THE REGULATION OF BRANCHED-CHAIN ESTER PRECURSOR BIOSYNTHESIS IN RIPENING FRUITS

By

Philip Engelgau

A DISSERTATION

Submitted to
Michigan State University
in partial fulfillment of the requirements
for the degree of

Horticulture – Doctor of Philosophy
Molecular Plant Sciences – Dual Major

2023

ABSTRACT

The aroma of fruits is an important indicator of ripeness to potential consumers. It is appreciated by humans as being essential to the organoleptic quality of fresh fruits. The two most consumed fruits in the United States, bananas and apples, have aroma profiles dominated by straight- and branched-chain esters. These compounds confer the characteristic flavors of these fruits. Despite the value of these esters to quality perception, their biosynthesis is still poorly understood. The central theme of this work is to understand how these fruits produce an ample supply of precursors for the biosynthesis of esters. The application of acetohydroxyacid synthase inhibitors demonstrated, through aroma and amino acid analyses of treated apple, banana, and ornamental quince, that the precursors to branched-chain esters are ultimately supplied through *de novo* synthesis and not from protein degradation. Inhibitor treatment, paired with ^{13}C-labeled acetate, allowed further elucidation of biochemical networks. Sensory analysis of inhibitor-treated apples, supplemented with population genetics analyses, demonstrated that humans can detect the absence of branched-chain esters and, via breeding/propagation efforts, have selected for fruit that are capable of branched-chain ester synthesis. Inhibitor application revealed a potentially unique means for butyl ester biosynthesis in banana fruit and inspired a precursor feeding study in plantain to better understand the origins of these important aroma compounds in banana. The specific mechanisms underlying banana aroma precursor biosynthesis were also explored. Aroma, respiration, and metabolic intermediate data demonstrated a coordinated shift of branched-chain amino acid metabolism that is facilitated by the alternative splicing of two otherwise feedback-regulated enzymes, acetohydroxyacid synthase and isopropylmalate synthase. The incidence of splicing and fold-change of the alternative transcripts was localized to only fruit pulp and increased with ripening. Enzymatic assays and transient expression in tobacco indicated these alternative isoforms to be immune to feedback regulation and to be able to supply ample precursors for branched-chain ester synthesis. Banana fruit aroma biodiversity was also explored, identifying several promising cultivars for future studies. Finally, artificial banana flavor was also investigated, revealing that the ersatz flavor substitute in foodstuffs is not emblematic of the banana of the past, ‘Gros Michel’, nor the banana of today, ‘Cavendish’.

To Songwen

ACKNOWLEDGEMENTS

While a great many people helped and supported me through every step of graduate school, I will reserve this page for those who are most likely to read it. These are the people whose unwavering support buoyed me during difficult periods and whose praise encouraged me to strive for greatness in those fleeting moments of success. If given the space, I could fill pages expressing the gratitude I feel to each of the following people, however I will attempt to be succinct.

To Songwen, who, perhaps better than anyone else, knew of the myriad difficulties I regularly encountered. She listened to my problems patiently and responded tactfully to my incessant ideas for how to fix them. She inspired grace and resolve in me while also acting as my muse, supporting our many hobbies that provided refuge from the endless frustrations I faced. While apart for the final eighteen months of my schooling, she provided powerful motivation for me to push through to the finish.

To my parents, my sisters, and grandparents, who, whether here or not, grounded me and gave perspective to how much I had grown while away. To leave my home state of California to pursue graduate school somewhere as foreign as Michigan was frightening. To do so alone was heartrending. My family gave me the love and support to persevere. Even though they may not have been in my immediate vicinity, their presence was felt as I endured my departure from home and grew to be a scientist.

To my friends, who, for better or worse, gave a better distraction from work than I could have ever envisioned. Whether this was through my recollection of our past adventures and mischief to help calm nerves before a presentation, or from our regular calls that served as a platform to discuss the coarser things in life, their presence provided me a haven from the pressures of graduate school.

And lastly to Dr. Randy Beaudry, who was the best advisor and mentor I could have possibly had. He pushed me to think critically and yet creatively when attacking a problem. I was allowed to pursue uncertain avenues of research and gain an appreciation for focus and efficiency when they failed. He granted me the independence to truly become independent and self-reliable. I grew tremendously while in graduate school, both as a scientist and as a person. Much of this is thanks to Randy.

PREFACE

To the modern reader, a warning is unfortunately necessary before continuing. The following dissertation will likely be considered by many as disturbing and upsetting. The source of this reproach is not so much as what the following contains, but what it lacks. The ensuing pages contain no heatmaps, no principal component analyses and no volcano plots. The reader will be unable to find genome-wide association studies, transcriptomic analyses, or untargeted metabolomic data. Not even a newly assembled genome is present. Perhaps the most regrettable omission from this work is the complete lack of putative candidate genes for future studies.

The following work took a difference approach; one that is *undeniably* out of date and out of fashion in this modern age of omics. Quite simply, every metabolite measured, every gene investigated, and every metric quantified were deliberately selected with a hypothesis in mind. These hypotheses were not the product of mining gratuitous amounts of data for potential patterns, trends, or associations. They were instead generated with a deep understanding of the metabolic pathways at play, contemplation upon the sum of past research, and consideration of logical explanations to observed phenomena.

Such a method, although exceptionally blasphemous and heretical at present, still has merits. The following work is a testament to such an approach. Beyond the officious influence of omics, creative and novel approaches were employed to upend entire dogmas and to discover and describe pathways to specialized metabolism for some of the most popular flavors to humankind.

This is not to say that omics does not have a place in biology. The extensive and wide-ranging nature of these studies have obvious value. They do not, however, have focus. It appears as though it is significantly easier to perform these resolution-less studies, be blinded by the grandiose scale, and ultimately be left with vague and indeterminate results than to conceive a precise strategy.

It is my desire that the following work may serve as an example of what can be accomplished without the “aid” of omics, hopefully inspiring some to forgo today’s nearly omnipresent staple of biological research.

TABLE OF CONTENTS

CHAPTER I – INTRODUCTION

When a fruit abscises, it is taking a literal "leap of faith" that it will be able to attract a consumer; an act that will ultimately lead to seed dispersal. However, evolution doesn't work by faith. For the wellbeing of its offspring, plants forgo and compromise otherwise canonical physiological patterns and biochemical inhibitions to make the fruit as appealing as possible for the short time they have remaining as an edible, living, entity. During ripening, normally homeostatic processes related to maintenance of tissue structure and macromolecule organization are abandoned as fruits soften and become susceptible to bruising, or as starches convert to sugars, sometimes leading to severe osmotic imbalances in tissues. Risks are taken when primary metabolites such as amino acids or fatty acids have their biosynthetic pathways deregulated in order to build up a substrate pool for the production of color pigments or aroma compounds. Evolution has concocted a dizzying number of unique regulatory alterations and compromises to shift metabolism in such a way as to accomplish the goal of attracting a consumer.

Humans fall prey to these biochemical strategies as well. From a plant's perspective, several species have benefited exceptionally well from attracting human consumers. The progenitors to the domesticated apple, for example, were once confined to the forests of Central Asia but, after having enchanted humans with their biochemical charms, now have offspring growing worldwide. The same story can be said of nearly all cultivated horticultural crops.

The following work focuses on one set of the biochemical attractants that have been effective at enticing humans: volatile aroma compounds. From the sulfurous compounds of muskmelons, the trailing aldehydes of cucumber, and citrus' menagerie of terpenes, these volatile compounds provide fruits with a seemingly endless catalog of flavors to deploy. The majority of aroma volatiles are products of specialized metabolism, synthesized at critical developmental phases within defined fruit tissues and specific taxa. Branched-chain esters, which are substantially produced by two of the world's most popular fruits, bananas and apples, will be of principal interest herein. These compounds imbue banana fruits with their characteristic flavor and also contribute substantially to an apple fruit's complex bouquet.

In Chapter II, the state of branched-chain aroma biochemistry will be reviewed with an emphasis on the many unknowns concerning how fruits synthesize these important compounds. Despite decades of research, questions, ranging from the overarching fundamentals of biosynthesis to the subtleties of intermediary steps, still remain.

In Chapter III, the long-standing assumption that branched-chain esters are an eventual product of protein degradation will be challenged through the novel employment of one of the world's most common herbicides. Previously unknown biochemical pathways of aroma biosynthesis will also be exposed through the application of this new tool. Furthermore, while most of the research herein is biochemical in perspective, a brief excursion into sensory science and population genetics will suggest that even though the branched-chain esters of apple fruits share the spotlight with several other classes of esters, humans can distinguish their absence and have selected for fruit that produce these important compounds.

In Chapter IV, the means by which bananas synthesize their characteristic and unique aroma will be elucidated, demonstrating a previously unknown route to specialized metabolism from branched-chain amino acid metabolism. It will also highlight the second known example of this pathway's transformation to providing an 'unregulated' supply of precursors for branched-chain esters.

In Chapter V, the diversity of banana fruit aroma will be explored. Resulting in the identification of several cultivars with promising aroma profiles for the elucidation of several aroma biochemical pathways.

Lastly, within the appendix, the history and myth of artificial banana flavoring will be explored through both biochemical and historical lenses.

In summary, the following work challenges several longstanding assumptions of fruit aroma biochemistry through the use of novel tools and techniques, it unravels the biosynthetic processes behind one of the world's most popular flavors, and, ultimately, demonstrates some of the sophisticated means that plants employ for the successful dispersion of their offspring.

CHAPTER II – LITERATURE REVIEW

Humans can perceive five tastes: sweet, sour, salty, bitter, and umami. There are, however, hundreds of olfactory receptors that allow humans, on average, to perceive over a trillion distinct olfactory stimuli (Trimmer, et al., 2019) (Bushdid, Magnasco, Vosshall, & Keller, 2014). Together the senses of taste and aroma provide the phenomena of flavor. These senses, however, do not contribute equally. Aroma composes upwards of 80% of perceived flavor (Murphy, Cain, & Bartoshuk, 1977). Furthermore, taste sensations can be greatly affected by the presence of aroma compounds. For example, the presence of certain volatiles within strawberry fruit can increase perceived sweetness independent of sugar content (Schwieterman, et al., 2014). While taste can be considered foundational to a food's flavor, ultimately, it is aroma that provides identity, definition, and character.

In nature, over half of all plant species are estimated to be dependent upon animal-mediated seed dispersal (Rogers, Donoso, Traveset, & Fricke, 2021), many of which use aroma as an attractant and means to signal potential consumers of fruit ripeness (Rodríguez, Alquézar, & Peña, 2013). Fruit volatile biosynthesis and emission has coevolved with the behaviors and physiologies of dispersers, proliferating an expansive biodiversity of aroma volatiles that increases plant fitness (Borges, Bessière, & Hossaert-McKey, 2008) (Borges, Ranganathan, Krishnan, Ghara, & Pramanik, 2011) (Lomáscolo, Levey, Kimball, Bolker, & Alborn, 2010).

The appreciation of fruit flavor diversification is apparent in humans too, as evidenced by the popularity and interest of new fruit cultivars and fruit-based products which often heavily market their novel flavors (Palmer & Molloy, 2020) (Becot, Bradshaw, & Conner, 2016). However, despite this appreciation, fruit breeding has traditionally overlooked flavor and instead prioritized production traits, such as size, appearance, decay resistance, and uniformity, a story well documented in the case of tomatoes (Tieman, et al., 2017) (Klee & Tieman, 2018). Understanding the molecular underpinnings of flavor allows future breeders, who will indubitably be needed to address future challenges of disease pressure and changing markets, to breed with flavor as a priority.

Within the United States, the two most consumed fruits are bananas and apples (USDA, 2021). The aroma profiles of both are dominated by short chain esters that are generally twelve carbons or less in size, however other chemical classes can be found, including alcohols, aldehydes, ketones, terpenes, and phenylpropenes (Morton & MacLeod, 1990). Esters are

produced through the condensation of an alcohol and an acyl-CoA, generating the alkyl and alkanoate parts of an ester, respectively (Figure 2.1). Banana and apple fruits produce a wide array of esters, each of which imbue its unique aroma into the fruit's overall flavor.

Banana fruit commonly produce esters composed of butyl, 2-methylpropyl, 3-methylbutyl, 1-methylbutyl, and, to a much lesser extent, hexyl alkyl elements. Alkanoate elements are typically acetates and butanoates, but some cultivars produce various iso-branched-chain alkanoate elements too (Macku & Jennings, 1987).

In apple fruit, alkyl portions of esters are typically made of butyl, 2-methylbutyl, and hexyl elements, however minor amounts of propyl, pentyl, and unsaturated hexyl compounds are not uncommon (Sugimoto, Forsline, & Beaudry, 2015). Trace amounts of 2-methylpropyl esters can also be regularly detected. Of alkanoate ester elements, acetate esters predominate, but butanoate, 2-methylbutanoate, and hexanoate are widespread with minor contributions from propanoates and trace amounts of pentanoates and 2-methylpropanoates (Sugimoto, Forsline, & Beaudry, 2015).

The biosynthesis of these various alcohols and acyl-CoAs has largely been thought to be catabolic in nature, implying a reliance on scavenging precursors produced through senescent processes (Gonda, et al., 2010) (Rowan, Lane, Allen, Fielder, & Hunt, 1996) (Rowan, Allen, Fielder, & Hunt, 1999) (Tressl & Drawert, 1973) (Myers, Issenberg, & Wick, 1970).

Straight-chain esters have generally been believed to be derived from fatty acids, mainly relying upon β- and α-oxidation to produce saturated components (Rowan, Allen, Fielder, & Hunt, 1999). Unsaturated C_6 straight-chain esters are made through the action of lipoxygenases on linolenic acid, which generally rely upon cellular disruption for the interaction of substrate and enzyme to occur, however evidence has suggested that some lipoxygenase activity provides aroma precursors within intact apple fruit tissues (Contreras & Beaudry, 2013) (Schiller, et al., 2015). Lipoxygenase activity with linoleic acid can supply saturated straight-chain C_6 elements.

The biosynthesis of 1-methylbutyl compounds, which can be considered as being sec-branched, is, among all the esters described herein, the least studied and has been proposed as being derived from fatty acid metabolism (Tressl & Drawert, 1973).

The other branched-chain esters: 2-methylbutyl, which may be termed as being anteiso-branched, and 2-methylpropyl and 3-methylbutyl, both of which are iso-branched, have long been assumed to be derived from the branched-chain amino acids isoleucine, valine, and leucine,

respectively (Tressl & Drawert, 1973) (Rowan, Lane, Allen, Fielder, & Hunt, 1996) (Myers, Issenberg, & Wick, 1970). It has been observed that within the tissues of aroma biogenesis of ripening apple and banana fruits, only the branched-chain amino acids with corresponding branched-chain esters emanated accumulate concomitantly with ester biosynthesis. In apple fruit, only isoleucine (the supposed progenitor of 2-methylbutyl compounds) accumulates, whereas in banana fruits only valine and leucine (the supposed progenitors of 2-methylpropyl and 3-methylbutyl esters, respectively) accumulate (Alsmairat, Engelgau, & Beaudry, 2018) (Sugimoto, Jones, & Beaudry, 2011). Such findings are contradictory to the notion that these volatiles and their precursors are the product of nondiscriminatory catabolic processes, instead suggesting a developmentally induced anabolic means to branched-chain ester precursor production.

The biosynthesis of branched-chain amino acids occurs within the chloroplasts of plants and can be considered as two parallel paths. These paths serve as the sole means of *de novo* primary metabolic production of these compounds (Figure 2.2). The production of isoleucine is normally thought of as beginning with threonine, which in itself is an eventual product of the tricarboxylic acid cycle, with several of the intermediary enzymes subject to feedback regulation by threonine and methionine-related metabolites. Threonine, by the action of threonine deaminase, can be converted to α-ketobutyrate. Acetohydroxyacid synthase then combines α-ketobutyrate with a molecule of pyruvate, and, through a series of additional steps facilitated by ketol acid reductoisomerase and dihydroxyacid dehydratase, α-keto-β-methylvalerate is produced, the α-ketoacid of isoleucine. Transamination by branched-chain aminotransferase can freely convert the branched-chain α-ketoacids to their respective amino acids and vice versa.

Valine and leucine are produced by a route that parallels isoleucine (Figure 2.2). Their synthesis begins with two pyruvate molecules being processed by acetohydroxyacid synthase *et al.* to produce α-ketoisovalerate, the α-ketoacid of valine. To produce leucine, α-ketoisovalerate is extended by isopropylmalate synthase, isopropylmalate isomerase, and isopropylmalate dehydrogenase to generate leucine's α-ketoacid, α-ketoisocaproate.

Under normal metabolic conditions, these pathways are regulated by allosteric feedback inhibition through the binding of the branched-chain amino acids with upstream enzymes. Isoleucine regulates its own production at threonine deaminase (Halgand, Wessel, Laprévote, & Dumas, 2002), valine and leucine synergistically inhibit acetohydroxyacid synthase (Lee &

Duggleby, 2001), and leucine limits isopropylmalate synthase activity (de Kraker, Luck, Textor, Tokuhisa, & Gershenzon, 2007). While these can be considered the principal regulatory mechanisms of branched-chain amino acid metabolism, minor networks have also been observed, such as the antagonism of isoleucine feedback by valine, and the role of isoleucine as an inhibitor of acetohydroxyacid synthase in some organisms (Halgand, Wessel, Laprévote, & Dumas, 2002) (Lee & Duggleby, 2001). These feedback mechanisms prevent overaccumulation of the branched-chain amino acids and balance the supply of each (Xing & Last, 2017).

While the enzymes of branched-chain amino acid metabolism are considered to be products of 'housekeeping' genes and thus constitutively expressed, variation of mRNA abundance for these genes is regularly observed during fruit ripening (Gonda, et al., 2010) (Sugimoto, Park, van Nocker, & Beaudry, 2008) (Kochevenko & Fernie, 2011). Furthermore, a growing theme of aroma biology is the developmental and tissue-specific expression of enzymes that have been neofunctionalized for volatile biosynthesis and whose products feed into branched-chain metabolism (Sugimoto, Engelgau, Jones, Song, & Beaudry, 2021) (Gonda, et al., 2013). The overarching regulatory networks of these pathways during fruit ripening remain to be definitively known. Beyond the assumed dependence on ethylene, a proliferation of untargeted transcriptomic and metabolomic studies have identified potential players but have yet to elucidate any concrete networks (Guo, et al., 2018) (Asif, et al., 2014) (Feng, et al., 2016).

The processing of branched-chain metabolites to esters also remains to be an area with more questions than answers. In general, two pathways are thought to convert branched-chain α-ketoacids to their respective alcohols and acyl-CoAs (Figure 2.3). The branched-chain α-ketoacid dehydrogenase complex, the canonical means for branched-chain amino acid catabolism (Peng, Uygun, Shiu, & Last, 2015), and a hypothetical plant branched-chain α-ketoacid decarboxylase, which has been demonstrated to be present in *Saccharomyces cerevisiae* (Dickinson, Harrison, Dickinson, & Hewlins, 2000) (Dickinson, Harrison, & Hewlins, 1998) (Dickinson, et al., 1997), are often thought to facilitate the process. However other possibilities have been suggested, such as the direct generation of aldehydes from the branched-chain amino acids, or the action of an amino acid decarboxylase to produce an amine that could be further processed to an aldehyde, both of which have been observed within Solanaceae in the processing of aromatic amino acids (Tieman, et al., 2006) (Kaminaga, et al., 2006). Many of these options, as currently understood, require subcellular relocalization and are still only hypothetical in terms

of their role in plants, or their ability to catalyze branched-chain substrates. Furthermore, while the reduction of aldehydes to alcohols has long be accepted to be performed by alcohol dehydrogenase, the interconversion of alcohols to acyl-CoAs, and vice versa, a necessary process of these proposed pathways, has been observed through feeding studies but lacks further evidence (Jayanty, Song, Rubinstein, Chong, & Beaudry, 2002) (Rowan, Lane, Allen, Fielder, & Hunt, 1996).

The terminal step of ester synthesis has been well documented as being catalyzed by alcohol acyl transferase (Beekwilder, et al., 2004). After initial work on the enzyme, an outsized role of its effect on volatile composition was assigned to its preference of substrates (Beekwilder, et al., 2004). Today, while the role of alcohol acyl transferase is still believed to exert a degree of influence on ester synthesis, the availability of substrates is now considered to be of greater import (Beekwilder, et al., 2004) (Jayanty, Song, Rubinstein, Chong, & Beaudry, 2002) (Wyllie & Fellman, 2000).

After synthesis, the route taken by the ester to reach the headspace has largely been taken for granted, however research has shown complexity to exist for the exit strategy of some flower volatiles (Liao, et al., 2021) (Adebesin, et al., 2017). It may be that fruit-produced volatiles, that in some species must pass through entire tissue layers for emanation, likewise undergo sophisticated means of escape.

Overall, large portions of the branched-chain ester biosynthetic pathways, from the procurement of α-ketoacids, to the preparation of alcohols and acyl-CoAs, are still in need of further study.

Given the importance of precursor availability to a fruit's aroma profile, an understanding of the upstream biosynthetic processes should not only illuminate the forces behind aroma biodiversity, but also the means that plants have evolved to synthesize these specialized metabolites. For example, banana fruit uniquely produce high levels of 2-methylpropyl and 3-methylbutyl esters whereas apple fruit emit substantial quantities of 2-methylbutyl esters. The origin of these compounds has been shown as being related to branched-chain amino acid metabolism, and yet neither fruit produces all three classes of esters. Furthermore, and as previously stated, the tissues of aroma biogenesis in these fruits have been observed to accumulate only the branched-chain amino acids that correspond to the branched-chain esters found in their headspaces (Alsmairat, Engelgau, & Beaudry, 2018) (Sugimoto, Jones, &

Beaudry, 2011). These observations clash with the current dogma of protein degradation as the ultimate source of volatile-bound amino acids and instead suggest that coordinated, fine-tuned anabolic processes are occurring within these fruits in order to engage specific aspects of branched-chain amino acid metabolism for the production of branched-chain ester precursors. However, such proposed anabolic processes, and the accumulation of the branched-chain amino acids, are seemingly paradoxical. The branched-chain amino acids, as previously described, regulate their own synthesis through feedback inhibition of upstream enzymes. If the pathways in question continue to operate during fruit ripening and volatile biosynthesis as they do under normal metabolism, with no alternative influxes or circumvention of regulation, then the accrual of the branched-chain amino acids should not occur.

Two possible explanations present themselves to resolve such a paradox. One being that protein degradation, and thus catabolism, is in fact the true source of branched-chain ester precursors, suggesting a misinterpretation of the observed accumulations of the branched-chain amino acids in ripening banana and apple fruits. The other possible explanation is that branched-chain ester biosynthesis is, instead, an entirely anabolic process and that, in amplifying flux through branched-chain metabolism, fruits have evolved specialized means to overcome or minimize the conserved feedback regulation of branched-chain amino acids in the synthesis of these specialized products.

The latter has recently been found to very likely be the case in ripening apple fruits. Citramalate synthase, an enzyme previously thought to only be present in bacteria but appears to have evolved in apple from duplication and neofunctionalization of isopropylmalate synthase, facilitates the biosynthesis of an unregulated supply of 2-methylbutyl esters through the circumvention of isoleucine feedback inhibition (Sugimoto, Engelgau, Jones, Song, & Beaudry, 2021). The enzyme condenses a molecule of pyruvate and acetyl-CoA to produce citramalate, a structural analog to isopropylmalate that can be processed by isopropylmalate isomerase and isopropylmalate dehydrogenase to produce α-ketobutyrate, the first metabolite downstream of threonine deaminase, effectively avoiding isoleucine feedback inhibition. Citramalate synthase lacks the leucine-binding regulatory domain characteristic of isopropylmalate synthase and is not inhibited by any of the branched-chain amino acids. Furthermore, the enzyme is also capable of facilitating extension of α-ketobutyrate several more times. The subsequent α-ketoacids, as well

as α-ketobutyrate, serve as potential precursors to three, four, five, and, possibly, six-carbon straight-chain esters in an analogous fashion as the branched-chain α-ketoacids.

Despite these findings, the notion that branched-chain ester production is ultimately catabolically supplied from protein degradation continues to be broadly accepted (Maoz, Lewinsohn, & Gonda, 2022).

The following work had several aims. The first was to conclusively establish the role of *de novo* branched-chain α-ketoacid production on branched-chain ester biosynthesis in ripening banana and apple fruits. This was accomplished with the use of an inhibitor that arrests the activity of acetohydroxyacid synthase, the common enzyme of branched-chain α-ketoacid synthesis. The subsequent aim sought to elucidate the means by which banana fruit overcome feedback inhibition in order to generate copious quantities of 2-methylpropyl and 3-methylbutyl esters. The final aim was to explore the diversity of banana fruit aroma to identify potential candidate cultivars for future studies on banana aroma biochemistry.

Figures & Tables

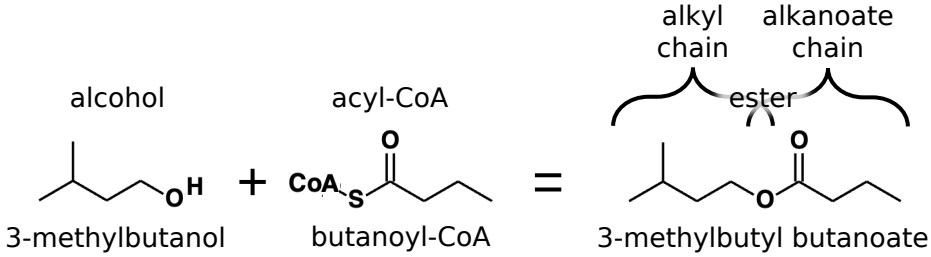

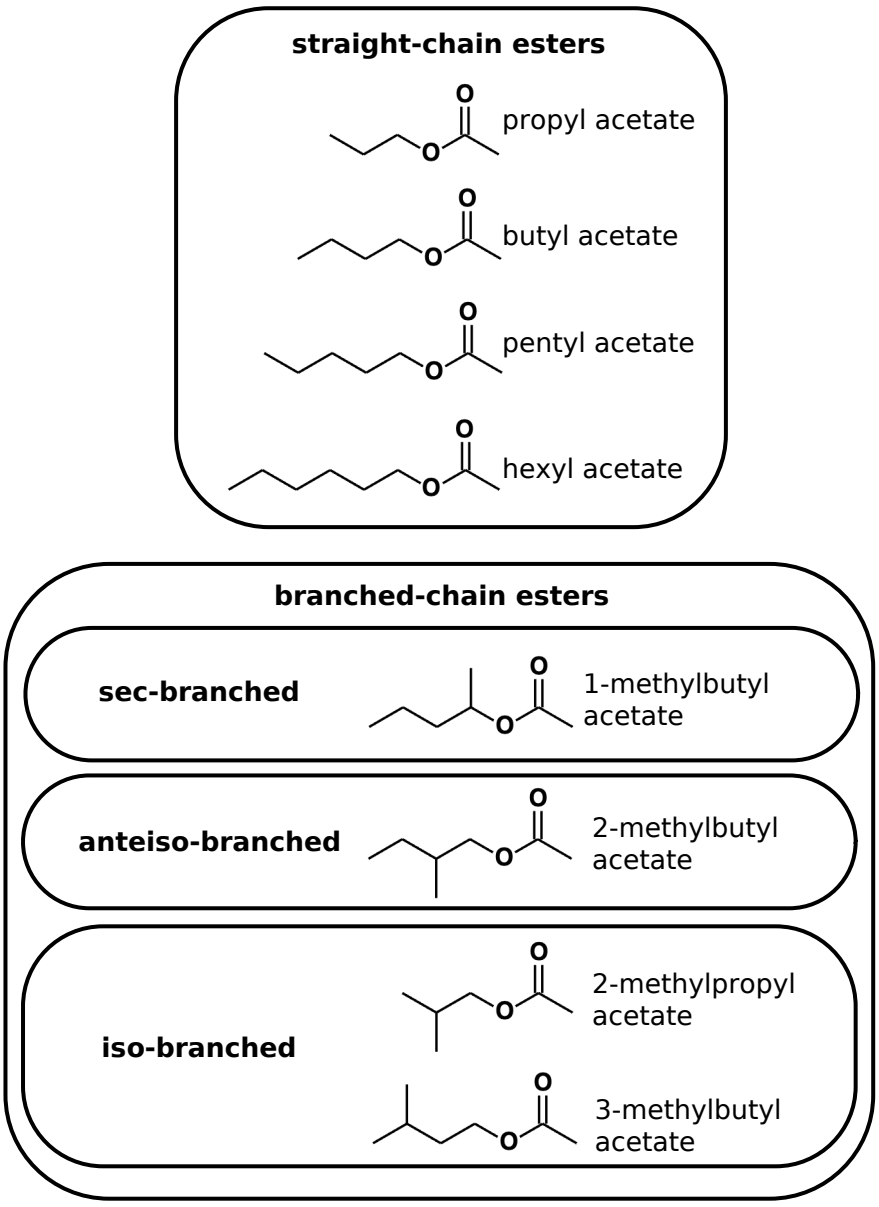

Figure 2.1. Nomenclature of esters and representative structures of the esters discussed in this dissertation. Acetate esters of each are depicted.

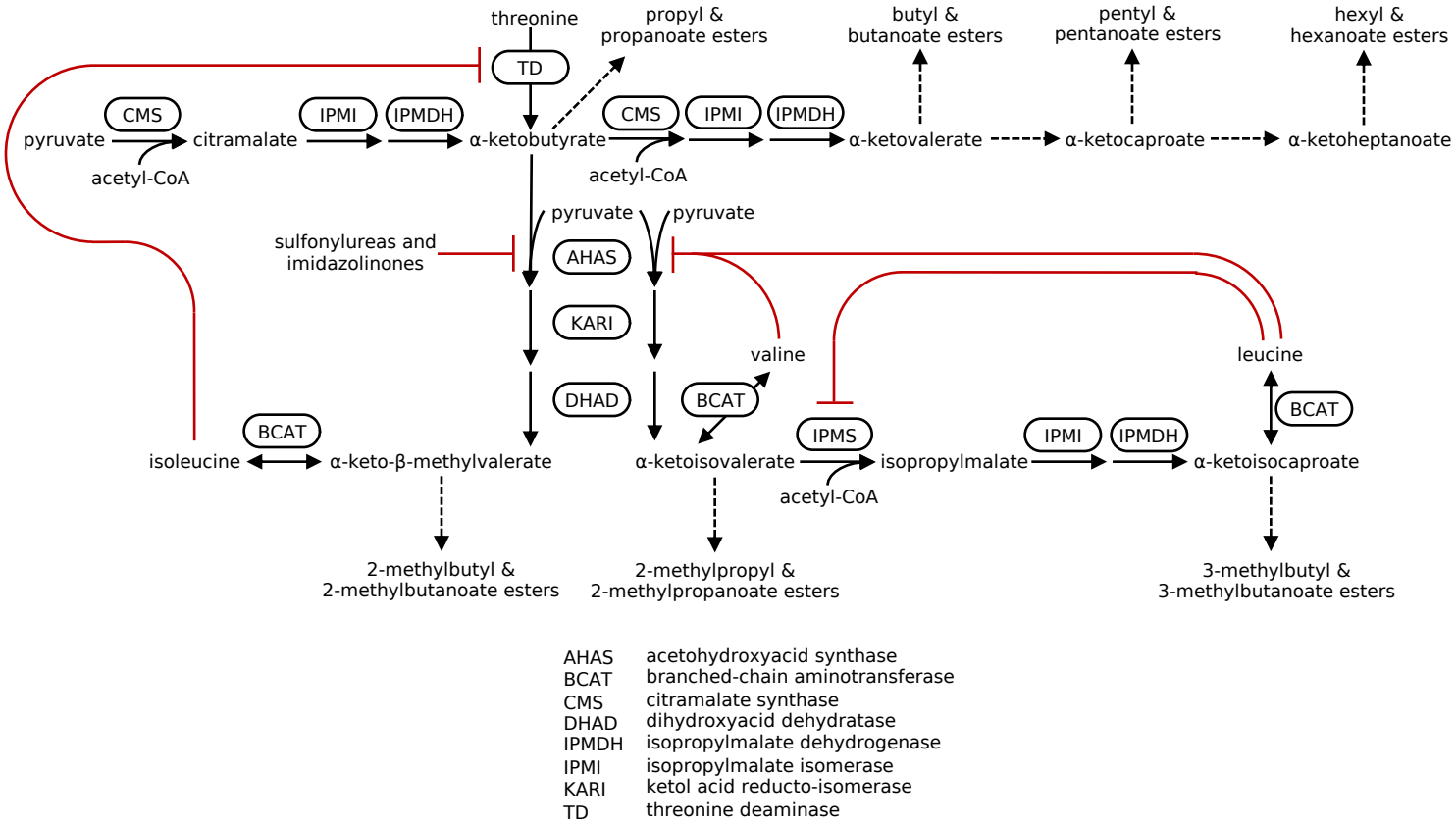

Figure 2.2. Branched-chain amino acid biosynthesis and the citramalate synthase pathway. Abbreviated pathways shown with dashed arrows. Reactions understood to be freely reversible are depicted with double-sided arrows. Enzymes shown in curved boxes. Principal inhibitory interactions drawn with red lines. Minor inhibitory mechanisms not shown: antagonism of isoleucine feedback at TD by valine and isoleucine inhibition of AHAS.

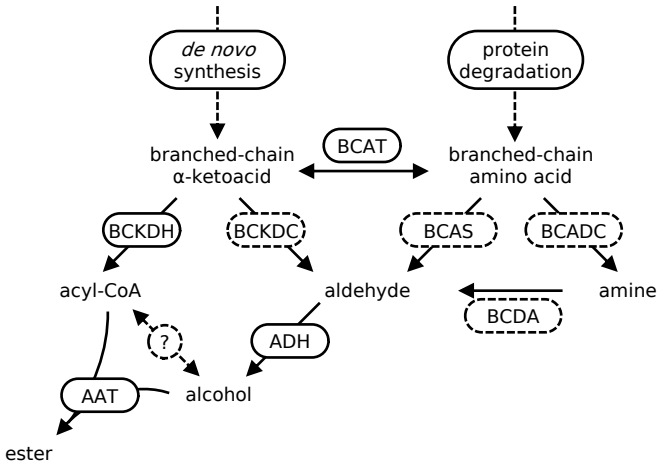

AAT	alcohol acyl transferase
ADH	alcohol dehydrogenase
BCADC	branched-chain amino acid decarboxylase
BCAS	branched-chain aldehyde synthase
BCAT	branched-chain aminotransferase
BCDA	branched-chain deaminase
BCKDC	branched-chain α-ketoacid decarboxylase
BCKDH	branched-chain α-ketoacid dehydrogenase complex

Figure 2.3. Proposed pathways for synthesis of branched-chain alcohols and acyl-CoAs. Abbreviated pathways shown with dashed arrows. Reactions understood to be freely reversible are depicted with double-sided arrows. Enzymes/processes shown in curved boxes. Hypothetical enzymes/processes are in dashed boxes. Analogous reactions to BCAS, BCADC, and BCDA have been observed in Solanaceae for aromatic amino acids. BCKDC has been detected in *Saccharomyces cerevisiae*. Interconversion of acyl-CoAs and alcohols has been observed in several fruits.

CHAPTER III – THE USE OF HERBICIDES TO INVESTIGATE ESTER PRECURSOR BIOSYNTHESIS IN RIPENING APPLE AND BANANA FRUITS

Introduction

For over half a century a relationship has been known to exist between the branched-chain esters that act as impact flavor notes for many popular fruits, and branched-chain amino acids; specifically, 2-methylbutyl and 2-methylbutanote esters and isoleucine, 2-methylpropyl and 2-methylpropanoate esters and valine, and 3-methylbutyl and 3-methylbutanoate esters and leucine (Myers, Issenberg, & Wick, 1970) (Rowan, Lane, Allen, Fielder, & Hunt, 1996) (Tressl & Drawert, 1973). However, the nature of this relationship has been disputed for some time.

Many groups have assumed that these amino acids act as direct precursors to their related volatiles via a catabolic relationship (Gonda, et al., 2010) (Rowan, Lane, Allen, Fielder, & Hunt, 1996) (Tressl & Drawert, 1973) (Myers, Issenberg, & Wick, 1970). However, such assertions overlook or outright disregard processes that must occur to supply said precursors. Ultimately a dogma has been conceived that heavily implies that aroma biosynthesis is a wholly catabolic process that relies upon amino acids sourced via protein degradation as a function of senescent processes (Maoz, Lewinsohn, & Gonda, 2022).

Ripening in fruit is a highly dynamic process involving sequentially induced and deliberate modifications to chlorophyll content, respiration, pigmentation, starch degradation, and sugar:acid balance, to name a few (Gortner, Dull, & Krauss, 1967). It would seem inconsistent to suggest that aroma biosynthesis, the often terminal feature of ripening and thus the ultimate attractant for consumption and seed dispersal, is not also an active process. Our research group's hypothesis is that aroma formation is under programmed regulation and thusly proposed that branched-chain volatiles are instead more directly derived from *de novo* synthesized precursors to branched-chain amino acids, the branched-chain α-ketoacids, via active, anabolic processes.

It has recently been observed that among the free amino acids of ripening apple and banana fruits, only those with related branched-chain volatiles produced by the fruit undergo a marked increase that is concomitant with aroma emanation (Alsmairat, Engelgau, & Beaudry, 2018) (Sugimoto, Jones, & Beaudry, 2011). Non-discriminatory protein degradative processes would not be expected to produce such coincidental results, implying that these fruits are actively engaging the processes of branched-chain amino acid synthesis.

Sugimoto et al. (2021) further demonstrated the importance of *de novo* precursor production through the elucidation of citramalate synthase's role of circumventing isoleucine inhibition at threonine deaminase in order to produce copious amounts of α-keto-β-methylvalerate to supply a precursor pool for 2-methylbutyl and 2-methylbutanoate ester production in apple fruit. Furthermore, it was found that apples lacking an active allele of citramalate synthase are unable to produce such esters.

Despite these discoveries, the mantra of branched-chain volatiles being directly descended from branched-chain amino acids, as well as its associated implications, continue to be prominently peddled (Maoz, Lewinsohn, & Gonda, 2022).

An experiment with a relatively simple premise can be used to dispel such questionable assertions and also further demonstrate the importance of *de novo* precursor biosynthesis. If the anabolic pathways predominate, inhibition of the biochemical pathway leading to the formation of the α-ketoacid precursors of amino acid synthesis should prevent the accumulation of the α-ketoacids, the amino acids, and the branched-chain esters simultaneously. On the other hand, if the amino acids are catabolically derived from previously formed proteins, branched chain ester synthesis should persist or be minimally disrupted by pathway inhibition.

The common enzyme of branched-chain amino acid biosynthesis, and thus branched-chain α-ketoacid production, is acetohydroxyacid synthase (Figure 2.2, EC 2.2.1.6). This enzyme is also the target of over fifty herbicides representing seven chemical families (Weed Science Society of America, 2021). The mode of action for two of these families, the sulfonylureas and imidazolinones, has been determined to be via binding and obstructing the channel leading to the enzyme's active site (McCourt, Pang, King-Scott, Guddat, & Duggleby, 2006), resulting in a loss of activity and, given the lack of an alternative biosynthetic pathway, arrested isoleucine, valine, and leucine biosynthesis that ultimately translates into severe inhibition of DNA synthesis, a halt of mitosis, and eventual plant death (Shaner & Reider, 1986). Furthermore, increased protein turnover, coupled with increases of total free amino acid levels, a likely effect of acute amino acid starvation, has been observed after inhibitor treatment (Shaner & Reider, 1986) (Goldberg & St. John, 1976).

The application of acetohydroxyacid synthase inhibitors to ripening fruits should likewise halt any *de novo* production of branched-chain amino acids, α-ketoacids, and related metabolites

while increasing overall protein degradation. The resulting effects on branched-chain volatiles and amino acids should be illuminating to the aroma biochemistry of fruits.

Results

Apple

The application of rimsulfuron, a sulfonylurea acetohydroxyacid synthase inhibitor, led to a reduction of the headspace concentrations of every 2-methylbutyl and 2-methylbutanoate ester analyzed in 'Gala', 'Empire', and 'Jonagold' fruits (Figures 3.1, 3.2, 3.3; Table 3.1). Further, 2-methylpropyl acetate, which is present in quantities under 2 nmol · L^{-1} in all three cultivars tested, was also reduced in the headspaces of treated 'Gala' and 'Empire' fruits.

While treatment of rimsulfuron had no discernable effect on butyl acetate, pentyl acetate was more abundant in all three of the cultivars when treated. Ethyl acetate was lower in 'Gala' and 'Empire' fruits. Propyl acetate and hexyl acetate were reduced in 'Empire' and 'Jonagold' headspaces, respectively.

Estragole, a phenylpropene produced at low levels by 'Jonagold' in quantities of 0.01 nmol · L^{-1}, was interestingly found to be nearly four-times higher in rimsulfuron-treated fruit.

To discern if herbicide-treated fruit were still capable of aroma production, and to test the importance of substrate availability, branched-chain α-ketoacids were fed, with and without inhibitor, to 'Empire' and 'Jonagold' peel tissues.

Feeding of α-keto-β-methylvalerate to rimsulfuron-treated 'Empire' and 'Jonagold' tissues led to a 'partial rescue' of the inhibitor-imposed disability for incorporation into the alkanoate moiety of 2-methylbutanoate esters in that the headspace concentrations of 2-methylbutanoate esters were higher than rimsulfuron-treated tissues without α-ketoacid supplementation, but less than control samples (Figures 3.2, 3.3, 3.4). Tissues not treated with rimsulfuron but supplemented with α-keto-β-methylvalerate had no increase of 2-methylbutanoate esters. On the other hand, 2-methylbutyl esters recovered well above control concentrations with α-keto-β-methylvalerate supplementation in treated fruits while also enhancing headspace concentrations in samples without inhibitor treatment.

'Empire' and 'Jonagold' fruit were also capable of converting supplied α-ketoisovalerate into copious amounts of methyl 2-methylpropanoate, ethyl 2-methylpropanoate, and 2-methylpropyl acetate (Figures 3.2, 3.3, 3.4). Interestingly, the pattern of reduced incorporation of the α-ketoacid into alkanoate portions of the esters, as compared to alkyl groups, by rimsulfuron-

treated tissues was consistent for α-ketoisovalerate feeding as described for α-keto-β-methylvalerate feeding.

Application of α-ketoisocaproate was likewise metabolized into appreciable amounts of ethyl 3-methylbutanoate and 3-methylbutyl acetate, neither of which are normally present apples, however the concentrations of both were found to be less when the tissue had been treated with inhibitor.

An interesting pattern presented itself when considering the ability of the fruits to convert the supplemented α-ketoacids. Both cultivars converted all three of the α-ketoacids into similar concentrations of acetate esters (~225 nmol · L^{-1} by 'Empire' and ~50 nmol · L^{-1} by 'Jonagold'). However, while α-ketoisovalerate and α-keto-β-methylvalerate were converted to similar amounts of ethyl esters by both cultivars (300-500 nmol · L^{-1} by 'Empire' and ~17 nmol · L^{-1} by 'Jonagold'), α-ketoisocaproate was converted into ethyl 3-methylbutanoate far less than its fellow branched-chain α-ketoacids (25.8 nmol · L^{-1} by 'Empire' and 1.2 nmol · L^{-1} by 'Jonagold').

Beyond the volatiles quantified, both cultivars were able to process α-ketoisovalerate and α-ketoisocaproate into an abundance of iso-branched-chain aldehydes, alcohols, and alkyl and alkanoate ester elements (Table 3.2). Furthermore, when fed α-ketoisovalerate, both cultivars produced 3-methylbutanal, 3-methylbutanol, and several 3-methylbutyl esters, indicating elongation of α-ketoisovalerate via isopropylmalate synthase (EC 2.3.3.13) into α-ketoisocaproate.

The citramalate synthase (EC 2.3.3.21) pathway of apple presents an interesting opportunity with regards to the use of acetohydroxyacid synthase inhibitors to study aroma production: namely, while the branched-chain portion of the pathway will be blocked due to the herbicide, the straight-chain portion, which is upstream of acetohydroxyacid synthase, will remain active. To study the possible changes of metabolism induced by the shunting of flux entirely towards the straight-chain route, 1,2-$^{13}C_2$ acetate was fed to the fruit, with and without inhibitor, to track possible changes of carbon movement (for expected carbon movement/labeling see (Sugimoto, Engelgau, Jones, Song, & Beaudry, 2021)).

Labeled acetate was fed to all three cultivars, however acetate incorporation into 'Gala' was very poor as compared to 'Empire' or 'Jonagold', as indicated by an average methyl acetate

M+2 incorporations of 3.0%, 21.6%, and 19.1%, respectively (Figures 3.5, 3.6, 3.7). The low incorporation of ‘Gala’ may be due to the aroma profile of ‘Gala’ fruit being almost entirely made up of acetate esters as compared to ‘Empire’ and ‘Jonagold’ fruit, which have a more diverse profile of alkanoate esters. Other acetate ester-dominated cultivars, such as ‘Redchief Delicious’, have been hypothesized to have saturating quantities of acetyl-CoA, hampering feeding experiments (Ferenczi, Sugimoto, & Beaudry, 2021). Thus, only the results from ‘Empire’ and ‘Jonagold’ were considered.

No significant differences of ^{13}C incorporation were found in rimsulfuron-treated fruits of either cultivar for methyl acetate, methyl propanoate or methyl butanoate. Rimsulfuron-treated ‘Empire’ produced low amounts of methyl 2-methylbutanoate, which showed no change of isotopolog enrichment patterning whereas treated ‘Jonagold’ produced none of the branched-chain volatile, so enrichment could not be assessed. M+1 and M+2 methyl pentanoate isotopologs were enriched in both cultivars when treated with rimsulfuron. This was paired with a corresponding decrease of the M isotopologs. Lastly, the M+1 isotopolog fraction of methyl hexanoate was significantly greater in rimsulfuron-treated ‘Jonagold’ fruit.

With regards to amino acid content, all three cultivars had a significant reduction of isoleucine content when treated with rimsulfuron, however neither valine nor leucine, which also depend upon acetohydroxyacid synthase for synthesis, were found to be different in the treated tissues (Tables 3.3, 3.4, 3.5). No other amino acids were found to be reduced by rimsulfuron treatment. Several amino acids were found to be elevated somewhat following treatment; however, no pattern of change was consistent across all three cultivars. Only ‘Gala’ fruit had a significant increase of total free amino acids in treated tissues. Lastly, treated ‘Jonagold’ fruit, which had an increase of estragole, did not have statistically different quantities of the amino acid precursors of phenylpropenes: phenylalanine and tyrosine.

Given our ability to cause fruit to fail to produce 2-methylbutyl and 2-methylbutanoate esters, and the lack of odor from the nonvolatile herbicide, we prepared samples to determine if humans could discriminate the absence of branched-chain volatiles. Participants were presented rimsulfuron-treated or untreated ‘Jonagold’ slices to smell in a “duo-trio” test. Briefly, subjects were tasked with matching a treated or untreated sample with a reference, which in this case was always an untreated sample. Twenty subjects completed 12 trials each (n = 240) and correctly

matched the samples significantly more often than by chance (Figure 3.8, 64% correct, $p = 6.7 \times 10^{-6}$).

The ability of panelists to discriminate the lack of 2-methylbutyl and 2-methylbutanoate esters in a complex aroma profile led us to consider what implications this may have had on apple breeding and the prevalence of these esters among commercially grown cultivars.

It has been demonstrated that the presence of an active allele of citramalate synthase is necessary for apples to synthesize a copious amount of 2-methylbutyl and 2-methylbutanoate esters in a dominant/recessive phenotypic relationship (Sugimoto, Engelgau, Jones, Song, & Beaudry, 2021) (Sugimoto, Forsline, & Beaudry, 2015). Among the 99 cultivars from the USDA Geneva *Malus* Core Collection previously analyzed, 6.1% were homozygous recessive, 36.4% were heterozygous, and 57.6% were homozygous dominant. Apples that were homozygous recessive had a significantly lower ratio of 2-methylbutyl and 2-methylbutanoate esters to straight-chain esters as compared to those with at least one copy of the active allele. From this data it cannot be determined if the observed allelic distribution favoring branched-chain ester-producing phenotypes is a result of natural or artificial selection.

However, among the apples screened, 'Cox's Orange Pippin', which has been identified through pedigree and sequencing-based analyses as a common breeding parent to many cultivars, was found to be homozygous recessive for citramalate synthase (Sugimoto, Engelgau, Jones, Song, & Beaudry, 2021) (Muranty, et al., 2020) (Noiton & Alspach, 1996). Through sequencing-based pedigree analyses of the USDA Geneva *Malus* Core Collection, several dozen cultivars with a first-degree (parent-offspring or clonal) relationship with 'Cox's Orange Pippin' have been identified (Migicovsky, et al., 2021). If no selective pressure were occurring, then, given that 'Cox's Orange Pippin' is homozygous recessive, a relatively greater number of its offspring will likewise be homozygous recessive and unable to produce 2-methylbutyl and 2-methylbutanoate esters. More than half of the cultivars within the germplasm have been found to be interconnected through first-degree relationships, suggesting a large degree of interbreeding and the reasonable assumption that the distribution of alleles observed by Sugimoto et al. (2021) is representative of the population of 'Cox's Orange Pippin's potential mates. We reasoned that should the proportion of 'Cox's Orange Pippin' offspring that are homozygous recessive be less than expected, assuming a parent population akin to previous observation, then it is likely that

humans have, likely unknowingly, been selecting for cultivars that are able to synthesize copious amounts of anteiso-branched-chain esters.

We sequenced the consequential single nucleotide polymorphism of citramalate synthase from 40 cultivars previously identified as having a first-degree relationship with ‘Cox’s Orange Pippin’ and termed this as the offspring population (Migicovsky, et al., 2021). The parent population (from Sugimoto et al. (2021) and Sugimoto et al. (2015)) and offspring population were mutually exclusive save for ‘James Grieves’, however this cultivar has been identified as being an offspring of ‘Cox’s Orange Pippin’ and was sequestered to the offspring population (Muranty, et al., 2020). Two cultivars, ‘Cherry Cox’ and ‘Potter Cox’, were identified as being sport mutations of ‘Cox’s Orange Pippin’ whereas another two cultivars, ‘Margil’ and ‘Rosemary Russet’ have been determined to be the parents of ‘Cox’s Orange Pippin’ (Muranty, et al., 2020) (Howard, et al., 2023). The sports (both homozygous recessive), and parents (both heterozygous) were removed from further analysis. In keeping with population definitions set by Migicovsky et al. (2021), cultivars listed as recently derived hybrids were removed from the parent and offspring populations as well. Furthermore, cultivars listed by alphanumeric codes were also removed. It was reasoned that these cultivars, given their lack of a common name and their status only as breeding lines, have not been publicly released and are thus not likely to be considered to be of high enough quality for commercial success.

Given our parent population, when crossed with ‘Cox’s Orange Pippin’ we would expect 29.1% of offspring to be homozygous recessive if no selection is occurring. However, among the 32 cultivars of the ‘Cox’s Orange Pippin’ offspring population, only 3 (9.4%) were homozygous recessive (Figure 3.8, $p = 0.0141$).

Lastly, intrigued and inspired by the change of estragole content in ‘Jonagold’ fruit treated with rimsulfuron, an attempt was made to influence the content of this phenylpropene with a different herbicide.

Glyphosate, an inhibitor of the shikimate pathway, and thus an inhibitor to the production of the aromatic amino acids tryptophan, tyrosine and phenylalanine, was applied to another estragole-producing cultivar: ‘Golden Delicious’. However, after almost two weeks of treatment there was no significant effect on estragole levels (Table 3.6). The amino acid levels of the peel tissues were also not found to be significantly different, save for alanine, which was 2.5-times

higher in treated tissues. Interestingly, the peels of glyphosate-treated fruits were found to be noticeably greener with higher levels of chlorophyll *a* than untreated tissues (Table 3.6).

Banana

The application of halosulfuron, another sulfonylurea acetohydroxyacid synthase inhibitor, led to a reduction of the headspace concentrations of every iso-branched-chain ester and alcohol analyzed in 'Cavendish' fruits (Figure 3.9; Table 3.7). Surprisingly, ethyl acetate, butyl acetate, and butyl butanoate were also less in treated tissues. None of the sec-branched esters or their related volatiles (2-pentanone, 2-pentanol, 1-methylbutyl acetate, and 1-methylbutyl butanoate) were affected by halosulfuron treatment.

Valine and leucine were significantly less abundant in halosulfuron-treated fruit, whereas isoleucine levels were unchanged (Table 3.8). No other amino acids were reduced in halosulfuron-treated fruits. Several amino acids were found to be higher after herbicide treatment with the total content of free amino acids having increased.

To further investigate 2-pentanone and 2-pentanol and their possible role as precursors to 1-methylbutyl esters, as well as the importance of substrate availability to aroma biosynthesis in bananas, sections of 'Horn Plantain' pulp were fed 2-pentanone, 2-pentanol, or butanol to assess this cultivar's ability to metabolize these compounds into esters.

'Horn Plantain' fruit have, compared to 'Cavendish', a very simple aroma profile that is restricted to ethyl acetate, 2-methylpropyl acetate, and 3-methylbutyl acetate. Notably, the cultivar produces very little 1-methylbutyl, butyl, or butanoate esters.

The feeding of 2-pentanol, but not 2-pentanone, resulted in the accumulation of 1-methylbutyl acetate in the headspace (Figures 3.10, 3.11). Furthermore, 2-pentanol feeding did not lead to an increase of 2-pentanone or vice versa. Butyl acetate and 2-methylpropyl butanoate production was increased when the tissues were fed butanol, however the levels of 2-methylpropyl butanoate, 0.6 nmol $\cdot$ L^{-1}, were much lower than butyl acetate, 168.0 nmol $\cdot$ L^{-1}. No other esters were determined to be affected by the feedings.

Ornamental quince

As a proof of concept, rimsulfuron was applied to the highly aromatic fruit of an ornamental quince hybrid (*Chaenomeles* × *superba*, cv. Dr Banks Pink); a species, when compared to apples and bananas, that there is practically no knowledge of its aroma biochemistry.

The aroma profile of the small, dense fruits was found to be dominated by the terpene linalool and the phenylpropene estragole, but low levels of the straight-chain esters propyl acetate, butyl acetate and ethyl butanoate as well as the branched-chain esters 2-methylpropyl acetate and 2-methylbutyl acetate are present. As this species is a member of Maleae (the tribe of Rosaceae that includes apples and pears), it was assumed that the peel is the site of aroma biogenesis. Thus, rimsulfuron was applied to the peels of aroma-active fruits and the effect upon aroma production and amino acid content was analyzed.

Rimsulfuron-treated fruits had less 2-methylpropyl acetate and 2-methylbutyl acetate, but more propyl acetate than untreated fruits. No difference was observed for butyl acetate, ethyl butanoate, estragole, or linalool (Table 3.9).

Valine and isoleucine were reduced in rimsulfuron-treated peel tissue (Table 3.10). No difference was seen of leucine, nor were any other amino acid concentrations decreased.

Discussion

The categorical suppression of every isoleucine, valine, and leucine-related volatile by fruits treated with an acetohydroxyacid synthase inhibitor emphatically demonstrates that these fruit tissues rely heavily, or perhaps solely, upon newly synthesized precursors for the production of these important sensory compounds.

Should the substrates for volatile biosynthesis be procured through non-anabolic processes, such as protein degradation as a function of senescence, then application of the acetohydroxyacid synthase inhibitors should have, at minimum, no effect upon volatile production. At best, their application should have boosted branched-chain volatile production through their noted effect of elevating protein turnover (Shaner & Reider, 1986) (Goldberg & St. John, 1976), as observed in several of the fruit cultivars tested that had increased total free amino acid contents.

However the volatiles in question were in fact reduced by the inhibitors, thus demonstrating that past observations of the marked increases of only branched-chain amino acids that have related volatiles being produced, such as isoleucine in apple, or valine and leucine in banana, are not a product of some coincidental catabolic phenomenon, but are due to a deliberate enhancement of these specific pathways (Sugimoto, Jones, & Beaudry, 2011) (Sugimoto, Forsline, & Beaudry, 2015) (Alsmairat, Engelgau, & Beaudry, 2018). The targeted production of specific branched-chain α-ketoacids is further illustrated by the explicit inhibitor-induced-

reduction of only the branched-chain amino acids in tissues that produce copious related volatiles. Furthermore, although valine levels were not found to be significantly less in treated apples, the reduction of the already trace quantities of 2-methylpropyl and 2-methylpropanoate esters suggest that even the synthesis these minor compounds of apple rely upon *de novo* substrates.

In apple, the supplementation of branched-chain α-ketoacids and the successful rescue of apple fruit aroma production not only demonstrates that the inhibitors were only influencing precursor supply and not negatively affecting downstream activities of ester biosynthesis, but it also highlights the importance of substrate availability. While apples do make a substantial amount of 2-methylbutyl and 2-methylbutanoate esters, they do not produce large amounts of 2-methylpropyl and 2-methylpropanoate or 3-methylbutyl and 3-methylbutanoate esters. However, when exogenously supplied with α-ketoisovalerate or α-ketoisocaproate, there is no general hindrance to incorporating these into their respective iso-branched-chain esters. This cross-compatibility of branched-chain α-ketoacids is mirrored by banana's ability to incorporate α-keto-β-methylvalerate into 2-methylbutyl esters (Wyllie & Fellman, 2000).

The experiments performed in this study were unable to determine why there is a difference of ability for apples to convert supplied α-ketoacids into alkyl or alkanoate ester elements. Perhaps the initial branched-chain α-ketoacid decarboxylase or dehydrogenase, the ultimate alcohol acyl transferases, or any of the enzymes in between, were exerting substrate preference and/or competition upon the processes downstream of the α-ketoacids. Selective esterase activity may also be possible. However, regardless of the cause, the use of inhibitors has clearly identified that such variation in the processing of the branched-chain α-ketoacids exists, and that future use of these inhibitors will undoubtedly aid in continuing research of the topic.

While several straight-chain esters were affected in the apple cultivars tested, the unanimous increase of pentyl acetate content as well as methyl pentanoate ^{13}C enrichment in fruit treated with inhibitor and, when applicable, ^{13}C-acetate, is of note. This consistent increase suggests that a significant proportion of precursors for pentyl and pentanoate ester elements in apple fruit are derived from the 1-C elongation pathway facilitated by citramalate synthase (Sugimoto, Engelgau, Jones, Song, & Beaudry, 2021).

There are several explanations for why similar results were not observed for the other short straight-chain esters and ester elements. If the precursors are substantially supplied from

other metabolic sources, such as β-oxidation of fatty acids to produce four and six-carbon substrates, then the application of inhibitor may not have disrupted overall α-ketoacid production sufficiently to have an observable effect. It may also be that shorter straight-chain α-ketoacids are too rapidly extended due to the increased flux imposed by the inhibitor to be processed into esters.

Our ability to generate fruit with highly similar aroma profiles, save for the loss of 2-methylbutyl and 2-methylbutanoate esters, provided an excellent opportunity to assess the importance of these branched-chain esters to the aroma profile of apples. It has been observed that different aromas are increasingly difficult to discriminate as they become more similar, with the prepared volatile mixtures of a study being indistinguishable when overlapping by more than 90% (Bushdid, Magnasco, Vosshall, & Keller, 2014). The capacity of subjects to discriminate a difference between treated and untreated 'Jonagold' fruit, an apple with a much more complex aroma profile than, for example, 'Gala', highlights the significance of the human ability to perceive the absence of branched-chain esters. Furthermore, the disequilibrium observed of apple cultivars towards those that do produce 2-methylbutyl and 2-methylbutanoate esters strongly suggests that humans have selectively bred for cultivars that produce these volatiles.

The increase of estragole in rimsulfuron-treated 'Jonagold' fruit may result from increased phenylalanine ammonia lyase activity, a phenomenon observed in soybean hypocotyls treated with sulfonylureas (Suttle & Schreiner, 1982).

Our inability to knock out estragole in 'Golden Delicious' fruit with glyphosate may be due to one or more factors. It could be that estragole production in apple fruit does not rely upon *de novo* precursor production, for neither of the phenylpropene-related aromatic amino acids have such a stark increase as isoleucine in ripening apple fruit peel (Sugimoto, Jones, & Beaudry, 2011). It is also possible that the degree of disruption required to observe a change of such a minor volatile was not achieved by our treatment methodology.

While applications of glyphosate under 1 mM lead to decreased chlorophyll accumulation in etiolated barley and corn shoots, a response attributed to disruption of the chloroplast envelope, among other subcellular alterations, it has also been observed that off-label use on field-grown soybeans, such as high rates or late season application, can delay senescence (Kitchen, Witt, & Rieck, 1981) (Campbell, Evans, & Reed, 1976) (Harbach, et al., 2016). This delay to senescence has been speculated to be due to a disruption of cross talk between auxin, an

eventual product of tryptophan and thus the shikimate pathway, and abscisic acid, a well-known modulator of senescence. Such phenomena may explain the preservation of chlorophyll *a* and greenness in glyphosate-treated apple peel.

In banana, the lack of suppression of 2-pentanol, 2-pentanone, and 1-methylbutyl esters by the sulfonylurea herbicide strongly suggests that these compounds are derived from a source that is not within the sphere of acetohydroxyacid synthase's influence. Furthermore, the ability of 'Horn Plantain' fruit to incorporate 2-pentanol, but not 2-pentanone, into 1-methylbutyl esters hints that the more stable ketone, detected in natural emanations from 'Cavendish', may be a dead-end byproduct of 1-methylbutanol oxidation. However, while we did not observe such an interconversion, it is possible that the short incubation period provided (~1-2 hours) was not sufficient. Lastly, it seems striking that banana fruit should produce two forms of branched-chain esters: iso- and sec-branched, but while iso-branched-chain esters are dependent upon acetohydroxyacid synthase activity, sec-branched esters are not.

Candidly, the depletion of butyl acetate and butyl butanoate in sulfonylurea-treated fruit was of great surprise. Besides some specialized instances of 1-C elongation that have been documented in apple and *Solanaceae* (Sugimoto, Engelgau, Jones, Song, & Beaudry, 2021), (Kroumova & Wagner, 2003), it has largely been assumed that butyl and butanoate esters are derived from β-oxidation of fatty acids; a catabolic process. As treatment of tissues with acetohydroxyacid synthase inhibitors does not lead to inhibition of fatty acid synthesis (Shaner & Singh, 1997), our results suggest that the source of these compounds in banana fruit is originally from branched-chain amino acid metabolism. Some of the first scientific work that attempted to establish a relationship between leucine and 3-methylbutyl esters found that bananas fed U-^{14}C-leucine produced a significantly enriched volatile fraction containing butyl butanoate and 1-methylbutyl butanoate (Tressl & Drawert, 1973).

It may be that banana fruit, brimming with a copious supply of α-ketoisocaproate, are able to process this surplus through the branched-chain recycling processes facilitated by the branched-chain α-ketoacid dehydrogenase complex to produce acetoacetate and acetyl-CoA (Peng, Uygun, Shiu, & Last, 2015). Either of these compounds, in theory, can be converted into acetoacetyl-CoA, which, through a series of steps, can be stripped of its ketone and become butanoyl-CoA. According to KEGG resources, a gene in banana has been putatively identified

for every theoretical step, save for the final reduction of crotonoyl-CoA into butanoyl-CoA (Figure 3.12).

Furthermore, the distinction of shared regulation between 1-methylbutyl esters, and 3-methylbutyl, 2-methylbutyl, butyl and butanoate esters, was also observed when the former were far less reduced compared to the latter after 1-methylcyclopropene treatment of bananas (Golding, Shearer, McGlasson, & Wyllie, 1999). Lastly, the derivation of butyl and butanoate esters from branched-chain α-ketoacid appears to be, among the fruits tested, unique to banana, as neither apple nor ornamental quince fruit demonstrated such a repression after inhibitor treatment.

The reduction of ethyl acetate by the sulfonylurea herbicide is also unclear, and it may even be that these precursors, which would be canonically considered primary metabolites, are also derived from a branched-chain source as another past study found that bananas fed U-^{14}C-leucine produced 3-methylbutyl acetate that was enriched in both the alkyl and alkanoate portions (Myers, Issenberg, & Wick, 1970).

The ability of 'Horn Plantain' to metabolize 2-pentanol into 1-methylbutyl acetate, and butanol into butyl acetate and 2-methylpropyl butanoate, further demonstrates the importance of precursor availability. Given that 'Horn Plantain' can synthesize both sets of iso-branched-chain esters and can utilize butanol, but do not produce high levels of butyl or butanoate esters, the fruit are evidently deficient at some phase of the interconversion of iso-branched-chain metabolism to four-carbon metabolism and that selectivity of an alcohol acyl transferase is not to blame.

In ornamental quince, the accumulation of propyl acetate by treated tissues on its own does not indicate whether or not the fruit produce α-ketobutyrate via the citramalate synthase pathway, however the lack of an enhancement of longer straight-chain esters (e.g., pentanoates), as seen by treated apple fruit, seems to indicate that these fruit do not perform the 1-C elongation steps beyond α-ketobutyrate.

Conclusion

In this work, a powerful new tool for the study of volatile biochemistry has been described. Through the application of herbicides, we have been able to demonstrate the importance of *de novo* synthesis of branched-chain α-ketoacids in the production of aroma compounds, identify a possibly novel pathway for the biosynthesis of butyl compounds in fruit,

highlight the importance of branched-chain compounds in complex aroma profiles, and gained insight into the nuances of α-ketoacid metabolism for ester biosynthesis. No doubt the use of herbicides on other fruits, whether those used herein or others that target different metabolic networks, will continue to shed light on the importance of substrate availability and aroma biochemistry in general.

However, already a significant point can be made: iso- and anteiso-branched-chain volatiles of apple and banana fruits are, to a significant degree, derived from newly synthesized α-ketoacids. If the biochemical steps between branched-chain α-ketoacid and ester begin with the action of a decarboxylase or the dehydrogenase complex as generally speculated, then the interconversion of branched-chain α-ketoacids to branched-chain amino acids, assuming the amino acid form is not needed for intracellular transport, is wholly unnecessary to the production of branched-chain volatiles. Thus, if the above conditions are true, the accumulated branched-chain amino acids in ripening fruit are a byproduct of, *and not precursors or intermediates to,* branched-chain volatile biosynthesis. Future studies will undoubtedly continue, as done here, to measure the amino acids rather than α-ketoacids due to the ease of preparation, routineness of the analyses, and the greater concentration of the former when in equilibria as compared to α-ketoacids. However, it is incumbent of aroma biochemists to be exact in their descriptions of branched-chain volatiles as being *related* to branched-chain amino acids, as opposed to being *derived* from them.

Finally, although this work has brought many exciting avenues of aroma biochemistry to light, there is one of significant note. Given that apples and banana fruits produce the α-ketoacids for aroma biosynthesis *de novo*, the canonical feedback mechanisms of branched-chain α-ketoacid synthesis present a paradox to how these fruits can accumulate precursors despite such strict regulation. While citramalate synthase explains how apple fruit circumvent regulation, it is still unknown what changes of metabolism must be occurring in banana fruits…

Materials and methods

Plant material

'Gala', 'Empire', 'Jonagold' and 'Golden Delicious' apple (*Malus ×domestica* Borkh.) fruit were harvested from local orchards at commercial maturity and transported to the laboratory during the 2022 season. Developmentally, the fruit were at the onset of ripening but no aroma volatiles could be discerned subjectively. 'Gala' and 'Empire' fruits began treatment

immediately after arrival. ‘Jonagold’ and ‘Golden Delicious’ fruit were held in air at 0 ℃ for two days before transfer to 1.5 O_2, 3% CO_2, 0 ℃. ‘Jonagold’ fruit were held in these conditions for twelve days before the initiation of treatment whereas ‘Golden Delicious’ fruit were held 2-3 weeks.

Banana (*Musa* spp. AAA group, Cavendish subgroup, cv. Valery; *Musa* spp. AAB group, Plantain subgroup, cv. Horn Plantain) fruit that had not been treated with ethylene were obtained from a local supermarket produce distribution and ripening center (Meijer/Chiquita, Lansing, MI). ‘Cavendish’ fruit were held at 13.5 ℃ until treatment. Plantains were held at room temperature (22 ℃) for 2-3 days before treatment.

‘Dr Banks Pink’ flowering quince (*Chaenomeles* ×*superba*) fruit were collected from accession CC7985*05 on the Michigan State University campus grounds. Fruits were actively producing aroma.

Treatment

Treatment with acetohydroxyacid synthase inhibitors were planned such that a mild, but regular application would be made starting prior to aroma production and thus before the start of accumulation of the branched-chain amino acids (Alsmairat, Engelgau, & Beaudry, 2018) (Sugimoto, Jones, & Beaudry, 2011). Trial and error proved this to be the most reliable method to suppress the pathway and have observable results.

Whole apple fruit were stored at room temperature (22 ℃) and rubbed daily with 3 mL of freshly made herbicide or water solution (1 mM rimsulfuron, made from Matrix®, 0.1% Tween 20) before preparation with further treatments. Quince fruit had 2 mL applied daily.

‘Gala’, ‘Empire’, and ‘Jonagold’ apple fruit were treated for four, nine, or seven days before further preparation, respectively. Quince were treated for six days before analysis. Whole fruit routinely had their headspace volatiles sampled for aroma production and treatment efficacy to determine appropriate times for further treatments.

Acetate and α-ketoacid feedings were performed by preparing vials of peel tissue as previously described by (Sugimoto, Engelgau, Jones, Song, & Beaudry, 2021). In detail, 11 mm disks of peel from treated fruits were cut away from the fruit and trimmed to have 1-2 mm of cortex tissue using a cork borer and scalpel. Five peel disks were laid upon five filter paper disks of equal diameter resting upon a glass microscope slide trimmed to fit within a 22 mL glass vial. Each disk of filter paper was wetted with 20 µL of treatment solution, described below, before

delicately placing a fruit tissue disk, peel side-up, upon the paper. More treatment solution, 20 µL, was then added on top of each peel disk before sliding the apparatus into the glass vial and sealing with a Mininert valve (Thermo Scientific). Samples were incubated overnight (22 ℃) before sampling.

'Gala' fruit were fed with 10 mM methanol, 10 mM acetate (unlabeled or 1,2-$^{13}C_2$) pH 7 balanced with KOH, 0.05% Tween 20, and 0.5 mM rimsulfuron if appropriate. These concentrations were doubled for 'Empire' and 'Jonagold' fruit and contained, when appropriate, 20 mM of α-keto-β-methylvalerate, α-ketoisovalerate, or α-ketoisocaproate.

'Golden Delicious' fruit were treated with 1 mM glyphosate, made from Roundup PowerMAX®, 0.1% Tween 20, for four days before being treated with 10 mM glyphosate, 0.1% Tween 20 for one day, followed by six days of treatment with 50 mM glyphosate, 0.1% Tween 20. Chlorophyll content was measured with a ΔA meter (Sintéleia, Forli, Italy, (Ziosi, et al., 2008)). Color measurements were performed with an AMT599 Colorimeter (Amtast, Lakeland, FL). The colorimeter and ΔA meters were calibrated according to manufacturer directions before use. Areas of blush on the fruit were avoided for chlorophyll and color analysis.

As inspired by past studies (Palmer & McGlasson, 1969), 'Cavendish' fruit were cut into ~1 cm^2 squares from fruit not treated with ethylene. Care was taken such that one edge of the square was from the edge of the pulp, thus representing an undisturbed or 'live edge' of cells that should be able to maintain unhindered gas exchange. Five of these were placed on filter paper disks on a trimmed microscope slide and placed into 22 mL vials as above described for apples. Each pulp section and piece of paper also received 20 µL of treatment solution with or without herbicide (0.5 mM halosulfuron, made from Sandea®, 0.1% Tween 20). The vials were sealed with Mininert valves. Fruit ripening was then induced by injecting 1 µL ethylene into the vials. The following day the vials were vented for 15 min before having the Mininert replaced on the vial but with a needle inserted to allow for gas diffusion. The following two days 20 µL of freshly made herbicide or water solution was added onto the pulp. The needles were kept in the valves to maintain gas diffusion. The next day, and thus four days since initially preparing the vials, the needles were removed and the vials were sealed and incubated for at least 1 hour at room temperature (22 ℃) before headspace sampling.

Plantains were prepared in a similar way but did not receive herbicide. Before analysis (~2-3 hours), 10 µL of water, 1 mM butanol, 1 mM 2-pentanone, or 1 mM 2-pentanol were added to the pulp sections.

Volatile analysis

Headspace volatiles from vials were sorbed for 30 s using a solid-phase micro extraction (SPME) fiber (65 µm PDMS-DVB; Supelco Analytical, Bellefonte, PA). The SPME fiber was then directly desorbed for 1 min in the injection port of a gas chromatograph (GC; HP-6890, Hewlett-Packard, Wilmington, DE) coupled to a time of flight mass spectrometer (MS; Pegasus II, LECO, St. Joseph, MI). Desorbed volatiles were cryofocused at the beginning of the column by immersing said region of the column in liquid nitrogen. After the desorption period, the run was initiated and the liquid nitrogen removed.

Quince and 'Golden Delicious' fruits selected for volatile analysis were incubated for 20 min at room temperature (22 °C) in 2 L sealed Teflon jars before a 3 min sorption and 2 min desorption protocol as described.

The conditions of the system were as follows. Injection port: 200 °C, splitless, helium carrier gas, front inlet flow was 1.5 mL/min constant, 10 mL/min purge flow, 11.5 mL/min total flow. Oven: initial temperature at 40 °C for 0 min, ramped by 43 °C/min to 185 °C for 0 min. Column: HP-5MS, 30 m × 0.25 mm i.d., 0.25 µm film thickness (Agilent, Santa Clara, CA). Transfer line temperature was 225 °C. MS: Electron ionization (-70 eV), ion source temperature was 200 °C, solvent delay was 50 sec, m/z 29 to 400 were scanned for, detector voltage was 1500 V, data collection rate was 20 Hz.

When α-ketoisocaproate was supplied to the fruit and separation of 2-methylbutyl acetate and 3-methylbutyl acetate was of interest, the following oven parameters were used: initial 40 °C for 0 min, 10 °C/min until 100 °C, 20 °C/min until 130 °C, 60 °C/min until 185 °C.

Compounds were identified by comparison with the retention time and mass spectrum against authenticated reference standards and spectra (National Institute of Standards and Technology Mass Spectral Search Program Version 2.0, 2001). Volatiles were quantified by calibration with a standard of 59 authenticated compounds (Sigma-Aldrich Co., St. Louis, MO and Fluka Chemika, Seelza, Germany). The standard was made by placing 0.5 µL of an equal-part mixture of the neat compounds onto a disc of filter paper before quickly placing the filter

paper into a 4 L sealed flask fitted with a Mininert valve (Valco Instruments Co. Inc., Houston, TX) for SPME fiber access. The quantification m/z of each compound can be seen in Table 3.11.

After volatile analysis, apple peel disks, collected peel of quince, and 'Cavendish' pulp samples were held at -80 ℃ for further amino acid analysis.

Sensory analysis

'Jonagold' fruit, previously stored in CA, as described above, were treated for seventeen consecutive days with herbicide or water solution (1 mM rimsulfuron, made from Matrix®, 0.1% Tween 20) as described above. Fruits were screened via GCMS, described above, to ensure successful treatment and suppression of 2-methylbutyl and 2-methylbutanoate esters. Treatment was stopped two days in advance of our initial target date for the sensory analysis. However, the experiment was delayed due to the February 13, 2023, mass shooting at Michigan State University. The fruit, having been treated and screened, were held in air at 1 ℃ under plastic bags seven days as the campus community recovered from the tragedy. The day before the new sensory study date, the fruit were removed from storage and allowed to warm to room temperature (22 ℃). The morning of the experiment, 1 x 5 cm segments weighing 2.5 – 3 g, were prepared from the apples. Cortex tissue was trimmed to maximize the proportion of peel tissue. Segments of fruit were prepared instead of discs to limit the surface area of cut tissues, minimizing oxidative volatiles. Fruit segments were then placed in 40 mL amber vials and sealed with PTFE-lined caps. Samples were allowed to incubate at least 2 hours before sensing.

Participant demographics were as follows: N = 20; age: (range = 18 – 41, average = 24.4); gender: (14 female, 6 male); sex assigned at birth: (14 female, 6 male); race:(1 African American or Black, 7 Asian (3 Asian Indian, 3 Chinese, 1 Vietnamese), 12 Caucasian or White); ethnicity: (17 Not of Hispanic, Latino/a or Spanish origin, 1 Mexican American, 1 unknown, 1 Spanish).

Participants performed twelve Duo Trio trials, each with a randomized treated and untreated sample, as well as an untreated sample as the reference. Participants were prompted: "In front of you is a set of three samples. Smell the reference sample labeled REF and then smell the two test samples. Select the sample code that smells the same as the REFERENCE sample. You must make a choice, even if it is only a guess. You may re-smell as often as you wish." Statistics were performed with Microsoft Excel v16.69.1. p-value = 1-BINOM.DIST(correct responses-1,total trials, 0.5, TRUE).

Amino acid analysis

Frozen samples were ground to a powder in liquid-nitrogen-chilled mortar and pestles. About 0.5 mg of tissue were vortexed for 10 sec in 2 mL of room temperature (22 ℃) 1:1:1 (water:acetonitrile:ethanol, v/v) spiked with 2 nmoles of U-^{13}C,^{15}N labeled amino acids (MilliporeSigma) before being heated for 15 min in a 65 ℃ water bath. Extracts were then briefly chilled on ice before being centrifuged at 4400 × g for 15 min at 4 ℃. The supernatant was filtered by centrifugation (0.2 µm nylon centrifugal filter; Costar, Corning) at 21000 × g for 5 min at room temperature. 10 µL of the filtrate was transferred to an autosampler vial and diluted 100-fold with 990 µL of 10.1 mM perfluorohexanoic acid (PFHA) spiked with 2 µmoles of internal standard. Thus the final concentration of internal standard was ~2 µM.

An amino acid standard series was prepared from a premade mixture (Millipore Sigma, AAS18) that contained equal molar amounts of cystine and all 20 proteinogenic amino acids save for tryptophan, asparagine, glutamine, and cysteine. An equal molar mixture of tryptophan, asparagine, glutamine, and cysteine was subsequently prepared. To avoid dilution errors or artefacts from differing buffers, these amino acid stocks were aliquoted and desiccated such that a five-part standard series ranging from 250 µM to 25 nM would be produced upon resuscitation with 10 µL of spiked extraction buffer and 990 µL spiked PFHA solution. Samples and amino acids were held overnight at -20 ℃ before analysis.

Amino acids were analyzed with a Xevo TQ-S Micro UPLC (H-Class)-MS/MS (Waters, Milford, MA) at the Michigan State University Mass Spectrometry and Metabolomics Core. Conditions were as follows. HPLC column: Acquirt UPLC HSS T3, 2.1 x 100 mm, 1.7 µm particle size (Waters), with a 0.2 µm pre-column filter (Waters). Mobile phase: A) 10 mM PFHA in water, B) acetonitrile. LC gradient: linear gradient, slope setting = 6, flow rate = 0.3 mL· min^{-1}, step 1) 0 min, 100% A, 0% B, 2) 1 min, 100% A, 0% B, 3) 8 min, 35% A, 65% B, 4) 8.01 min, 10% A, 90% B, 5) 9 min, 10% A, 90% B, 6) 9.01 min, 100% A, 0% B, 7) 13 min, 100% A, 0% B. Column temp: 40 ℃. Autosampler temp: 10 ℃. Injection volume: 10 µL. Tune parameters: electrospray ionization, standard ESI probe, capillary voltage = +1.0 kV , source temp = 120 ℃, desolvation temp = 350 ℃, desolvation gas = 800 L· hr^{-1}, cone gas = 40 L· hr^{-1}. MS collection was split into three phases and were adjusted after checking the retention time of several samples, however proline was missed for apple and quince samples. Parent and daughter ions,

cone and collision voltages, phases collected and approximate retention times can be seen in Table 3.12.

Data were quantified by first calculating a linear regression of log(unlabeled amino acid response/labeled amino acid response) transformed standard responses. R^2 values were all greater than 0.98 and the slope (m) and y-intercept (b) were used to calculate unknowns: µM of unknown sample = 10^[(log(unknown unlabeled response/unknown labeled response)-b/m].

Figures & Tables

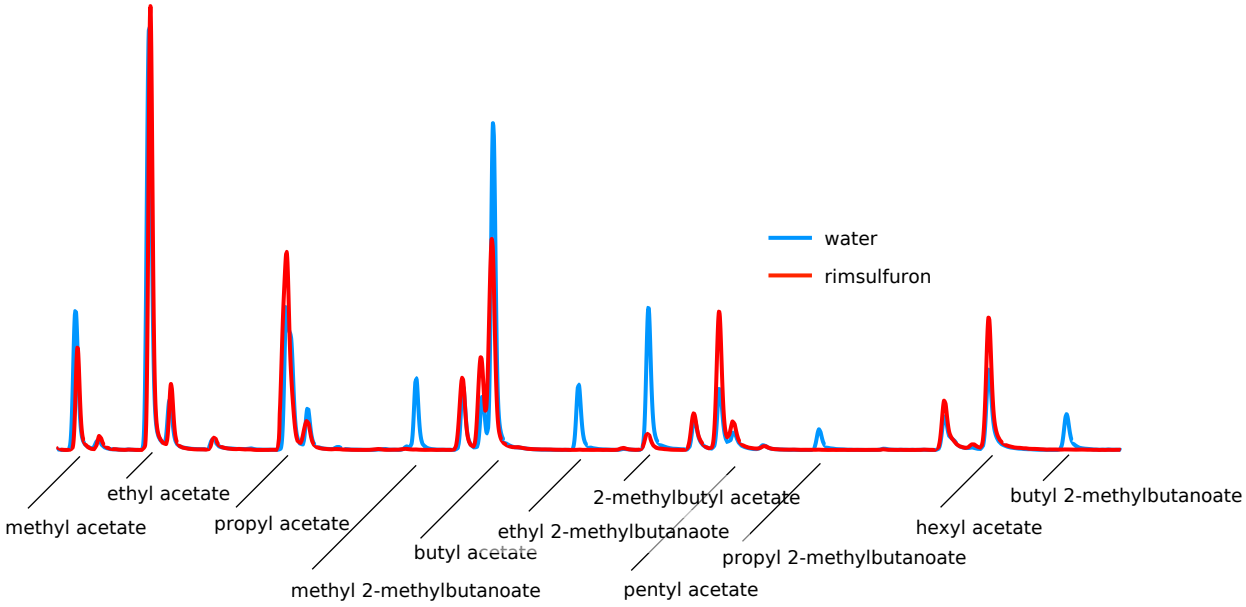

Figure 3.1. Representative chromatograms of the headspaces of 'Jonagold' apple fruit peels treated with water or rimsulfuron and fed methanol.

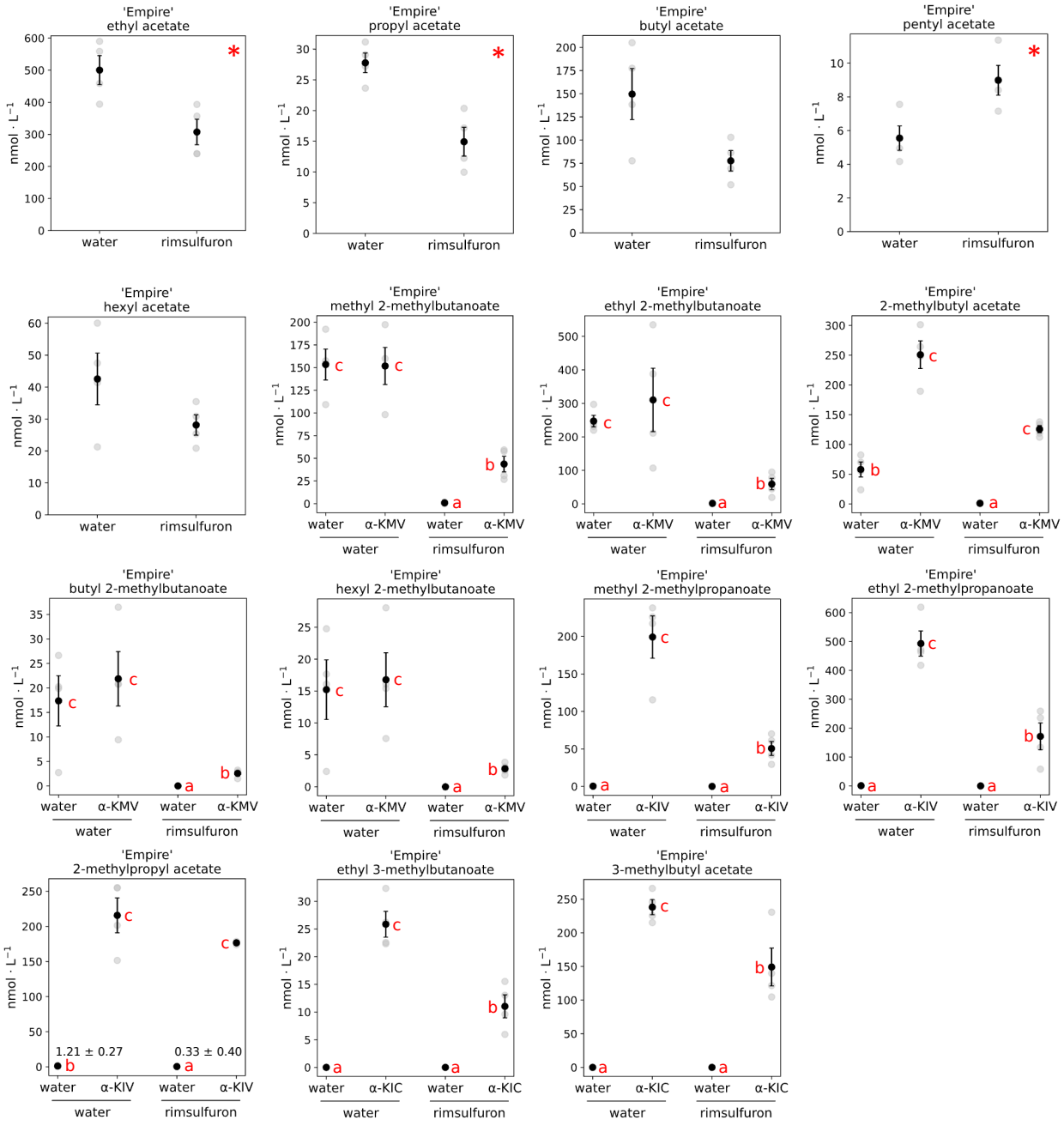

Figure 3.2. Volatile headspace concentrations of 'Empire' apple fruit peels treated with water or herbicide and fed branched-chain α-ketoacids. Presented as means ± ½ SD of four biological reps. α-KMV = α-keto-β-methylvalerate; α-KIV = α-ketoisovalerate; α-KIC = α-ketoisocaproate. Significantly different straight-chain ester concentrations are denoted by * (two-tailed two-sample equal variance t-test, α=0.05). Significantly different branched-chain ester concentrations are denoted by different letters adjacent to means (data transformed for statistical analysis via log(x+1) due to unequal variance of α-ketoacids fed samples; Tukey's test, α=0.05). The concentrations of 2-methylpropyl acetate tissues not treated with α-KIV are shown in figure.

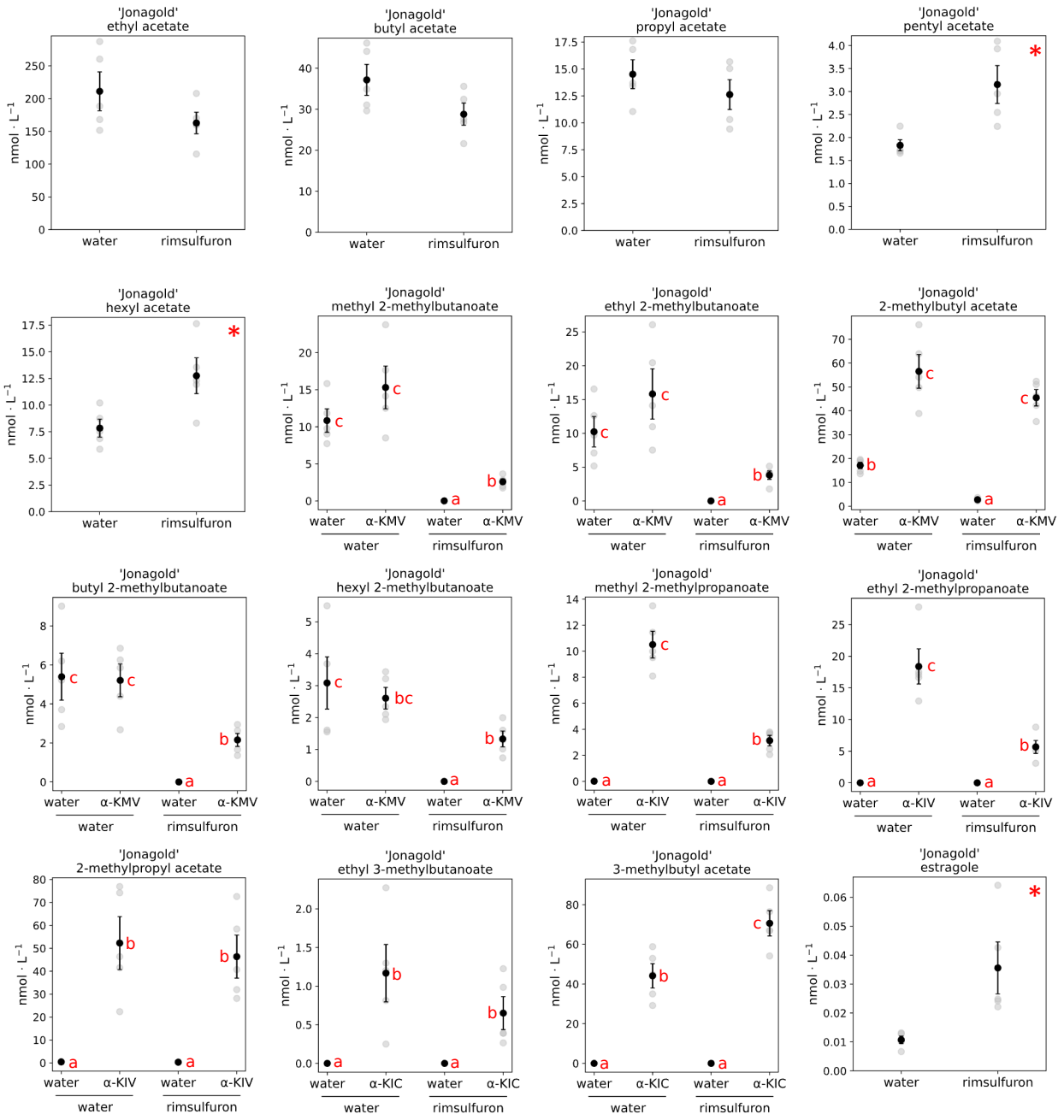

Figure 3.3. Volatile headspace concentrations of ‘Jonagold’ apple fruit peels treated with water or herbicide and fed branched-chain α-ketoacids. Presented as means ± ½ SD of four biological reps. α-KMV = α-keto-β-methylvalerate; α-KIV = α-ketoisovalerate; α-KIC = α-ketoisocaproate. Significantly different straight-chain ester concentrations are denoted by * (two-tailed two-sample equal variance t-test, α=0.05). Significantly different branched-chain ester concentrations are denoted by different letters adjacent to means (data transformed for statistical analysis via log(x+1) due to unequal variance of α-ketoacids fed samples; Tukey’s test, α=0.05).

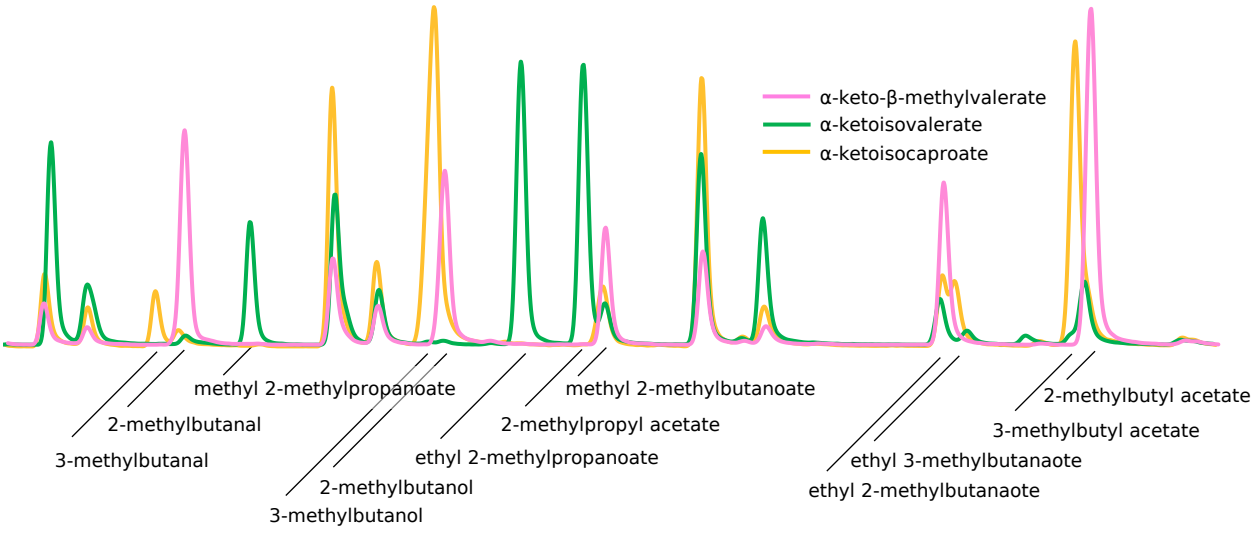

Figure 3.4. Representative chromatograms of the headspaces of ‘Empire’ apple fruit peels fed branched-chain α-ketoacids and methanol.

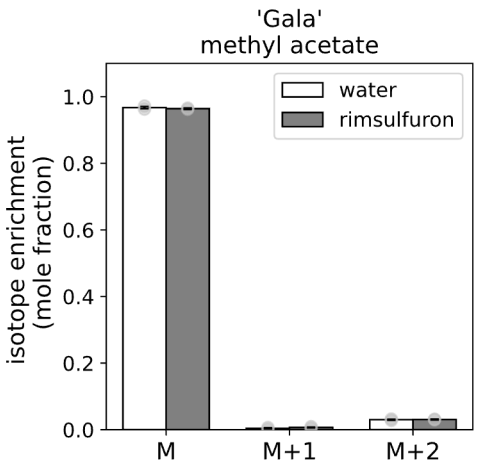

Figure 3.5. Mass isotopolog distribution of methyl acetate from 'Gala' apple fruit peels treated with water or herbicide and fed 1,2-$^{13}C_2$ acetate and methanol. Presented as means ± ½ SD of two biological reps. Significantly different distributions are denoted by * (two-tailed two-sample equal variance t-test, α=0.05).

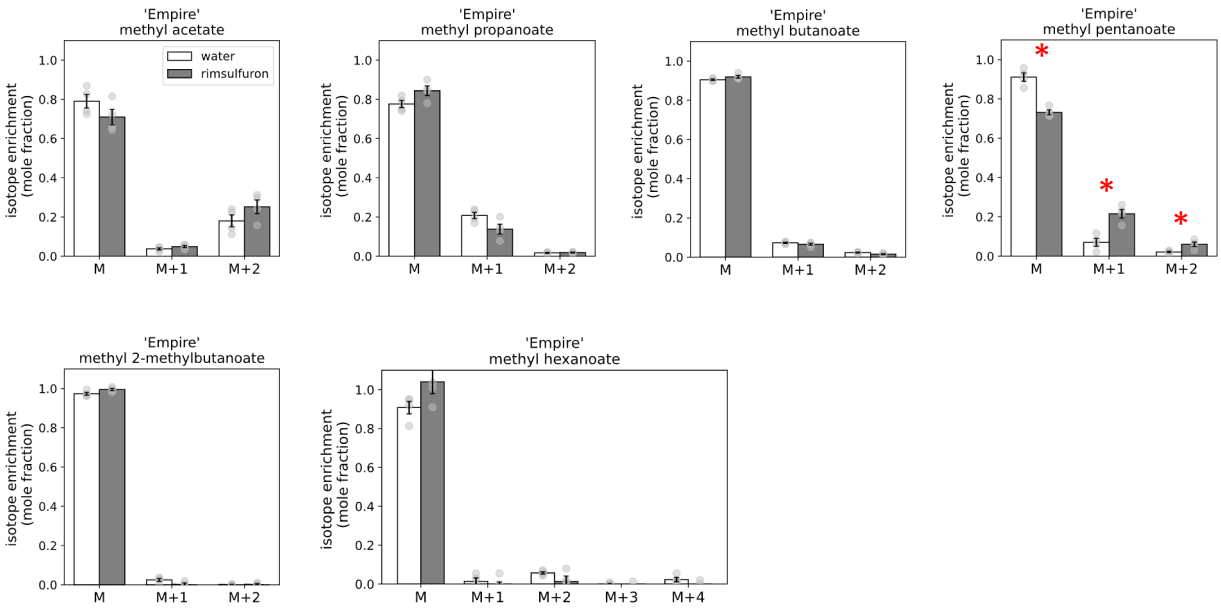

Figure 3.6. Mass isotopolog distribution of methyl esters from 'Empire' apple fruit peels treated with water or herbicide and fed 1,2-$^{13}C_2$ acetate and methanol. Presented as means ± ½ SD of four biological reps. Significantly different distributions are denoted by * (two-tailed two-sample equal variance t-test, α=0.05).

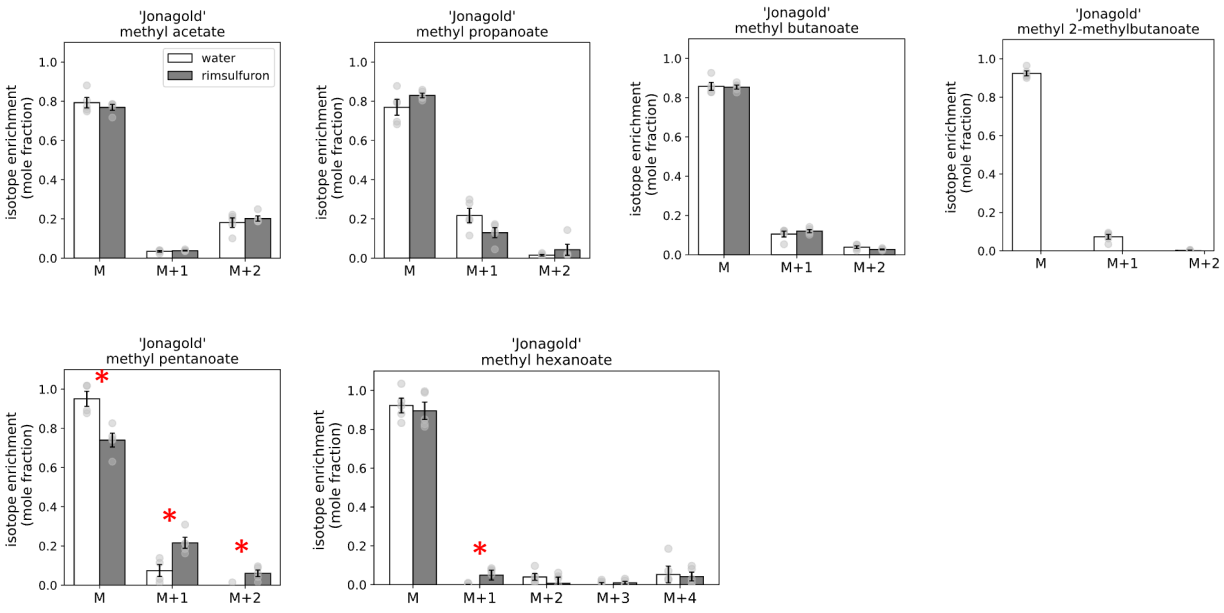

Figure 3.7. Mass isotopolog distribution of methyl esters from 'Jonagold' apple fruit peels treated with water or herbicide and fed 1,2-$^{13}C_2$ acetate and methanol. Presented as means ± ½ sD of five biological reps. Significantly different distributions are denoted by * (two-tailed two-sample equal variance t-test, α=0.05).

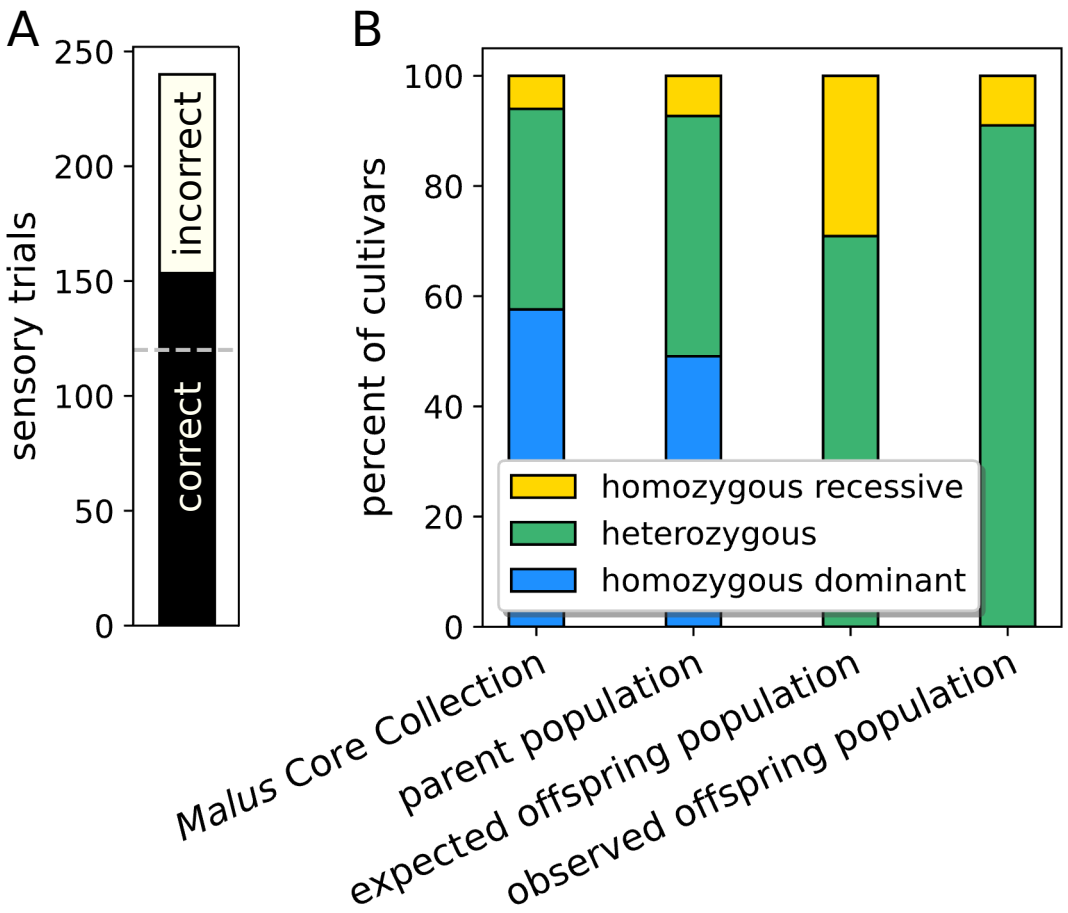

Figure 3.8. Results of sensory trials and population genetics analyses. A: Complied results from duo-trio sensory tests between rimsulfuron and water treated 'Jonagold' fruit. Dashed line shows expected number of correct trials if determined by chance (n = 240, 64% correct, $p = 6.7 \times 10^{-6}$). B: Distribution of citramalate synthase genotypes. *Malus* Core Collection is distribution of 99 cultivars as assessed by Sugimoto et al., 2021. Parent population is derived from USDA Geneva *Malus* Core Collection to mimic population definitions of Migicovsky et al., 2022 (n = 55). Offspring populations are derived from 'Cox's Orange Pippin' (homozygous recessive) and parent population (n = 32). Excepted vs observed (χ^2, p = 0.0141).

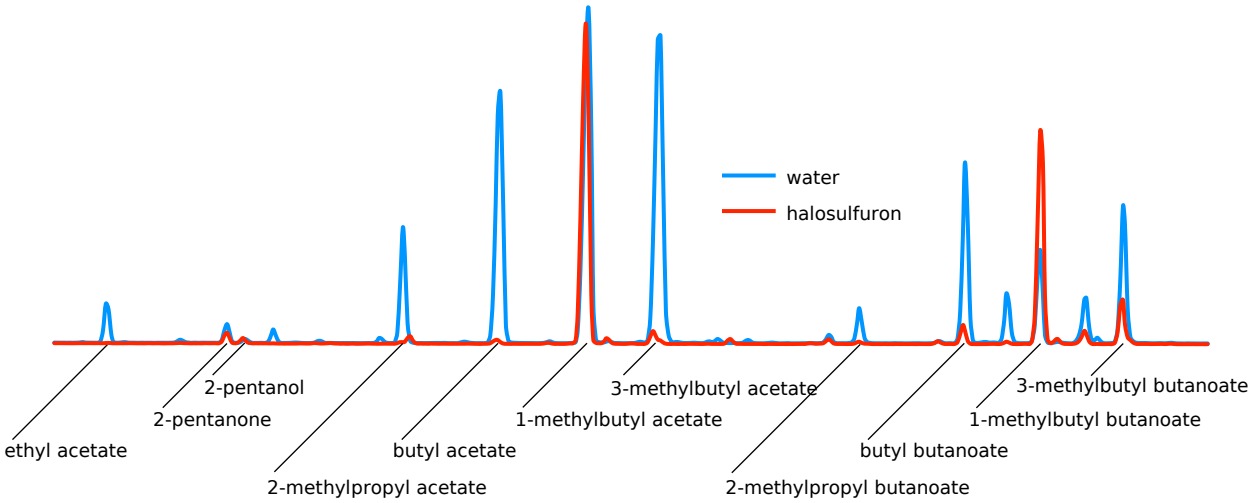

Figure 3.9. Representative chromatograms of the headspaces of ‘Cavendish’ banana fruit pulp sections treated with water or halosulfuron.

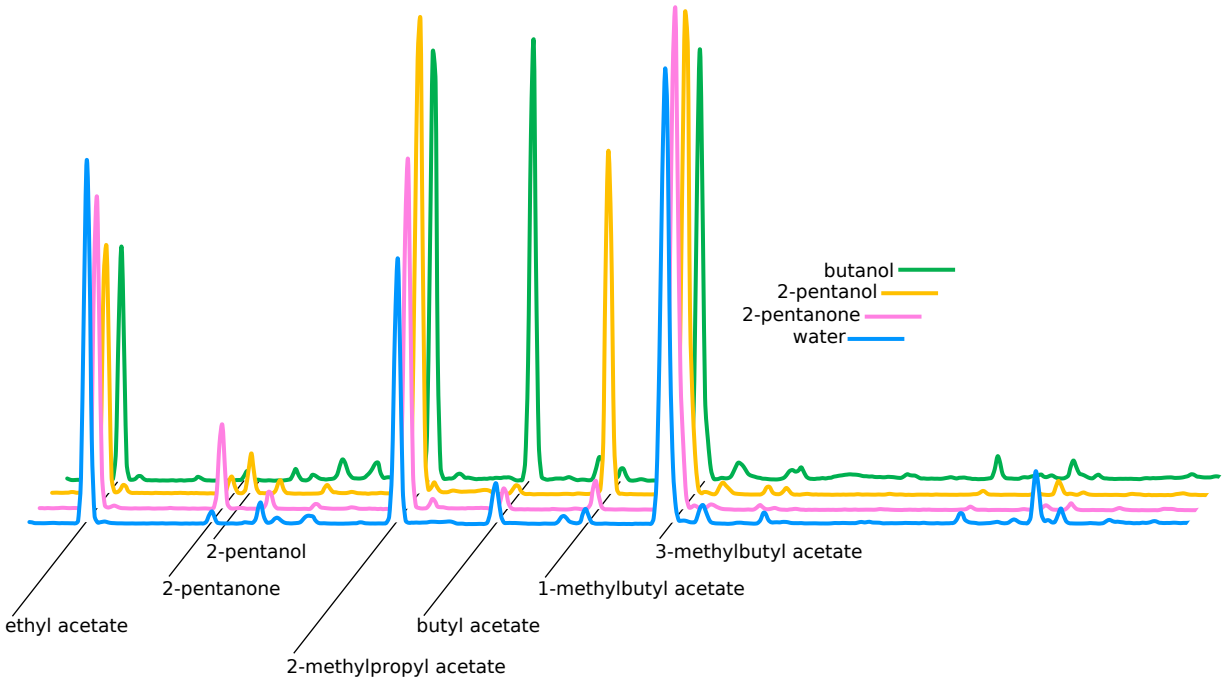

Figure 3.10. Representative chromatograms of the headspaces of ‘Horn Plantain’ banana fruit pulp sections fed with potential ester precursors or water.

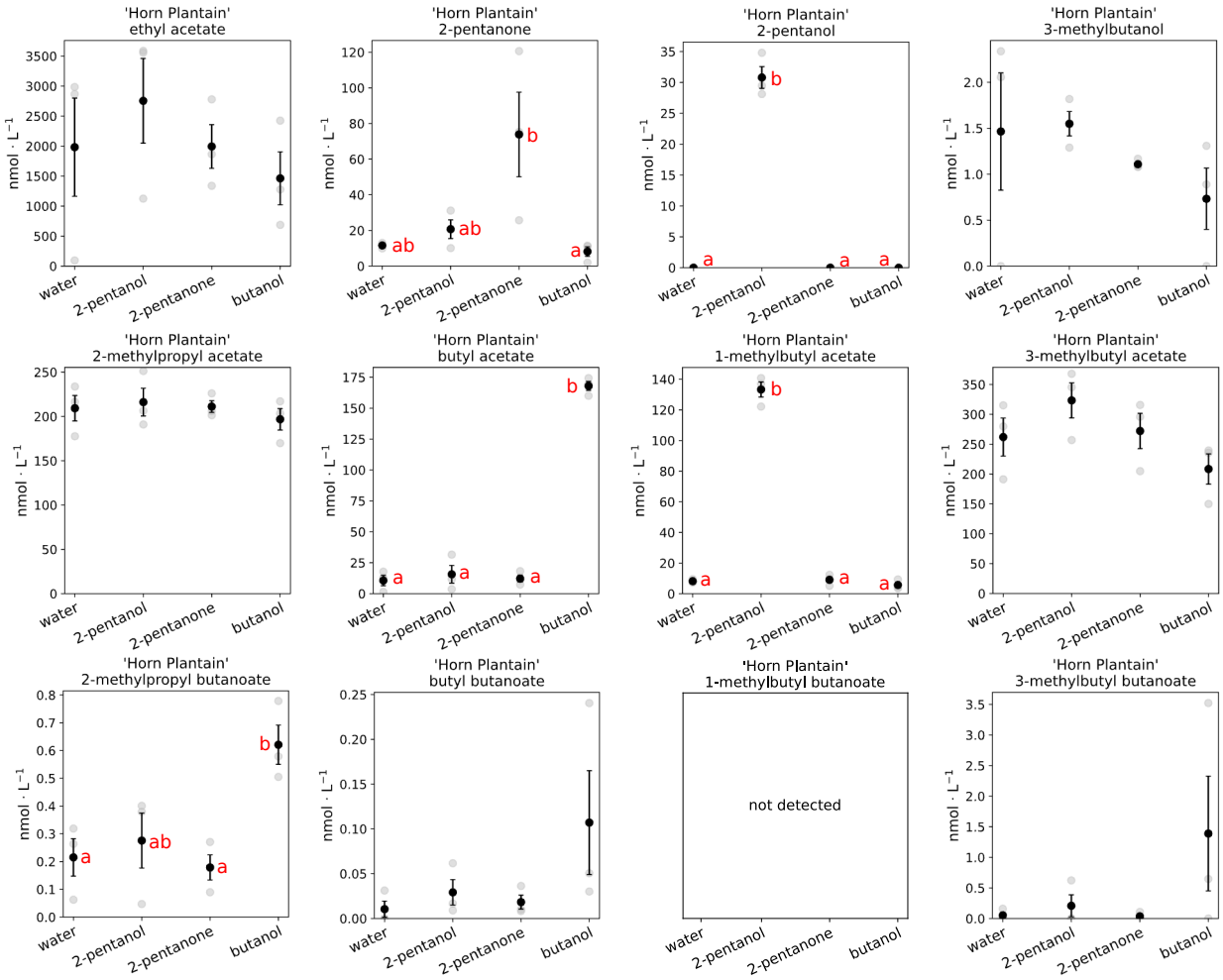

Figure 3.11. Volatile headspace concentrations of 'Horn Plantain' banana fruit pulp sections treated with potential aroma precursors. Presented as means ± ½ SD of three biological reps. Significantly different volatile concentrations are denoted by different letters adjacent to means (Tukey's test, α=0.05).

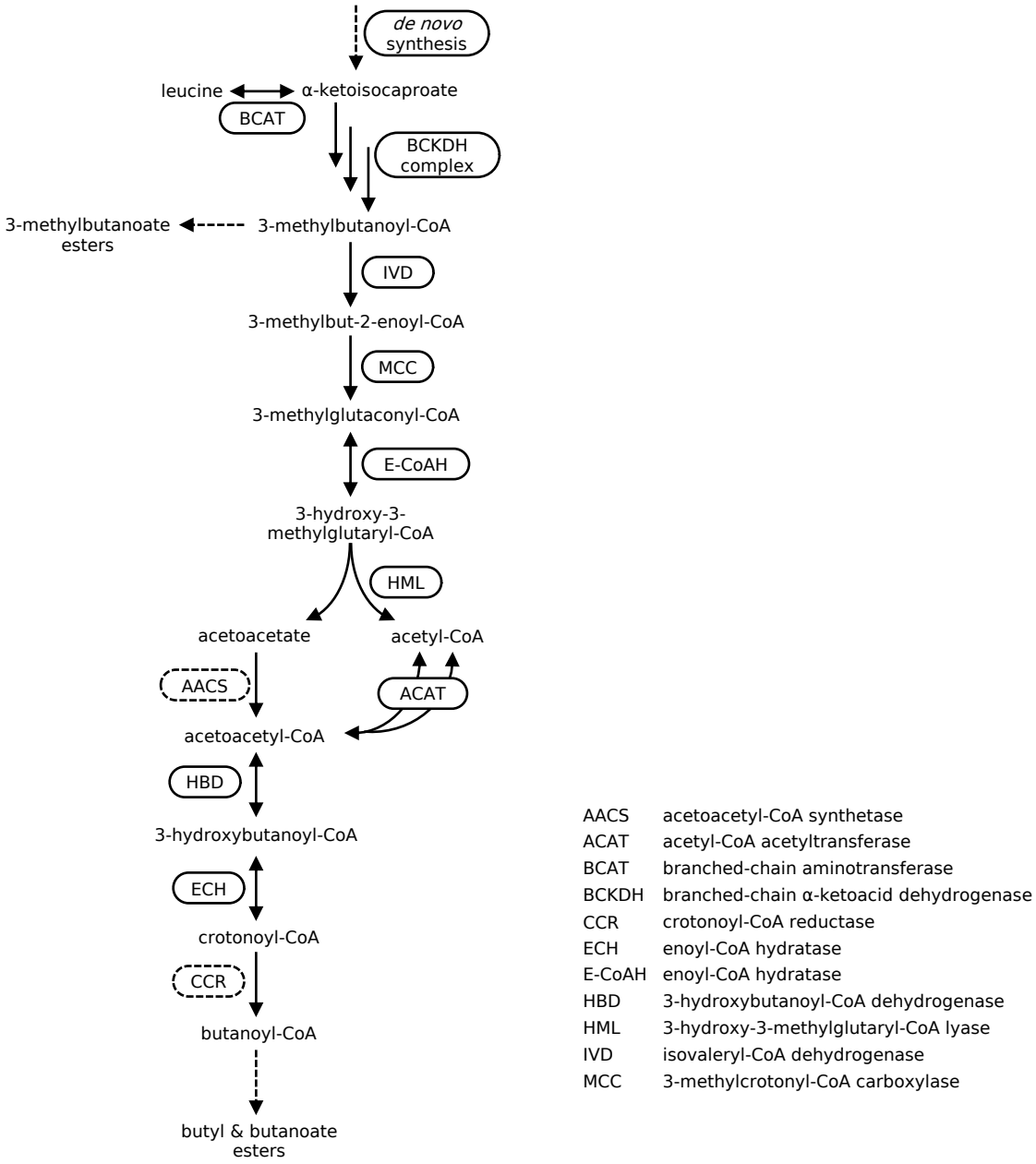

Figure 3.12. Proposed pathway for synthesis of butyl and butanoate compounds in banana fruit starting from α-ketoisocaproate. Abbreviated pathways shown with dashed arrows. Reactions understood to be freely reversible are depicted with double-sided arrows. Enzymes with putative candidates in banana are shown in curved boxes. Those without a candidate are in dashed boxes.

volatile	nmol · L^{-1} water	nmol · L^{-1} rimsulfuron	p-value	fold-change
ethyl acetate	320.76 ± 53.52	184.97 ± 33.28	0.043	▼ 1.7
propyl acetate	38.12 ± 8.36	25.53 ± 4.73	0.181	–
butyl acetate	262.62 ± 30.73	204.27 ± 35.78	0.204	–
pentyl acetate	6.57 ± 0.80	10.20 ± 1.28	0.028	▲ 1.6
hexyl acetate	82.36 ± 11.31	98.18 ± 20.27	0.468	–
2-methylpropyl acetate	1.13 ± 0.09	0.41 ± 0.06	0.000	▼ 2.7
2-methylbutanol	7.09 ± 0.53	2.41 ± 0.57	0.000	▼ 2.9
2-methylbutyl acetate	71.84 ± 5.39	19.39 ± 5.06	0.000	▼ 3.7
ethyl 2-methylbutanoate	5.03 ± 1.29	0.12 ± 0.09	0.003	▼ 42.0
butyl 2-methylbutanoate	16.40 ± 2.74	0.58 ± 0.31	0.000	▼ 28.0
hexyl 2-methylbutanaote	18.87 ± 3.20	0.99 ± 0.61	0.000	▼ 19.0

Table 3.1. Headspace volatile concentrations of water or rimsulfuron-treated ripe 'Gala' apple fruit peel. Presented as means ± ½ sD of three biological reps. Fold-change of means of rimsulfuron-treated tissue presented if significant (t-test; two-tailed; two-sample equal variance; $\alpha = 0.05$). Tissues were also fed acetate and methanol, see methods for further detail.

volatile	α-ketoisovalerate	α-ketoisocaproate
2-methylpropanal	'Empire'	
2-methylpropanol	both	
2-methylpropyl acetate[a]	both	
2-methylpropyl propanoate	both	
2-methylpropyl butanoate	both	
2-methylpropyl hexanoate	both	
2-methylpropyl 2-methylpropanoate	both	
2-methylpropyl 2-methylbutanoate	both	
2-methylpropyl 3-methylbutanoate		'Jonagold'
methyl 2-methylpropanoate[a]	both	
ethyl 2-methylpropanoate[a]	both	
propyl 2-methylpropanaote	both	
butyl 2-methylpropanoate	both	
pentyl 2-methylpropanoate	both	
hexyl 2-methylpropanoate	'Empire'	
3-methylbutanal	both	both
3-methylbutanol	both	both
3-methylbutyl formate		'Jonagold'
3-methylbutyl acetate[a]	both	both
3-methylbutyl propanoate	both	both
3-methylbutyl butanoate	'Jonagold'	both
3-methylbutyl pentanoate	'Empire'	'Jonagold'
3-methylbutyl hexanoate		both
3-methylbutyl 2-methylpropanoate	both	both
3-methylbutyl 2-methylbutanoate		both
methyl 3-methylbutanoate		both
ethyl 3-methylbutanoate[a]		both
propyl 3-methylbutanoate		both
butyl 3-methylbutanoate		both

Table 3.2. Iso-branched-chain volatiles identified in the headspace of 'Empire' and/or 'Jonagold' ripe fruit peel fed with supplementary iso-branched-chain α-ketoacids. Fruit were also supplied with methanol. [a] quantified.

amino acid	nmol · g^{-1} FW water	nmol · g^{-1} FW rimsulfuron	p-value	fold-change
alanine	33.8 ± 3.9	92.3 ± 10.3	0.001	▲ 2.7
arginine	24.6 ± 0.5	22.8 ± 1.4	0.268	–
asparagine	11.4 ± 5.1	109.3 ± 81.4	0.275	–
aspartate	195.8 ± 31.6	453.8 ± 39.4	0.001	▲ 2.3
cysteine	0.6 ± 0.2	1.0 ± 0.2	0.140	–
glutamate	147.7 ± 20.9	216.1 ± 9.2	0.013	▲ 1.5
glutamine	5.6 ± 1.0	14.0 ± 2.1	0.008	▲ 2.5
glycine	9.2 ± 4.2	19.1 ± 11.2	0.434	–
histidine	7.3 ± 0.6	7.5 ± 1.1	0.921	–
isoleucine	68.3 ± 4.6	11.2 ± 4.8	0.025	▼ 6.1
leucine	2.8 ± 0.3	6.1 ± 1.3	0.171	–
lysine	40.0 ± 3.2	37.6 ± 1.4	0.478	–
methionine	2.5 ± 1.0	9.2 ± 2.9	0.064	–
phenylalanine	7.0 ± 0.2	6.4 ± 0.5	0.342	–
proline	n.d.	n.d.	n.d.	n.d.
serine	65.6 ± 5.6	196.9 ± 20.3	0.000	▲ 3.0
threonine	16.3 ± 2.6	29.7 ± 2.6	0.006	▲ 1.8
tryptophan	0.6 ± 0.1	0.5 ± 0.2	0.605	–
tyrosine	3.4 ± 0.2	3.2 ± 0.8	0.792	–
valine	6.0 ± 1.6	4.7 ± 1.3	0.265	–
total	648.3 ± 70.4	1241.5 ± 147.8	0.008	▲ 1.9

Table 3.3. Amino acid content of water or rimsulfuron-treated ripe 'Gala' apple fruit peel. Presented as means ± ½ sD of four biological reps. Fold-change of means of rimsulfuron-treated tissue presented if significant (two-sample equal variance t-test; one-tailed test for valine, leucine and isoleucine; two-tailed test for all others; $\alpha = 0.05$). Proline was not determined.

amino acid	nmol · g^{-1} FW water	nmol · g^{-1} FW rimsulfuron	p-value	fold-change
alanine	84.9 ± 12.9	129.3 ± 24.6	0.161	–
arginine	25.7 ± 3.3	29.6 ± 5.6	0.575	–
asparagine	304.5 ± 117.4	368.1 ± 267.1	0.835	–
aspartate	307.9 ± 43.3	319.4 ± 27.5	0.830	–
cysteine	3.1 ± 1.5	8.2 ± 1.0	0.030	▲ 2.6
glutamate	156.7 ± 20.8	162.5 ± 15.2	0.830	–
glutamine	23.2 ± 4.5	39.0 ± 15.0	0.354	–
glycine	7.2 ± 3.6	8.3 ± 2.6	0.806	–
histidine	7.6 ± 0.9	9.8 ± 1.3	0.197	–
isoleucine	159.9 ± 45.9	5.3 ± 1.1	0.011	▼ 30.2
leucine	2.3 ± 0.7	9.5 ± 2.3	0.156	–
lysine	39.9 ± 3.8	50.1 ± 8.9	0.331	–
methionine	3.8 ± 0.5	8.1 ± 1.0	0.010	▲ 2.1
phenylalanine	7.0 ± 0.8	8.6 ± 1.3	0.313	–
proline	n.d.	n.d.	n.d.	n.d.
serine	141.6 ± 7.2	220.0 ± 34.6	0.068	–
threonine	27.3 ± 3.3	24.0 ± 2.6	0.464	–
tryptophan	0.6 ± 0.1	0.6 ± 0.1	0.955	–
tyrosine	2.3 ± 0.7	3.6 ± 0.9	0.275	–
valine	5.9 ± 0.8	8.0 ± 2.3	0.212	–
total	1311.4 ± 224.0	1412.2 ± 328.6	0.808	–

Table 3.4. Amino acid content of water or rimsulfuron-treated ripe 'Empire' apple fruit peel. Presented as means ± ½ sD of four biological reps. Fold-change of means of rimsulfuron-treated tissue presented if significant (two-sample equal variance t-test; one-tailed test for valine, leucine and isoleucine; two-tailed test for all others; $\alpha = 0.05$). Proline was not determined.

amino acid	nmol · g^{-1} FW water	nmol · g^{-1} FW rimsulfuron	p-value	fold-change
alanine	32.9 ± 9.6	44.1 ± 5.8	0.295	–
arginine	24.6 ± 1.7	24.2 ± 2.7	0.871	–
asparagine	79.8 ± 67.8	70.2 ± 38.3	0.893	–
aspartate	158.9 ± 49.8	184.9 ± 33.5	0.641	–
cysteine	1.6 ± 0.4	6.4 ± 0.9	0.000	▲ 4.1
glutamate	82.3 ± 18.5	94.3 ± 16.4	0.601	–
glutamine	8.7 ± 3.1	17.5 ± 3.8	0.079	–
glycine	4.1 ± 1.1	7.8 ± 3.9	0.341	–
histidine	8.8 ± 0.6	9.6 ± 1.5	0.561	–
isoleucine	102.3 ± 23.4	4.2 ± 1.5	0.002	▼ 24.1
leucine	3.5 ± 0.3	13.9 ± 2.9	0.314	–
lysine	35.5 ± 2.8	40.5 ± 4.3	0.312	–
methionine	4.7 ± 0.9	10.3 ± 1.6	0.011	▲ 2.2
phenylalanine	6.5 ± 0.6	6.8 ± 0.4	0.627	–
proline	n.d.	n.d.	n.d.	n.d.
serine	75.5 ± 12.5	145.0 ± 27.1	0.032	▲ 1.9
threonine	18.0 ± 3.2	11.0 ± 1.1	0.051	–
tryptophan	0.8 ± 0.1	0.9 ± 0.3	0.596	–
tyrosine	3.4 ± 0.5	3.4 ± 0.5	0.914	–
valine	3.5 ± 1.3	5.2 ± 0.9	0.138	–
total	655.4 ± 186.5	700.2 ± 106.0	0.821	–

Table 3.5. Amino acid content of water or rimsulfuron-treated ripe 'Jonagold' apple fruit peel. Presented as means ± ½ sD of five biological reps. Fold-change of means of rimsulfuron-treated tissue presented if significant (two-sample equal variance t-test; one-tailed test for valine, leucine and isoleucine; two-tailed test for all others; $\alpha = 0.05$). Proline was not determined.

trait	water		glyphosate		p-value	fold-change
estragole[a]	0.28 ±	0.06	0.14 ±	0.04	0.063	–
alanine[b]	36.9 ±	5.9	93.0 ±	25.5	0.044	▲ 2.5
arginine	15.3 ±	1.4	16.4 ±	2.0	0.625	–
asparagine	223.2 ±	102.3	489.1 ±	183.0	0.194	–
aspartate	422.1 ±	54.0	428.0 ±	88.4	0.951	–
cysteine	0.4 ±	0.1	0.5 ±	0.1	0.359	–
glutamate	9.2 ±	2.1	16.9 ±	5.0	0.153	–
glutamine	188.3 ±	23.6	232.5 ±	34.9	0.274	–
glycine	5.9 ±	1.2	9.7 ±	2.7	0.179	–
histidine	6.3 ±	1.1	6.2 ±	1.1	0.953	–
isoleucine	152.6 ±	44.5	113.1 ±	15.7	0.377	–
leucine	3.7 ±	0.8	4.7 ±	1.9	0.603	–
lysine	21.0 ±	2.1	24.5 ±	3.9	0.400	–
methionine	10.5 ±	3.3	12.5 ±	4.9	0.723	–
phenylalanine	4.8 ±	0.6	3.8 ±	0.4	0.082	–
proline	n.d.		n.d.		n.d.	n.d.
serine	126.9 ±	29.7	183.1 ±	43.0	0.264	–
threonine	29.8 ±	5.4	31.7 ±	5.5	0.794	–
tryptophan	0.4 ±	0.1	0.5 ±	0.1	0.408	–
tyrosine	1.8 ±	0.4	1.9 ±	0.4	0.481	–
valine	22.1 ±	3.5	17.8 ±	5.0	0.449	–
total	1281.2 ±	251.5	1685.6 ±	364.1	0.337	
I_{AD}[c]	0.63 ±	0.08	1.28 ±	0.11	0.001	
lightness	70.2 ±	0.5	68.5 ±	0.5	0.019	
chroma	52.8 ±	0.8	53.7 ±	0.5	0.311	
hue angle[d]	96.2 ±	0.9	104.5 ±	1.6	0.001	

Table 3.6. Traits of water or glyphosate-treated ripe 'Golden Delicious' apple fruit peel. Presented as means ± ½ SD of five biological reps. Fold-change of estragole or amino acid means of glyphosate-treated tissue presented if significant (two-sample equal variance t-test; one-tailed test for phenylalanine, tyrosine and tryptophan; two-tailed test for all others; $\alpha = 0.05$). Proline was not determined. IAD calculated from 4 technical reps, color metrics are from 2 technical reps each. [a] estragole presented as nmol · L^{-1}. [b] amino acids presented as nmol · g^{-1} FW. [c] IAD, index of absorbance difference, the difference of absorbance of 670 and 720 nm; corresponds to the content of chlorophyll a (Ziosi et al., 2008). [d] 90 = green, 180 = yellow.

volatile	nmol · L^{-1} water	nmol · L^{-1} halosulfuron	p-value	fold-change
ethyl acetate	210.8 ± 26.0	9.6 ± 6.0	0.013	▼ 22.0
butyl acetate	457.1 ± 60.2	21.7 ± 14.5	0.014	▼ 21.1
butyl butanoate	87.1 ± 4.9	12.3 ± 5.3	0.001	▼ 7.1
2-methylpropyl acetate	133.9 ± 7.9	2.8 ± 1.0	0.004	▼ 47.8
2-methylpropyl butanoate	20.2 ± 1.4	0.6 ± 0.2	0.009	▼ 33.7
3-methylbutanol	0.8 ± 0.1	0.1 ± 0.0	0.022	▼ 16.6
3-methylbutyl acetate	298.3 ± 11.7	32.3 ± 15.7	0.001	▼ 9.2
3-methylbutyl butanoate	44.0 ± 1.6	14.0 ± 1.4	0.000	▼ 3.1
2-pentanone	23.6 ± 1.8	15.9 ± 5.4	0.412	–
2-pentanol	5.2 ± 0.7	5.2 ± 0.3	0.966	–
1-methylbutyl acetate	299.3 ± 20.8	274.1 ± 31.8	0.443	–
1-methylbutyl butanoate	34.4 ± 2.9	50.7 ± 4.0	0.171	–

Table 3.7. Headspace volatile concentrations of water or halosulfuron-treated ripe 'Cavendish' banana fruit pulp. Presented as means ± ½ SD of three biological reps. Fold-change of means of halosulfuron-treated tissue presented if significant (paired t-test; two-tailed; $\alpha = 0.05$).

amino acid	µmol · g^{-1} FW water	µmol · g^{-1} FW halosulfuron	p-value	fold-change
alanine	0.149 ± 0.010	0.593 ± 0.052	0.020	▲ 4.0
arginine	0.183 ± 0.010	0.200 ± 0.012	0.228	–
asparagine	0.508 ± 0.073	0.825 ± 0.017	0.092	–
aspartate	0.279 ± 0.017	0.916 ± 0.026	0.004	▲ 3.3
cysteine	0.245 ± 0.031	0.617 ± 0.044	0.009	▲ 2.5
glutamate	0.773 ± 0.126	1.843 ± 0.157	0.028	▲ 2.4
glutamine	0.247 ± 0.012	0.531 ± 0.034	0.080	–
glycine	0.079 ± 0.014	0.124 ± 0.007	0.033	▲ 1.6
histidine	3.288 ± 0.125	3.399 ± 0.085	0.215	–
isoleucine	0.033 ± 0.002	0.038 ± 0.003	0.069	–
leucine	0.248 ± 0.026	0.161 ± 0.013	0.042	▼ 1.5
lysine	0.072 ± 0.006	0.061 ± 0.004	0.060	–
methionine	0.003 ± 0.000	0.003 ± 0.000	0.522	–
phenylalanine	0.028 ± 0.001	0.024 ± 0.003	0.168	–
proline	0.104 ± 0.006	0.194 ± 0.006	0.014	▲ 1.9
serine	0.283 ± 0.009	0.524 ± 0.024	0.005	▲ 1.9
threonine	0.144 ± 0.010	0.172 ± 0.008	0.061	–
tryptophan	0.058 ± 0.003	0.068 ± 0.004	0.159	–
tyrosine	0.055 ± 0.007	0.075 ± 0.004	0.032	▲ 1.4
valine	0.206 ± 0.015	0.029 ± 0.001	0.005	▼ 7.0
total	6.984 ± 0.377	10.398 ± 0.248	0.025	▲ 1.5

Table 3.8. Amino acid content of water or halosulfuron-treated ripe 'Cavendish' banana fruit pulp. Presented as means ± ½ sD of three biological reps. Fold-change of means of halosulfuron-treated tissue presented if significant (paired t-test; one-tailed test for valine, leucine and isoleucine; two-tailed test for all others; $\alpha = 0.05$).

volatile	nmol · L^{-1} [a] water	rimsulfuron	p-value	fold-change
propyl acetate	0.034 ± 0.007	0.931 ± 0.357	0.002	▲ 27.1
butyl acetate	0.155 ± 0.033	0.198 ± 0.048	0.328	–
ethyl butanoate	0.354 ± 0.168	0.467 ± 0.273	0.621	–
2-methylpropyl acetate	0.110 ± 0.036	0.002 ± 0.003	0.025	▼ 45.1
2-methylbutyl acetate	0.095 ± 0.030	0.009 ± 0.007	0.029	▼ 10.1
estragole	0.425 ± 0.044	0.289 ± 0.123	0.123	–
linalool[a]	464248 ± 41116	386155 ± 117608	0.318	–

Table 3.9. Headspace volatile concentrations of water or rimsulfuron-treated ripe 'Dr Banks Pink' ornamental quince fruit. Presented as means ± ½ SD of four biological reps. Fold-change of means of rimsulfuron-treated tissue presented if significant (t-test; two-tailed; two-sample equal variance; $\alpha = 0.05$). [a] linalool presented as m/z 71 response.

amino acid	nmol · g^{-1} FW water	nmol · g^{-1} FW rimsulfuron	p-value	fold-change
alanine	39.7 ± 11.9	29.9 ± 1.0	0.447	–
arginine	19.0 ± 1.4	20.4 ± 2.6	0.645	–
asparagine	25.2 ± 10.0	40.2 ± 5.6	0.239	–
aspartate	289.4 ± 83.8	274.6 ± 45.4	0.881	–
cysteine	0.2 ± 0.1	0.2 ± 0.0	0.785	–
glutamine	9.6 ± 2.3	16.5 ± 2.5	0.086	–
glutamate	197.4 ± 45.8	236.5 ± 21.1	0.466	–
glycine	9.2 ± 3.0	22.0 ± 9.5	0.246	–
histidine	5.8 ± 0.7	9.6 ± 1.2	0.028	▲ 1.7
isoleucine	6.5 ± 0.7	3.3 ± 0.6	0.030	▼ 1.9
leucine	7.5 ± 0.4	6.2 ± 0.4	0.288	–
lysine	20.5 ± 0.7	25.6 ± 2.5	0.097	–
methionine	2.0 ± 0.5	4.8 ± 0.8	0.020	▲ 2.5
phenylalanine	5.1 ± 0.5	5.4 ± 0.3	0.576	–
proline	n.d.	n.d.	n.d.	n.d.
serine	52.1 ± 15.0	157.3 ± 16.7	0.003	▲ 3.0
threonine	18.2 ± 4.2	19.0 ± 2.3	0.875	–
tryptophan	16.0 ± 5.8	16.0 ± 4.8	0.999	–
tyrosine	2.2 ± 0.4	1.8 ± 0.3	0.426	–
valine	12.8 ± 1.2	3.6 ± 0.5	0.000	▼ 3.6
total	738.3 ± 184.5	893.0 ± 102.9	0.492	–

Table 3.10. Amino acid content of water or rimsulfuron-treated ripe 'Dr Banks Pink' ornamental quince fruit peel. Presented as means ± ½ SD of four biological reps. Fold-change of means of rimsulfuron-treated tissue presented if significant (two-sample equal variance t-test; one-tailed test for valine, leucine and isoleucine; two-tailed test for all others; $\alpha = 0.05$). Proline was not determined.

for quantification			for isotope enrichment	
m/z	volatile	fruit	*m/z*	volatile
TIC	1-methylbutyl acetate[a]		43-45	methyl acetate
TIC	1-methylbutyl butanoate[a]		88-90	methyl propanoate
43	2-methylbutyl acetate	quince	87-89	methyl butanoate
70	2-methylbutyl acetate	apple	88-90	methyl 2-methylbutanoate
43	2-methylpropyl acetate		87-89	methyl pentanoate
71	2-methylpropyl butanoate		101-105	methyl hexanoate
TIC	2-pentanol[a]			
86	2-pentanone			
41	3-methylbutanol			
70	3-methylbutyl acetate			
55	3-methylbutyl butanoate			
57	butyl 2-methylbutanaote			
43	butyl acetate	quince		
61	butyl acetate	apple/banana		
89	butyl butanoate			
148	estragole			
57	ethyl 2-methylbutanoate			
71	ethyl 2-methylpropanoate			
57	ethyl 3-methylbutanaote			
61	ethyl acetate			
43	ethyl butanoate			
103	hexyl 2-methylbutanoate			
61	hexyl acetate			
71	linalool			
85	methyl 2-methylbutanoate			
87	methyl 2-methylpropanoate			
61	pentyl acetate			
43	propyl acetate	quince		
61	propyl acetate	apple		

Table 3.11. Ions used for integration of volatile compounds. [a] No standard was available for several compounds, thus they were integrated under their total ion count and then quantified against an isomer within the standard.

compound	parent ion (*m/z*)	daughter ion (*m/z*)	cone voltage	collision voltage	approximate retention time (min)	phase
Gly	76	30	17	8	2.05	1
[13C2,15N]-Gly	79	32	17	8	2.05	1
Ala	90.1	44	35	17	3.54	1
[13C3,15N]-Ala	94.1	47.1	17	8	3.54	1
Ser	106.1	60	30	10	1.79	1
[13C3,15N]-Ser	110.1	63	19	10	1.79	1
Thr	120.1	74	19	8	2.46	1
[13C4,15N]-Thr	125.1	78.1	19	8	2.46	1
Cys	122	76	18	15	2.32	1
[13C3,15N]-Cys	126	79	18	15	2.32	1
Asn	133.1	74	35	14	1.79	1
Asp	134.1	74	35	10	1.42	1
[13C4,15N]-Asp	139.1	77	19	11	1.42	1
Gln	147.1	84	35	14	2.24	1
Glu	148.1	84	34	14	2.01	1
[13C5,15N]-Gln	154.1	89.1	17	14	2.24	1
Pro	116	70	35	10	5.13	2
[13C5,15N]-Pro	122.1	75.1	35	10	5.13	2
Val	118.1	72	35	9	6.05	2
[13C5,15N]-Val	124.1	77.1	35	9	6.05	2
Met	150.1	104	19	9	5.89	2
[13C5,15N]-Met	156.1	109.1	19	9	5.89	2
Tyr	182.1	136.1	20	12	5.44	2
[13C9,15N]-Tyr	192.1	145.1	20	12	5.44	2
Ile and Leu	132.1	86	35	9	6.76 and 6.9	3
[13C5,15N]-Ile and Leu	139.1	92	35	9	6.76 and 6.9	3
Lys	147.1	84	19	14	7.7	3
[13C6,15N2]-Lys	155.1	90.1	19	14	7.7	3
His	156.1	110	20	12	7.73	3
[13C6,15N3]-His	165.1	118.1	20	12	7.73	3
Phe	166.1	120	20	10	6.98	3
[13C9,15N]-Phe	176.1	129.1	20	10	6.98	3
Arg	175.1	70	24	18	7.85	3
[13C6,15N4]-Arg	185.1	75	24	18	7.85	3
Trp	205.1	146	19	14	7.04	3
[13C11,15N2]-Trp	218.1	156	19	14	7.04	3

Table 3.12. Ions and other parameters used for amino acid analysis.

CHAPTER IV – ALTERNATIVE SPLICING OF TWO OTHERWISE FEEDBACK INHIBITED ENZYMES PROVIDES MEANS FOR BIOSYNTHESIS OF CHARACTERISTIC BANANA AROMA

Introduction

The characteristic flavor of banana (*Musa* spp.) fruit is exceedingly rare in nature. Among commercially produced fruits, whether of temperate or tropical origin, the compounds that are responsible for a banana fruit's distinctive aroma, 2-methylpropyl and 3-methylbutyl esters, are occasionally emanated in trace amounts, but no other fruit generates these volatiles to the degree that banana fruit do (Morton & MacLeod, 1990).

The synthesis of these volatiles, as well as butyl esters, which are not necessarily 'banana-like' but contribute to the overall 'fruitiness' of the fruit's flavor (McCarthy, Palmer, Shaw, & Anderson, 1963), has recently been demonstrated to be dependent upon the *de novo* production of branched-chain α-ketoacids via the same metabolic routes as branched-chain amino acid biosynthesis, with 2-methylpropyl and 3-methylbutyl compounds most closely related to valine and leucine, respectively (Chapter III).

While these iso-branched-chain amino acids, and by implication their α-ketoacids, have been observed among the proteinogenic amino acids to uniquely accumulate in ripening pulp, the tissue of aroma biogenesis, it is unclear how this is possible (Alsmairat, Engelgau, & Beaudry, 2018). The processes that produce these compounds are regulated by strict feedback mechanisms that should prevent such stark increases under normal metabolism (Figure 2.2) (Lee & Duggleby, 2001) (de Kraker, Luck, Textor, Tokuhisa, & Gershenzon, 2007). Specifically, acetohydroxyacid synthase (AHAS), the regulator of the total pool of iso-branched-chain amino acids, is synergistically inhibited by valine and leucine whereas isopropylmalate synthase (IPMS), the fulcrum that determines the balance of these compounds by facilitating the extension of α-ketoisovalerate to α-ketoisocaproate, is regulated by leucine (Xing & Last, 2017). The observed phenomena of banana fruits accumulating an ample supply of precursors for aroma biosynthesis seems to be in paradox to these canonical regulatory networks.

IPMS has been documented as being recruited to specialized metabolism several times, each of which involved loss of leucine feedback regulatory elements and, in some, shifts in substrate specificity. In *Solanaceae*, *Brassicaceae*, and *Lamiaceae*, neofunctionalized enzymes derived from IPMS have been documented to provide precursors for defensive compounds in

vegetative organs (de Kraker & Gershenzon, 2011) (Ning, et al., 2015) (Wang, et al., 2022). Citramalate synthase, an enzyme likewise believed to have evolved from IPMS, has been found to be responsible for the ability of apple (*Malus ×domestica* Borkh.) fruits to produce copious amounts of 2-methylbutyl and 2-methylbutanoate esters, an important contributor to apple flavor, by circumventing the feedback mechanisms of isoleucine and anteiso-branched-chain metabolite synthesis (Sugimoto, Engelgau, Jones, Song, & Beaudry, 2021).

Thus, given the numerous examples of IPMS deregulation and neofunctionalization, we began exploration of the paradox of banana aroma biosynthesis with this noted gateway enzyme of specialized metabolism.

Results

Discovery and characterization of alternate splice forms and their predicted proteins

Gel electrophoresis of polymerase chain reaction (PCR) products from the amplification of *MaIPMS* from ripe banana (*Musa* spp. AAA group, Cavendish subgroup, cv. Valery) fruit pulp RNA yielded two bands differing by approximately 200 base pair (bp) (Figure 4.1). While sequencing of the excised bands revealed that the longer of the two possessed the complete *MaIPMS* sequence as expected, the shorter band lacked the entirety of exons 9 and 10, representing a 219 bp loss. Due to the structure of the gene, this internal truncation would be predicted to produce a protein lacking 73 internal amino acids with no frameshifts or substitutions (Figure 4.2).

Current genomic resources for banana indicate only one copy of IPMS to be present (Table 4.1) and no further work with the gene suggested the different transcripts to be allelic or of different genes, thus the transcripts were inferred to be the result of alternative splicing. The longer isoform was named *MaIPMS.1* and the shorter named *MaIPMS.2*.

Alignment of the predicted MaIPMS isoform structures with the crystal structure of *Mycobacterium tuberculosis* IPMS (Koon, Squire, & Baker, 2004) indicated that the missing regions of *MaIPMS.2* correspond with the entire loss of the residues comprising, in the nomenclature of Koon et al. (2004), α13 of subdomain II, and β11, β12, β13, and α14 of the leucine-binding regulatory (R) domain of IPMS (Figures 4.3, 4.4, 4.5, 4.6). On a tertiary scale, the loss of these motifs of the R-domain effectively removes the upper βββα unit that would otherwise fold with a likewise unit to form a pair of β-wrapped α-helices. Such a loss exposes a relatively large and otherwise internal region of the enzyme. Overall, while the models suggest

that the catalytic TIM barrel's structure is minorly affected in MaIPMS.2, subdomain II and the R-region are predicted to have major reorganizations compared to MaIPMS.1.

Given the predicted maintenance of the catalytic domain's structure, the observed binding of leucine to the N-terminals of α14 and α15' of the R-domain (Koon, Squire, & Baker, 2004), as well as the functional variations in other neofunctionalized IPMS enzymes from other plant species, each with modification to the R-domain but preservation of catalytic activity (de Kraker & Gershenzon, 2011) (Ning, et al., 2015) (Wang, et al., 2022) (Sugimoto, Engelgau, Jones, Song, & Beaudry, 2021), it was hypothesized that MaIPMS.2 lacks feedback inhibition to leucine but retains enzymatic activity (Figure 4.7, 4.8).

We next investigated the other rate-limiting enzyme of branched-chain amino acid biosynthesis, acetohydroxyacid synthase (AHAS). Transcriptomic data (Asif, et al., 2014) of unripe and ripe (*Musa* spp. AAA group, Cavendish subgroup, cv. Dwarf Cavendish) fruit indicated there to be an alternative transcript of the regulatory subunit (RSU) of AHAS present in ripe fruit pulp that lacks exon 3, corresponding with an 84 bp loss that would result in a protein with an internal deletion of 28 amino acids with no frameshifts or substitutions compared to the full-length isoform (Figure 4.9). These transcripts were likewise named *MaAHAS_RSU1.1* and *MaAHAS_RSU1.2*.

PCR amplification and gel electrophoresis confirmed the presence of the alternative transcript in ripe fruit pulp, as well as a lack of splicing for the second copy of MaAHAS_RSU present in banana, MaAHAS_RSU2 (Figure 4.10).

Analysis against the cryo-electron microscopy structure of *Arabidopsis thaliana* AHAS (Lonhienne, et al., 2020) indicated the predicted MaAHAS_RSU1.2 isoform to lack the residues composing the C-terminal of β4 of the first ACT domain's βαββαβ motif, as well as the entirety of β5 and the N-terminal of α3 of the oligomerization domain (Figure 4.11, 4.12). Models of MaAHAS_RSU1.2 show further disruptions to the secondary structures in the form of altered β6, β7, and α4 lengths in addition to loss of the α3, β8, and β9 folds (Figure 4.13). The overall structure, however, was not predicted to undergo major rearrangements with the most dramatic shift taking the form of a shortened β4 directly connecting via an unstructured coil to β6 followed by a general maintenance of form save for the loss of the β8 and β9 folds which normally interact with β5.

The conserved βαββαβ motif of ACT domains has been shown to bind the branched-chain amino acids that confer feedback inhibition (Lee & Duggleby, 2001), however the compromised β4 structure is on the periphery of the domain and farthest from the observed amino acid binding sites. It was unclear what effects these changes may have on feedback inhibition by valine and leucine, as well as what the modifications to the oligomerization domains would have on generation of the holoenzyme, and thus activation of the catalytic domain via binding of the catalytic subunits (CSU), or on the overall flexibility of the regulatory subunit, an important property for imbuing feedback sensitivity.

Trends of respiration, aroma production, and metabolic intermediate accumulation in ripening fruit pulp

To explore the trends of important aspects of fruit ripening in the context of these enzyme isoforms (Figure 4.14), a population of ungassed, but mature 'Valery' banana fruit were ripened and analyzed in the laboratory. The fruit were gassed with propylene, which allows for observation of endogenous ethylene production while still synchronizing the ripening processes with minimal physiological alterations (McMurchie, McGlasson, & Eaks, 1972).

Gassed fruits reached a climacteric peak two days after the start of propylene treatment (Figure 4.15). Internal propylene levels of the gassed fruits were over 500 $\mu L \cdot L^{-1}$ after being exposed to ~1200 $\mu L \cdot L^{-1}$ propylene for 12 hours, and gradually dissipated to 0.15 $\mu L \cdot L^{-1}$ nine days later (Figure 4.15). This decay closely followed the curve $y = 42.6 \cdot x^{-2.547}$; ($y = \mu L \cdot L^{-1}$ internal propylene, x = days after propylene treatment, $R^2 = 0.98$). The internal propylene concentration at the end of treatment and one day after the start of treatment was equivalent to 5.34 and 0.25 $\mu L \cdot L^{-1}$ of ethylene, respectively, but thereafter contributed a likely inconsequential degree as an ethylene analog (Burg & Burg, 1967). A set of subsamples were collected immediately after propylene treatment to observe what processes may have been triggered due to a high internal concentration of ripening hormone in fruits not yet in the climacteric.

A maximum of 0.2 $\mu L \cdot L^{-1}$ of propylene was measured to have penetrated control fruit, however they failed to enter the climacteric during the period of the study (Figure 4.16). Samples were collected after nine days to serve as a temporal comparator of metabolites and gene expression to ripening fruits.

In ripening fruits, most aroma compounds began to be detected within the headspace three-four days after the climacteric peak and continued to rise steadily thereafter (Figure 4.17, 4.18). 2-Methylpropyl & 2-methylpropanoate, and 3-methylbutyl & 3-methylbutanoate ester elements reached headspace concentrations of 114 and 116 nmol · L^{-1}, respectively (Figure 4.19). Overall, the trends of aroma production and respiration followed trends consistent with normal banana ripening (Macku & Jennings, 1987) (Alsmairat, Engelgau, & Beaudry, 2018).

Within the pulp tissue, pyruvate peaked sharply one day after the climacteric peak (Figure 4.20), as previously observed (Beaudry, Severson, Black, & Kays, 1989). Amino acid levels were also consistent with previous reports (Alsmairat, Engelgau, & Beaudry, 2018) and demonstrated steady increases of valine and leucine beginning two days after the climacteric peak, reaching maximum observed concentrations of 1.9 and 2.6 μmol · g^{-1}, respectively (Figure 4.20). Isoleucine and threonine failed to accumulate appreciably throughout ripening.

The branched-chain α-ketoacids, α-ketoisovalerate and α-ketoisocaproate, accumulated in concert with their branched-chain amino acid counterparts, however the ratios of the branched-chain amino acid to their α-ketoacids were observed to drop dramatically after the onset of accumulation and settle two days after the climacteric peak to a ratio at least 10-fold less than that of unripe fruits (Figure 4.20). α-Isopropylmalate levels also began to increase in tandem with the α-ketoacids and branched-chain amino acids and reached a peak concentration of 0.016 μmol · g^{-1} a week after entering the climacteric.

The straight-chain α-ketoacids, α-ketovalerate, α-ketocaproate, and α-ketooctanoate, likewise increased throughout ripening, albeit at much lower concentrations than the branched-chain α-ketoacids (Figure 4.20). Furthermore, the amount of α-ketoacid accumulated decreased with chain length.

Citramalate levels increased slightly from 0.001 μmol · g^{-1} at the onset of ripening to 0.004 μmol · g^{-1} a week later (Figure 4.20).

Fruits not gassed with propylene did not accumulate any of the volatile compounds or volatile-related metabolites measured (Figures 4.17, 4.18, 4.19, 4.20) They also maintained uninduced ratios of branched-chain amino acids to branched-chain α-ketoacids. Levels of threonine and isoleucine, which are not considered to be related to aroma production in banana fruit, were present in indistinguishable concentrations in nongassed and gassed fruits (Figure 4.20).

Gene expression of *MaAHAS*, *MaIPMS*, and their splice forms

The fold-changes of expression of both copies of *MaAHAS_CSU* and *MaAHAS_RSU*, as well as *MaIPMS*, were found to sharply spike at the immediate end of propylene treatment within pulp tissue (1½ days before the climacteric peak), while internal propylene concentrations were relatively high, as compared to before exposure to propylene (Figure 4.21). Twelve additional hours later, following the dissipation of propylene, the expression of these genes reduced.

A day after the climacteric peak, the expression of *MaAHAS_CSU1*, *MaAHAS_RSU1* and *MaIPMS* spiked to levels above those at the end of propylene treatment, a likely indication that normal ripening physiology was now occurring and that the influence of propylene was past.

MaAHAS_CSU1 expression peaked 10-times higher in ripening fruit compared to unripe control fruit and thereafter was maintained at levels 8-times greater than control fruit. Both *MaAHAS_RSU1* and *MaIPMS* expression peaked to ~5-fold greater than unripe fruit a day after entering the climacteric but decreased again a day later. For the remainder of the study, *MaAHAS_RSU1* was expressed near basal levels whereas *MaIPMS* was maintained to nearly double that of ungassed fruits until 6 days past the climacteric peak when levels began to increase again.

After their initial peak of expression, *MaAHAS_CSU2* and *MaAHAS_RSU2* failed to undergo another increase of expression as compared to their respective copies. This was interpreted as being indicative of these genes not normally being involved during ripening.

The percent of transcripts that were of each isoform was determined by gel densitometry via PCR amplification of the genes with primers external to, but facing toward the splice sites, and the subsequent measurement of the density of the two bands by gel electrophoresis. The technique was found to be simple, accurate and precise for these transcripts. The shorter isoforms of *MaAHAS_RSU1* and *MaIPMS* steadily increased in proportion throughout ripening, making up 5.7% and 22% of *MaAHAS_RSU1* and *MaIPMS* transcripts at maximum, respectively (Figures 4.22, 4.23).

The fold-change of expression for the specific isoforms was calculated by normalizing the product of the percent of the isoform multiplied by the calculated fold-change expression of both isoforms. *MaAHAS_RSU1.2* expression peaked a day after the climacteric peak to be 9-times greater than unripe fruit and was thereafter maintained close to double that of pre-induced fruits (Figure 4.22). *MaAHAS_RSU1.1* underwent a slight increase at the end of propylene treatment

prior to a 4-fold peak a day after entering the climacteric before returning to basal or less levels for the remainder of ripening.

MaIPMS.2 expression steadily increased after the climacteric peak, eventually reaching levels of expression 95-times greater than unripe fruit (Figure 4.23). *MaIPMS.1* expression increased 4-fold at the termination of propylene treatment before peaking to levels about 5-times higher than pre-initiated fruit prior to being expressed less than double pre-induced fruit levels for the remainder of the study.

In non-fruit tissues, no expression of *MaAHAS_RSU1.2* was detected (Table 4.2). In ripe fruit peel *MaAHAS_RSU1.2* was found to comprise 3.2% of *MaAHAS_RSU1* transcripts. While *MaIPMS.2* was detected in several of the tissues tested, it was not found to represent more than 1.5% of *MaIPMS* transcripts. Within ripe fruit peels, *MaIPMS.2* comprised 1.1% of *MaIPMS* transcripts.

Properties of MaAHAS, MaIPMS, and their isoforms

MaAHAS

The *in vitro* activity of MaAHAS, regardless of RSU isoform, was found to inhibited by levels of sodium pyruvate ≥ 50 mM in the reaction buffer, a phenomenon not observed for Arabidopsis AHAS (Lee & Duggleby, 2001) but similar to findings for pea AHAS (Hawkes, Howard, & Pontin, 1989) (Figure 4.24). Thus, our assays, at maximum, used 20 mM sodium pyruvate as a substrate.

Preparations of MaAHAS holoenzyme, whether expressed in bacteria or tobacco, were always prepared/coexpressed with MaAHAS_CSU1 and either one of the MaAHAS_RSU1 isoforms or equal molar amounts of both. These treatments will be referred to only by the RSUs present. Lastly, to simplify language, ‘maximum activity’ will refer to the amount of enzyme activity with no inhibitor present, however slight variation was regularly observed at low inhibitor concentrations.

MaAHAS_RSU1.2 had half the activity of MaAHAS_RSU1.1 with pyruvate (Figure 4.24, Table 4.3). This was found to be the result of a reduction of V_{max} by half with a minimal increase of the K_m. A mixture of the regulatory subunits (MaAHAS_RSU1.1+2) had intermediate V_{max} values with a slight decrease of K_m as compared to MaAHAS_RSU1.1.

Valine, at levels of 0.2 mM, was found to inhibit MaAHAS_RSU1.1 to 80.6% maximum activity. It was further reduced to 70.6% of maximal activity at 1 mM and 58.9% at 5 mM

(Figure 4.25). MaAHAS_RSU1.2, on the other hand, was less affected by valine and plateaued to ~90% maximum activity at 0.2 mM valine. The inhibition of MaAHAS_RSU1.1+2 by valine more closely followed the trend of MaAHAS1.1 with a minimum activity of 67.1%.

Leucine steadily inhibited MaAHAS_RSU1.1 and MaAHAS_RSU1.1+2 to 50.6% and 64.9% of maximum activity at 5 mM, respectively. MaAHAS_RSU1.2 was minimally affected by leucine and maintained >95% maximum activity at 5 mM leucine.

Equal molar mixtures of valine and leucine, which have been shown to act synergistically as feedback inhibitors (Lee & Duggleby, 2001), rapidly reduced the activity of MaAHAS1.1 to 62.2% maximal activity at 0.1 mM and further inhibited to 32.3% activity when 5 mM was present. MaAHAS1.1+2 was likewise rapidly inhibited but maintained 49.8% maximum activity at 5 mM. The alternative isoform MaAHAS1.2, compared to the full-length isoform, was only mildly inhibited and maintained 80.7% activity when 5 mM of the inhibitor mix was present.

Each of the holoenzymes tested responded similarly to isoleucine with only minor inhibition (>90% maximum activity) at 1 mM. This inhibition increased at 5 mM isoleucine (~80% maximum activity).

MaIPMS

There was difficulty in successfully expressing soluble MaIPMS.2 in bacteria (*Escherichia coli*) or tobacco (*Nicotiana benthamiana*), described below. In its stead we prepared two mutant forms for MaIPMS to recreate, in stages of intensity, the predicted removal of residues in MaIPMS.2 (Figure 4.4). For one of these mutations, MaIPMS.PV523-524AA, the terminal residues of α14, which are implicated to help bind leucine and are lost in MaIPMS.2, were substituted to alanine. MaIPMS.PV523-524AA was analyzed for kinetic properties, substrate preference tests, and expression in tobacco. The other mutation, MaIPMS.α14del, lacked the entirety of α14 and was only used for leucine inhibition studies.

MaIPMS.PV523-524AA had about half the activity of MaIPMS.1 with equal molar mixtures of the two (MaIPMS.1+PV523-524AA) having an intermediate level of activity (Table 4.4). For all kinetic parameters tested, save for the K_m of acetyl-CoA which was ~5-times less than MaIPMS.1, MaIPMS.PV523-524AA was less efficient. This ultimately translated into comparable K_{cat}/K_m values for the holoenzymes tested when acetyl-CoA was considered, but a 3.4-fold reduction of the K_{cat}/K_m of MaIPMS.PV523-524AA as compared to MaIPMS.1 with α-ketoisovalerate.

The MaIPMS.PV523-524AA mutation did not result in major modifications to substrate preference and thus the following values are averages of the three holoenzymes tested against activity with α-ketoisovalerate (Table 4.5). The enzymes had no activity with α-ketoisocaproate and an average of 6% activity with α-keto-γ-(methylthio)butyric acid. Activity with pyruvate was slightly higher at 9.9%. Interestingly, MaIPMS had relatively high activity with medium length α-ketoacids with 84.1% and 22.3% activity with α-ketobutyric acid and α-ketovaleric acid, respectively.

MaIPMS.1 was steeply inhibited by leucine and was reduced to 63.7% activity at 0.05 mM leucine (Figure 4.25). It was maximally inhibited to 27.3% activity at 5 mM. MaIPMS.1+PV523-524AA followed a similar pattern but was only inhibited to 58.4% and 43% activity, at 0.05 and 5 mM leucine, respectively. MaIPMS.PV523-524AA was inhibited to no less than 90% of maximum activity by 5 mM leucine and MaIPMS.α14del activity was found to be unaffected by leucine.

Transient expression

Combinations of MaAHAS and MaIPMS were expressed in tobacco (*Nicotiana benthamiana*) leaves followed by analysis of relevant metabolites. Treatments including MaIPMS.2 resulted in similar metabolite pools to identical treatments lacking MaIPMS.2. It was thus inferred that, given the extreme difficulty of expressing MaIPMS.2 in bacteria, expression in tobacco had also failed. In response to this, MaIPMS.PV523-524AA was transiently expressed in another set of treatments in order to observe the *in planta* effects on branched-chain amino acid metabolism when MaIPMS is deregulated.

Expression of MaAHAS_RSU1.2 alone led to greater amounts of α-ketoisovalerate, valine, leucine, and the two amino acids combined, as compared to MaAHAS_RSU1.1 (Figure 4.26). When both MaAHAS_RSU1 isoforms were coexpressed the concentrations of metabolites were not significantly different from MaAHAS_RSU1.1 alone.

When an IPMS isoform was expressed alone there was no significant changes to the metabolite pools save that the ratio of valine:leucine was decreased (Figure 4.27). Coexpression of IPMS with MaAHAS_RSU1.2 was required in order for plants to accumulate α-ketoisocaproate, α-isopropylmalate and greater amounts of leucine than when only MaAHAS_RSU1.2 was expressed. However, while the total pool of valine and leucine was not

affected, the distribution of the two, as demonstrated by a significantly reduced valine:leucine ratio, had changed.

Expression of MaIPMS.PV523-524AA with MaAHAS_RSU1.2 led to greater amounts of α-ketoisocaproate, α-isopropylmalate, and leucine compared to the analogous treatment with MaIPMS.1 (Figure 4.27). There was no difference between the total amount of valine and leucine between said treatments, but the shift of balance between the iso-branched amino acids was evident by the greater amount of valine in the MaAHAS_RSU1.2 + MaIPMS.1 treatment.

The pattern of isoleucine accumulation mirrored that of valine (Figures 4.26, 4.27). It may be that this pattern was the result of valine antagonism to threonine deaminase (Halgand, Wessel, Laprévote, & Dumas, 2002). None of the treatments influenced threonine, α-ketovalerate, α-ketocaproate or citramalate content.

Discussion

The virtual exclusivity of *MaAHAS_RSU1.2* and *MaIPMS.2* to the tissues of aroma biogenesis and their concomitant expression with iso-branched-chain α-ketoacid accumulation and aroma biosynthesis during ripening strongly implicates these isoforms as being involved with aroma biosynthesis. Furthermore, the *in planta* outperformance of the alternative isoforms or their surrogates, with only half the activity of their canonical counterparts *in vitro*, suggests that despite shortfalls of catalytic efficiencies, their demonstrated lack of feedback inhibition ultimately allows for a greater capacity to produce the precursors of aroma compounds. Moreover, the concentrations of valine and leucine present in banana pulp, throughout the entirety of ripening, would impose close to or maximal inhibition to the isoforms of MaAHAS and MaIPMS of normal metabolism. It thus appears very likely that *MaAHAS_RSU1.2* and *MaIPMS.2* are incumbent for the biosynthesis of the characteristic flavor of banana fruit.

Acetohydroxyacid synthase

MaAHAS_RSU1.2, to the best of our knowledge, is the first example of a naturally occurring variant of a plant AHAS_RSU to have impaired feedback inhibition as a function of recruitment to specialized metabolism. Its role in the context of banana aroma precursor biosynthesis appears to act as a deregulated facilitator for increasing the total pool of iso-branched-chain metabolites.

It is noteworthy that AHAS has not been observed to act in concert with any of the other neofunctionalized IPMS enzymes (de Kraker & Gershenzon, 2011) (Sugimoto, Engelgau, Jones, Song, & Beaudry, 2021) (Ning, et al., 2015) (Wang, et al., 2022). While MdCMS and MAM act

on pathways either upstream or beyond the influence of AHAS, PcIBMS and SlIPMS3 are dependent upon AHAS. Furthermore, while the role of SlIPMS3 is believed to act as a fulcrum between iso-branched-chain acyl precursors to acylsugars, PcIBMS, in theory, would rely not only upon AHAS, but also IPMS to provide its substrate α-ketoisocaproate. Thus, our work herein demonstrates not only the novelty of increasing total iso-branched-chain pool for plant specialized metabolism, but also the importance of consideration to both of the regulatory enzymes of branched-chain amino acid metabolism.

It seems likely, given the solved structure of AtAHAS (Figure 4.13) (Lonhienne, et al., 2020), that many of the observed differences of feedback inhibition and catalytic activity of MaAHAS_RSU1.2, as compared to MaAHAS_RSU1.1, are the result of reduced flexibility of the RSU. AHAS_RSUs activate the AHAS holoenzyme through binding of the CSUs and enabling formation of the catalytic sites between CSU monomers. The binding of valine results in a change of conformation facilitated by the hinge-like movement of the RSU, expanding the holoenzyme slightly and thus disrupting the interface between the bound CSUs, leading to a loss of activity. A loss of this flexibility, which may be incurred by the modifications of MaAHAS_RSU1.2, would not only affect the ability of bound branched-chain amino acids to impose inhibition, but in theory would also interfere with the successful formation of the catalytic sites. If true, this seems, in the context of kinetics, to have manifested in a reduction of V_{max} with no impairment of K_m. Thus, the removal of residues within the oligomerization domain may be of greater consequence than the shortening of the ACT domain's peripheral fold.

However, the shortening of this motif may still be of importance, particularly regarding the complete cessation of leucine's ability to inhibit MaAHAS_RSU1.2. Given the proposed hypothesis that each ACT domain is preferential to one or the other of the iso-branched-chain amino acids (Lee & Duggleby, 2001), it may be that the ACT1 domain of MaAHAS_RSU1 is more tailored to leucine, rather than valine, thus providing explanation for the partial disruption of valine inhibition but complete abolition of leucine feedback for MaAHAS_RSU1.2.

Lastly, the modifications that have occurred in MaAHAS_RSU1.2 do not impede the ability of sulfonylureas to impose inhibition, as evidenced by the successful arrest of *de novo* iso-branched-chain metabolite biosynthesis through the application of halosulfuron to banana fruit pulp (Chapter III). Thus the substrate channels of the CSUs, the determined binding site of

sulfonylureas, are unaffected in the alternative isoform (McCourt, Pang, King-Scott, Guddat, & Duggleby, 2006).

Isopropylmalate synthase

Our struggles to express MaIPMS.2 in *E. coli* and the lack of perceived activity in *N. benthamiana* strongly suggest that if MaIPMS.2 is utilized by banana, some additional form of stabilization that is absent in these model organisms is seemingly necessary. This need likely stems from the large area of otherwise internally folded residues exposed by the deletion of one of the R-domain's two βββα motifs. Such stabilization may take the form of a chaperone protein or perhaps a post-translational modification, such as proteolytic truncation of the likely disordered C-terminal of IPMS.2. There is a distinct poetry to this latter possibility: the resulting IPMS protein, lacking the regions downstream of subdomain II, would be analogous to the evolutionary modifications that have occurred to release SlIPMS3, MdCMS, and MAM from feedback inhibition (Figures 4.7, 4.8) (Ning, et al., 2015) (Sugimoto, Engelgau, Jones, Song, & Beaudry, 2021) (de Kraker & Gershenzon, 2011).

Nonetheless, the changes that have occurred in MaIPMS.2, as demonstrated by our designed MaIPMS mutants, are clearly sufficient to likewise relieve MaIPMS.2 of inhibition to leucine. Therefore the MaIPMS.2 splice variant represents an additional member to the growing family of neofunctionalized IPMS enzymes (Figure 4.28). However, unlike other members of this family, MaIPMS.2 relies upon developmentally specific alternative splicing instead of alteration to a duplicated IPMS gene. MaIPMS.2 also represents another IPMS enzyme recruited to specialized metabolism to produce aroma compounds in reproductive organs (Sugimoto, Engelgau, Jones, Song, & Beaudry, 2021).

While our *in vitro* results of substrate specificity of MaIPMS.1 proportionally mirrored the observed increases of citramalate and straight-chain α-ketoacids within ripening banana pulp, *in planta* expression of MaIPMS.1 and MaIPMS.PV523-524AA did not corroborate such findings and definitive conclusions are not possible. It may be that, in the case of 2-ethylmalate synthase and 2-propylmalate synthase activity, tobacco leaves do not house a sufficient substrate supply for an observable shift of metabolite pools, despite the relatively high activity of these reactions measured *in vitro*. Specificity of the isopropylmalate isomerase and isopropylmalate dehydrogenase enzymes present in tobacco may also be acting as limiters to metabolite flow, as hypothesized by Sugimoto et al. (2021). Additionally, as highlighted by MaIPMS.PV523-524AA

having similar substrate preferences as MaIPMS.1, and given that relatively large modifications to the C-terminal are capable of shifts of substrate preference (de Kraker & Gershenzon, 2011), it may be that MaIPMS.2, with a substantially greater loss within the R-domain compared to MaIPMS.PV523-524AA, is responsible for these increasing metabolites in banana pulp as a function of a divergence of substrate preference from MaIPMS.1 on account of its considerable modification to the R-domain.

Lastly, the stark reduction of catalytic activity induced by the modest modifications of MaIPMS.PV523-524AA are of note with regard to the interplay of subunits and the enzyme's catalytic mechanism, however such efficiency shortfalls have been observed of other neofunctionalized IPMS enzymes (Sugimoto, Engelgau, Jones, Song, & Beaudry, 2021) (Wang, et al., 2022) and, given their deregulated nature, are likely inconsequential from a holistic perspective.

Branched-chain amino acid metabolism and banana ripening

The observed interplay between AHAS and IPMS in ripening banana, acting as regulator and balancer, respectively, of the iso-branched-chain metabolites, closely agrees with the proposed roles of these enzymes by Xing & Last (2017). Furthermore, the lack of isoleucine accumulation by ripening banana pulp, despite deregulation of AHAS, an enzyme necessary for its *de novo* production in plants, highlights the separation of regulation between anteiso- and iso-branched-chain metabolism with the former being most tightly controlled by threonine deaminase.

The necessity of *de novo* iso-branched-chain metabolites has been recently demonstrated for the first time through the application of sulfonylurea AHAS inhibitors (Chapter III). Our observation of accumulating α-isopropylmalate, an otherwise fleeting intermediate of α-ketoisovalerate extension, further reinforces the notion that the production of aroma precursors is an anabolic process.

Another observation of note in this study is the stark adjustment of the ratios of iso-branched-chain amino acids to their respective α-ketoacids. The dramatic reduction of this ratio, thus favoring the α-ketoacids 10-fold more during aroma biosynthesis as compared to unripe fruit, suggests a reduction of branched-chain amino transferase (BCAT) activity. Under past dogmas of aroma biosynthesis, the relative increase in the α-ketoacids would be interpreted as an increase of BCAT activity under the assumption that amino acids are the ultimate precursors of these volatiles. However, given that banana aroma biosynthesis is an anabolic process actively

generating α-ketoacids, our observations strongly suggest that a decrease of BCAT activity is occurring during ripening, limiting the interconversion of newly synthesized branched-chain α-ketoacids to their amino acids, a step that otherwise would be counterproductive to aroma synthesis as the α-ketoacids are likely more direct precursors. Expression of BCAT in ripening apple fruits, which produce large amounts of anteiso-branched-chain esters that are likewise supplied via *de novo* synthesis of α-keto-β-methylvalerate, the α-ketoacid of isoleucine, has been observed to categorically decrease in expression during ripening (Chapter III) (Sugimoto, Jones, & Beaudry, 2011). These results calls into question the nearly omnipresent postulation that increased BCAT expression is a means to fruit aroma biosynthesis (Maoz, Lewinsohn, & Gonda, 2022).

Alternative splicing as a metabolic regulator in plants

Alternative splicing allows for proteome diversification with minimal genomic expansion. However, while the role of alternative splicing is widely recognized as an important process of human transcriptional regulation, the extent and importance of alternative splicing in plants is burgeoning. Advances in the understanding of alternative splicing with regards to fruit development as well as plant metabolism are a part of this growing field.

In cucumber, melon, papaya, and peach fruit, ~15% of genes have been observed to undergo alternative splicing during ripening and a growing number of examples demonstrate the ways alternative splicing can facilitate specialized metabolism in plants, including the synthesis of volatile fatty acid derivatives in tea leaves (*Camellia sinensis*), alkaloids in Madagascar periwinkle (*Catharanthus roseus*), anthocyanins in peach flowers (*Prunus persica*), and starch degradation in ripening banana fruit, to name a few (Yan, Bai, Song, & Pang, 2021) (Lam, Wang, Lo, & Zhu, 2022) (Xu, et al., 2019). (Carqueijeiro, et al., 2020) (Yin, Zhen, & Li, 2019) (Jiang, et al., 2021).

The alternative splicing of AHAS and IPMS in ripening banana pulp demonstrates, to our knowledge, the first known example of a pair of enzymes being recruited to specialized metabolism via alternative splicing. Furthermore, the observed restriction of alternative transcript expression to the developmental period after the climacteric peak, and notably not while internal propylene concentrations were relatively high, as well as the virtual restriction of the alternative transcripts to pulp tissues demonstrate that there exists a highly specific system for modulating these splice events to select tissues and developmental phases.

Conclusion

Fruits are sacrificial organs that are dependent upon the attraction of a consumer for their successful dispersion. Failure translates into a substantial waste of resources and a loss of fitness. Thus, the biochemical manipulations enacted by ripening fruits are of no surprise when one considers what is at stake. This research has elucidated another example of the evolutionary specializations that fruits have conceived to improve their palatability. This work, paired with the findings of citramalate synthase's role in ripening apple fruits (Sugimoto, Engelgau, Jones, Song, & Beaudry, 2021) and of methionine gamma lyase in muskmelons (Gonda, et al., 2013), illustrates a growing number of unique mechanisms not only of how fruits convert primary metabolites to specialized ones, but also of the unique ways that branched-chain amino acid metabolism can be modified for fruit aroma biosynthesis. Future work on the means of volatile production in other fruits will likely also expose previously unknown routes to specialized metabolism in plants.

Materials and Methods

Fruit material and ripening scheme

United States Department of Agriculture certified organic, mature, unripe, green bananas (*Musa* spp. AAA group, Cavendish subgroup, cv. Valery) originating from Ecuador, that were not treated with ethylene, were obtained from a local supermarket produce distribution and ripening center (Meijer/Chiquita, Lansing, MI). Fruits were held in the laboratory at room temperature (22 °C) under opaque plastic bags with dampened newspaper to reduce incidence of light and dehydration when not being analyzed or treated.

Fruits were separated from hands into individual fingers and had 2.4 mL glass cylinders attached with non-corrosive rubber silicone (3140 RTV; Dow-Corning, Midland, MI). The other end of the cylinders were sealed with rubber septa. During curing the septa were temporarily pierced with a needle to allow for escape of gasses produced during curing. The silicone was allowed to cure for 3 days before removal of needles and any tape used to hold the apparatus in place. This sealed compartment was used to measure the fruit's internal composition of CO_2, ethylene, and propylene (see below; (Beaudry, Paz, Black, & Kays, 1987)).

The following day all but five fruits were treated with ~1200 ppm propylene, equivalent to 12 ppm ethylene (Burg & Burg, 1967), for 12 hours in a 900 L sealed aluminum chamber. Three of the five non-gassed fruits had internal gas composition and aroma profiles analyzed (see

below) before having pulp tissue collected, flash frozen in liquid nitrogen, and held at -80 ℃ for further analysis. The remaining two non-gassed fruits were held separately from the gassed bananas and analyzed as above nine days later. Immediately after propylene treatment, five of the gassed bananas were analyzed for gas composition and the median three were then used for aroma analysis and had tissue sampled. The remaining population of fruit, including those gassed and not gassed, had internal gas composition analyzed daily until one week after entering the climacteric. Each day three gassed fruits with gas concentrations representing the approximate average of the population were selected for aroma analysis before having pulp tissue collected, flash frozen in liquid nitrogen, and held at -80 ℃ for further analysis. Fruits which failed to follow the population's ripening trends, such as delays entering the climacteric or a lack of de-greening, were removed from the study as they were identified.

Peel tissues were collected from a hand of bananas (*Musa* spp. AAA group, Cavendish subgroup, cv. Valery) originating from Guatemala and obtained from a local grocery store (Kroger/Chiquita). The fruits were held at room temperature (18 ℃) for six days until aroma-active with brown specks present (a similar physiological state as the fruit of our main study a week after entering the climacteric). Peel tissue was then collected, flash frozen in liquid nitrogen, and held at -80 ℃ for further analysis.

Non-fruit materials

Root, pseudostem, leaf, peduncle, bract, anther, and ovary tissues (*Musa* spp. AAA group, Cavendish subgroup, cv. Dwarf Cavendish) were kindly collected and flash frozen in liquid nitrogen by Dr. Alan Chambers of The University of Florida's Institute of Food and Agricultural Sciences Tropical Research and Education Center before being shipped on dry ice overnight to the laboratory. Pseudostem and peduncle tissues were collected with a cork borer before freezing. Upon arrival the samples were held at -80 ℃ until further analysis.

Internal CO_2

A 100 µL gas sample was drawn from the above described attached glass cylinder using a 0.5 mL plastic syringe and injected into an infrared gas analyzer (225-MK3; Analytical Development Company, Hoddesdon, UK) with N_2 as the carrier gas (150 mL · min^{-1}) as previously described (Beaudry, Cameron, Shirazi, & Dostal-Lange, 1992). The concentration of CO_2 was calculated using a certified gas standard (Matheson Gas Products, Montgomeryville, PA) containing 0.979 ppm ethylene, 4.85% CO_2, and 1.95% O_2, balanced with N_2.

Internal ethylene and propylene

After measuring CO_2, a 1 mL gas sample was drawn from the attached cylinder using a 1 mL plastic syringe and injected into a gas chromatograph (Carle Series 400 AGC; Hach Company, Loveland, CO) fitted with a 6 m long, 2 mm internal diameter stainless steel column packed with activated alumina F-1 (80/100 mesh) and equipped with a flame ionization detector. Ethylene was calculated using the aforementioned certified gas standard and propylene was calculated using a homemade 10 ppm propylene standard (Matheson Gas Products, Montgomeryville, PA).Propylene decay curve calculated with Microsoft Excel, v16.58, power trendline option.

Aroma analysis

Fruits selected for volatile analysis had glass cylinders and silicone gently removed before being incubated for 20 min at room temperature (22 ℃) in 2 L sealed Teflon jars (Savillex Corporation, Minnetonka, MN). Headspace volatiles were then sorbed for 3 min using a solid-phase micro extraction (SPME) fiber (65 μm PDMS-DVB; Supelco Analytical, Bellefonte, PA). The SPME fiber was then directly desorbed for 2 min in the injection port of a gas chromatograph (GC; HP-6890, Hewlett-Packard, Wilmington, DE) coupled to a time-of-flight mass spectrometer (MS; Pegasus II, LECO, St. Joseph, MI). Desorbed volatiles were cryofocused at the beginning of the column by immersing said region of the column in liquid nitrogen. After the desorption period, the run was started and the liquid nitrogen removed.

The conditions of the system were as follows. Injection port: 200 ℃, splitless, helium carrier gas, inlet pressure was initially 13.7 psig for 0 min, then ramped up at 3.5 psi/min to 26.5 psig, 3 sec purge, 10 mL · min^{-1} purge flow, 11.76 mL · min^{-1} total flow. Oven: initial temperature at 40 ℃ for 0 min, ramped by 10 ℃/min to 50 ℃ for 0 min, then ramped by 50 ℃/min to 230 ℃ for 0 min. Column: DB-5MS, 30 m × 0.25 mm i.d., 0.25 μm film thickness (Agilent, Santa Clara, CA). Transfer line temperature was 210 ℃. MS: Electron ionization (-70eV), ion source temperature was 209 ℃, solvent delay was 50 sec, m/z 29 to 300 were scanned for, detector voltage was 1400 V, data collection rate was 10 Hz.

Compounds were identified by comparison with the retention time and mass spectrum against authenticated reference standards and spectra (National Institute of Standards and Technology Mass Spectral Search ProgramVersion 2.0, 2001). Volatiles were quantified by calibration with a standard of authenticated compounds (Sigma-Aldrich Co., St. Louis, MO and

Fluka Chemika, Seelza, Germany). The standard was made by placing 0.5 µL of an equal-part mixture of the neat compounds onto a disc of filter paper before quickly placing the filter paper into a 4-L sealed flask fitted with a Mininert valve (Valco Instruments Co. Inc., Houston, TX) for SPME fiber access. The quantification m/z of each compound can be seen in Table 4.6. No prominent unique m/z was identified for butyl 2-methylpropanoate and 2-methylpropyl butanoate, which co-eluted, however the lack of other 2-methylpropanoate esters prompted us to assume peaks of this retention time to be wholly 2-methylpropyl butanoate.

To quantify 2-pentanol, 1-methylbutyl acetate, and 1-methylbutyl butanoate, which were not present in the standard used, TIC of these compounds, as identified by reference spectra, were integrated and quantified against the TIC of isoforms present in the standard (3-methylbutanol, 3-methylbutyl acetate, 3-methylbutyl butanoate). None of these 6 peaks appeared to co-elute with any other compounds.

Non-volatile metabolite analysis

Valine, leucine, isoleucine, threonine, citramalate, α-isopropylmalate, α-ketoisovalerate, α-ketoisocaproate, α-ketovalerate, α-ketocaproate, and α-ketooctanoate were measured via GCMS analysis of derivatized extracts.

Previously collected and frozen pulp tissues were ground via liquid nitrogen-chilled mortar and pestle. 0.5 g of tissue was then extracted in 2.2 mL of a prewarmed 1:1 acetonitrile:water solution containing 0.4 µmoles of U-^{13}C, ^{15}N labeled amino acids (MilliporeSigma) for 15 min in a 65 ℃ water bath. Extracts were then briefly chilled on ice before being centrifuged at 4400 × g for 10 min at 4 ℃. The supernatant was then filtered by centrifugation (0.2 µm nylon centrifugal filter; Costar, Corning) at 21000 × g for 30 min until 1 mL of cleared filtrate was collected. The pH was then raised above 7.5 by the addition of ~50 uL 1M NaOH and verified by the presence of a bright yellow color after adding 75 uL of 1% w/v α-nitrophenol. The samples were then desiccated via rotovac (DNA100 Speed Vac, Savant, Hyannis, Mass.) at 22 °C for 23 hr. The samples were first derivatized at 60 °C for 24 hr via methoxyamination by the addition of 500 µL of 40 mg · mL^{-1} methoxamine hydrochloride in anhydrous pyridine. They were then further derivatized at 60 °C for 24 hr via *tert*-butyldimethylsilyation by the addition of 500 µL of *N*-methyl-*N*-*tert*-butyldimethylsilyltrifluoroacetamide containing 1% *tert*-butyldimethylsilyl chloride. The

derivatized samples were then centrifuged at 21000 × g for 5 min before having supernatant aliquoted into autosampler vials.

1.0 µL of each sample was analyzed with a GC (Agilent 7890A) coupled to a quadrapole MS (5975C inert XL MSD with Triple-Axis Detector). The conditions of the system were as follows. Injection port: 250 ℃, splitless, helium carrier gas, inlet pressure 13.1 psi, 3 mL/min purge flow, 44 mL/min total flow, 40 mL/min at 1 min purge flow to split vent. Oven: initial temperature at 80 ℃ for 0 min, ramped by 30 ℃/min to 130 ℃ for 0 min, then ramped at 15 ℃/min to 250 ℃ for 0 min, then ramped at 40 ℃/min to 320 ℃ for 4 min. Column: VF-5ms, 30 m x 0.25 mm i.d., 0.25 µm film thickness (Agilent, Santa Clara, CA). Transfer line temperature was 300 ℃. MS: Electron ionization (-70eV), MS source temperature was 230 ℃, MS quadrapole temperature was 150 ℃, solvent delay was 5 min, detector voltage was 1824 V, data collection rate was 30-75 Hz depending on the number of *m/z* scanned for per segment, selected ion monitoring was used with the run separated into three segments.

Compounds were identified by retention time and spectra of derivatized authenticated standards (Table 4.7). Quantification was performed by comparison of the ratios of peak areas of metabolites to labeled internal standards. Valine, α-ketoisovalerate, α-ketoisocaproate, α-ketovalerate, α-ketocaproate, and α-ketooctanoate were compared to labeled valine. Leucine was compared to labeled leucine. Isoleucine, threonine, citramalate and α-isopropylmalate were compared to labeled isoleucine. Calibration standards consisted of 0.001 to 1.0 µM of the analyzed compounds (MilliporeSigma).

A note on the extraction and derivatization process. Early attempts at the above method used only 100 µL of each derivatizing agent but indicated extremely low values of both the endogenous metabolites as well as the spiked internal standard in samples collected from ripe tissues. It was hypothesized that these low values were due to either residual enzyme activity resulting from what was possibly a too-mild extraction process, or that high carbohydrate levels in the ripe tissues were competing with the metabolites of interest for the derivatizing agents. The latter was proposed to be the cause as further testing with more rigorous extraction conditions, including incubation in a 75 ℃ for 10 min while using a 1:1:1 water:ethanol:[acetonitrile v/v 1% formic acid] buffer, or using an excess of derivatizing agents, including 500 µL or 1 mL of each indicated the issue was a lack of derivatizing agent. Adding

500 µL was sufficient to overcome competition with the carbohydrates without needlessly diluting the extract further.

A note on isomers resulting from derivatization. and selected peaks. The resulting imine of methoxyamination can form steric isomers that may separate based on the chromatography used. The isomers of derivatized α-keto-β-methylvalerate and α-ketoisovalerate were separated in our analysis and, in the case of derivatized α-ketoisovalerate, the larger peak was used for quantification.

A note on α-keto-β-methylvalerate (KMV) derivatization. We attempted to measure KMV with the above methods, however only a trace signal could be detected. This is most likely due to 1) KMV, whose corresponding amino acid isoleucine is in relatively low levels in banana pulp compared to leucine and valine, would be expected to present at approximately 10 $nmol \cdot g^{-1}$. 2) KMV racemizes in alkaline solutions, such as the conditions present in preparation of sample desiccation 3) methoxyamination also leads to racemization, as described above. Thus derivatized KMV is theoretically present in four isomers. This dilution of signal, combined with likely low native levels, made quantification impossible with the current method.

Pyruvate was initially attempted to be analyzed by the above method, however pyruvate was found to evaporate quickly from warmed extraction buffer when in the presence of acetonitrile, making quantification with a reliable internal standard very difficult. Thus, an enzymatic analysis approach was taken (Lamprecht & Heinz, 1984):

Of the aforementioned ground tissue, 5 g was extracted in 10 mL of an ice-cold 0.6 N $HClO_4$ solution for 30 min on wet ice with occasional shaking. The extraction was then centrifuged at 14000 × g for 30 min at 1 °C. The supernatant was neutralized to between pH 7.0 and 7.4 with 5 N K_2CO_3 and then incubated on ice for 10 min before centrifugation at 20000 × g for 30 min at 1 °C to pellet insoluble $KClO_4$. The resulting supernatant was then aliquoted, flash frozen in liquid nitrogen, and held and -80 °C until enzyme analysis. Extraction recovery was 97.1%.

The conditions of the enzymatic assay were as follows in a total volume of 1 mL: 0.5 mL sample extract, 98 mM triethanolamine (pH 7.6), 60 mM KCl, 30 mM $MgSO_4$, 0.1 mM NADH, 12 U L-lactic acid dehydrogenase from rabbit muscle (SigmaAldrich). Quantification was performed by measuring absorbance of NADH ($\varepsilon_{NADH,\ 25\ °C,\ 339.85\ nm} = 629.2\ mL \cdot mmol^{-1} \cdot mm^{-1}$)

by subtracting the absorbance of sample with buffer against the absorbance of the reaction 10 min after addition of enzyme (U-3000, Hitachi, Tokyo, Japan).

Nucleic acid extraction

RNA was extracted from tissues with a hot borate buffer and several salt-ethanol precipitations and washes as inspired by (Lopez-Gomez & Gomez-Lim, 1992).

In detail, 3-4 g of the aforementioned ground pulp tissue had 0.25-0.5 g polyvinylpolypyrrolidone added. This mixture was then dumped into 12 mL of prewarmed extraction buffer (150 mM Trizma Base, 50 mM ethylenediaminetetraacetic acid , 2% sodium dodecyl sulfate, 1% β-mercaptoethanol, adjusted to pH 7.5 with boric acid), vortexed for 15 s before incubation for 5 min in a 65 ℃ water bath. Afterwards, 0.25 volumes 100% ethanol were added, followed by a brief vortexing and the addition of 0.11 volumes 5M potassium acetate and a subsequent vortexing for 1 min. This mixture was then vortexed for 1 min with one volume of 49:1 chloroform:3-methylbutanol followed by centrifugation at 1560 × g for 15 min at 4 ℃. The supernatant was likewise extracted with one volume of 1:1 chloroform:phenol and again with one volume of 49:1 chloroform:3-methylbutanol. The RNA was then precipitated by the adjustment to 3M lithium chloride with 8M LiCl and incubation at -20 ℃ overnight.

The following day the RNA was collected by centrifugation at 14636 × g for 90 min at 4 ℃. The pellet was washed with 5 mL of ice-cold 70% ethanol before further centrifugation for 30 min. The resulting pellet was dissolved in 400 µL water and had 25 µL 5M potassium acetate and 1 mL of ice-cold 100% ethanol added before precipitation at -80 ℃ for 2 hr.

The RNA was pelleted by centrifugation at 21000 × g for 15 min at 4 ℃ before being washed with 500 µL 75% ethanol and dissolved in 300 µL water. Immediately following resuspension, 150 µL of ice-cold 100% ethanol was added and the sample was incubated on ice for 30 min to precipitate sugars and pectins. After centrifugation at 14000 × g for 10 min at 4 ℃, the supernatant had 300 µL 3M sodium acetate, pH 5.2, and 825 µL ice-cold 100% ethanol added before a final precipitation overnight at -20 ℃.

The sample was centrifuged at 21000 × g for 10 min at 4 ℃ and the resulting pellet was washed with 500 µL 70% ice-cold ethanol. The pellet was then air-dried for several minutes before resuspension in 200 µL water. Quantity and quality were assessed with a Nanodrop.

DNA extraction was inspired by (Gawel & Jarret, 1991).

In detail, 0.6 g of ground leaf tissue was incubated in pre-warmed extraction buffer (4% cetyltrimethyl ammonium bromide, 100 mM Tris HCl pH 8.0, 1.4 M NaCl, 20 mM ethylenediaminetetraacetic acid, 0.1% β-mercaptoethanol, 0.5g polyvinylpolypyrrolidone) and incubated at 65 ℃ for 30 min with occasional mixing. This was then extracted with 15 mL of 24:1 chloroform:3-methylbutanol by vortexing for 1 min. The mixture was centrifuged at 5000 × g at room temperature for 5 min before precipitation of the supernatant with an equal volume of ice-cold isopropanol. The solution was allowed to precipitate overnight at -20 ℃.

The following day the solution was briefly vortexed before centrifugation 20000 × g for 15 min. The pellet was then washed with 10 mL 70% ethanol by centrifugation with the solution 14636 × g for 5 min. The washed pellet was next dissolved in 500 µL of TE buffer (10 mM Tris, 1 mM ethylenediaminetetraacetic acid, pH 8.0). The DNA was then reprecipitated with 50 µL 3M sodium acetate, pH 5.2 and 1 mL 100% ethanol before being allowed to precipitate overnight at -20 ℃.

The next day the DNA was pelleted at 20000 × g for 15 min followed by another wash with 70% ethanol and a final dissolve into 500 µL TE buffer.

Quantitative PCR

Extracted RNA was treated with DNase I (Thermofisher) and converted to cDNA (High-Capacity cDNA Reverse Transcription Kit, Thermofisher).

Quantification of total expression of the genes of interest was performed with a SYBR-based qPCR approach using primers targeting genetic regions that are not spliced. Amplicons were under 250 bp in length. Primers used can be seen in (Table 4.8) and were optimized to have similar melting points. MaDNAJ and MaRPS4 were used as reference genes (Chen, et al., 2011). The 20 µL reaction mixture was as follows: 1X Power SYBR Green Master Mix (Thermofisher), 0.2 µM of each primer, and ~60 ng of cDNA, balanced with water. The reaction conditions were as follows: 10 min 95 ℃, followed by 40 cycles of 15 s 95 ℃, 60 s 60 ℃. All C_t values were less than 30 and the efficiency of reactions across runs were 100% ± 15%. Fold-change of expression was calculated with the $2^{-\Delta\Delta Ct}$ method and normalized against the average of pre-induced fruit.

Quantification of transcript distribution was performed with a gel densitometry approach. Primers facing towards the splice junction were used to produce amplicons of two different lengths, one including the excised portion and one without. The products were then viewed by

gel electrophoresis and the band densities were digitally integrated. The composition of each transcript was calculated by dividing the area of each band by the total area of the two combined. The method was verified with standards derived from plasmids prepared for protein expression, see below. To prepare the standards, purified plasmid solutions composed of a single isoform were quantified via Qubit Fluorometric Quantification (Thermofisher) and then mixed with the alternate isoform in 9:1, 3:1, 1:1, 1:3, and 1:9 (w/w) ratios. These mixes were then amplified using 50, 5, and 0.5 pg · rxn^{-1} in triplicate. The results indicated this method to be within a tolerable range of accuracy and precision, however the lowest template concentration led to inadequate results. When 50 to 5 pg · rxn^{-1} of template were used, MaAHAS_RSU1 had a 4.9% error and a 2.1% standard deviation, and MaIPMS had a 5.6% error and a 5.2% standard deviation.

Primers used can be seen in (Table 4.8). The 20 µL reaction mixture was as follows: 1X Phusion ® High-Fidelity DNA Polymerase Buffer (New England Biolabs), 1 U 1X Phusion ® High-Fidelity DNA Polymerase (New England Biolabs), 200 µM dNTPs (Promega), 0.5 µM of each primer, ~100 ng of cDNA, balanced with water. The reaction conditions were as follows: 30 s 98 ℃, followed by 30 cycles of 10 s 98 ℃, 30 s 64 ℃, 15 s 72 ℃. The entirety of the PCR products were mixed to have 1X Purple Gel Loading Dye (New England Biolabs). The dye casts no UV shadow and includes additives to improve band brightness and tightness. MaAHAS_RSU1 and MaIPMS amplicons were viewed on 2.5 and 2% agarose gels, respectively, containing 1.2 µg · mL^{-1} ethidium bromide. Gel electrophoresis was performed in TAE buffer with 0.5 µg · mL^{-1} of ethidium bromide using constant voltage: 5 min 100 V, 50 min 70 V. The gel was exposed to the maximum duration of UV light to just avoid over-exposing the bands. The two bands were then integrated with ImageJ v1.53r. All samples were performed in triplicate and each run included at least three no-template controls (NTC). Runs with any sign of amplification in the NTC samples were discarded. Regularly cleaning lab equipment and space with a 1% sodium hypochlorite solution greatly reduced cross-contamination.

The fold-change of specific isoforms was calculated by multiplying the percent of an isoform (determined by gel densitometry) by the normalized fold-change expression of both (determined by SYBR qPCR). This product was then renormalized against pre-induced fruit.

Cloning

All cloning, unless otherwise stated, proceeded with initial amplification from cDNA followed by ligation and propagation with the entry vector cloneJET1.2 (Thermo Scientific). The insert with proper restriction sites was produced through restriction enzyme digestion, gel purified, and ligated with the destination backbone. DH5α cells were used for vector preparation. All vectors were confirmed with at least two Sanger sequencing reactions at the Michigan State University Research Technology Support Facility Genomics Core.

Acetohydroxyacid synthase

Methods for the expression and testing of the acetohydroxyacid synthase subunits was inspired by (Xing & Last, 2017) (Lee & Duggleby, 2001)

MaAHAS_CSU1 was initially amplified from genomic DNA (gDNA from 3-61) using primers 139 and 140 to include 5' NdeI and 3' XhoI splice sites and to exclude the predicted chloroplast targeting peptide (Emanuelsson, Nielsen, & Von Heijne, 1999). Initial attempts to amplify from RNA sources failed for unknown reasons, however the lack of introns made sourcing from genomic DNA simple (this is common for AHAS_CSU). The insert was cloned into the NdeI and XhoI sites of pET-41 (Novagen) resulting in a C-terminal 8X-His-Tag.

MaAHAS_RSU1.1 and .2 were amplified from cDNA collected from ripe banana fruit pulp using primers 230 and 136 to include 5' NcoI and 3' XhoI restriction sites and to exclude the predicted chloroplast targeting peptide (ChloroP). CloneJET1.2 constructs were screened for colonies of each splice form. Inserts were subsequently cloned into the NcoI and XhoI splice sites of pET-41 (Novagen) resulting in constructs with N-terminal GST tags, and internal and C-terminal 6X or 8X, respectively, His-Tags.

To produce protein, the above-described vectors were transformed into Rosetta™ 2(DE3)pLysS cells (Novagen) and incubated overnight in LB (Miller) media with 25 µg/mL chloramphenicol and 50 µg/mL kanamycin at 37 °C, 250 rpm. The following morning this was used at a rate of 0.05 mL inoculum per mL culture to inoculate 300 mL batches of fresh LB (Miller) with antibiotics in 1 L Erlenmeyer flasks. These were grown at 37 °C, 250 rpm until reaching an OD_{600} of 0.8 – 0.9 whereupon the cultures were chilled at 1 °C for 10-15 min before the collection of a pre-induced sample. The cells were subsequently induced with 357 µM isopropyl β-D-1-thiogalactopyranoside (IPTG) and incubated at 24.8°C, 250 rpm for 6 hours.

Cells were collected by centrifugation (2500 – g for 15 - 30 min at 4 ℃). Pellets were held at -80 ℃ before extraction.

Cells were resuspended at 5 ℃ at a 25-fold concentration factor with lysis buffer (50 mM Tris-HCl, pH 7.5, 300 mM NaCl, 5 mM $MgCl_2$, 15% glycerol, 1mg/mL lysozyme, 1U · mL^{-1} Benzonase® Nuclease) and incubated on a linear wave rocker for 30 min. Each 300 mL equivalent of culture was then sonicated at 5 ℃ for two 7.5 min regiments of 50% power, 50% pulse with the sonication tip immersed to 1.5-times tip diameter (Omni Ruptor 250) while the sample was immersed in ice-water. Samples were cooled in ice water for at least 30 min in-between sonications. Samples of the crude lysate were then collected before centrifugation (12500 × g for 15 min at 4 ℃) to pellet insoluble material. A sample of cleared lysate was then collected before incubation with resin equilibrated with the appropriate construct's wash buffer (specifics described below).

MaAHAS_CSU1 was extracted via the C-terminal 8X-His-Tag with Ni-NTA agarose (Qiagen). Wash buffer: 50 mM Tris-HCl pH 7.5, 300 mM NaCl, 30 mM imidazole, 5 mM $MgCl_2$. Elution buffer: 50 mM Tris-HCl pH 7.5, 300 mM NaCl, 200 mM imidazole, 5 mM $MgCl_2$.

MaAHAS_RSU1.1 and .2 were extracted via the N-terminal GST tag with Pierce™ glutathione agarose. Wash buffer: 50 mM Tris-HCl pH 7.5, 300 mM NaCl, 5 mM $MgCl_2$. Elution buffer: 50 mM Tris-HCl pH 7.5, 300 mM NaCl, 10 mM reduced glutathione, 5 mM $MgCl_2$

Cleared lysate was incubated with 0.5 mL of appropriate resin per 300 mL of CSU culture or 600 mL of RSU culture for 1-2 hours at 5 ℃ on a linear wave rocker. Collection of 'flow-through' and all resin wash or elution steps were performed by centrifugation of the resin (1000 × g for 2 min at 4 ℃) followed by aspiration of the supernatant. Following incubation, cleared lysate (flow-through) was separated from the resin as above-described. The resin was then washed twice with 5 mL of appropriate wash buffer followed by five 0.5 mL elutions. All five elutions were desalted with PD-10 desalting columns packed with Sephadex G-25 resin (Cytiva) via the manufacturer's spin protocol into desalt buffer (25 mM potassium phosphate pH 7.5, 5mM $MgCl_2$, 15% glycerol). The sample was then concentrated at 7500 × g for 10 min at 4 ℃ with Amicon™ Ultra-4 10 kDa molecular weight cutoff filters. This finished product was then quantified via Bradford assay against a bovine serum albumin standard series. These

methods typically yielded 1.4 mg MaAHAS_CSU1, 200 µg MaAHAS_RSU1.1 and 230 µg MaAHAS_RSU1.2 per 300 mL of culture. Proteins were verified by SDS-PAGE analysis and via sequencing at the Michigan State University Research Technology Support Proteomics Facility.

Initial tests found that removal of the GST tag from the regulatory subunits was unnecessary for catalytic activity or inhibition, consistent with previous studies (Xing & Last, 2017) (Lee & Duggleby, 2001), and thus cleavage was not performed.

Holoenzymes were prepared *immediately* before use. First, 0.00204 nmoles catalytic subunit with 0.051 nmoles regulatory subunit in 10 µL per reaction balanced with water were incubated for 10 min at 30 ℃. 142 µL of freshly made cofactor buffer (295.8 mM potassium phosphate pH 7.5, 1.48 mM thiamine diphosphate, 14.8 µM flavin adenine dinucleotide, 14.8 mM $MgCl_2$) was then added to the enzymes and incubated for 10 min at 30 ℃. The activated holoenzyme was added at a rate of 152 µL to 58 µL of substrate. Thus the final concentrations of the 210 µL reaction were: 9.71 nM catalytic subunit, 242.86 nM regulatory subunit, 200 mM potassium phosphate pH 7.5, 1 mM thiamine diphosphate, 10 µM flavin adenine dinucleotide, 10 mM $MgCl_2$). Reactions were then incubated for 40 min at 30 ℃. If not quenched immediately, the reaction was stopped and stored via immersion in liquid nitrogen.

The reactions were measured with a modified Voges-Proskauer test. 25 µL of 3M H_2SO_4 was added to quench the frozen reactions followed by incubation for 20 min at 60 ℃ to convert acetolactate to acetoin. 250 µL of 1:1 (freshly dissolved 1.25% α-naphthol in 10M NaOH):(0.5% creatine) was then added and incubated for 30 min at 60 ℃ to develop a pink color. Samples were well mixed for the oxidative reaction to progress. Non-proteinogenic precipitates were pelleted via centrifugation (21000 × g for 5 min) before absorbance was measured without delay at 525 nm. Product was quantified by subtraction against identical reactions without enzyme and with an eight-part acetoin standard series ranging from 0 to 0.12 mM acetoin in 485 µL that included cofactor and desalt buffer to mimic the reactions as closely as possible.

The holoenzyme was found to have linear activity through 50 min. For each experiment (kinetics, valine inhibition, leucine inhibition, etc.), each reaction was performed in triplicate using the same enzyme preparation. Due to the inhibitory effects observed when more than 20 mM Na pyruvate was present, kinetics parameters were calculated from reactions consisting of 5,

6.66, 10, and 20 mM Na pyruvate. All amino acid inhibitory studies were done with 20 mM Na pyruvate.

Isopropylmalate synthase

Methods for the expression and testing of IPMS was inspired by (de Kraker, Luck, Textor, Tokuhisa, & Gershenzon, 2007) and (Xing & Last, 2017).

MaIPMS.1 and .2 were amplified from cDNA derived from ripe banana fruit pulp to include 5' NcoI and 3' XhoI splice sites and to exclude the predicted chloroplast targeting peptide (Emanuelsson, Nielsen, & Von Heijne, 1999). CloneJET1.2 constructs were screened for colonies of each splice form. Inserts were subsequently cloned into the NcoI and XhoI splice sites of pET-28 (Novagen) resulting in constructs with C-terminal 6X His-Tags.

To generate mutated versions of MaIPMS, gBlock gene fragments (IDT) were designed and ordered to incorporate the desired modifications into a sequence of the region to be modified spanning from two naturally occurring restriction sites, BsaI and MfeI. The region was then replaced in the MaIPMS.1 pET28 vector to produce MaIPMS.PV523-524AA and MaIPMS.α14del.

MaIPMS.1 and these mutated versions then additionally clone into a custom DE3 vector using LIC sites added via PCR. The vector, termed pAL-MBP, which was graciously given by Dr. Ning Zheng of University of Washington, is comparable in machinery to the pET vector line (Novagen), save for cam^R, and results in proteins with N-terminal 6X His-Tag, MBP tag, and TEV cut site.

To produce protein, the pET vectors were transformed in Rosetta™ 2(DE3)pLysS cells and the pAL vectors in BL21 Star™ (DE3) cells and incubated overnight in LB (Miller) media with 50 µg/mL kanamycin and/or at 37 ℃, 250 rpm. The following morning this was used at a rate of 0.05 mL inoculum per mL culture to inoculate 300 mL batches of fresh LB (Miller) with antibiotics in 1 L Erlenmeyer flasks. These were grown at 37 ℃, 250 rpm until reaching an OD_{600} of 0.8 – 0.9 whereupon the cultures were chilled at 1 ℃ for 10-15 min before the collection of a pre-induced sample. The cells were subsequently induced with 357 µM isopropyl β-D-1-thiogalactopyranoside (IPTG) and incubated at 16 ℃, 250 rpm overnight. Cells were collected by centrifugation (2500 × g for 30 min at 4 ℃). Pellets were held at -80 ℃ before extraction.

Cells were resuspended at 5 ℃ at a 25-fold concentration factor with lysis buffer (50 mM Tris-HCl, pH 8, 300 mM NaCl, 5 mM $MgCl_2$, 15% glycerol, 1 mg/mL lysozyme, 1 U/mL

Benzonase® Nuclease) and incubated on a linear wave rocker for 30 min. Each 300 mL equivalent of culture was then sonicated at 5 ℃ for two 7.5 min regiments of 50% power, 50% pulse with the sonication tip immersed to 1.5-times tip diameter (Omni Ruptor 250) while the sample was immersed in ice-water. Samples were cooled in ice water for at least 30 min in-between sonications. Samples of the crude lysate were then collected before centrifugation (12500 × g for 15 min at 4 ℃) to pellet insoluble material. A sample of cleared lysate was then collected before incubation with resin equilibrated with the appropriate construct's wash buffer (specifics described below).

pET proteins were extracted via the C-terminal 6X His-Tag with Ni-NTA agarose (Qiagen). Wash buffer: 50 mM Tris-HCl pH 8, 300 mM NaCl, 30 mM imidazole, 5 mM $MgCl_2$. Elution buffer: 50 mM Tris-HCl pH 8, 300 mM NaCl, 200 mM imidazole, 5 mM $MgCl_2$.

pAL proteins were extracted via the N-terminal MBP tag with amylose resin (NEB). Wash buffer: 50 mM Tris-HCl pH 8, 300 mM NaCl, 5 mM $MgCl_2$. Elution buffer: 50 mM Tris-HCl pH 8, 300 mM NaCl, 10 mM maltose, 5 mM $MgCl_2$.

Cleared lysate was incubated with 0.5 mL of appropriate resin per 300-600 mL culture for 1-2 hours at 5 ℃ on a linear wave rocker. Collection of 'flow-through' and all resin wash or elution steps were performed by centrifugation of the resin (1000 × g for 2 min at 4 ℃) followed by aspiration of the supernatant. Following incubation, cleared lysate (flow-through) was separated from the resin as above-described. The resin was then washed twice with 5 mL of appropriate wash buffer followed by five 0.5 mL elutions. All five elutions were desalted with PD-10 desalting columns packed with Sephadex G-25 resin (Cytiva) via the manufacturer's spin protocol into desalt buffer (50 mM Tris pH 8.0, 5 mM $MgCl_2$, 15% glycerol). This finished product was then quantified via Bradford assay against a bovine serum albumin standard series. These methods typically yielded 1 mg MaIPMS.1-His, MaIPMS.PV523-524AA-His, His-MBP-MaIPMS.1, and His-MBP-MaIPMS.PV523-524AA per 300 mL of culture. MaIPMS.α14del was most reliably extracted with the His-MBP version, resulting in an average of 350 µg per 300 mL of culture. Proteins were verified by SDS-PAGE analysis and via sequencing at the Michigan State University Research Technology Support Proteomics Facility.

There was considerable difficulty in expressing MaIPMS.2. Decreased induction temperatures (10 ℃), different cell lines (Rosetta-gami™ 2 (DE3), and added tags (MBP) were among the attempted modifications that did not lead to any soluble protein. GST tags were

avoided as any trace carryover of the reduced glutathione needed for elution would react with the reaction indicator, described below, and lead to over-exposure on our spectrophotometer.

All reactions were prepared daily with fresh enzyme preparations. Substrates solutions were prepared daily or from -80 ℃ stored Li Acetyl-CoA aliquots. The 150 µL reactions were composed of 20 µL enzyme and 130 µL of substrate and buffer. Equal molar mixtures of enzymes were pre-mixed and held on ice. The final reaction concentrations were 0.032 nmoles enzyme, 100 mM Tris HCl pH 8.0, 4 mM $MgCl_2$, and substrate. Standard substrate conditions were composed of 10 mM sodium α-ketoisovalerate and 0.25 mM lithium acetyl-CoA. Removal of the tags was deemed unnecessary as the enzymes maintained similar properties with or without them, however pET proteins were found to be linear through 20 min and pAL proteins linear through 40 min. Thus pET protein reactions were performed for 15 min whereas pAL proteins for 30 min. The reactions were initiated by pipetting the enzyme mixture into the lid of micro-centrifuge tubes containing the substrate and buffer mixture. The reactions were then initiated by briefly centrifuging at 10000 × g for 10 sec before incubation at 30 ℃. Reactions were stopped by placing the tubes in liquid nitrogen and held overnight before analysis.

The reactions were measured via the reaction of the freed thiol groups of coenzyme A with 5,5′-dithiobis-(2-nitrobenzoic acid) (DTNB). The frozen reactions were quenched with 200 µL 100% ethanol followed by the addition of 200 µL 100 mM Tris HCl pH 8.0, 1 mM DTNB. The samples were well mixed by inversion and allowed to incubate at room temperature for ~30 min to allow yellow color development. Absorbance was measured without delay at 412 nm. Product was quantified against identical reactions without α-ketoacid, or, when α-keto-γ-(methylthio) butyrate was tested, against identical reactions without acetyl-CoA. The content of the yellow 3-carboxy-1-nitrothiophenol anion was quantified with ε_{412} of 14140 $M^{-1} \cdot cm^{-1}$ (Kohlaw, 1988).

The kinetics with α-ketoisovalerate were tested with 0.33, 0.45, 0.66, 1.33, and 16 mM sodium α-ketoisovalerate, however these values were not found to be low enough to sufficiently reduce MaIPMS.1 activity and thus 0.01, 0.05, 0.1, 0.2, and 8.67 mM sodium α-ketoisovalerate were also used. The kinetics with acetyl-CoA were tested with 0.0166, 0.02, 0.0286, 0.05, and 0.2 mM lithium acetyl-CoA. Leucine inhibition was tested with 0, 0.01, 0.025, 0.05, 0.1, 0.5, 1, and 5 mM leucine. Tests of substrate preference used 10 mM of the following α-ketoacids:

sodium α-ketoisovalerate, sodium α-ketoisocaproate, sodium pyruvate, α-ketobutyric acid, α-ketovaleric acid, sodium α-keto-γ-(methylthio) butyrate.

Transient expression in *Nicotiana benthamiana*

Methods for transient expression in tobacco were inspired by (Bedewitz, Jones, D'Auria, & Barry, 2018) and (Sugimoto, Engelgau, Jones, Song, & Beaudry, 2021).

Nicotiana benthamiana seeds were sown in covered tray of Greenworld potting mix (ASB, Mount Elgin, Ontario). After the second true leaf plants were transplanted to four-inch square pots filled with Greenworld potting mix and grown in a growth room at 23 °C under fluorescent lights (145 μmol m^{-2} s^{-1}) under a 16-h photoperiod and were supplemented with full-strength Hoagland's solution.

MaAHAS_CSU1, MaAHAS_RSU1.1, MaAHAS_RSU1.2, MaIPMS.1, MaIPMS.2, and MaIPMS.PV523-524AA were cloned from protein expression vectors into a modified pEAQ vector (Sainsbury, Thuenemann, & Lomonossoff, 2009) containing the chloroplast target peptide sequence of *Arabidopsis thaliana* ribulose bisphosphate carboxylase small chain 1A (At1g67090) via restriction site cloning. The constructs were cloned into *Agrobacterium tumefaciens* strain LBA4404 and incubated with 50 μg/mL kanamycin and 150 μg/mL rifampicin overnight at 30°C, 250 rpm in YEB buffer (5 g/L beef extract, 1 g/L yeast extract, 5 g/L peptone, 5 g/L sucrose, 0.5 g/L $MgCl_2$). The following day these were diluted 1:25 into fresh YEB containing antibiotics and grown overnight at 30 °C, 250 rpm.

The following day the cells were pelleted (2500 × g, 10 min , 22 °C) and gently resuspended in ½ volume infiltration buffer (10 mM $MgCl_2$, 10 mM MES KOH pH 5.6) before repelleting and resuspending in infiltration buffer. The cells were then diluted to an OD_{600} = 1 before induction with 200 μM acetosyringone for 4 hours, 22 °C and gentle rocking. If gene stacking were desired then appropriate cultures were mixed in equal parts.

Three full-sized leaves were completely infiltrated per plant with 1 mL syringes. After 6 days the leaves were collected and flash frozen in liquid nitrogen before being held at -80 °C for further analysis.

Metabolites were extracted and analyzed as described above for banana pulp, however only 100 mg of tissue was extracted and only 100 μL of each derivatizing reagent was used.

Genes and protein models used in this study

Banana loci are from the DH-Pahang genome v2 (Martin, et al., 2016). MaAHAS_CSU1: Ma06_t18100, MaAHAS_CSU2: Ma10_t11980, MaAHAS_RSU1: Ma06_t14010, MaAHAS_RSU2: Ma06_t30380, MaIPMS: Ma08_t09270. MaDNAJ GeneBank: HQ853242, MaRPS4 GeneBank: HQ853247. MaAHAS_RSU1.2 transcript from (Asif, et al., 2014): XM_009406005.

Predictive modeling was performed with ColabFold (Mirdita, et al., 2022) with sequences lacking predicted chloroplast targeting peptides (Emanuelsson, Nielsen, & Von Heijne, 1999). Proteins were aligned with Clustal Omega (Sievers, et al., 2011) and diagrammed with ESPript 3.0 (Robert & Gouet, 2014).

Arabidopsis AHAS: At2g31810. Cryo-electron microscopy structure with bound valine (PDB 6VZ8) (Lonhienne, et al., 2020). Tuberculosis IPMS: LeuA. Crystal structure with bound leucine (PDB 3FIG) (Koon, Squire, & Baker, 2004).

Figures & Tables

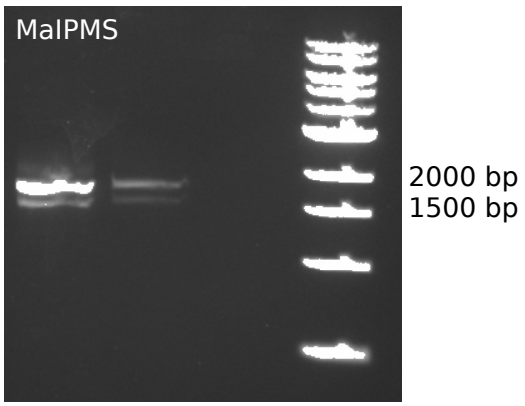

Figure 4.1: Initial discovery of *MaIPMS* alternative splicing from the amplification of *MaIPMS* from ripe banana pulp cDNA. Left most lanes are of different biological reps. bp = base pair.

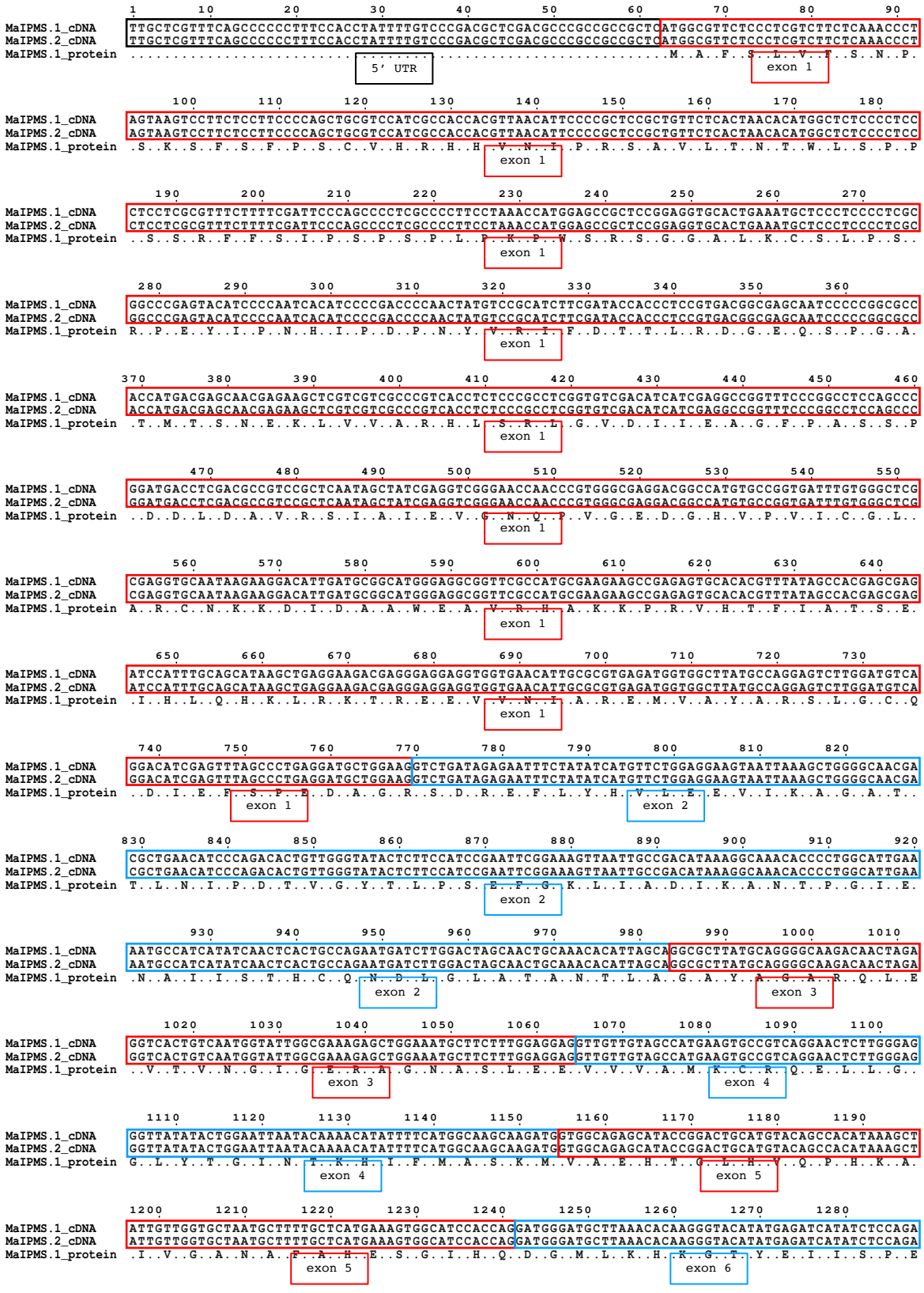

Figure 4.2: DNA and protein sequences of MaIPMS.

Figure 4.2 (cont'd)

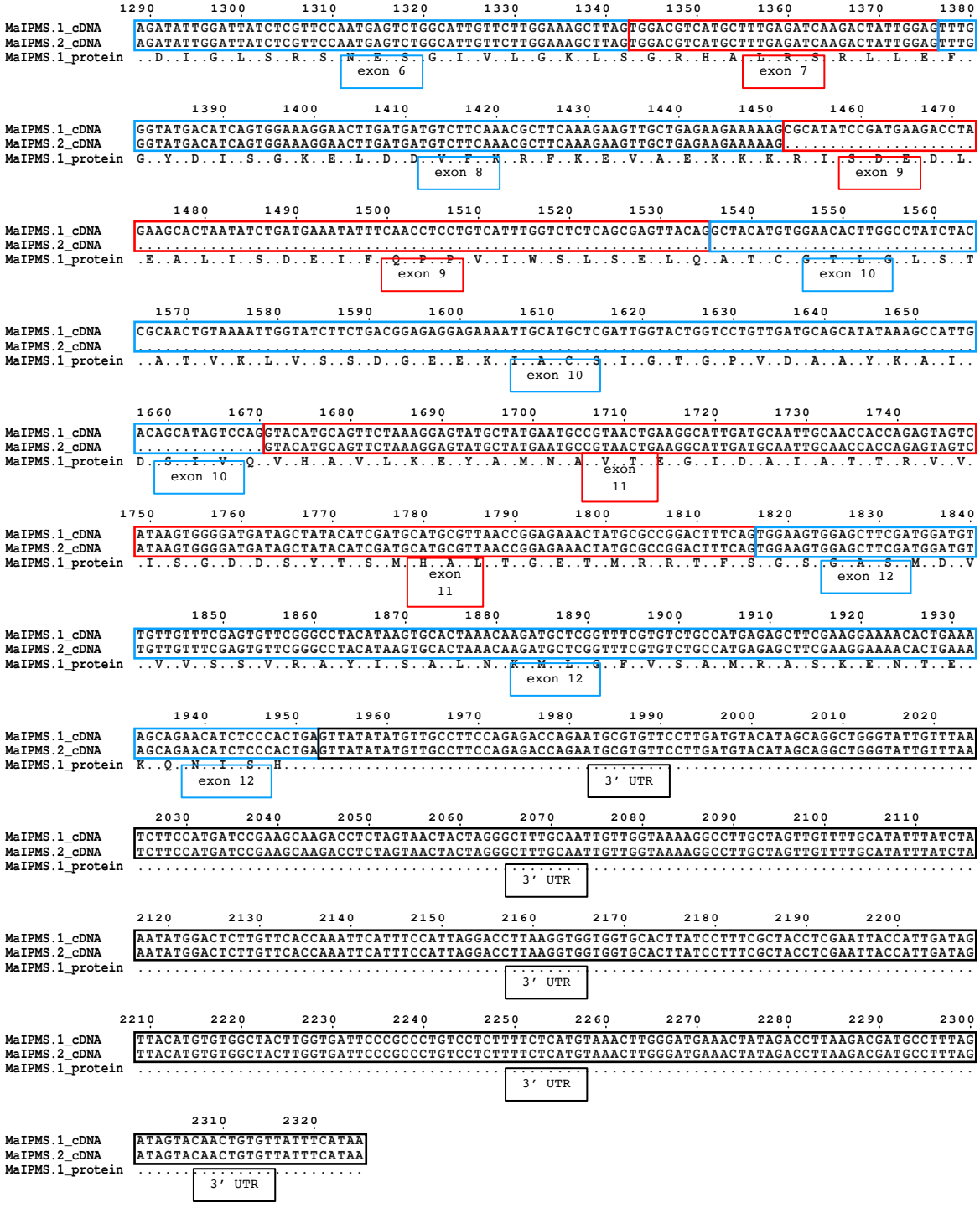

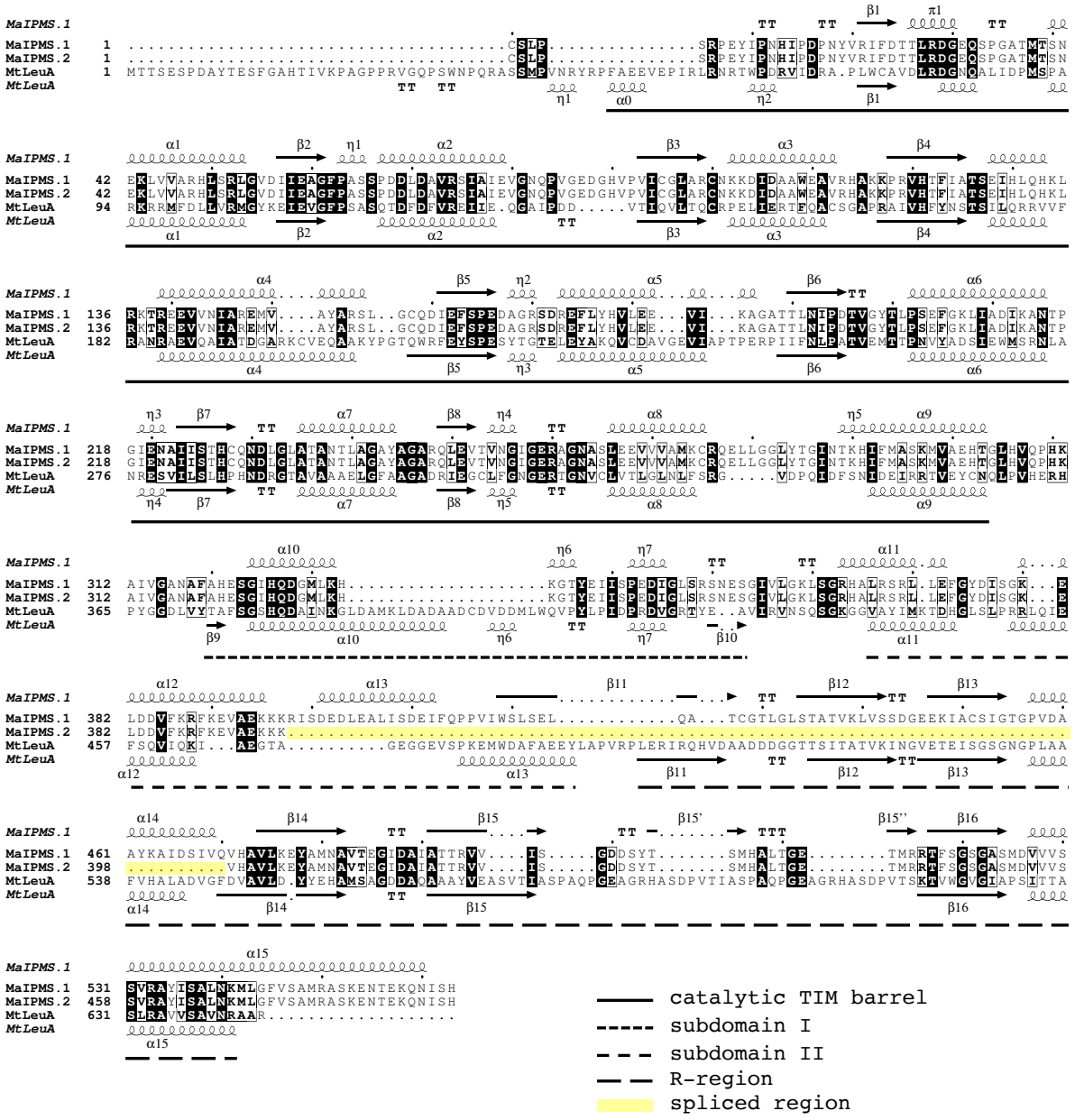

Figure 4.3: Alignment of MaIPMS.1 predicted structure, MaIPMS.2 sequence, and *Mycobacterium tuberculosis* IPMS crystal structure (MtLeuA). Nomenclature of secondary structures follows that of Koon et al. (2004). Plant sequences are without their predicted chloroplast targeting peptides.

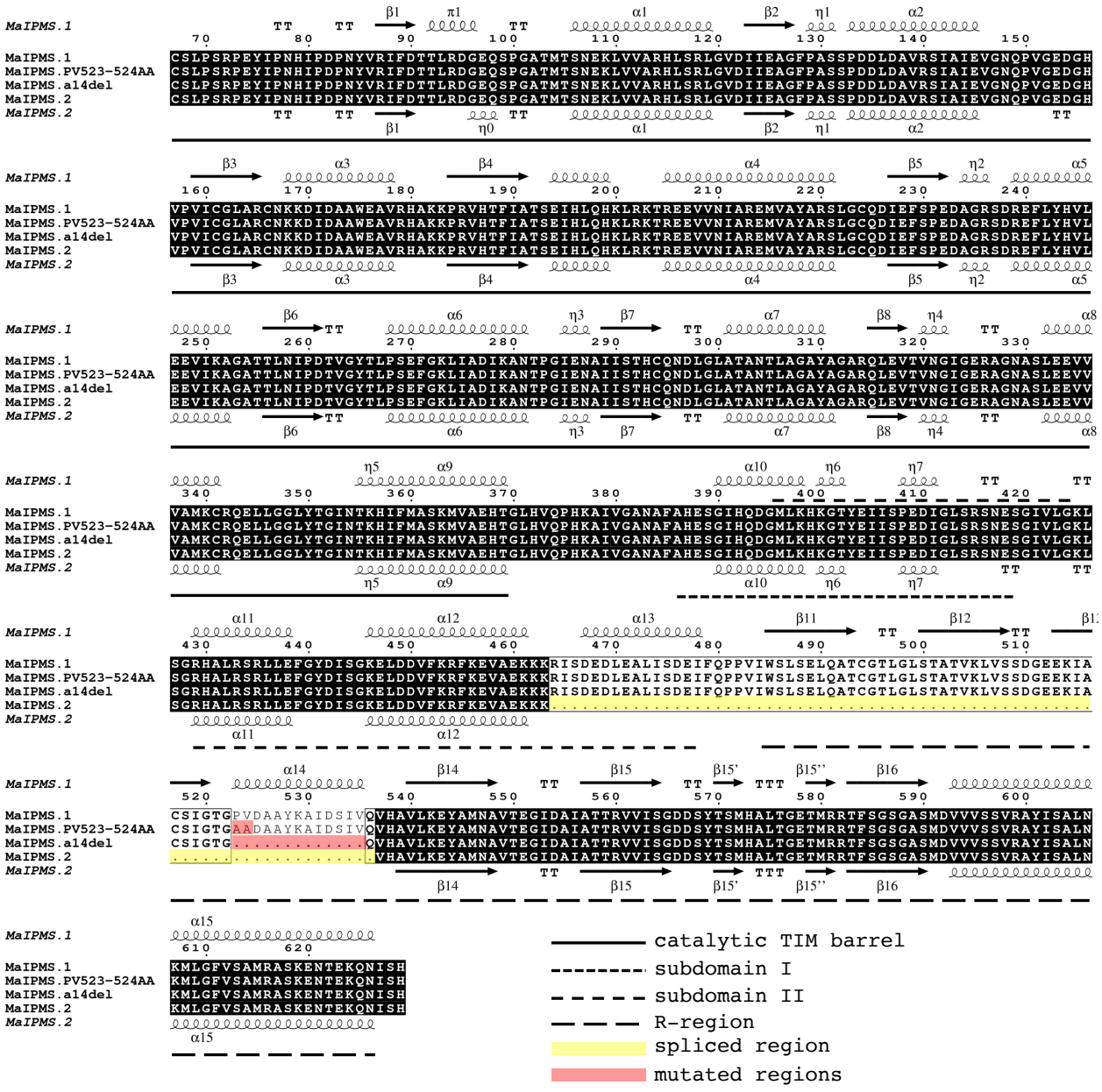

Figure 4.4: Alignment of predicted MaIPMS.1 structure, predicted MaIPMS.2 structure, and prepared MaIPMS mutants. MaIPMS.1 sequence numbered in reference to start codon. Nomenclature of secondary structures follows that of Koon et al. (2004). Plant sequences are without their predicted chloroplast targeting peptides.

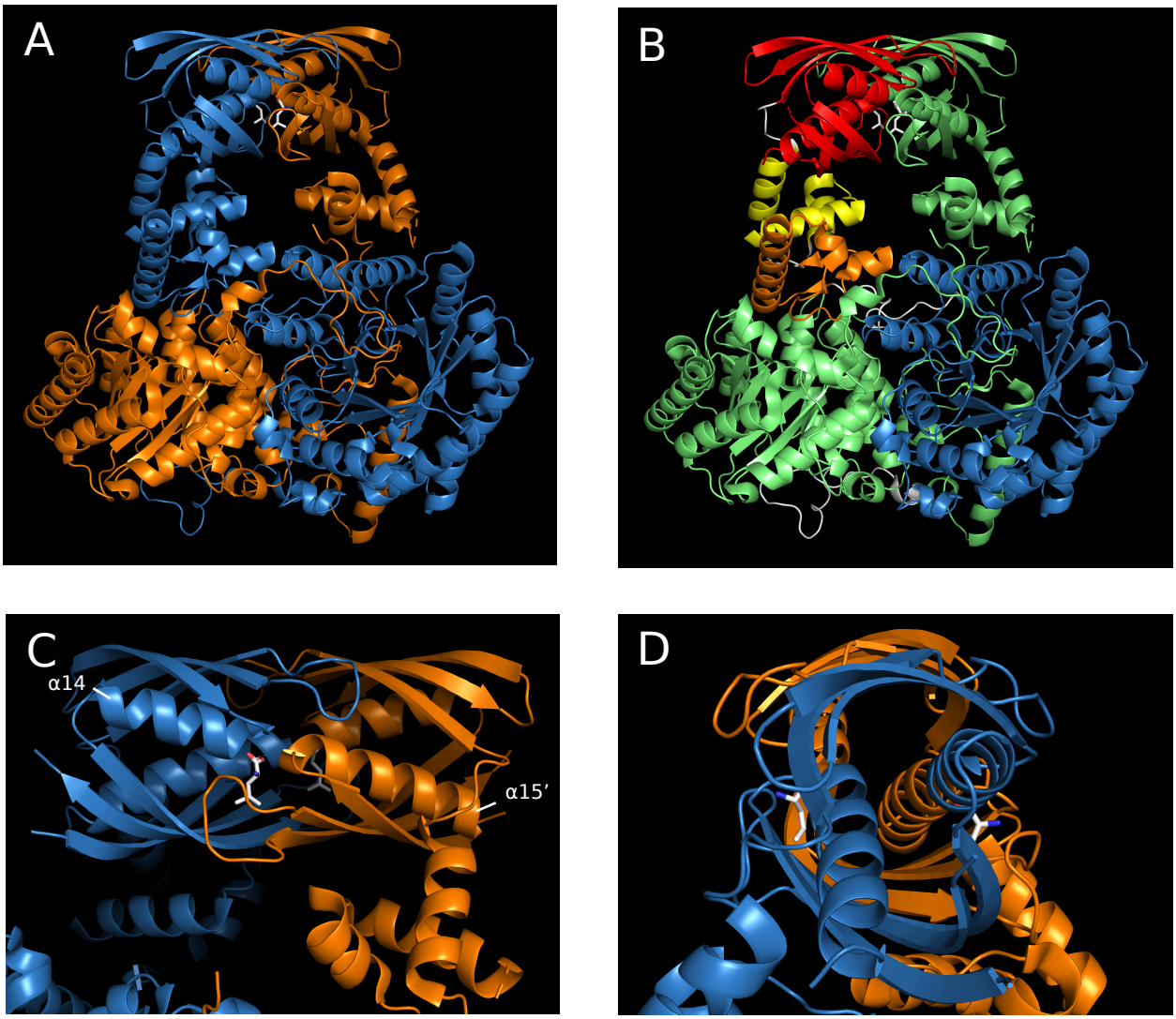

Figure 4.5: Crystal structure of *Mycobacterium tuberculosis* IPMS with bound leucine, adapted from Koon et al., 2004. A: Overview of the dimer. Monomers colored in orange and blue. B: Overview of dimer. One monomer in light green, of other monomer: catalytic domain is blue, subdomain I orange, subdomain II yellow, and regulatory (R)-domain red. C, D: Views of R-domain with bound leucine (white stick models) and critical α-helices labeled. Coloration as in A.

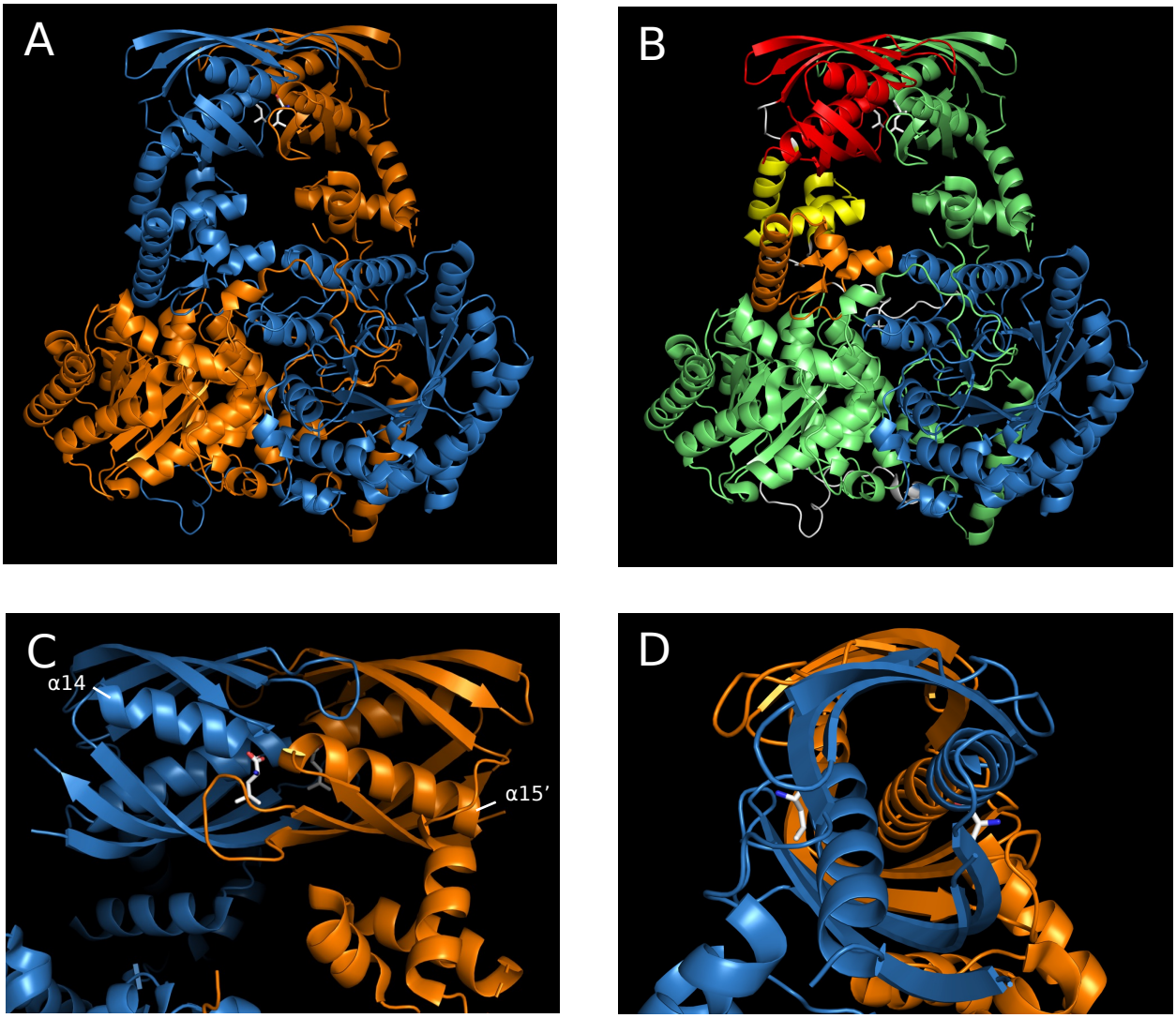

Figure 4.5: Crystal structure of *Mycobacterium tuberculosis* IPMS with bound leucine. A: Overview of the dimer. Monomers colored in orange and blue. B: Overview of dimer. One monomer in light green, of other monomer: catalytic domain is blue, subdomain I orange, subdomain II yellow, and regulatory (R)-domain red. C, D: Views of R-domain with bound leucine (white stick models) and critical α-helices labeled. Coloration as in A.

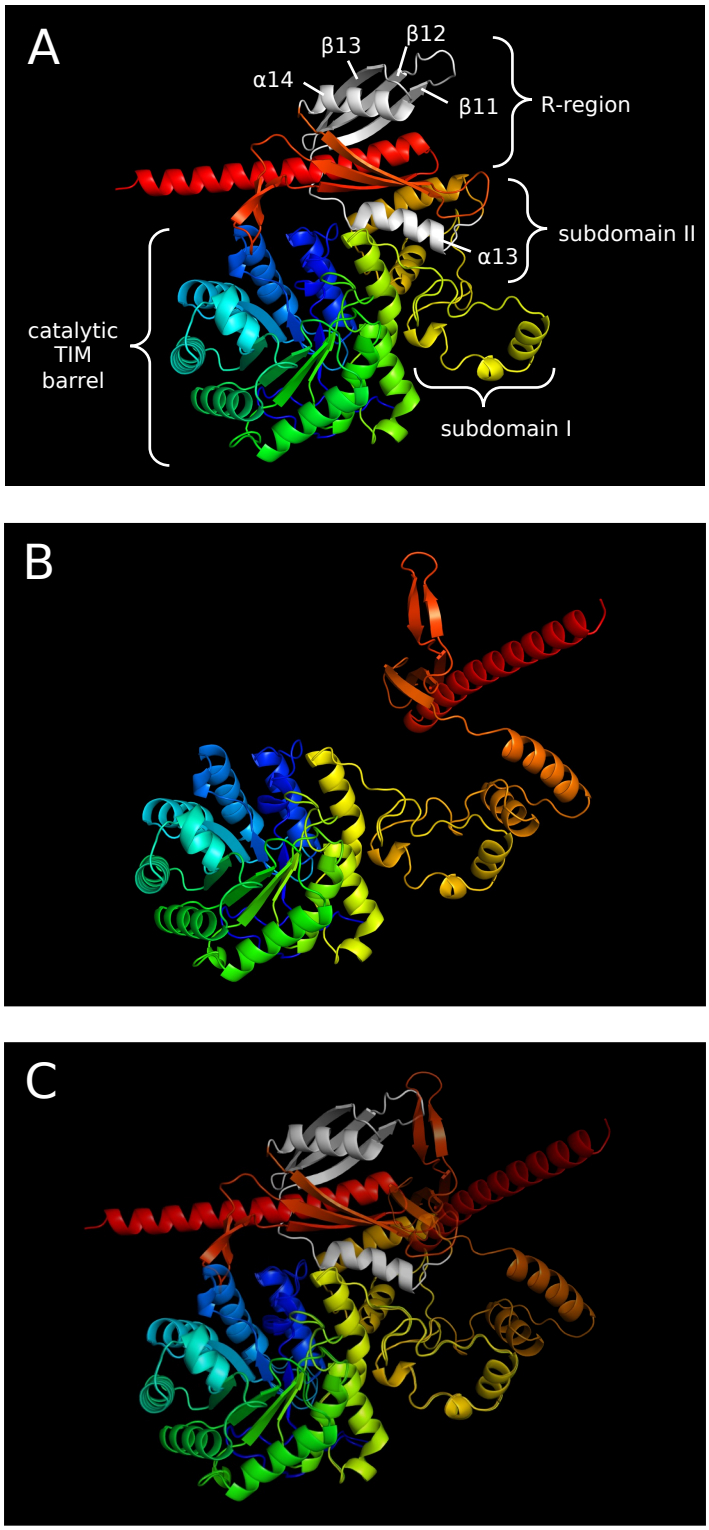

Figure 4.6: Predicted structures of MaIPMS.1 and MaIPMS.2. Enzymes are colored from blue to red (N to C-terminal). Spliced regions in white. A: MaIPMS.1 with domains and secondary structures of note labeled. B: MaIPMS.2. C: Overlay of predicted structures.

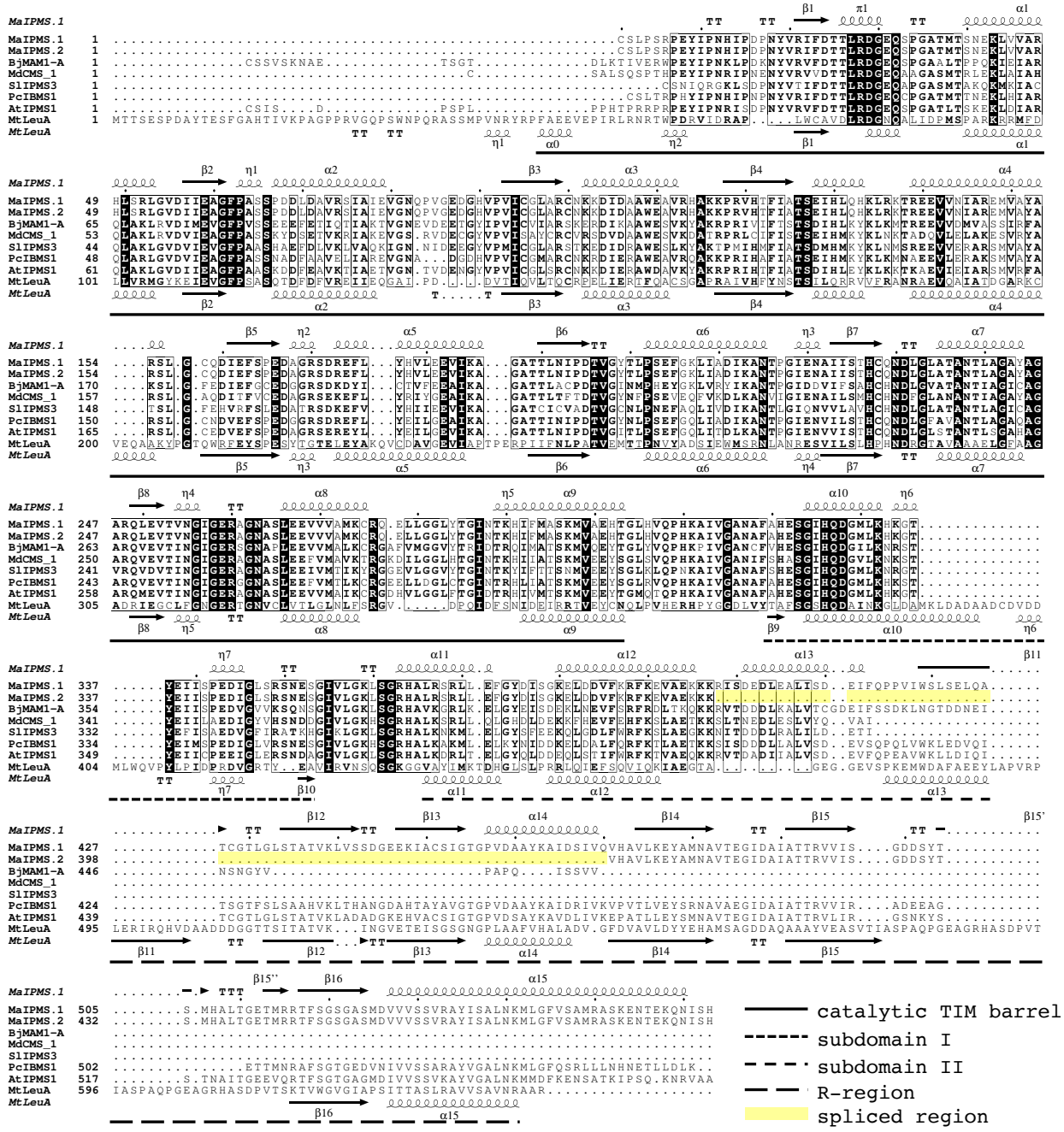

Figure 4.7: Alignment of IPMS and neofunctionalized IPMS enzymes against MaIPMS.1 predicted structure and *Mycobacterium tuberculosis* IPMS crystal structure (MtLeuA). Nomenclature of secondary structures follows that of Koon et al. (2004). Plant sequences are without their predicted chloroplast targeting peptides.

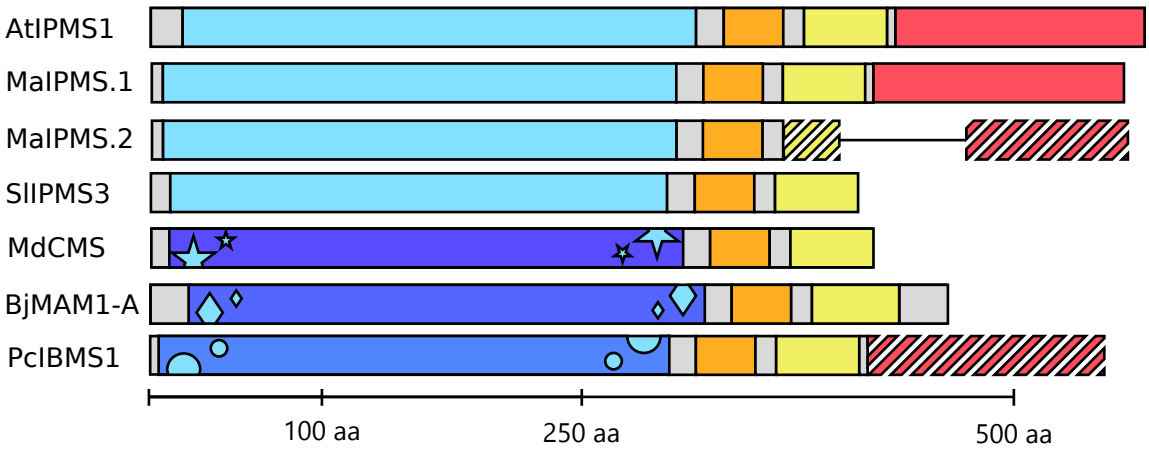

Figure 4.8: Schematic of IPMS and IPMS-neofunctionalized enzymes. Catalytic TIM barrel in light blue, subdomain I in orange, subdomain II in yellow, regulatory region in red. Domains with compromised functions or folds shown hashed. Darker catalytic domains signify modified substrate preference. Predicted chloroplast targeting peptides removed.

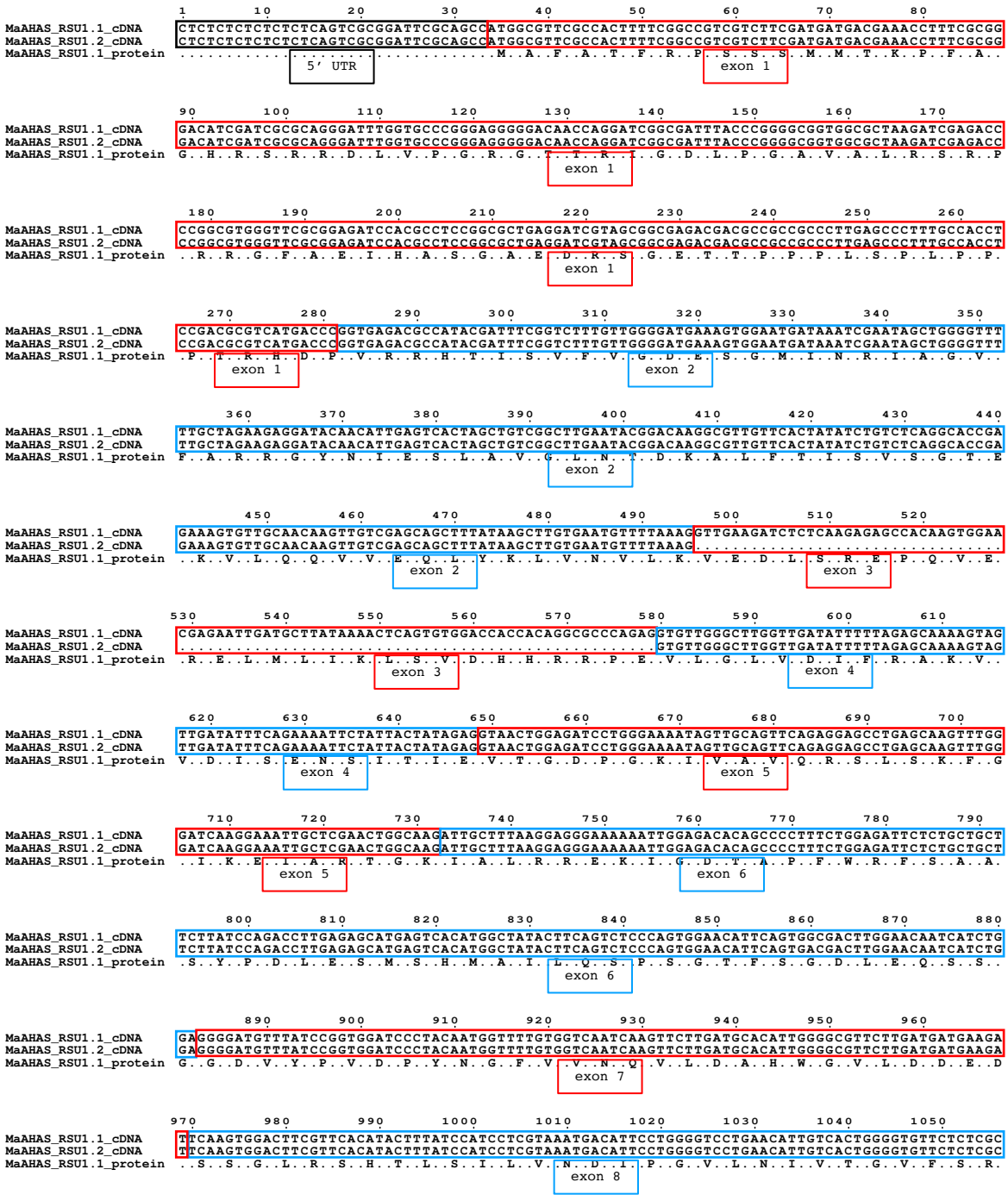

Figure 4.9: DNA and protein sequences of MaAHAS_RSU1.

Figure 4.9 (cont'd)

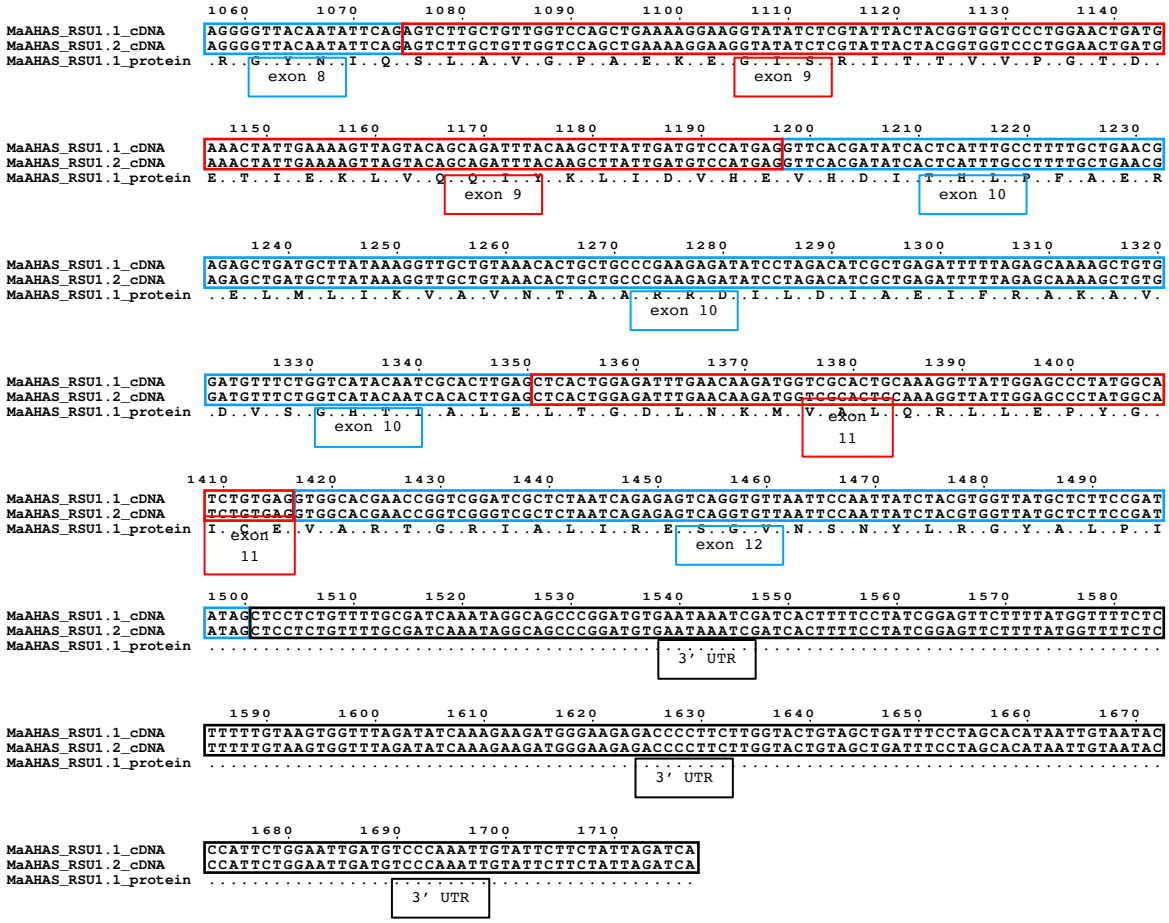

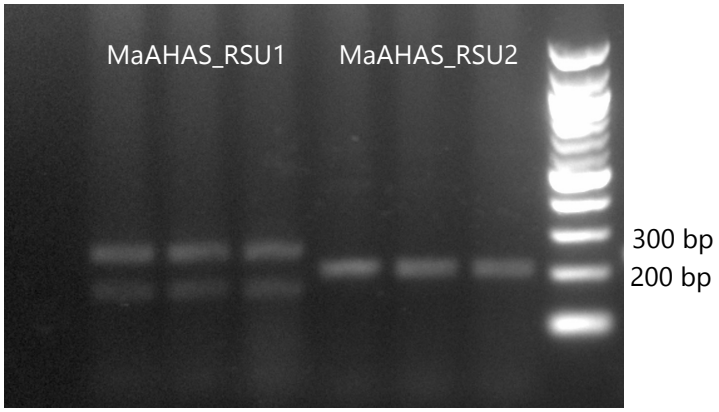

Figure 4.10: Results from investigation of MaAHAS_RSU splicing. Three biological reps are shown. bp = base pair.

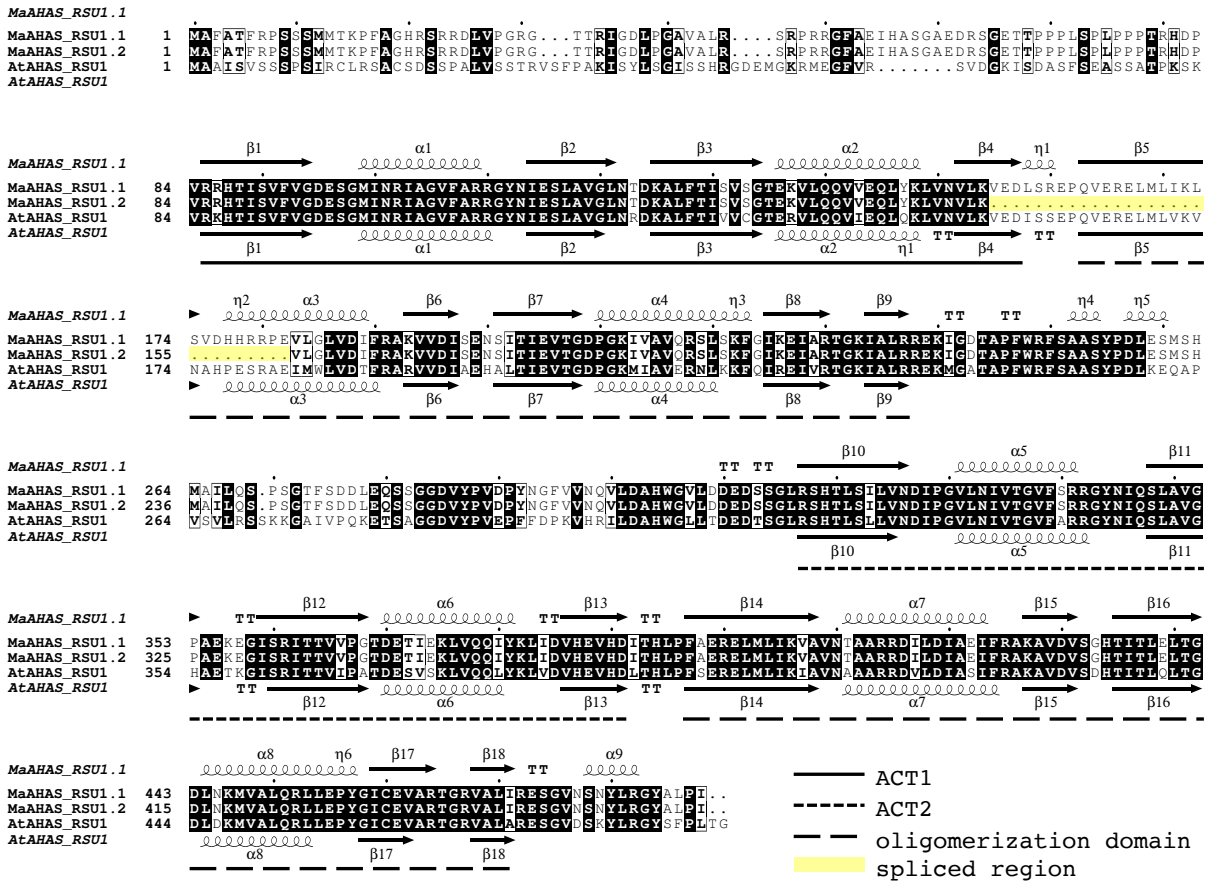

Figure 4.11: Alignment of predicted MaAHAS_RSU1.1 structure, MaAHAS_RSU1.2 sequence, and cryo-electron microscopy AtAHAS structure. Plant sequences are without their predicted chloroplast targeting peptides.

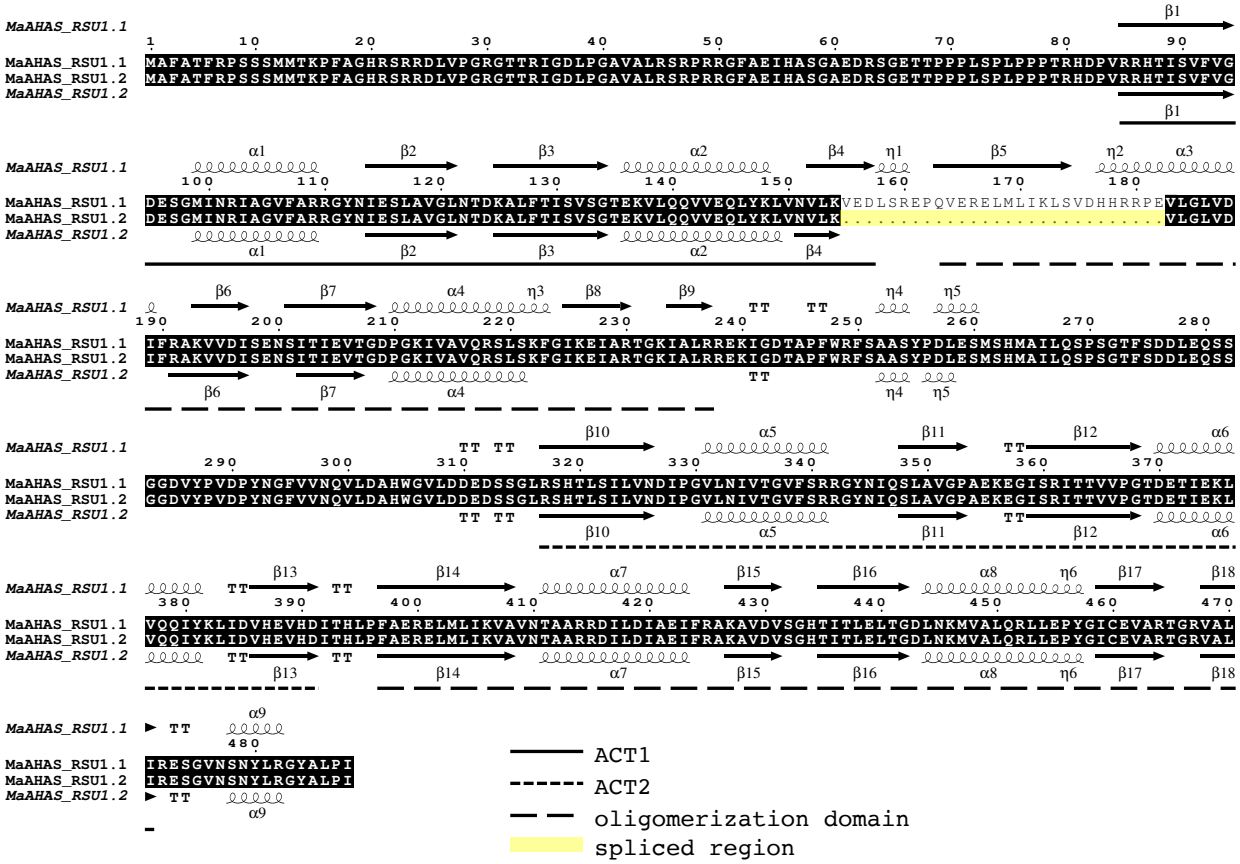

Figure 4.12: Alignment of predicted MaAHAS_RSU1 structures. Plant sequences are without their predicted chloroplast targeting peptides.

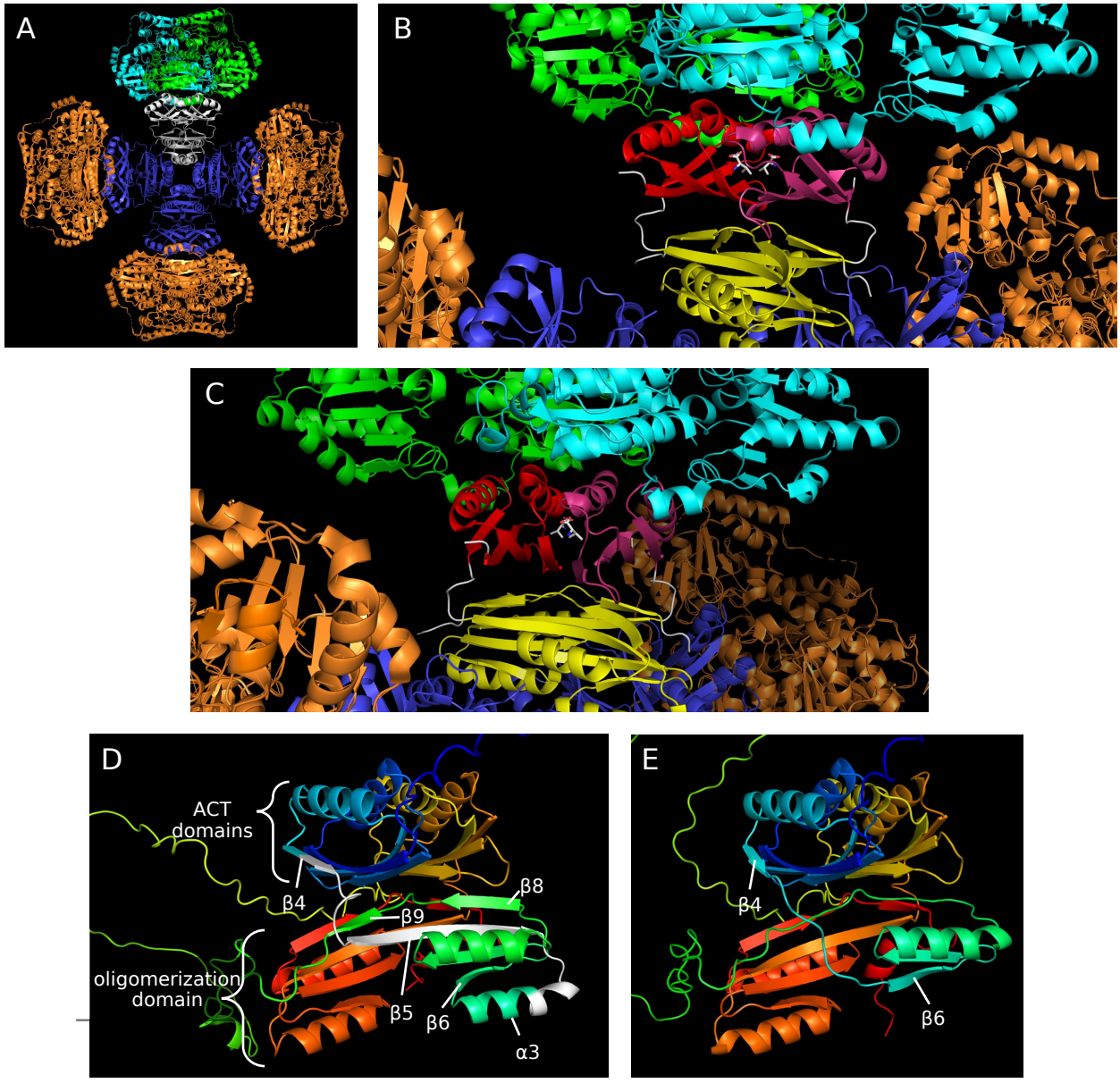

Figure 4.13: Cryo-electron microscopy structure of AtAHAS with bound valine and predicted MaAHAS_RSU1 structures. A: View of entire AHAS holoenzyme dodecamer. Three of the CSU-CSU-RSU trimers colored in orange, orange, and blue, respectively. Final trimer has CSUs in cyan and green, RSU in white. B, C: Zoom in of RSU. ACT domains colored in red and dark pink. Oligomerization domain colored in yellow. Valine as white stick models. D, E: Predicted structures of MaAHAS_RSU1.1 and MaAHAS_RSU1.2, respectively. Colored red to blue (N to C-terminal), spliced region colored in white. Domains of MaAHAS_RSU1.1 labeled. Secondary structures of note are labeled.

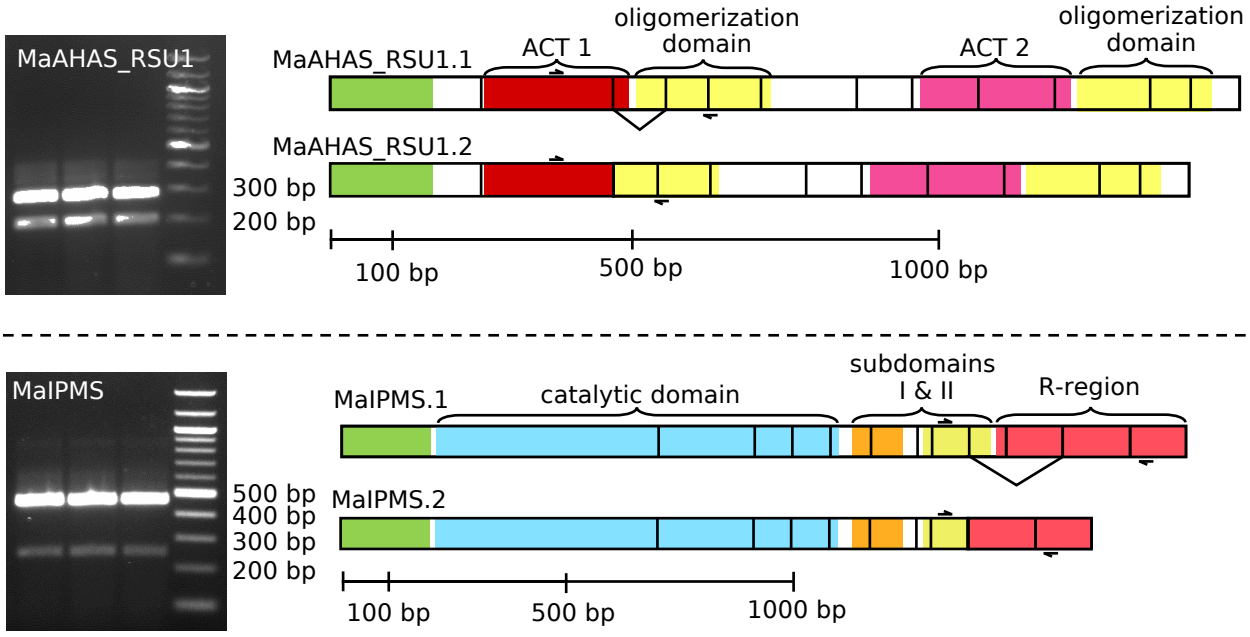

Figure 4.14: Schematic overview of the exon divisions of MaAHAS_RSU1 and MaIPMS isoforms as well as evidence of alternative splicing. Green domains represent predicted chloroplast targeting peptides. Gels depict three biological reps and the binding sites of primers used are indicated within the schematics. bp = base pair.

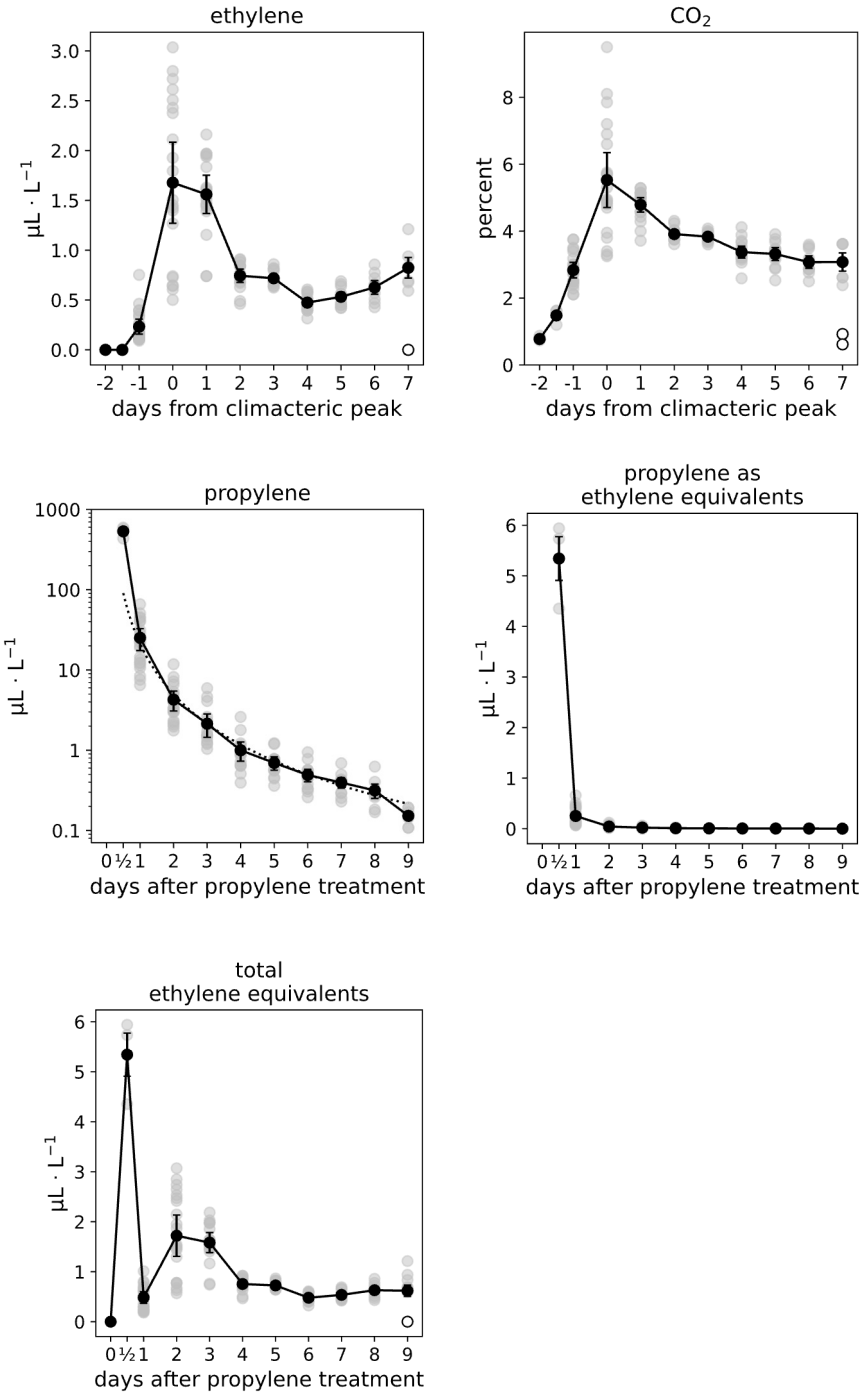

Figure 4.15: Internal gas concentrations of fruit treated with propylene. Different x-axes are used when logical. Propylene converted to ethylene equivalents with 100 µL · L^{-1} propylene to 1 µL · L^{-1} ethylene ratio (Burg & Burg, 1967). Presented as means ± ½ SD. Dotted black line follows fitted curve of propylene data. Ripening was initiated two days prior to climacteric peak with propylene.

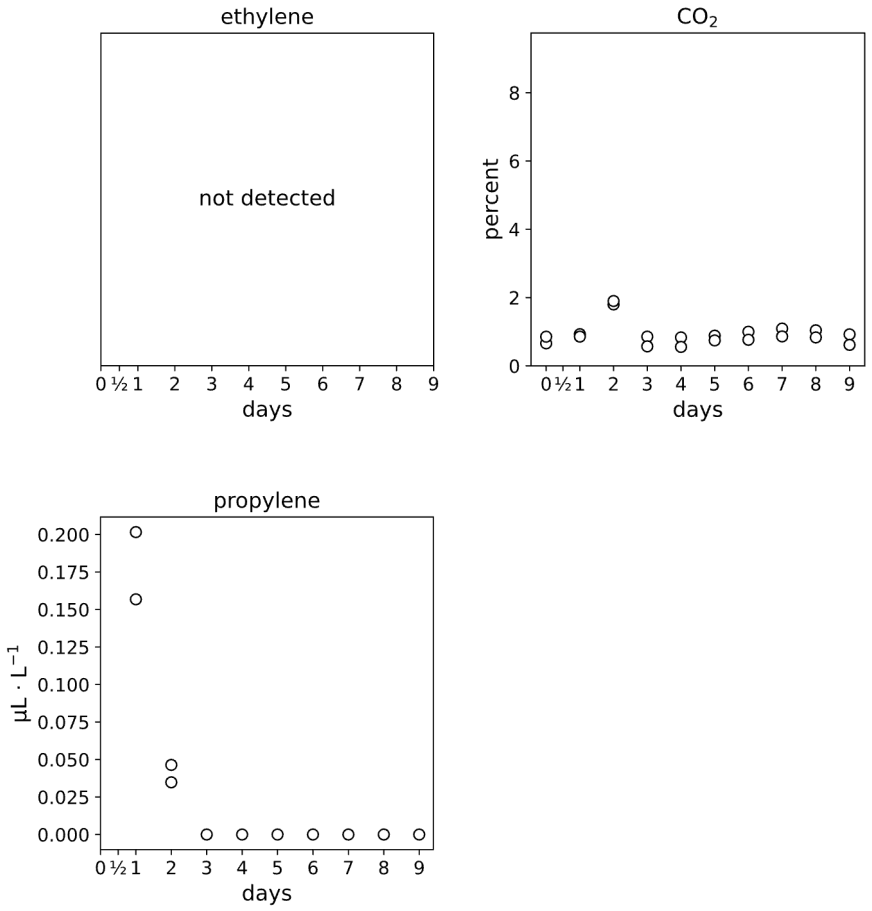

Figure 4.16: Internal gas concentrations of fruit not treated with propylene. Presented as individual data points.

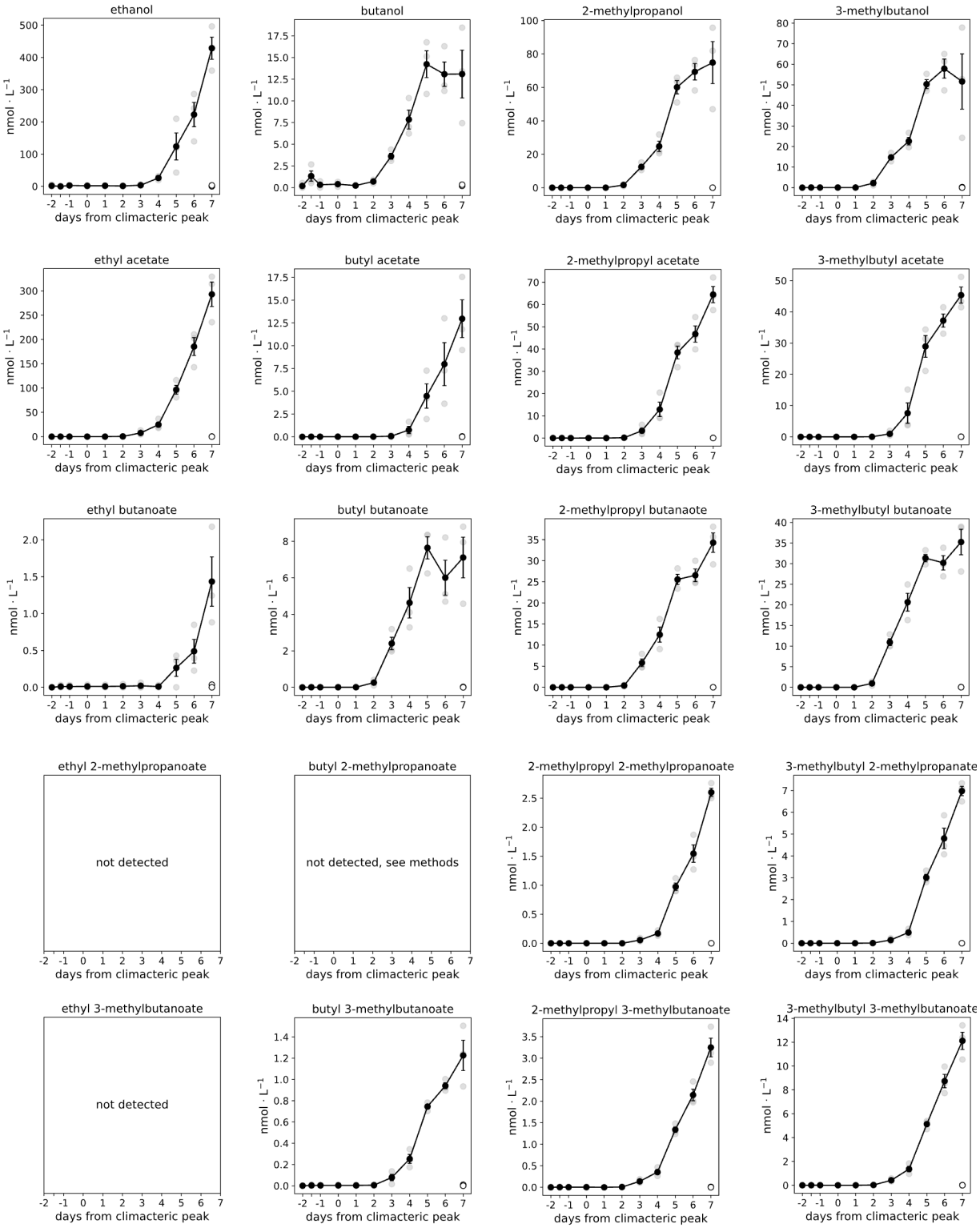

Figure 4.17: Headspace volatile concentrations. Presented as means ± ½ SD of three biological reps. Ripening was initiated two days prior to climacteric peak with propylene. Fruit not treated with propylene shown as open circles.

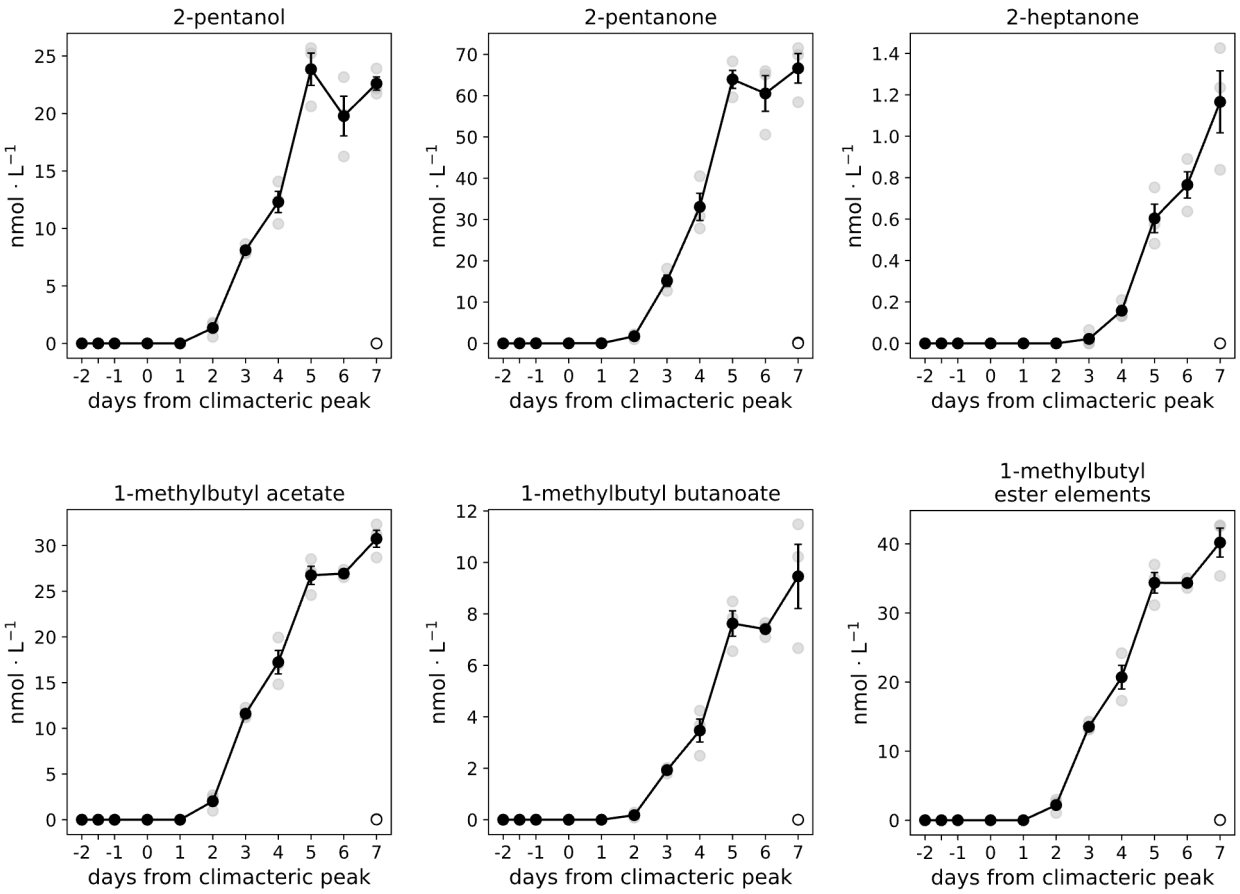

Figure 4.18: Headspace volatile concentrations of sec-branched compounds. Presented as means ± ½ SD of three biological reps. Ripening was initiated two days prior to climacteric peak with propylene. Fruit not treated with propylene shown as open circles.

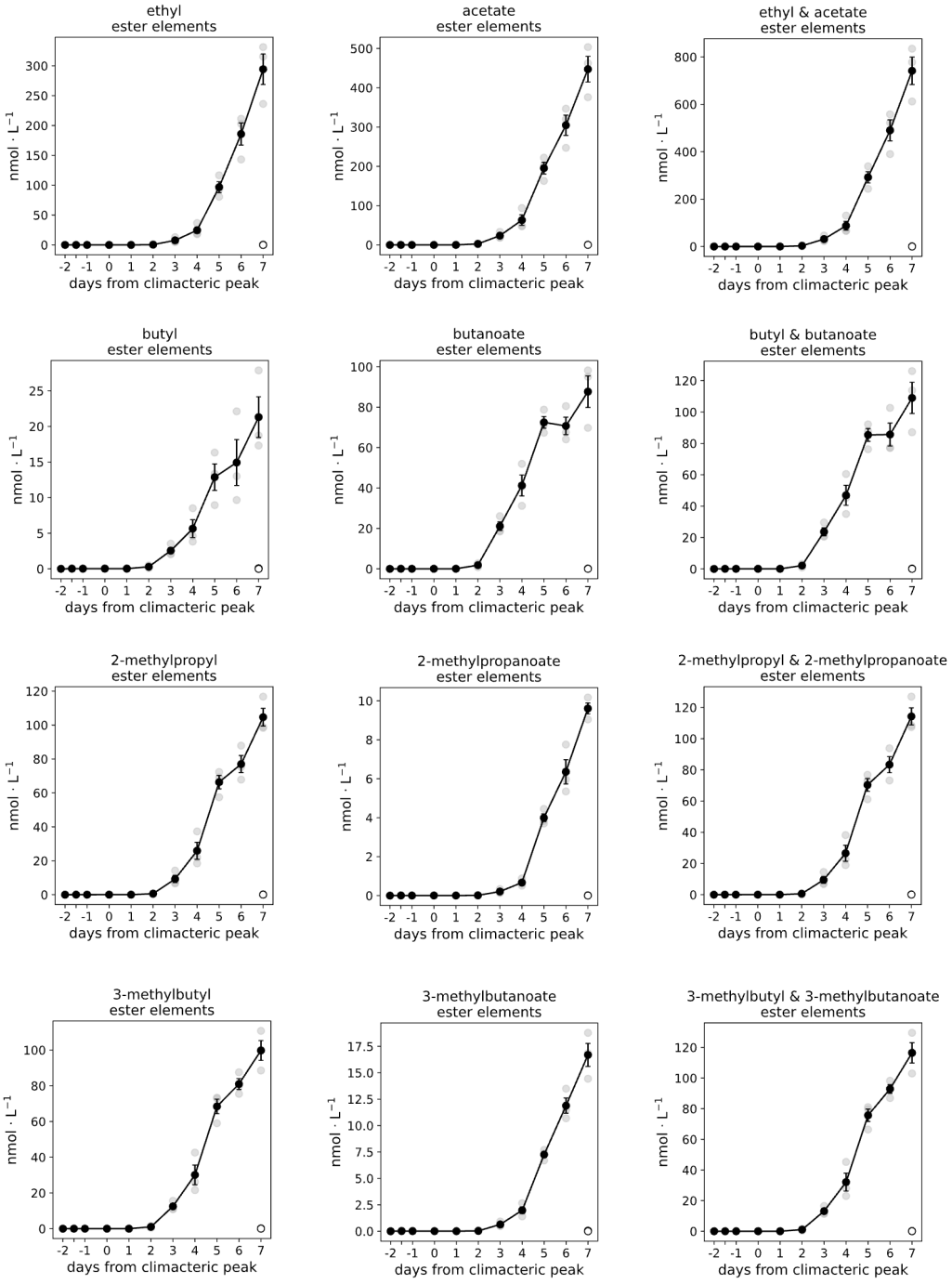

Figure 4.19: Summaries of ester elements in fruit headspaces. Presented as means ± ½ SD of three biological reps. Ripening was initiated two days prior to climacteric peak with propylene. Fruit not treated with propylene shown as open circles.

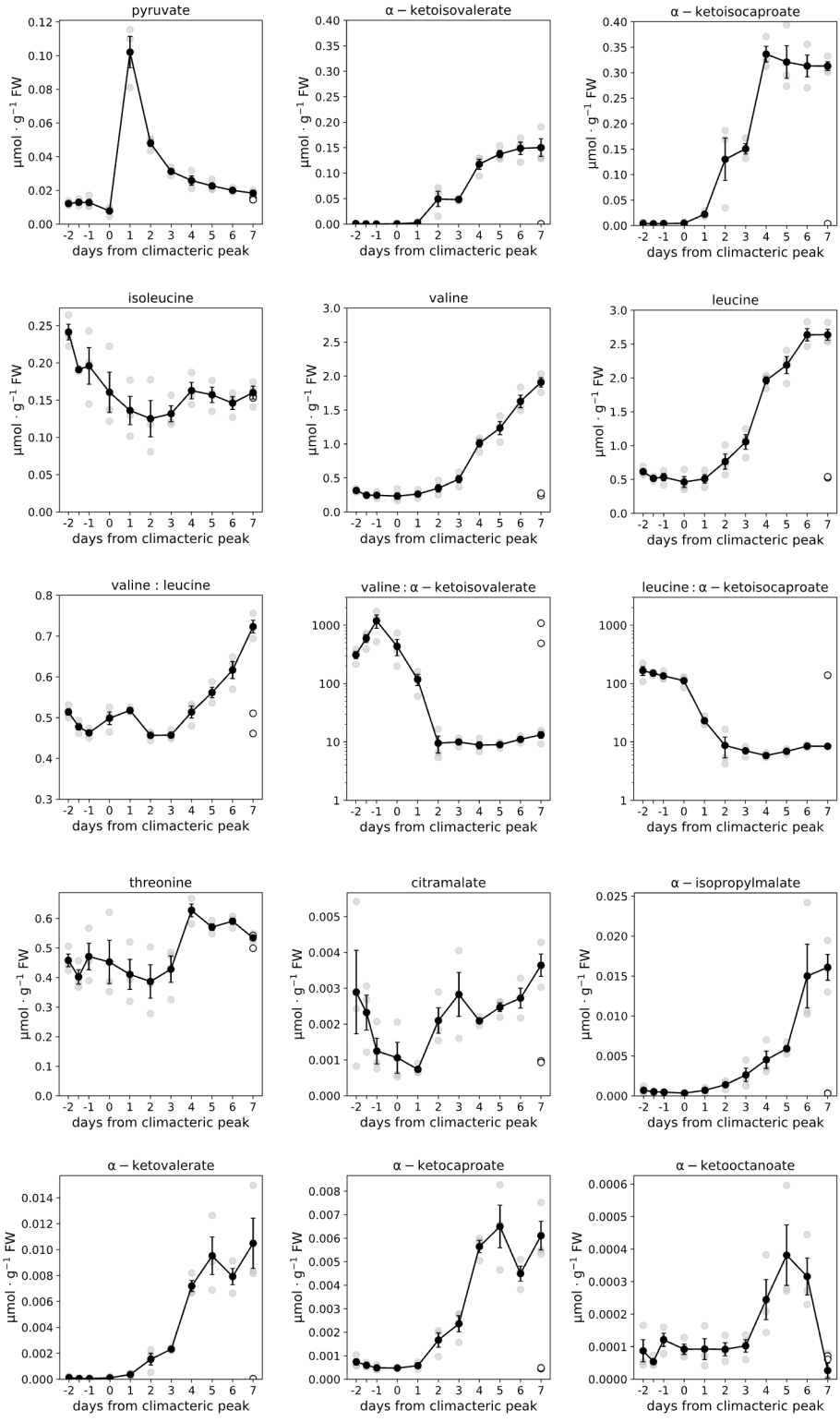

Figure 4.20: Concentrations of relevant metabolites in fruit pulp. Presented as means ± ½ SD of three biological reps. Ripening was initiated two days prior to climacteric peak with propylene. Fruit not treated with propylene shown as open circles.

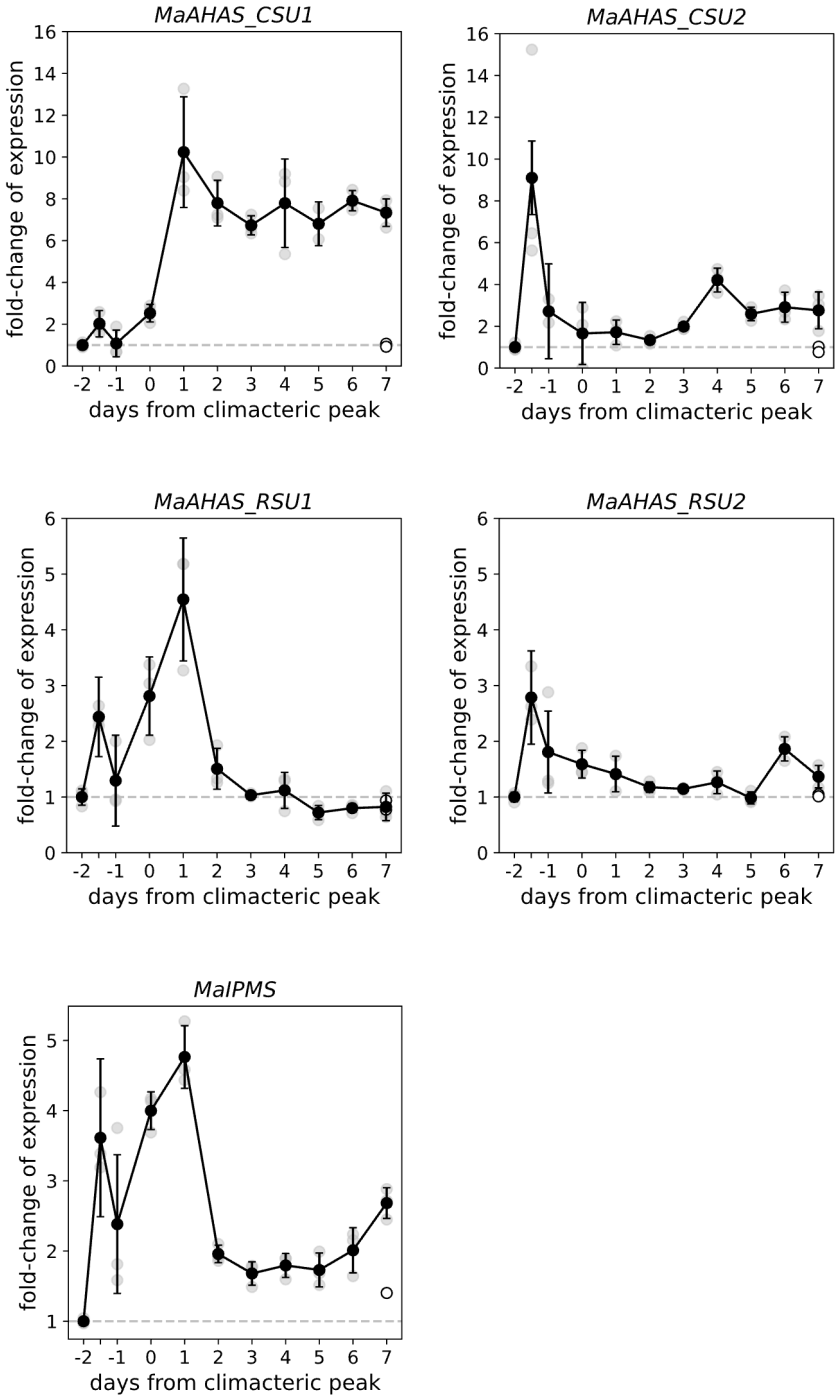

Figure 4.21: Relative expression of *MaAHAS* and *MaIPMS*. Enzyme isoforms are collectively quantified here. Data normalized against average of fruit prior to propylene treatment (dashed line). Presented as means ± ½ SD of three biological reps. Ripening was initiated two days prior to climacteric peak with propylene. Fruit not treated with propylene shown as open circles.

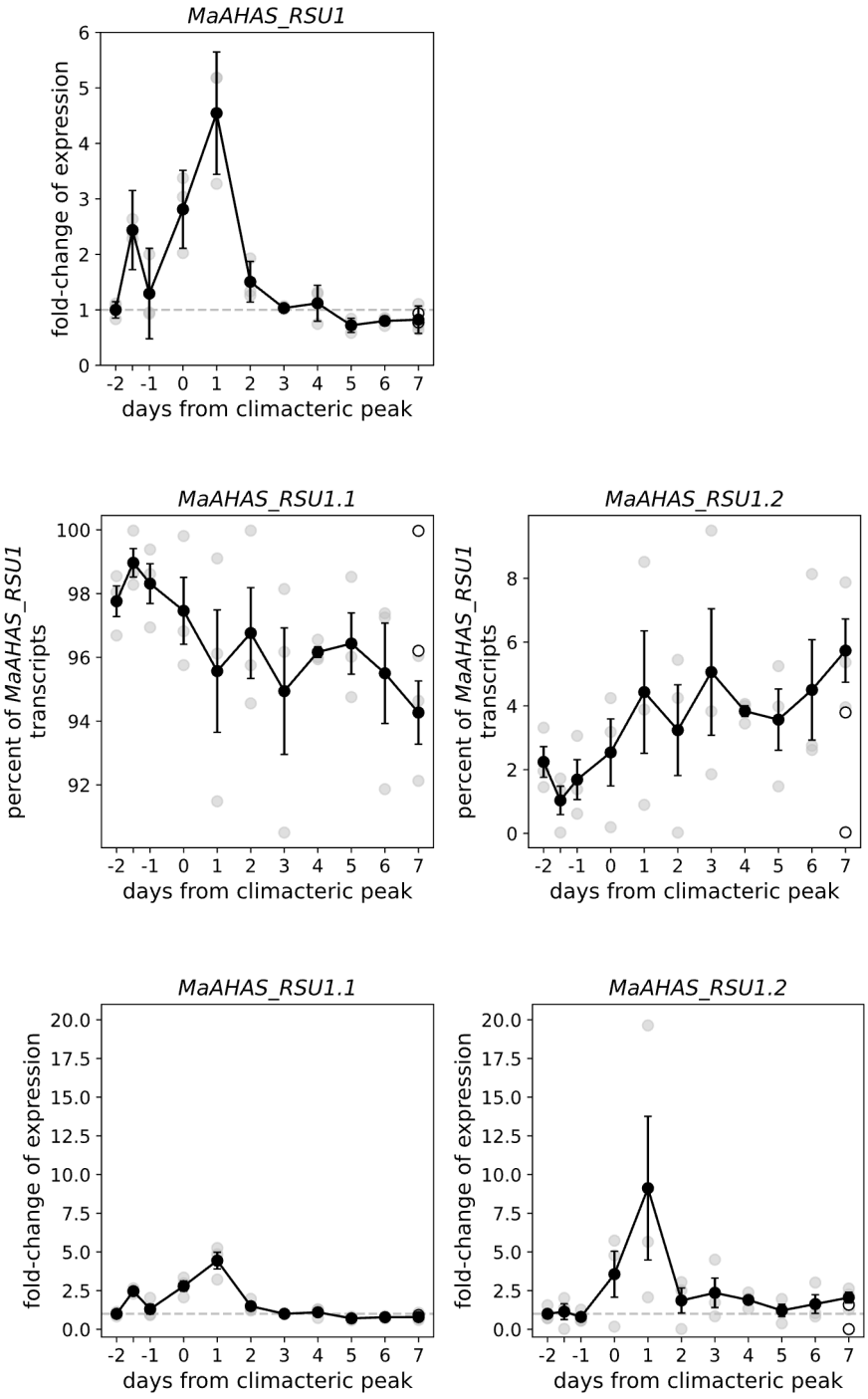

Figure 4.22: Relative expression and distribution of *MaAHAS_RSU1* transcripts. Data normalized against average of fruit prior to propylene treatment (dashed line). Presented as means ± ½ SD of three biological reps. Ripening was initiated two days prior to climacteric peak with propylene. Fruit not treated with propylene shown as open circles.

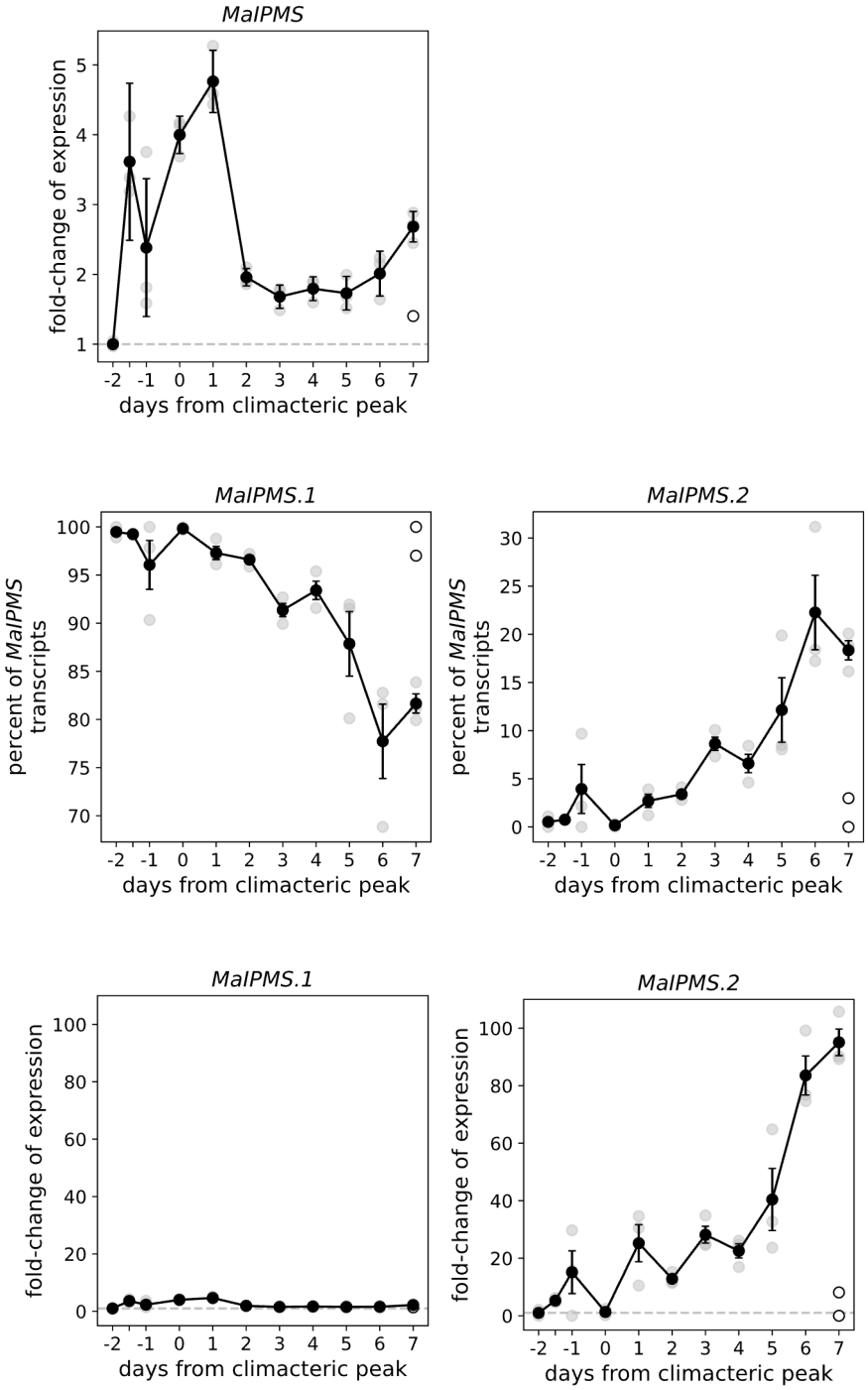

Figure 4.23: Relative expression and distribution of *MaIPMS* transcripts. Data normalized against average of fruit prior to propylene treatment (dashed line). Presented as means ± ½ SD of three biological reps. Ripening was initiated two days prior to climacteric peak with propylene. Fruit not treated with propylene shown as open circles.

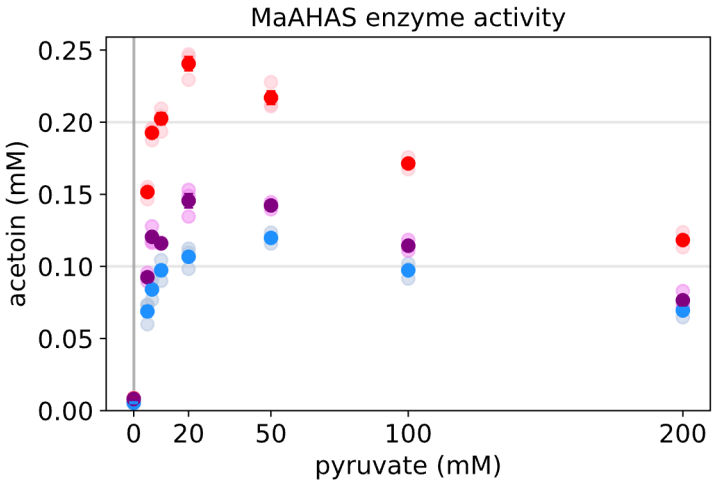

Figure 4.24: Activity of MaAHAS with sodium pyruvate. Red, blue, and purple data points represent holoenzymes composed of MaAHAS_CSU1 and either MaAHAS_RSU1.1, MaAHAS_RSU1.2, or an equal molar mix of both, respectively. Presented as means ± ½ SD of three technical reps. Vertical lines represent approximate pulp pyruvate concentrations throughout ripening.

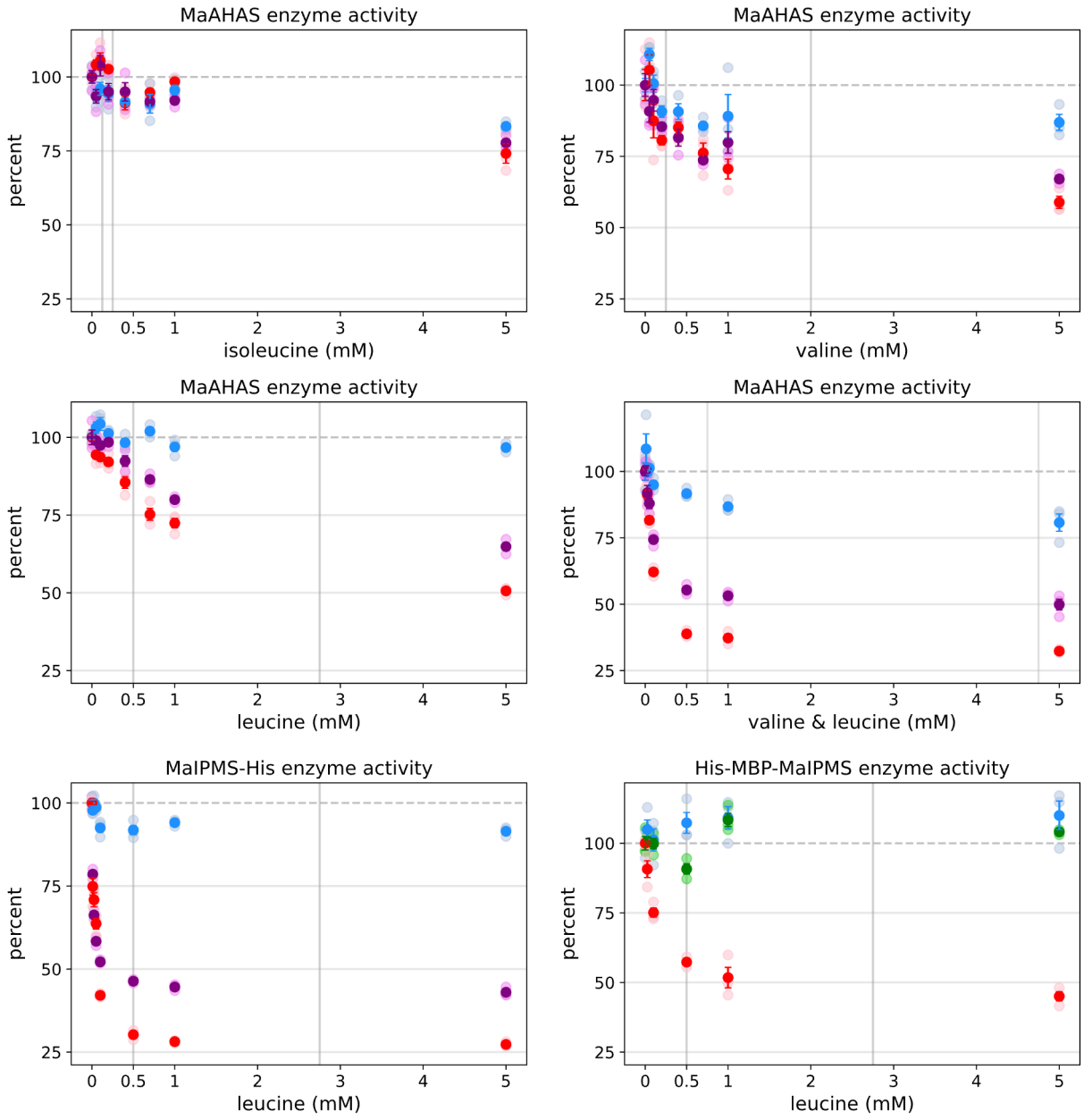

Figure 4.25: Activity of MaAHAS and MaIPMS with branched-chain amino acid inhibitors. MaAHAS data: red, blue, and purple data points represent holoenzymes composed of MaAHAS_CSU1 and either MaAHAS_RSU1.1, MaAHAS_RSU1.2, or an equal molar mix of both, respectively. IPMS data: red, blue, green, and purple data points represent MaIPMS.1, MaIPMS.PV523-524AA, MaIPMS.α14del, or an equal molar mixture of MaIPMS.1 and MaIPMS.PV523-524AA, respectively. Data normalized against activity with no inhibitor present (dashed horizontal line). Presented as means ± ½ SD of three technical reps. Vertical lines represent approximate inhibitor concentrations present in pulp tissue throughout ripening.

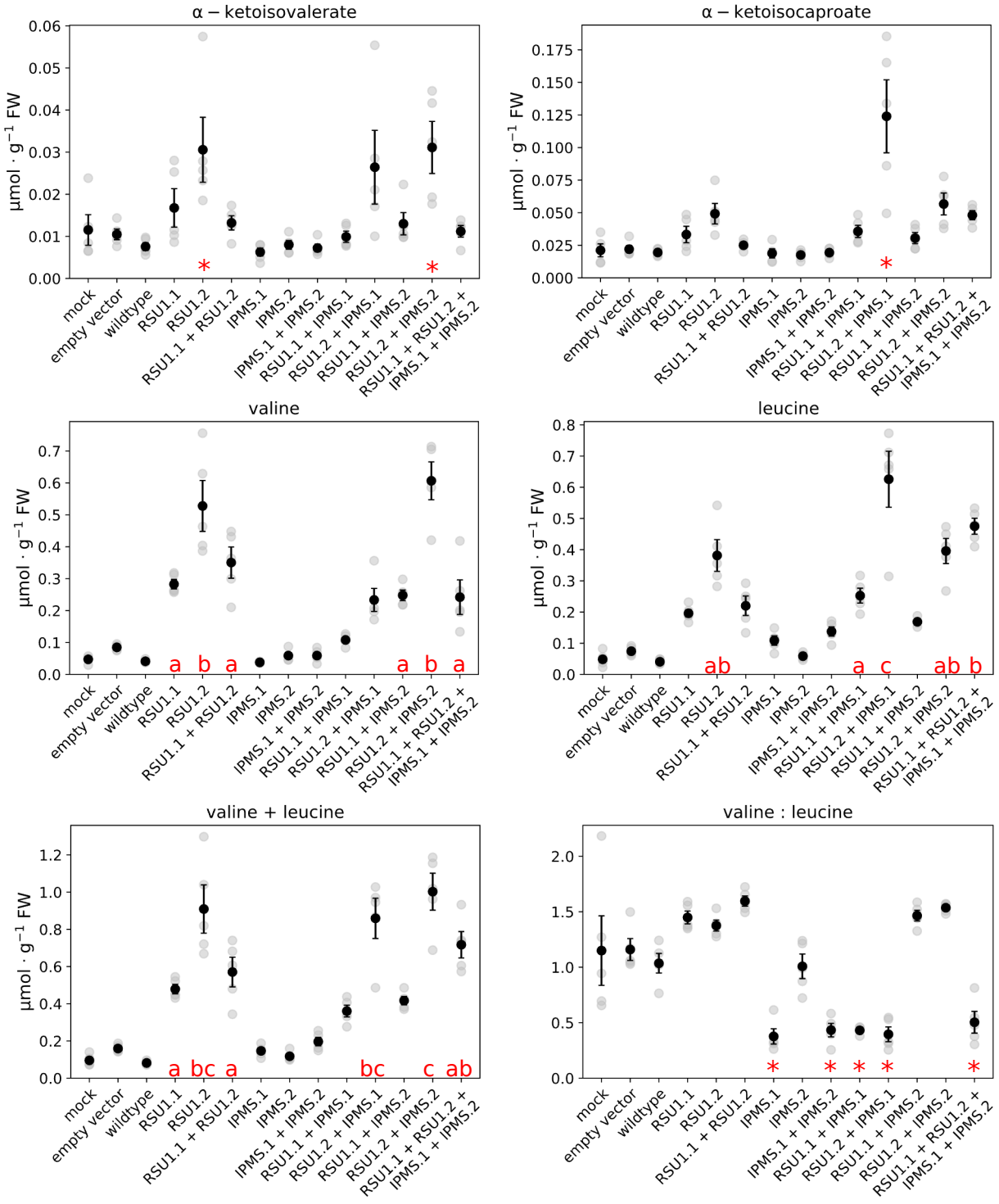

Figure 4.26: Relevant metabolite concentrations of transfected *N. benthamiana* leaves; experiment one. Treatments with MaAHAS used MaAHAS_CSU1 and one or both MaAHAS_RSU1 isoforms. These treatments have only the RSU used labeled. Presented as means ± ½ SD of five biological reps. Metabolite concentrations significantly different from the mock infiltration (mock), empty vector, and wildtype controls are denoted by *, or different letters if found to be significantly different to one another; Tukey's test, α =0.05).

Figure 4.26 (cont'd)

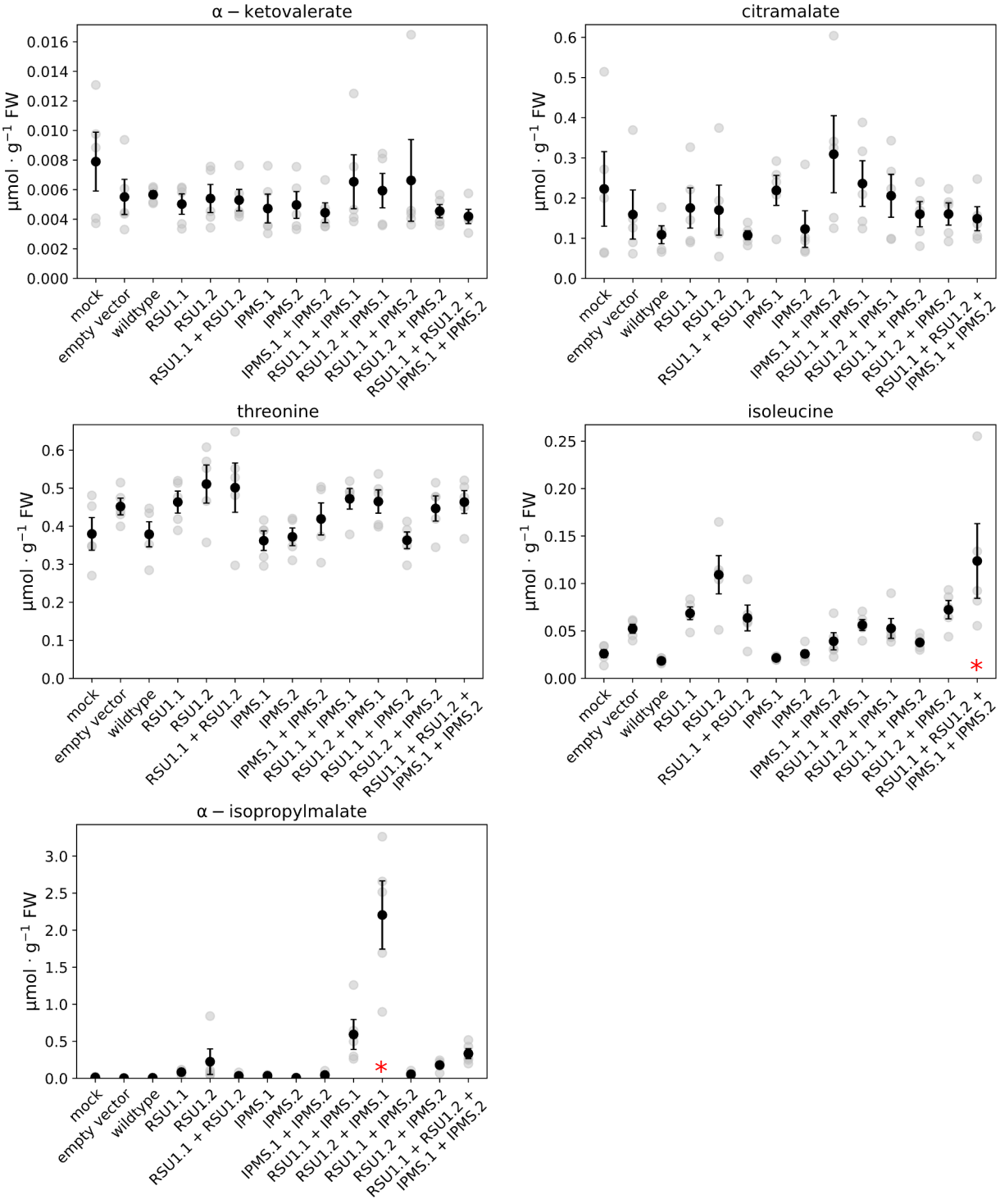

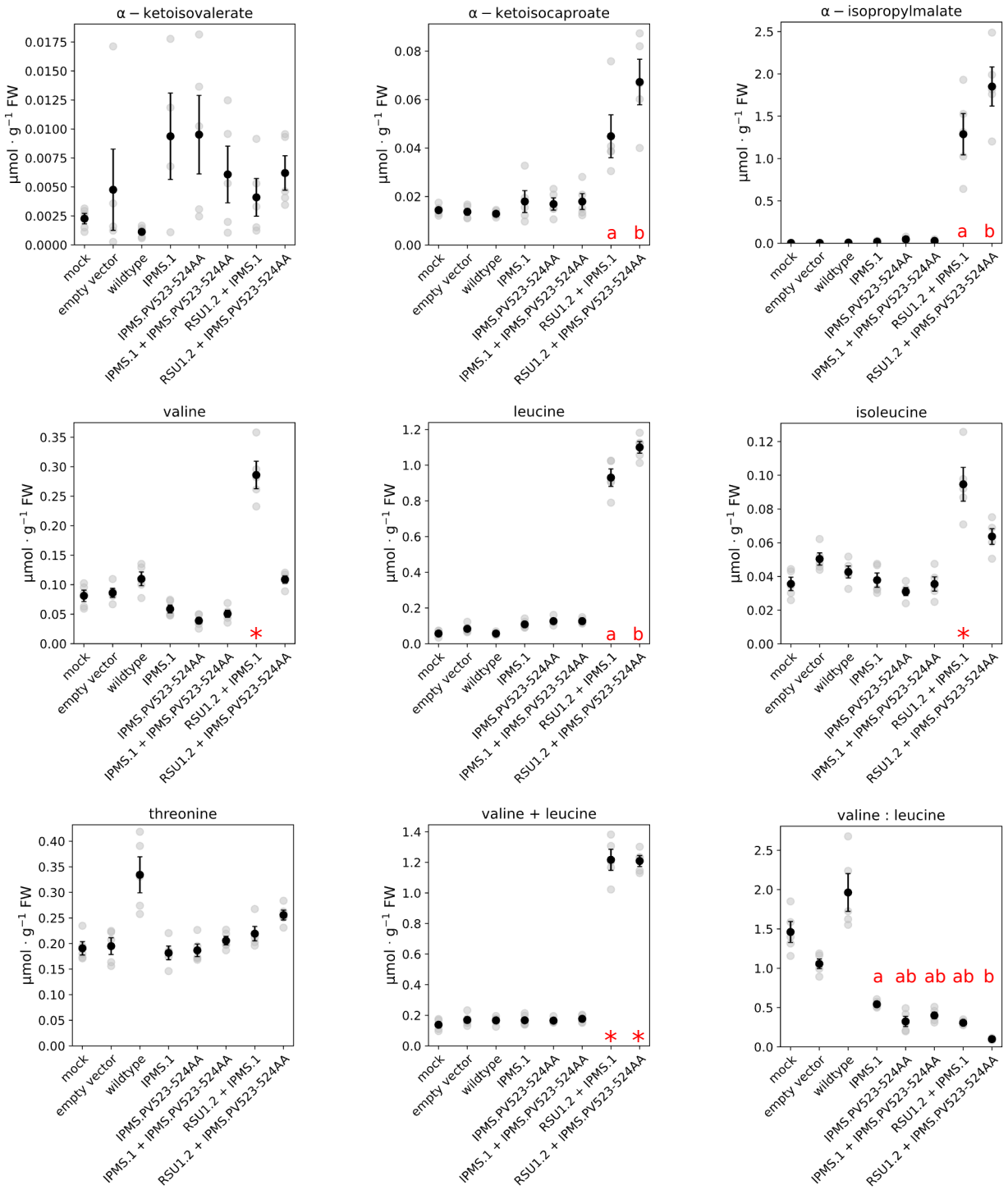

Figure 4.27: Relevant metabolite concentrations of transfected *N. benthamiana* leaves; experiment two. Treatments with MaAHAS used MaAHAS_CSU1 and MaAHAS_RSU1.2. These treatments are labeled with 'RSU1.2'. Presented as means ± ½ SD of five biological reps. Metabolite concentrations significantly different from the mock infiltration (mock), empty vector, and wildtype controls are denoted by *, or different letters if found to be significantly different to one another; Tukey's test, α =0.05).

Figure 4.27 (cont'd)

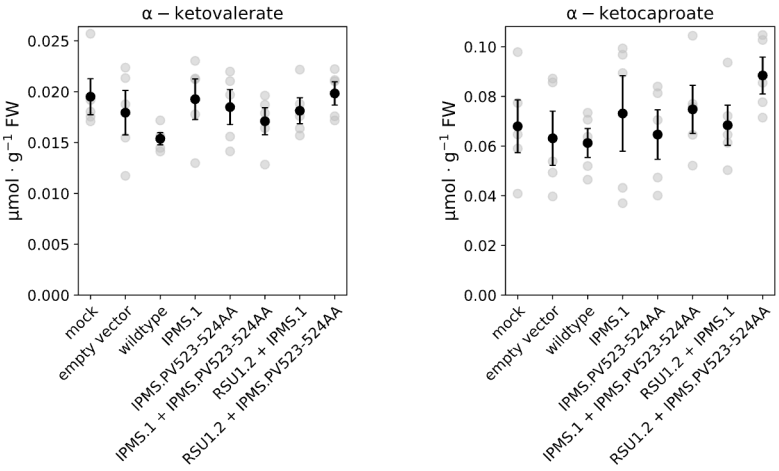

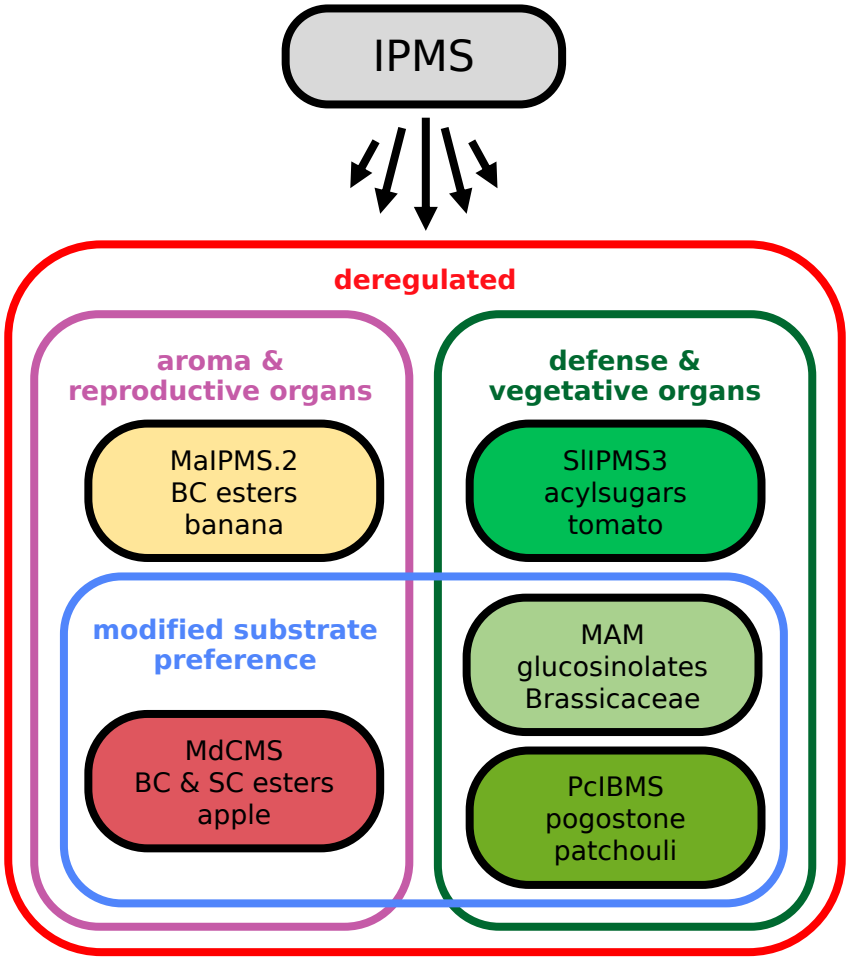

Figure 4.28: Venn diagram of neofunctionalized IPMS enzymes, including specialized metabolites and organisms/families. BC = branched-chain, SC = straight-chain.

hit name	organism/ genome	*Musa acuminata* subspecies	putative ID	Score (Bits)	E value
Ma08_t09270.1 2-isopropylmalate synthase	DH-Pahang genome v4	malaccensis	IPMS	1120	0
Macma4_08_g09160.1	DH-Pahang genome v2	malaccensis	IPMS	1120	0
Mabur_Contig11682_t000010	Calcutta 4	burmannica	IPMS	1115	0
Maban_Contig166_t002240	Banksii	banksii	IPMS	1114	0
Mazeb_scaffold481_t000100	Zebrina	zebrina	IPMS	811	0
Mabur_Contig2717_t000060	Calcutta 4	burmannica	hydroxymethylglutaryl-CoA lyase, mitochondrial	43.5	0.002
Ma04_t10090.1 Hydroxymethylglutaryl-CoA lyase, mitochondrial	DH-Pahang	malaccensis	hydroxymethylglutaryl-CoA lyase, mitochondrial	43.1	0.002
Macma4_04_g10410.1	DH-Pahang	malaccensis	hydroxymethylglutaryl-CoA lyase, mitochondrial	43.1	0.002
Maban_Contig411_t000290	Banksii	banksii	hydroxymethylglutaryl-CoA lyase, mitochondrial	43.1	0.002
Maban_Contig94_t004620	Banksii	banksii	hydroxymethylglutaryl-CoA lyase, mitochondrial	37	0.18
Mabur_Contig18776_t000150	Calcutta 4	burmannica	hydroxymethylglutaryl-CoA lyase, mitochondrial	35.4	0.49
Maban_Contig285_t001340	Banksii	banksii	hydroxymethylglutaryl-CoA lyase, mitochondrial	35	0.72
Ma08_t24740.1 Hydroxymethylglutaryl-CoA lyase, mitochondrial	DH-Pahang	malaccensis	hydroxymethylglutaryl-CoA lyase, mitochondrial	34.3	1.1

Table 4.1. tBLASTn results against MaIPMS.1 without the predicted chloroplast transit peptide (ChloroP) against available banana genomic resources.

tissue	*MaAHAS_RSU1.1*	*MaAHAS_RSU1.2*	*MaIPMS.1*	*MaIPMS.2*
bract	100.0 ± 0.0	0.0 ± 0.0	99.5 ± 0.4	0.5 ± 0.4
anther	100.0 ± 0.0	0.0 ± 0.0	100.0 ± 0.0	0.0 ± 0.0
pseudostem	100.0 ± 0.0	0.0 ± 0.0	99.3 ± 0.4	0.7 ± 0.4
ovary	100.0 ± 0.0	0.0 ± 0.0	100.0 ± 0.0	0.0 ± 0.0
root	100.0 ± 0.0	0.0 ± 0.0	100.0 ± 0.0	0.0 ± 0.0
leaf	100.0 ± 0.0	0.0 ± 0.0	100.0 ± 0.0	0.0 ± 0.0
peduncle	100.0 ± 0.0	0.0 ± 0.0	98.6 ± 0.8	1.4 ± 0.8
ripe fruit peel	96.8 ± 1.4	3.2 ± 1.4	98.9 ± 0.5	1.1 ± 0.5
ripe fruit pulp[a]	94.3 ± 1.0	5.7 ± 1.0	81.7 ± 1.0	18.3 ± 1.0

Table 4.2. Percent of MaAHAS_RSU1 or MaIPMS transcripts by isoform in various tissues. Presented as means ± ½ SD of three biological reps. [a] 7 days after climacteric peak.

MaAHAS_RSU1 isoform	V_{max} ($mM \cdot min^{-1}$)	K_m (mM)	K_{cat} (s^{-1})	K_{cat}/K_m ($s^{-1} \cdot M^{-1}$)	R^2
MaAHAS_RSU1.1	0.00750	4.54	12.9	2835	0.898
MaAHAS_RSU1.2	0.00346	4.82	5.9	1230	0.781
MaAHAS_RSU1.1 & MaAHAS_RSU1.2 (equal molar)	0.00431	3.95	7.4	1872	0.796

Table 4.3. Kinetic properties of MaAHAS. Reactions were composed of MaAHAS_CSU1 and MaAHAS_RSU1 subunits, with sodium pyruvate and performed in triplicate. R2 values are of derived Lineweaver-Burk equations. See methods for further detail.

MaIPMS isoform	substrate	V_{max} ($mM \cdot min^{-1}$)	K_m (mM)	K_{cat} (s^{-1})	K_{cat}/K_m ($s^{-1} \cdot M^{-1}$)	R^2
MaIPMS.1	α-ketoisovalerate	0.00884	0.109	0.692	6360	0.995
	acetyl-CoA	0.04485	0.805	3.51	4358	0.995
MaIPMS.PV523-524AA	α-ketoisovalerate	0.00477	0.202	0.373	1848	0.970
	acetyl-CoA	0.00871	0.151	0.681	4517	0.993
MaIPMS.1 & MaIPMS.PV523-524AA (equal molar)	α-ketoisovalerate	0.00841	0.135	0.658	4857	0.928
	acetyl-CoA	0.03611	0.621	2.825	4548	0.991

Table 4.4. Kinetic properties of MaIPMS with sodium α-ketoisovalerate or lithium acetyl-CoA. Reactions were performed in triplicate or, for MaIPMS.1 with α-ketoisovalerate, in quadruplicate. R2 values are of derived Lineweaver-Burk equations. See methods for further detail.

MaIPMS isoform	α-keto-isovalerate	α-keto-isocaproate	pyruvate	α-keto-butyric acid	α-keto-valeric acid	α-keto-γ-(methylthio) butyric acid
MaIPMS.1	100.0 ± 6.4	0.5 ± 0.4	12.3 ± 0.4	87.4 ± 0.7	27.6 ± 0.1	4.0 ± 0.1
MaIPMS.PV523-524AA	100.0 ± 0.5	0.1 ± 0.4	7.6 ± 0.6	77.3 ± 0.4	17.1 ± 0.7	7.7 ± 1.1
MaIPMS.1 & MaIPMS.PV523-524AA (equal molar)	100.0 ± 10.5	-0.2 ± 0.2	9.7 ± 0.5	87.5 ± 2.7	22.1 ± 0.2	6.3 ± 0.3

Table 4.5. Percent of activity of MaIPMS isoforms with confirmed substrates of IPMS derivatives. Presented as precent activity relative to activity with α-ketoisovalerate as means ± ½ SD from three technical replicates.

m/z	volatile
TIC[a]	1-methylbutyl acetate
TIC[a]	1-methylbutyl butanoate
71	2-heptanone
33	2-methylpropanol
56	2-methylpropyl 2-methylpropanoate
103	2-methylpropyl 3-methylbutanoate
56	2-methylpropyl acetate
TIC[a]	2-pentanol
86	2-pentanone
57	3-methylbutanol
71	3-methylbutyl 2-methylpropanaote
103	3-methylbutyl 3-methylbutanoate
73	3-methylbutyl acetate
55	3-methylbutyl butanoate
33	butanol
103	butyl 3-methylbutanoate
61	butyl acetate
89	butyl butanoate
31	ethanol
71	ethyl 2-methylpropanoate
102	ethyl 3-methylbutanoate
61	ethyl acetate
88	ethyl butanoate
41	mix of 2-methylpropyl butanoate and butyl 2-methylpropanoate

Table 4.6. Ions used for integration of volatile compounds. [a] No standard was available for several compounds, thus they were integrated under their TIC and then quantified against an isoform within the standard.

m/z	U-^{13}C, ^{15}N labeled *m/z*	underivatized form
202		a-ketoisovalerate
202		a-ketovalerate
216		a-ketoisocaproate
216		a-ketocaproate
244		a-ketooctanoate
186	191	valine
200	206	leucine
200	206	isoleucine
303/404	306/409	threonine
433		citramalate
461		isopropylmalate

Table 4.7. Ions used for integration of derivatized compounds. Samples were derivatized via methoxyamination followed by tert-butyldimethylsilyation. Compounds are in order of retention time.

gene	purpose	forward primer	reverse primer
MaRPS4	general qPCR	TGAGAGTGGCTTGACCCTGA	GTGACATTTAGTCGTCTGCTGG
MaDNAJ	general qPCR	ATCAGAGAAAGAACACCCCGT	AAGAACCATCCTGTGAGAGCAT
MaAHAS_CSU1	general qPCR	CTTGCATTTGGTGTAAGGTTTGAT	CTTCTGCTTGTCCAGTTCTTCT
MaAHAS_CSU2	general qPCR	TTGGCGTCAGGTTCGAC	TTCAGTTGGTCCAGCTCTTTC
MaAHAS_RSU1	general qPCR	TCCGGTGGATCCCTACAATG	CCCAGTGACAATGTTCAGGAC
MaAHAS_RSU2	general qPCR	CCAATAAAGTATTGCAACAGGTCATG	TCTCCTGTTACCTCAATGGTTAGT
MaIPMS	general qPCR	CAATGAGTCTGGCATTGTTCTTG	CTTCTCAGCAACTTCTTTGAAGC
MaAHAS_RSU1	splice percentage	CCAGGATCTCCAGTTACCTCT	ACTAGCTGTCGGCTTGAATAC
MaIPMS	splice percentage	GATGATGTCTTCAAACGCTTCAAAG	TCCATCGAAGCTCCACTTCC

Table 4.8. Primers used for quantitative PCR in this study. See methods for more detail.

CHAPTER V – OBSERVATIONS AND COMMENTARY ON THE DIVERSITY OF BANANA FRUIT AROMA BIOCHEMISTRY

Introduction

Bananas are enjoyed around the world. While half of the estimated 100 million tons of banana fruit produced globally per year are cultivars of the 'Cavendish' group, thousands of other cultivars play important roles both culturally and as caloric staples in many regions (FAO, 2022). Pulp and peel color, the conversion of starch to sugars during ripening, and thus the use of a cultivar for cooking or dessert preparations, pulp texture, sugar-acid balance, and aroma are some of the organoleptic traits that have diversified among cultivated varieties (Ploetz, Kepler, Daniells, & Nelson, 2007).

Among these qualities of the fruit, aroma is of particular interest. The characteristic flavor of banana fruits is attributed to esters composed of 2-methylpropyl and 3-methylbutyl elements (Morton & MacLeod, 1990) (McCarthy, Palmer, Shaw, & Anderson, 1963). Butyl and 1-methylbutyl esters also contribute to the aroma profile, providing 'fruity' notes (McCarthy, Palmer, Shaw, & Anderson, 1963) (Shiota, 1993). Other compounds, albeit present in much lesser amounts, can also be found in the fruits, such as hexyl esters and various alcohols, ketones, aldehydes, and phenol ethers. However, as acetate and butanoate esters are considered the principal flavor impact compounds of banana fruit, we directed our focus towards them.

Several biochemical pathways are postulated to be the source of esters within banana fruits. For many decades 2-methylpropyl and 3-methylbutyl compounds have been known to be metabolically linked to valine and leucine, respectively (Figure 2.2) (Myers, Issenberg, & Wick, 1970) (Tressl & Drawert, 1973). Recently this relationship has been shown to be anabolic in nature with the synthesis of these iso-branched-chain esters dependent upon *de novo* synthesis of α-ketoacids via the branched-chain amino acid biosynthesis pathway (Chapter III). This was determined to likely be facilitated by the alternative splicing of two otherwise feedback regulated, and thus limiting, enzymes of the pathway: acetohydroxyacid synthase (AHAS), the regulator of the total pool of iso-branched-chain metabolites, and isopropylmalate synthase (IPMS), the fulcrum between valine and leucine-related metabolites (Chapter IV). Evidence has also suggested that butyl compounds are likewise derived from iso-branched-chain metabolism (Chapter III). 1-Methylbutyl and hexyl compounds are thought to arise from fatty acid metabolism with the latter attributed to lipoxygenase activity (Tressl & Drawert, 1973).

As indicated, many features of the biochemical origins of these compounds remains to be definitively known. The regulatory systems that control the activation and relative contribution of these pathways, as well as the role of cellular disruption, and thus mastication, have on the biosynthesis and emanation of banana volatiles are likewise poorly understood.

To investigate these features of aroma biology, natural variation can serve as an excellent resource in the identification of natural mutations and correlations that illuminate biochemical pathways and networks (Sugimoto, Forsline, & Beaudry, 2015) (Sugimoto, Engelgau, Jones, Song, & Beaudry, 2021) (Tieman, et al., 2017). However, as previously noted, cultivars of the 'Cavendish' group dominate global production and thus the vast majority of research upon this topic has been performed with 'Cavendish' cultivars. Furthermore, there have been no published studies concerning the diversity of banana fruit volatiles. Our goal was to perform such a study to begin exploring the breadth and depth of the diversity of banana fruit aroma in the context of ester biosynthesis, ultimately identifying natural variants that may serve as models for further investigation of potential biochemical pathways.

Results and Discussion

To explore banana fruit aroma biochemistry diversity, we collected seventeen cultivars representing a diversity of geographic provenances, ploidies, and culinary uses from small-holder American farmers in southern Florida, uncommon cultivars that are sold only in certain US regions and are produced by major commercial growers operating in Central America, specialty cultivars from local Asian grocery stores, and fruit from accessions maintained at the USDA-ARS Tropical Agriculture Research Station in Puerto Rico (Table 5.1). After arrival at the laboratory, a population of each cultivar had ripening synchronized with a propylene treatment, however data collected on the internal ethylene and CO_2 concentrations of the fruits suggested that all cultivars investigated had entered the climacteric prior to analysis. Thus, the fruits were monitored for any additional changes of respiration as well as for aroma development.

We investigated nine esters representing five biosynthetic precursors of alkyl ester elements. These were butyl, 2-methylpropyl, 3-methylbutyl, and 1-methylbutyl acetate esters, their respective butanoate esters, as well as hexyl acetate. We observed a large degree of diversity in the aroma profiles of the cultivars. Some ester classes were effectively absent in that their presence was either not detectable or they were present only at trace levels. However, no

cultivar lacked 2-methylpropyl or 3-methylbutyl esters, a disappointing result considering the importance of these compounds to the flavor of banana fruit (Figure 5.1).

The simplest aroma profile observed was produced by 'Horn Plantain' fruits, which only emanate appreciable amounts of 2-methylpropyl and 3-methylbutyl acetate (Figure 5.1). 'Red' and 'Manzano' fruits had likewise simple profiles but produced, in addition to 2-methylpropyl and 3-methylbutyl acetate, either 1-methylbutyl acetate or butyl acetate, respectively. These commercially available cultivars may alone serve as powerful systems to explore the biosynthetic origins of butyl and 1-methylbutyl esters in banana fruit.

Several cultivars that did not have any apparent biosynthetic shortcomings and produced esters from each of the biosynthetic alkyl precursor classes in question (2-methylpropyl, 3-methylbutyl, 1-methylbutyl, butyl, and hexyl) were observed to have markedly different distributions of aroma compounds as compared to most other cultivars analyzed (Figure 5.1). For example, the aroma profile of 'Pisang Awak' fruit is dominated by butyl and 1-methylbutyl acetate, 'Gran Nain' fruit by 3-methylbutyl acetate, and 'Senorita' fruit by 1-methylbutyl acetate. Investigation of cultivars with such deviations to headspace composition may be insightful to understanding what regulatory processes may be affecting the utilization of different biochemical pathways.

3-Methylbutyl and 2-methylpropyl esters are derived from the same metabolic pathways as the iso-branched-chain amino acids leucine and valine, respectively, thus the production of these esters and the iso-branched-chain amino acids are metabolically interlinked. The ratio of 3-methylbutyl to 2-methylpropyl esters (3MB:2MP) within the aroma profiles of the analyzed cultivars was found to be bimodal (Figure 5.2). Cultivars that emitted less than 50 nmoles $\cdot$ L^{-1} of 2-methylpropyl and 3-methylbutyl esters within the 2-L test container headspace yielded a 3MB:2MP ratio of 2.50 (R^2 = 0.82). The remaining cultivars, excluding 'Red' and 'Laknau', described below, produced a 3MB:2MP ratio of 0.80 (R^2 = 0.81). The headspace of 'Red' fruit, unlike the other cultivars tested, was greatly weighted towards 2-methylpropyl esters with a 3MB:2MP ratio of 0.26. 'Laknau' fruit, despite producing greater than 135 nmoles $\cdot$ L^{-1} of 2-methylpropyl and 3-methylbutyl esters, had a 3MB:2MP ratio of 2.6, consistent with the cultivars with lower amounts of 2-methylpropyl and 3-methylbutyl esters within their headspaces.

Peeling and cutting the fruit pulp often led to the release of volatiles otherwise not present when the headspace of whole, intact fruit was assessed (Figure 5.1). Among the monitored volatiles, hexyl acetate was almost exclusively emanated after cutting. Lipoxygenase activity has been previously detected within banana fruits (Tressl & Drawert, 1973) and the limitation of hexyl esters production to only cut tissues suggests that tissue disruption is required to allow otherwise segregated substrates and enzymes to interact. This in contrast to apple fruits, which are able to generate hexyl compounds from intact tissues via β-oxidation and lipoxygenase activity (Rowan, Allen, Fielder, & Hunt, 1999) (Contreras & Beaudry, 2013). Lipoxygenase activity, nonetheless, is greatly enhanced in cut apples too (Contreras & Beaudry, 2013).

'Goldfinger' fruits, while intact, produce only trace amounts of butanoate esters. However, after slicing, butanoate esters increased to compose almost a quarter of the container headspace (Figure 5.1). 'Pisang Mas' fruit presented an interesting reciprocal: intact fruits produced substantial amounts of 2-methylpropyl butanoate and 3-methylbutyl butanoate and only trace amounts of the corresponding acetate esters. However, after slicing, 2-methylpropyl acetate and 3-methylbutyl acetate were present in the headspace. Whether these observed changes of aroma profiles are a function of a peel-based suppression or a result of slicing is not clear from our methodology. Future work on these cultivars will help to explain the effects of cutting, and thus mastication, on banana fruit aroma profiles, as well as what processes may be independently regulating the synthesis or emission of acetate and butanoate esters.

Seven cultivars had the volatile emanations of their fruits tracked for at least three consecutive days (Figure 5.3). Two of these tested cultivars, 'Senorita' and 'Huamoa' were also evaluated without propylene treatment. Overall, fruit treated or not treated with propylene followed similar trends save for a one-day advancement of several ester moieties produced by untreated 'Senorita' fruits, and a slight increase of aroma headspace content and a reduction of volatile content variability in treated 'Huamoa'.

Among the trends of aroma production, of note is the significant temporal difference of 1-methylbutyl versus butyl, 2-methylpropyl, and 3-methylbutyl ester production by 'Senorita' fruit (Figure 5.3). Other tested cultivars indicated a general coordination of the synthesis of esters from these varying biochemical pathways. Our results reinforce the notion of a common biosynthetic origin for butyl, 2-methylpropyl and 3-methylbutyl esters, and a separate source for

1-methylbutyl esters (Chapter III). While the regulation of these various pathways may be synchronized in most fruits, that of 1-methylbutyl esters seems to be capable of decoupling. Furthermore, 'Huamoa' fruit produced 2-methylpropyl esters approximately one day in advance of butyl, 3-methylbutyl, and 1-methylbutyl esters, suggesting that fine-tuned regulation within iso-branched-chain metabolism is possible as well. It may that the regulation of AHAS and IPMS are slightly desynchronized in 'Huamoa' fruit such that utilization of IPMS and its ability to extend α-ketoisovalerate to α-ketoisocaproate is delayed compared to AHAS activation.

The amino acid content was quantified for fourteen cultivars at ripe and unripe stages (Tables 5.2, 5.3). Greater than two-thirds of the amino acid indices across the measured cultivars were found to be significantly different between unripe and ripe samples. Notably, valine was significantly greater in the ripe pulp of every cultivar tested. Leucine was also greater in all but one cultivar: the nearly inodorous 'Dwarf Chamaluco'. The common increase of valine and leucine during ripening lends explanation to the ubiquity of 2-methylpropyl and 3-methylbutyl esters within the cultivars tested. Furthermore, the leucine:valine ratio was found to be consistent across cultivars tested (1.28, $R^2 = 0.85$), suggesting that IPMS, the regulator between valine and leucine distribution (Figure 5.2) (Chapter IV) (Xing & Last, 2017), has a consistent role of balancing valine and leucine content across cultivars. None of the other amino acids were observed to undergo such a universal upward trend during ripening, however some (notably aspartate, glutamate, and glutamine) were regularly found to have decreased several-fold in ripe fruit (Tables 5.2, 5.3).

When the sum of valine and leucine content was regressed against the sum of 2-methylpropyl and 3-methylbutyl esters within the headspaces, two populations were observed (Figure 5.2). One group, composed of 'Valery', 'Gros Michel', 'Mysore', 'Kelat', and 'Laknau', had more than double the concentration of iso-branched-chain esters within their headspaces compared to cultivars with comparable amounts of valine and leucine.

It is unclear what phenomena manifests this bimodal distribution. It would seem, given that the cultivars analyzed maintained a consistent ratio of leucine to valine and that the total amount of valine and leucine was not the sole predictor of iso-branched-chain ester content, that this difference of ability is likely not a result of differing AHAS or IPMS activity and is instead due to processes downstream of the iso-branched-chain α-ketoacids. These discrepancies may also be responsible for the bimodal distribution of 3MB:2MP ratios previously described.

Among the esters analyzed, the biochemical origins of 1-methylbutyl esters are the least studied, however they have been hypothesized to be derived from fatty acid metabolism (Tressl & Drawert, Biogenesis of banana volatiles, 1973). They are, however, a branched-chain ester. Given that the biosynthetic origin of the other major branched-chain esters of fruits are each metabolically linked to amino acids (2-methylbutyl and isoleucine, 2-methylpropyl and valine, and 3-methylbutyl and leucine), it seemed reasonable to suspect that the same may be the case of 1-methylbutyl compounds. To test this possibility, the pulp amino acid content of 'Senorita' fruit was analyzed from tissues collected throughout the progression of ripening (Figure 5.4). The large temporal difference of 1-methylbutyl production by 'Senorita' fruit as compared to 2-methylpropyl, 3-methylbutyl, and butyl ester production should allow any trends to clearly present themselves. However, no such association was found, strongly suggesting that 1-methylbutyl ester synthesis is not related to that of any of the proteinogenic amino acids.

Nonetheless, the trends of valine and leucine accumulation within ripening 'Senorita' was concomitant with 2-methylpropyl and 3-methylbutyl ester biosynthesis, consistent with previous observations of 'Valery' fruit (Alsmairat, Engelgau, & Beaudry, 2018).

Conclusion

After sampling only a small number of the thousands of cultivars grown globally, we have been able to identify a tremendous degree of aroma diversity. Several promising cultivars have been identified that may prove useful to determining the molecular underpinnings of butyl and 1-methylbutyl ester production as well as the regulation of the various biochemical pathways that contribute to a banana fruit's final aroma.

Our failure to find a cultivar that lacks 2-methylpropyl or 3-methylbutyl esters is disappointing. It may be that these compounds that imbue banana fruit with their characteristic flavor are exceptionally common, necessitating a much greater search to find such an exception.

Furthermore, our study focused only on the most prominent esters of banana fruit. A broader study, both in terms of volatiles analyzed and cultivars screened, may reveal further insights. Apple fruits, for example, have aroma profiles dominated by esters, however several cultivars have meaningful amounts of the phenylpropene estragole, which imbues an 'anise or spicy' flavor to the fruit (Morton & MacLeod, 1990). Perhaps such 'specialty' volatiles may be present in some banana cultivars as well, providing an unexpected but perhaps appreciated alternative to 'standard' banana flavor.

Ultimately it may be, when one considers the current threat of *Fusarium* wilt to 'Cavendish' banana production (Lambert, 2019), that the banana of the future brings with it a new meaning to 'banana flavor'.

Materials and methods

Plant material

Fruit was collected during the spring of 2022 from small-holder American farmers in southern Florida, uncommon cultivars that are sold only in certain US regions and are produced by major commercial growers operating in Central America, specialty cultivars from local Asian grocery stores, and fruit from accessions maintained at the USDA-ARS Tropical Agriculture Research Station in Puerto Rico. Table 5.1 indicates all cultivars used in this work and, when known, their country of origin.

Fruits were stored in the laboratory under opaque plastic bags with damped paper towels to reduce the incidence of light and desiccation. Propylene treatment, and the measurement of internal ethylene, CO_2 and propylene were as previously described (Chapter IV).

Volatile analysis

Whole fruit were incubated for 20 min at room temperature (22 ℃) in 2 L sealed Teflon jars before headspace volatiles from vials were sorbed for 3 min using a solid-phase micro extraction (SPME) fiber (65 μm PDMS-DVB; Supelco Analytical, Bellefonte, PA). Fruit slices were prepared as 1 cm wide peeled discs of pulp and were incubated in 1 L Teflon jars for 20 min while upright, maximizing surface area. After sorption, the SPME fiber was directly desorbed for 1 min in the injection port of a gas chromatograph (GC; HP-6890, Hewlett-Packard, Wilmington, DE) coupled to a time of flight mass spectrometer (MS; Pegasus II, LECO, St. Joseph, MI). Desorbed volatiles were cryofocused at the beginning of the column by immersing said region of the column in liquid nitrogen. After the desorption period, the run was initiated and the liquid nitrogen removed.

The conditions of the system were as follows. Injection port: 200 ℃, splitless, helium carrier gas, front inlet flow was 1.5 mL/min constant, 10 mL/min purge flow, 11.5 mL/min total flow. Oven: initial temperature at 40 ℃ for 0 min, ramped by 43 ℃/min to 185 ℃ for 0 min. Column: HP-5MS, 30 m × 0.25 mm i.d., 0.25 μm film thickness (Agilent, Santa Clara, CA). Transfer line temperature was 225 ℃. MS: Electron ionization (-70 eV), ion source temperature

was 200 ℃, solvent delay was 50 sec, m/z 29 to 400 were scanned for, detector voltage was 1500 V, data collection rate was 20 Hz.

Compounds were identified by comparison with the retention time and mass spectrum against authenticated reference standards and spectra (National Institute of Standards and Technology Mass Spectral Search Program Version 2.0, 2001). Volatiles were quantified by calibration with a standard of 59 authenticated compounds (Sigma-Aldrich Co., St. Louis, MO and Fluka Chemika, Seelza, Germany). The standard was made by placing 0.5 µL of an equal-part mixture of the neat compounds onto a disc of filter paper before quickly placing the filter paper into a 4 L sealed flask fitted with a Mininert valve (Valco Instruments Co. Inc., Houston, TX) for SPME fiber access. The quantification m/z of each compound can be seen in Table 5.4.

If said sample was destined for amino acid analysis, pulp tissues were collected and held at -80 ℃ for further processing.

The headspace of banana flavored foodstuffs was prepared by placing ~0.5 g of product into a 40 mL vial, adding 2 mL of water, and then incubating at 40 ℃ before 30 s sorption and 1 min desorption as described above. Headspace composition was quantified by integrating under total ion count for each volatile, dividing by molecular weight, and then calculating percent of total per volatile. Ethanol and propylene glycol content were ignored.

Volatile data of whole ‘Valery’ fruit are from Chapter IV. ‘Gros Michel’ and ‘Valery’ data used for artificial banana analysis were from fruit 7 days after treatment with propylene.

Amino acid analysis

Frozen samples were ground to a powder in liquid-nitrogen-chilled mortar and pestles. About 0.5 mg of tissue were vortexed for 10 s in 2 mL of room temperature (22 ℃) 1:1:1 (water:acetonitrile:ethanol, v/v) spiked with 2 nmoles of U-^{13}C,^{15}N labeled amino acids (MilliporeSigma) before being heated for 15 min in a 65 ℃ water bath. Extracts were then briefly chilled on ice before being centrifuged at 4400 × g for 15 min at 4 ℃. The supernatant was filtered by centrifugation (0.2 µm nylon centrifugal filter; Costar, Corning) at 21000 × g for 5 min at room temperature. 10 µL of the filtrate was transferred to an autosampler vial and diluted 100-fold with 990 µL of 10.1 mM PFHA spiked with 2 µmoles of internal standard. Thus the final concentration of internal standard was ~2 µM.

An amino acid standard series were prepared from a premade mixture (Millipore Sigma, AAS18) that contained equal molar amounts of cystine and all 20 proteinogenic amino acids

save for tryptophan, asparagine, glutamine, and cysteine. Another equal molar mixture of the stragglers was also prepared. To avoid dilution errors or artefacts from differing buffers, these amino acid stocks were aliquoted and desiccated such that a 5-part standard series ranging from 250 µM to 25 nM would be produced upon resuscitation with 10 µL of spiked extraction buffer and 990 µL spiked PFHA solution.

Samples and amino acids were held overnight at -20 ℃ before analysis.

Amino acids were analyzed with a Xevo TQ-S Micro UPLC (H-Class)-MS/MS (Waters, Milford, MA) at the Michigan State University Mass Spectrometry and Metabolomics Core. Conditions were as follows. HPLC column: Acquirt UPLC HSS T3, 2.1 x 100 mm, 1.7 µm particle size (Waters), with a 0.2 µm pre-column filter (Waters). Mobile phase: A) 10 mM PFHA in water, B) acetonitrile. LC gradient: linear gradient, slope setting = 6, flow rate = 0.3 mL· min^{-1}, step 1) 0 min, 100% A, 0% B, 2) 1 min, 100% A, 0% B, 3) 8 min, 35% A, 65% B, 4) 8.01 min, 10% A, 90% B, 5) 9 min, 10% A, 90% B, 6) 9.01 min, 100% A, 0% B, 7) 13 min, 100% A, 0% B. Column temp: 40 ℃. Autosampler temp: 10 ℃. Injection volume: 10 µL. Tune parameters: electrospray ionization, standard ESI probe, capillary voltage = +1.0 kV , source temp = 120 ℃, desolvation temp = 350 ℃, desolvation gas = 800 L· hr^{-1}, cone gas = 40 L· hr^{-1}. MS collection was split into three phases and were adjusted after checking the retention time of several samples. Parent and daughter ions, cone and collision voltages, phases collected and approximate retention times can be seen in Table 5.5.

Data were quantified by first calculating a linear regression of log(unlabeled amino acid response/labeled amino acid response) transformed standard responses. R^2 values were all greater than 0.98 and the slope (m) and y-intercept (b) were used to calculate unknowns: µM of unknown sample = 10^[(log(unknown unlabeled response/unknown labeled response)-b/m]. Amino acid data of ‘Valery’ fruit are from Chapter IV.

Figures & Tables

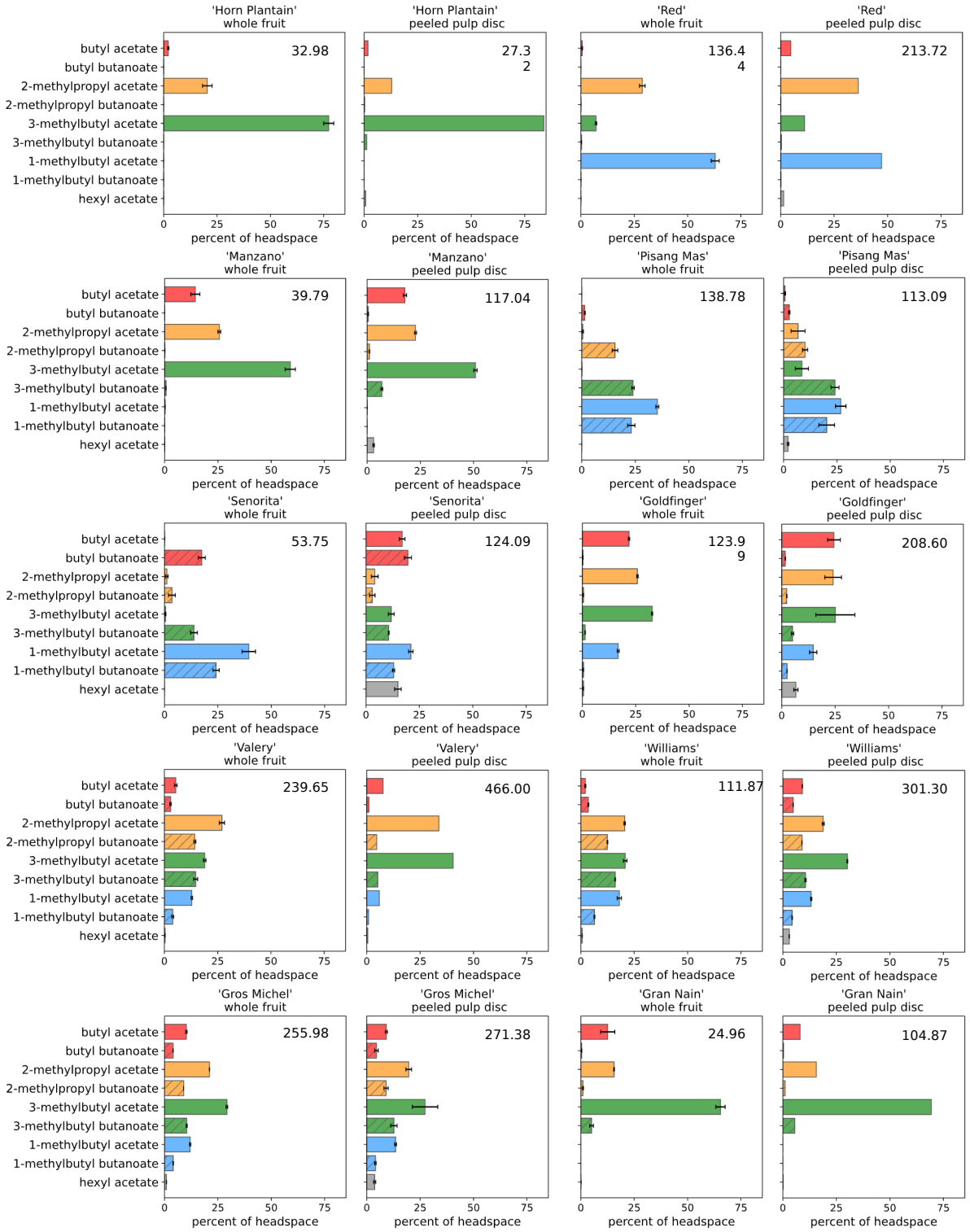

Figure 5.1. Aroma profiles of ripe banana cultivars. Calculated only with displayed esters. Other volatiles may be present in headspace but were not quantified. Presented as means ± ½ SD. Average of total concentration of quantified esters displayed in upper right corner in nmol · L^{-1}. Whole fruit and peeled pulp discs are not necessarily from the same fruit.

Figure 5.1 (cont'd)

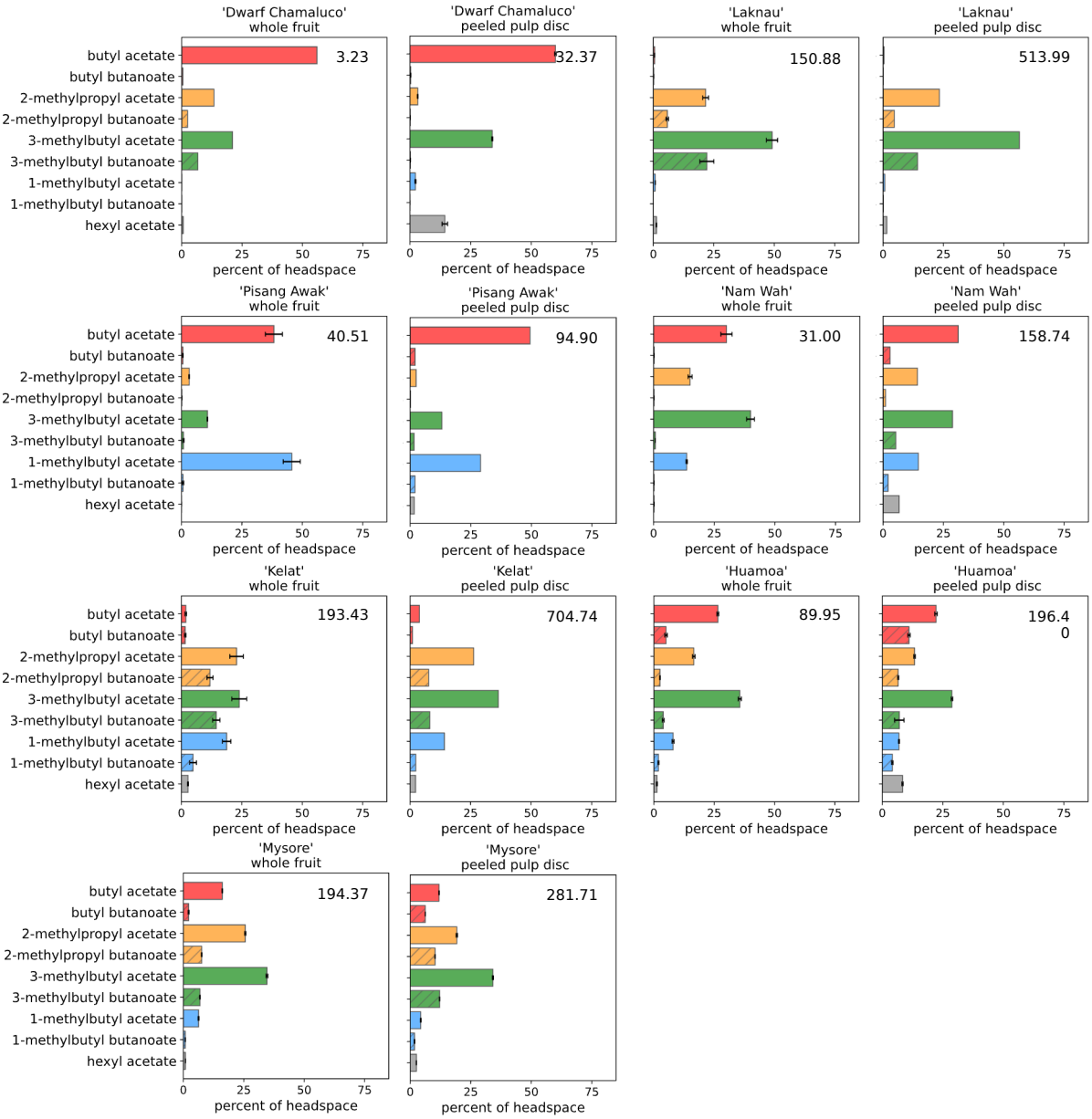

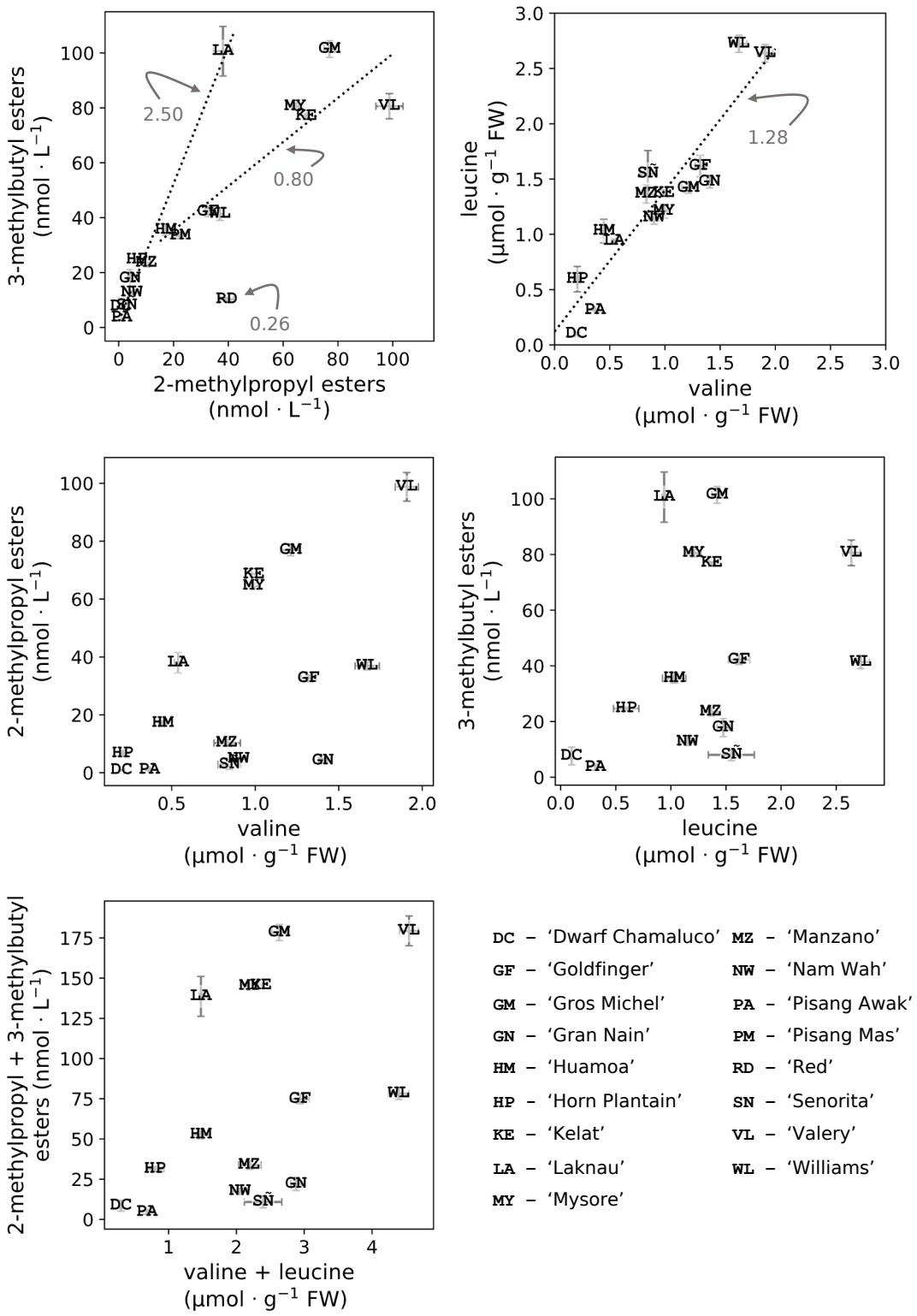

Table 5.2. Ratios of iso-branched-chain esters and iso-branched-chain amino acids in ripe banana fruit pulp. Slopes of regressed data presented. Outlier ratio of 'Red' also shown. Presented as means ± ½ SD.

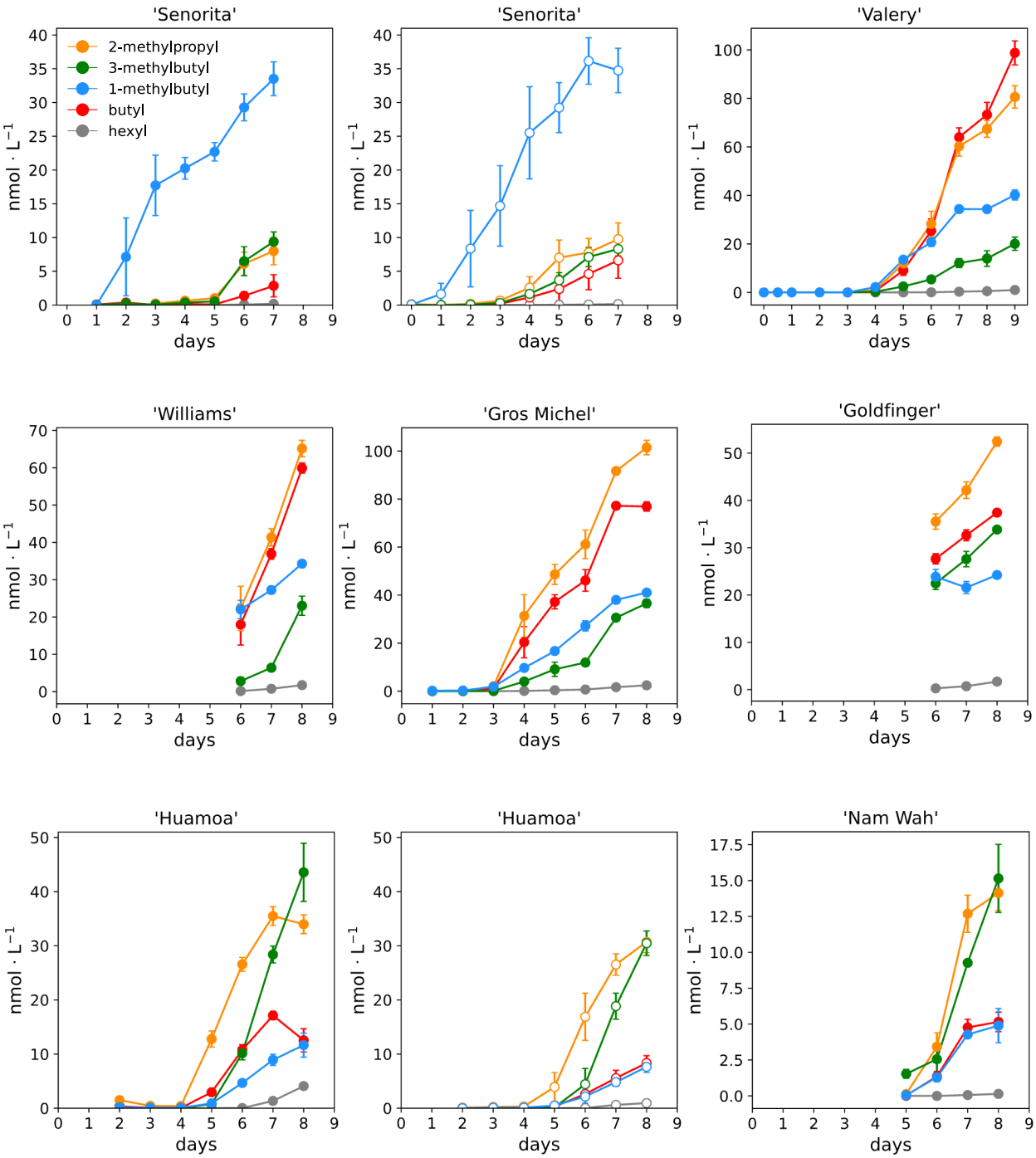

Figure 5.3. Accumulation of esters within the headspace of ripening banana cultivars. Data are of alkyl elements from pooled acetate and butanoate esters. Data of fruit not treated with propylene are open circles, whereas those treated with propylene are solid circles. Presented as means ± ½ SD. Fruit were treated with propylene on day 0. Butyl esters = red, 2-methylpropyl esters = yellow, 3-methylbutyl esters = green, 1-methylbutyl esters = blue, hexyl acetate = gray.

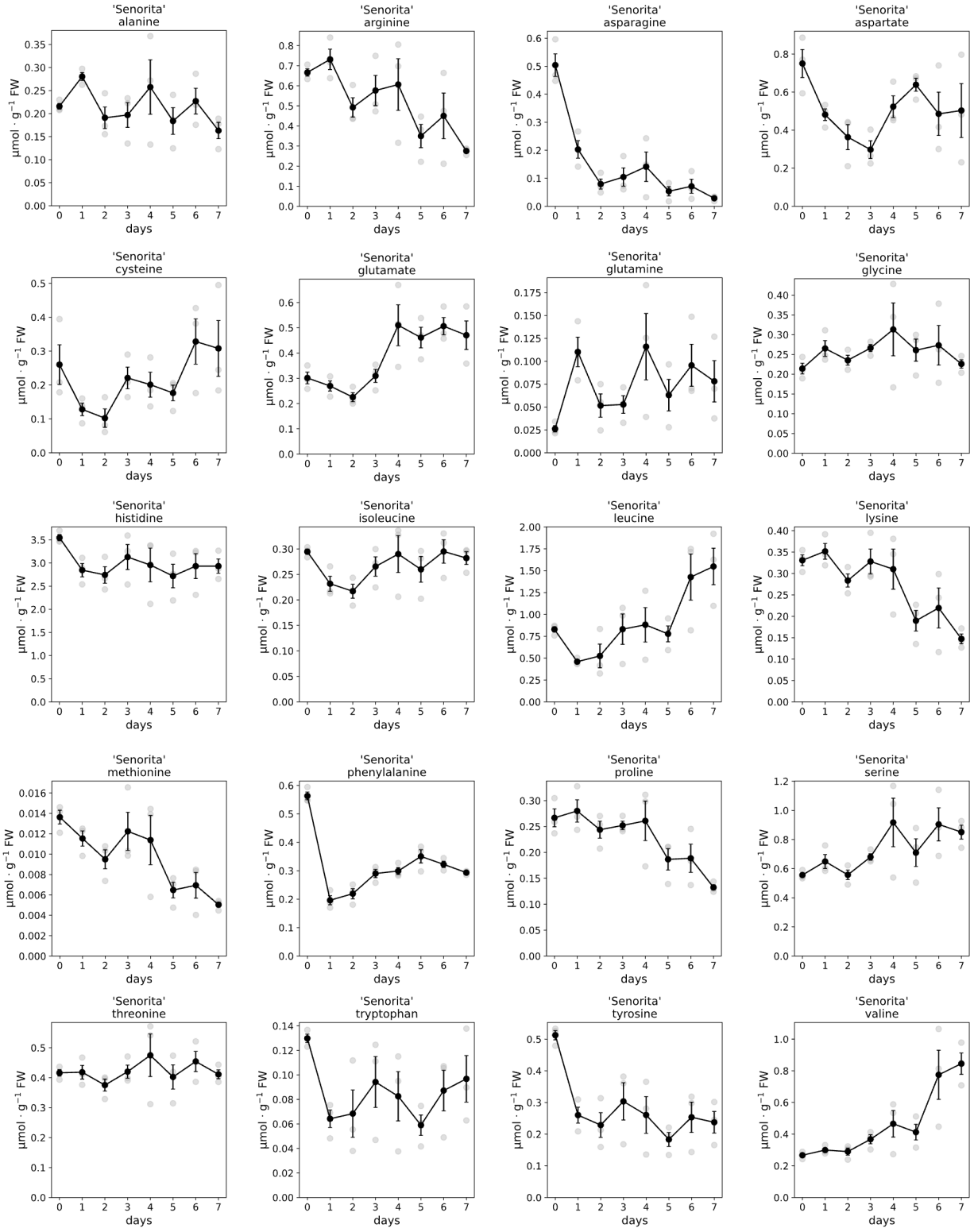

Figure 5.4. Fruit pulp amino acid content of ripening ‘Senorita’ banana fruit. Fruit were gassed with propylene on day 0. Presented as means ± ½ SD.

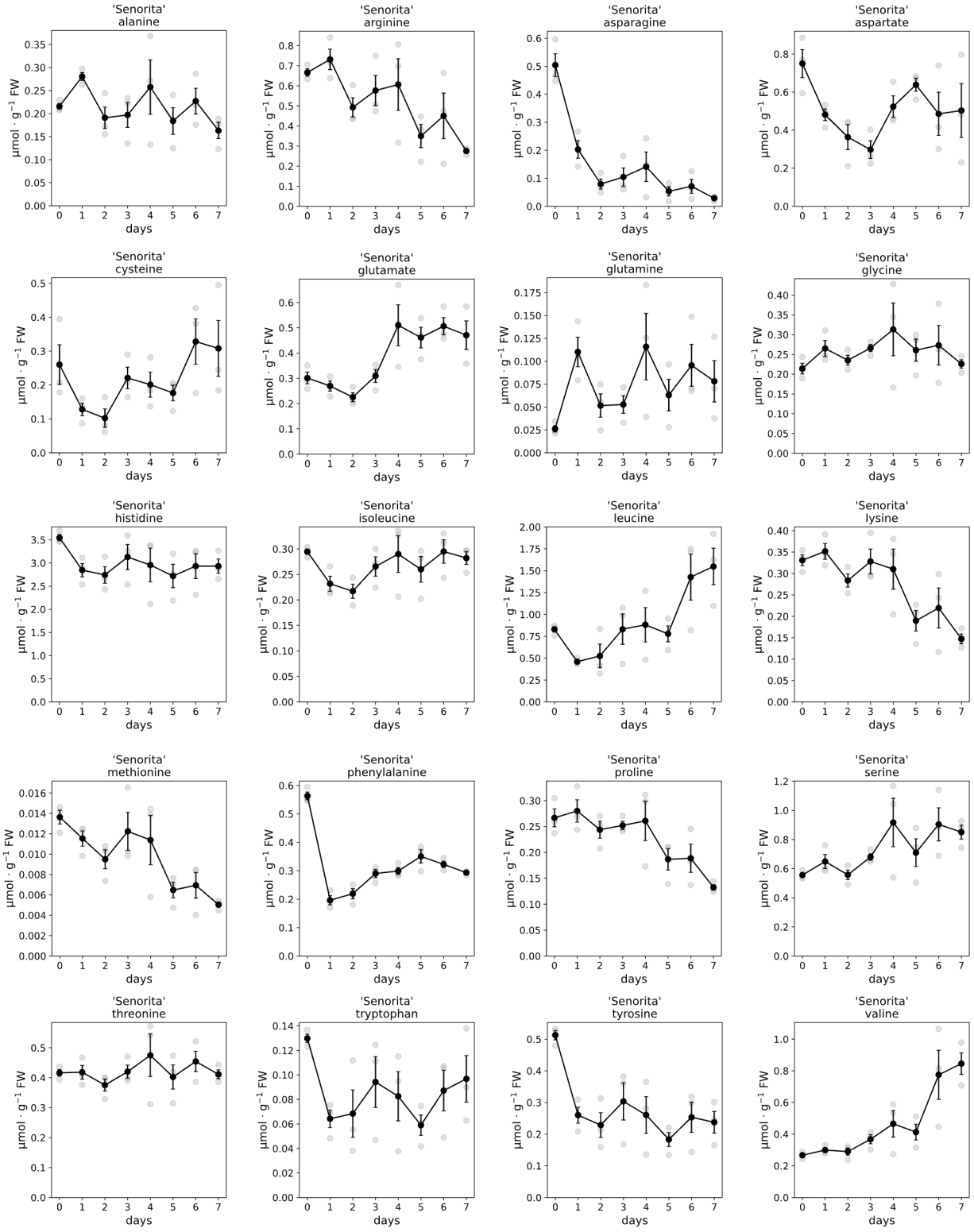

Table 5.4. Fruit pulp amino acid content of ripening ‘Senorita’ banana fruit. Fruit were gassed with propylene on day 0. Presented as means ± ½ SD.

cultivar/accession	marketed name & company	PLU	ploidy	type	country of origin
Senorita	Baby - Del Monte	4234	AA	miscellaneous AA	Ecuador
Pisang Mas	Minis - Chiquita	4234	AA	Sucrier	Guatemala
Gran Nain / NGRL 947			AAA	Cavendish	PR, USA
Valery	Yellow - Chiquita	4011	AAA	Cavendish	NA
Williams			AAA	Cavendish	FL, USA
Gros Michel			AAA	Gros Michel	FL, USA
Red	Reds - Del Monte	4236	AAA	Red	NA
FHIA-01	Goldfinger		AAAB	synthetic hybrid	FL, USA
Kelat / PI 19354			AAB	Kelat	PR, USA
Laknau - 23479 / TARS 16515			AAB	Laknau	PR, USA
Mysore			AAB	Mysore	FL, USA
Horn Plantain	Plantain - Chiquita	4235	AAB	Plantain	Ecuador
Huamoa			AAB	Popoulu	FL, USA
Manzano	Apple - Del Monte	4233	AAB	Silk	Colombia
Dwarf Chamaluco / TARS 17128			ABB	Bluggoe	PR, USA
Nam Wah			ABB	Pisang Awak	FL, USA
Pisang Awak			ABB	Pisang Awak	Thailand

Table 5.1. Cultivars used in this study. PLU = price look-up code, listed when applicable.

cultivar	ploidy	type	stage	µmol · g^{-1} FW alanine	arginine	asparagine
'Senorita'	AA	misc. AA	unripe	0.216 ± 0.006	**0.667 ± 0.018**	**0.504 ± 0.040**
			ripe	0.163 ± 0.018	**0.275 ± 0.009**	**0.029 ± 0.004**
'Gran Nain'	AAA	Cavendish	unripe	**0.360 ± 0.012**	**0.249 ± 0.009**	3.429 ± 0.088
			ripe	**0.198 ± 0.024**	**0.669 ± 0.064**	3.136 ± 0.239
'Williams'	AAA	Cavendish	unripe	**0.177 ± 0.016**	**0.685 ± 0.069**	3.633 ± 0.387
			ripe	**0.380 ± 0.014**	**0.966 ± 0.003**	4.365 ± 0.198
'Gros Michel'	AAA	Gros Michel	unripe	0.027 ± 0.004	0.128 ± 0.030	0.662 ± 0.133
			ripe	0.029 ± 0.003	0.162 ± 0.009	0.532 ± 0.079
'Goldfinger'	AAAB	synthetic hybrid	unripe	0.071 ± 0.010	0.408 ± 0.040	**4.894 ± 0.318**
			ripe	0.059 ± 0.004	0.558 ± 0.032	**3.545 ± 0.123**
'Kelat'	AAB	Kelat	unripe	0.175 ± 0.018	0.977 ± 0.039	1.595 ± 0.129
			ripe	0.116 ± 0.011	0.704 ± 0.067	1.286 ± 0.134
'Laknau'	AAB	Laknau	unripe	**0.044 ± 0.002**	1.130 ± 0.121	**0.212 ± 0.019**
			ripe	**0.013 ± 0.001**	1.050 ± 0.115	**0.006 ± 0.001**
'Mysore'	AAB	Mysore	unripe	0.292 ± 0.125	0.399 ± 0.096	1.218 ± 0.292
			ripe	0.041 ± 0.003	0.356 ± 0.010	0.374 ± 0.042
'Horn Plantain'	AAB	Plantain	unripe	0.087 ± 0.024	**0.576 ± 0.125**	**1.331 ± 0.242**
			ripe	0.025 ± 0.004	**0.113 ± 0.020**	**0.147 ± 0.037**
'Huamoa'	AAB	Popoulu	unripe	0.114 ± 0.026	1.563 ± 0.431	3.507 ± 0.961
			ripe	0.128 ± 0.008	0.212 ± 0.025	0.746 ± 0.046
'Manzano'	AAB	Silk	unripe	**0.188 ± 0.007**	**0.075 ± 0.013**	1.460 ± 0.136
			ripe	**0.347 ± 0.025**	**0.257 ± 0.019**	2.042 ± 0.126
'Dwarf Chamaluco'	ABB	Bluggoe	unripe	**1.284 ± 0.037**	0.236 ± 0.019	**4.036 ± 0.116**
			ripe	**0.828 ± 0.023**	0.218 ± 0.005	**2.993 ± 0.134**
'Nam Wah'	ABB	Pisang Awak	unripe	**0.056 ± 0.002**	**0.063 ± 0.005**	1.734 ± 0.018
			ripe	**0.253 ± 0.013**	**0.698 ± 0.009**	1.339 ± 0.211
'Pisang Awak'	ABB	Pisang Awak	unripe	0.318 ± 0.026	**0.053 ± 0.001**	**0.127 ± 0.008**
			ripe	0.192 ± 0.023	**0.192 ± 0.018**	**0.060 ± 0.007**

Table 5.2. Fruit pulp amino acid content of ripe and unripe bananas. Presented as means ± ½ SD of three biological reps. Significantly different concentrations between ripe and unripe fruit are in bold (two-tailed equal-variance t.test, α=0.05).

Table 5.2 (cont'd)

		µmol · g^{-1} FW				
cultivar	stage	aspartate	cysteine	glutamate	glutamine	glycine
'Senorita'	unripe	0.750 ± 0.074	0.260 ± 0.059	0.301 ± 0.023	0.026 ± 0.003	0.214 ± 0.014
	ripe	0.503 ± 0.142	0.308 ± 0.082	0.471 ± 0.057	0.078 ± 0.023	0.226 ± 0.011
'Gran Nain'	unripe	**1.238 ± 0.097**	**0.102 ± 0.007**	**1.234 ± 0.058**	3.315 ± 0.206	0.142 ± 0.005
	ripe	**0.568 ± 0.067**	**0.170 ± 0.003**	**0.677 ± 0.048**	3.438 ± 0.100	0.195 ± 0.016
'Williams'	unripe	**2.344 ± 0.147**	**0.031 ± 0.010**	**0.854 ± 0.034**	**6.703 ± 0.286**	**0.101 ± 0.005**
	ripe	**0.812 ± 0.010**	**0.635 ± 0.061**	**0.454 ± 0.015**	**4.598 ± 0.170**	**0.605 ± 0.015**
'Gros Michel'	unripe	**0.558 ± 0.041**	0.019 ± 0.008	**0.172 ± 0.016**	0.494 ± 0.105	**0.050 ± 0.010**
	ripe	**0.048 ± 0.005**	0.016 ± 0.003	**0.084 ± 0.007**	0.247 ± 0.031	**0.113 ± 0.012**
'Goldfinger'	unripe	**2.038 ± 0.213**	**0.005 ± 0.001**	**0.840 ± 0.080**	**2.572 ± 0.319**	**0.076 ± 0.009**
	ripe	**0.351 ± 0.016**	**0.034 ± 0.006**	**0.267 ± 0.016**	**1.541 ± 0.028**	**0.135 ± 0.013**
'Kelat'	unripe	**1.665 ± 0.061**	**0.056 ± 0.003**	**0.703 ± 0.027**	**3.974 ± 0.414**	**0.273 ± 0.002**
	ripe	**0.514 ± 0.038**	**0.030 ± 0.006**	**0.341 ± 0.001**	**1.550 ± 0.181**	**0.329 ± 0.012**
'Laknau'	unripe	**1.172 ± 0.066**	**0.020 ± 0.002**	**0.254 ± 0.013**	**0.382 ± 0.017**	**0.039 ± 0.006**
	ripe	**0.006 ± 0.000**	**0.131 ± 0.006**	**0.017 ± 0.001**	**0.023 ± 0.001**	**0.116 ± 0.008**
'Mysore'	unripe	**1.257 ± 0.064**	0.270 ± 0.025	**0.417 ± 0.102**	0.939 ± 0.330	0.089 ± 0.025
	ripe	**0.049 ± 0.004**	0.338 ± 0.018	**0.023 ± 0.001**	0.143 ± 0.014	0.072 ± 0.004
'Horn Plantain'	unripe	**1.503 ± 0.265**	**0.005 ± 0.001**	**1.201 ± 0.284**	**1.341 ± 0.209**	0.089 ± 0.020
	ripe	**0.012 ± 0.003**	**0.163 ± 0.019**	**0.070 ± 0.015**	**0.067 ± 0.017**	0.174 ± 0.020
'Huamoa'	unripe	**3.580 ± 0.186**	**0.005 ± 0.001**	**1.140 ± 0.156**	**4.604 ± 1.152**	0.137 ± 0.040
	ripe	**0.171 ± 0.006**	**0.055 ± 0.008**	**0.365 ± 0.020**	**0.257 ± 0.017**	0.111 ± 0.004
'Manzano'	unripe	0.415 ± 0.034	**0.640 ± 0.023**	0.263 ± 0.020	**1.535 ± 0.229**	**0.083 ± 0.005**
	ripe	0.391 ± 0.033	**0.911 ± 0.039**	0.315 ± 0.044	**4.068 ± 0.439**	**0.217 ± 0.016**
'Dwarf Chamaluco'	unripe	**2.761 ± 0.198**	**0.236 ± 0.016**	1.751 ± 0.098	**3.472 ± 0.204**	0.136 ± 0.013
	ripe	**1.601 ± 0.037**	**0.135 ± 0.008**	1.697 ± 0.088	**1.565 ± 0.193**	0.417 ± 0.166
'Nam Wah'	unripe	**1.060 ± 0.065**	**0.070 ± 0.003**	**0.361 ± 0.017**	**4.561 ± 0.506**	**0.027 ± 0.002**
	ripe	**0.719 ± 0.032**	**0.368 ± 0.012**	**0.552 ± 0.030**	**1.753 ± 0.188**	**0.109 ± 0.008**
'Pisang Awak'	unripe	**1.135 ± 0.010**	**0.461 ± 0.015**	**0.547 ± 0.020**	0.140 ± 0.016	**0.034 ± 0.004**
	ripe	**0.382 ± 0.026**	**0.659 ± 0.008**	**0.372 ± 0.033**	0.164 ± 0.011	**0.085 ± 0.007**

Table 5.2 (cont'd)

		µmol · g^{-1} FW					
cultivar	stage	histidine	isoleucine	leucine	lysine	methionine	phenylalanine
'Senorita'	unripe	**3.547 ± 0.067**	0.295 ± 0.005	**0.829 ± 0.030**	**0.331 ± 0.013**	**0.014 ± 0.001**	**0.563 ± 0.014**
	ripe	**2.933 ± 0.155**	0.282 ± 0.013	**1.548 ± 0.209**	**0.147 ± 0.011**	**0.005 ± 0.000**	**0.293 ± 0.004**
'Gran Nain'	unripe	2.919 ± 0.096	**0.030 ± 0.002**	**0.098 ± 0.009**	**0.073 ± 0.001**	**0.010 ± 0.001**	**0.021 ± 0.003**
	ripe	3.202 ± 0.175	**0.214 ± 0.018**	**1.475 ± 0.056**	**0.133 ± 0.013**	**0.021 ± 0.002**	**0.048 ± 0.003**
'Williams'	unripe	**1.862 ± 0.127**	**0.032 ± 0.002**	**0.045 ± 0.004**	**0.405 ± 0.038**	**0.005 ± 0.000**	0.107 ± 0.014
	ripe	**3.361 ± 0.120**	**0.118 ± 0.006**	**2.723 ± 0.077**	**0.687 ± 0.010**	**0.024 ± 0.000**	0.094 ± 0.001
'Gros Michel'	unripe	**2.392 ± 0.385**	**0.027 ± 0.003**	**0.095 ± 0.014**	0.061 ± 0.010	0.010 ± 0.003	**0.439 ± 0.066**
	ripe	**4.047 ± 0.111**	**0.053 ± 0.004**	**1.419 ± 0.047**	0.077 ± 0.004	0.007 ± 0.001	**0.069 ± 0.005**
'Goldfinger'	unripe	1.121 ± 0.128	**0.017 ± 0.002**	**0.045 ± 0.002**	0.127 ± 0.012	0.012 ± 0.002	**0.092 ± 0.013**
	ripe	1.424 ± 0.056	**0.040 ± 0.002**	**1.618 ± 0.096**	0.141 ± 0.007	0.010 ± 0.001	**0.021 ± 0.000**
'Kelat'	unripe	6.207 ± 0.240	**0.068 ± 0.004**	**0.230 ± 0.016**	0.380 ± 0.015	**0.051 ± 0.004**	**0.322 ± 0.039**
	ripe	5.585 ± 0.157	**0.040 ± 0.002**	**1.372 ± 0.031**	0.265 ± 0.032	**0.021 ± 0.004**	**0.064 ± 0.013**
'Laknau'	unripe	**2.711 ± 0.170**	0.020 ± 0.004	**0.083 ± 0.015**	0.118 ± 0.008	0.005 ± 0.001	**0.092 ± 0.010**
	ripe	**3.509 ± 0.090**	0.032 ± 0.001	**0.939 ± 0.017**	0.145 ± 0.006	0.007 ± 0.001	**0.017 ± 0.001**
'Mysore'	unripe	3.817 ± 0.328	**0.036 ± 0.003**	**0.096 ± 0.021**	0.126 ± 0.028	0.005 ± 0.001	**0.039 ± 0.005**
	ripe	3.789 ± 0.189	**0.054 ± 0.003**	**1.210 ± 0.064**	0.133 ± 0.006	0.005 ± 0.000	**0.071 ± 0.008**
'Horn Plantain'	unripe	**2.129 ± 0.208**	0.023 ± 0.008	**0.059 ± 0.015**	0.064 ± 0.014	0.004 ± 0.001	0.048 ± 0.013
	ripe	**3.257 ± 0.173**	0.054 ± 0.007	**0.595 ± 0.115**	0.048 ± 0.005	0.006 ± 0.001	0.031 ± 0.002
'Huamoa'	unripe	**4.676 ± 0.283**	**0.024 ± 0.003**	**0.063 ± 0.008**	0.208 ± 0.050	**0.012 ± 0.001**	0.062 ± 0.011
	ripe	**5.989 ± 0.261**	**0.075 ± 0.003**	**1.029 ± 0.106**	0.066 ± 0.007	**0.006 ± 0.000**	0.075 ± 0.001
'Manzano'	unripe	**1.184 ± 0.136**	**0.029 ± 0.003**	**0.096 ± 0.023**	**0.056 ± 0.007**	**0.002 ± 0.000**	**0.030 ± 0.003**
	ripe	**1.856 ± 0.038**	**0.129 ± 0.008**	**1.366 ± 0.084**	**0.151 ± 0.007**	**0.009 ± 0.000**	**0.082 ± 0.004**
'Dwarf Chamaluco'	unripe	3.657 ± 0.226	**0.026 ± 0.004**	0.071 ± 0.005	**0.048 ± 0.001**	0.007 ± 0.000	0.044 ± 0.008
	ripe	2.957 ± 0.167	**0.063 ± 0.005**	0.100 ± 0.013	**0.028 ± 0.000**	0.006 ± 0.001	0.071 ± 0.005
'Nam Wah'	unripe	**1.039 ± 0.057**	**0.012 ± 0.001**	**0.019 ± 0.001**	**0.028 ± 0.002**	**0.011 ± 0.001**	**0.031 ± 0.003**
	ripe	**1.515 ± 0.035**	**0.130 ± 0.012**	**1.151 ± 0.060**	**0.054 ± 0.004**	**0.005 ± 0.000**	**0.147 ± 0.007**
'Pisang Awak'	unripe	0.395 ± 0.025	**0.030 ± 0.002**	**0.027 ± 0.001**	**0.024 ± 0.001**	**0.001 ± 0.000**	**0.044 ± 0.002**
	ripe	0.413 ± 0.006	**0.152 ± 0.007**	**0.313 ± 0.001**	**0.030 ± 0.001**	**0.002 ± 0.000**	**0.080 ± 0.002**

Table 5.2 (cont'd)

cultivar	stage	µmol · g^{-1} FW proline	serine	threonine	tryptophan	tyrosine	valine
'Senorita'	unripe	**0.267 ± 0.017**	**0.556 ± 0.015**	0.416 ± 0.011	0.130 ± 0.003	**0.513 ± 0.015**	**0.267 ± 0.011**
	ripe	**0.132 ± 0.005**	**0.851 ± 0.048**	0.411 ± 0.015	0.097 ± 0.019	**0.238 ± 0.034**	**0.845 ± 0.068**
'Gran Nain'	unripe	0.251 ± 0.002	**0.679 ± 0.035**	**0.260 ± 0.005**	0.032 ± 0.006	**0.036 ± 0.007**	**0.119 ± 0.016**
	ripe	0.295 ± 0.020	**1.777 ± 0.056**	**0.373 ± 0.015**	0.049 ± 0.002	**0.112 ± 0.006**	**1.406 ± 0.026**
'Williams'	unripe	**0.075 ± 0.008**	**0.487 ± 0.046**	**0.227 ± 0.018**	**0.007 ± 0.000**	**0.034 ± 0.003**	**0.089 ± 0.009**
	ripe	**0.311 ± 0.006**	**1.420 ± 0.023**	**0.456 ± 0.010**	**0.133 ± 0.005**	**0.325 ± 0.001**	**1.670 ± 0.072**
'Gros Michel'	unripe	**0.075 ± 0.016**	**0.133 ± 0.019**	**0.124 ± 0.019**	**0.032 ± 0.004**	**0.063 ± 0.012**	**0.045 ± 0.005**
	ripe	**0.138 ± 0.004**	**0.494 ± 0.027**	**0.229 ± 0.010**	**0.062 ± 0.002**	**0.140 ± 0.008**	**1.212 ± 0.060**
'Goldfinger'	unripe	0.102 ± 0.005	**0.311 ± 0.035**	0.188 ± 0.017	0.012 ± 0.003	**0.010 ± 0.001**	**0.049 ± 0.006**
	ripe	0.095 ± 0.003	**1.166 ± 0.024**	0.210 ± 0.011	0.018 ± 0.003	**0.026 ± 0.003**	**1.319 ± 0.045**
'Kelat'	unripe	**0.311 ± 0.007**	**0.504 ± 0.013**	0.628 ± 0.022	0.023 ± 0.004	0.072 ± 0.011	**0.139 ± 0.007**
	ripe	**0.269 ± 0.006**	**0.768 ± 0.005**	0.539 ± 0.023	0.029 ± 0.010	0.077 ± 0.017	**0.992 ± 0.013**
'Laknau'	unripe	**0.055 ± 0.004**	**0.194 ± 0.008**	**0.111 ± 0.005**	0.021 ± 0.002	**0.031 ± 0.002**	**0.049 ± 0.007**
	ripe	**0.132 ± 0.004**	**0.380 ± 0.003**	**0.159 ± 0.002**	0.024 ± 0.002	**0.049 ± 0.004**	**0.538 ± 0.022**
'Mysore'	unripe	0.172 ± 0.025	0.391 ± 0.051	**0.147 ± 0.011**	0.041 ± 0.013	0.059 ± 0.016	**0.064 ± 0.019**
	ripe	0.109 ± 0.008	0.539 ± 0.020	**0.081 ± 0.003**	0.025 ± 0.002	0.056 ± 0.004	**0.994 ± 0.026**
'Horn Plantain'	unripe	**0.286 ± 0.023**	0.355 ± 0.062	0.183 ± 0.034	0.016 ± 0.009	**0.018 ± 0.006**	**0.057 ± 0.012**
	ripe	**0.456 ± 0.033**	0.304 ± 0.019	0.135 ± 0.010	0.032 ± 0.004	**0.130 ± 0.005**	**0.206 ± 0.016**
'Huamoa'	unripe	0.302 ± 0.062	0.572 ± 0.121	0.332 ± 0.059	0.018 ± 0.009	**0.010 ± 0.003**	**0.102 ± 0.023**
	ripe	0.241 ± 0.009	0.532 ± 0.016	0.169 ± 0.004	0.018 ± 0.002	**0.048 ± 0.006**	**0.446 ± 0.023**
'Manzano'	unripe	**0.146 ± 0.016**	**0.376 ± 0.034**	**0.121 ± 0.011**	**0.016 ± 0.003**	**0.034 ± 0.003**	**0.085 ± 0.011**
	ripe	**0.284 ± 0.016**	**1.130 ± 0.096**	**0.240 ± 0.011**	**0.043 ± 0.005**	**0.127 ± 0.010**	**0.832 ± 0.079**
'Dwarf Chamaluco'	unripe	**0.298 ± 0.016**	**1.414 ± 0.029**	**0.206 ± 0.008**	**0.010 ± 0.001**	0.008 ± 0.000	**0.119 ± 0.006**
	ripe	**0.155 ± 0.006**	**1.931 ± 0.081**	**0.168 ± 0.006**	**0.020 ± 0.001**	0.011 ± 0.002	**0.200 ± 0.013**
'Nam Wah'	unripe	0.054 ± 0.003	**0.375 ± 0.007**	**0.062 ± 0.005**	**0.003 ± 0.001**	**0.006 ± 0.000**	**0.051 ± 0.003**
	ripe	0.068 ± 0.004	**1.716 ± 0.025**	**0.113 ± 0.006**	**0.007 ± 0.001**	**0.031 ± 0.003**	**0.901 ± 0.043**
'Pisang Awak'	unripe	0.037 ± 0.001	**0.606 ± 0.036**	**0.070 ± 0.001**	**0.003 ± 0.000**	**0.005 ± 0.000**	**0.075 ± 0.002**
	ripe	0.041 ± 0.001	**1.094 ± 0.041**	**0.088 ± 0.001**	**0.008 ± 0.001**	**0.020 ± 0.000**	**0.365 ± 0.004**

cultivar	ploidy	type	alanine	arginine	asparagine	aspartate	cysteine	glutamate
'Senorita'	AA	misc. AA	0.76	**0.41**	**0.06**	0.67	1.18	1.56
'Gran Nain'	AAA	Cavendish	**0.55**	**2.69**	0.91	**0.46**	**1.66**	**0.55**
'Valery'	AAA	Cavendish						
'Williams'	AAA	Cavendish	**2.15**	**1.41**	1.20	**0.35**	**20.47**	**0.53**
'Gros Michel'	AAA	Gros Michel	1.10	1.27	0.80	**0.09**	0.86	**0.49**
'Goldfinger'	AAAB	synthetic hybrid	0.83	1.37	**0.72**	**0.17**	**6.93**	**0.32**
'Kelat'	AAB	Kelat	0.66	0.72	0.81	**0.31**	**0.54**	**0.48**
'Laknau'	AAB	Laknau	**0.29**	0.93	**0.03**	**0.01**	**6.51**	**0.07**
'Mysore'	AAB	Mysore	0.14	0.89	0.31	**0.04**	1.25	**0.05**
'Horn Plantain'	AAB	Plantain	0.29	**0.20**	**0.11**	**0.01**	**32.93**	**0.06**
'Huamoa'	AAB	Popoulu	1.12	0.14	0.21	**0.05**	**11.35**	**0.32**
'Manzano'	AAB	Silk	**1.85**	**3.41**	1.40	0.94	**1.42**	1.20
'Dwarf Chamaluco'	ABB	Bluggoe	**0.65**	0.92	**0.74**	**0.58**	**0.57**	0.97
'Nam Wah'	ABB	Pisang Awak	**4.52**	**11.11**	0.77	**0.68**	**5.24**	**1.53**
'Pisang Awak'	ABB	Pisang Awak	0.60	**3.65**	**0.47**	**0.34**	**1.43**	**0.68**

Table 5.3. Fold change of unripe to ripe fruit pulp amino acid content. Presented as fold change of ripe to unripe means. Significantly different concentrations between ripe and unripe fruit are bold and colored by intensity, relative to extremes. Red indicates a decrease during ripening, blue indicates an increase. (two-tailed equal-variance t-test, α=0.05).

Table 5.3 (cont'd)

cultivar	glutamine	glycine	histidine	isoleucine	leucine	lysine	methionine	phenylalanine
'Senorita'	2.98	1.05	**0.83**	0.96	**1.87**	**0.45**	**0.37**	**0.52**
'Gran Nain'	1.04	1.38	1.10	**7.07**	**15.13**	**1.82**	**1.99**	**2.26**
'Valery'				**0.66**	**4.28**			
'Williams'	**0.69**	**5.98**	**1.81**	**3.69**	**60.24**	**1.69**	**4.50**	0.88
'Gros Michel'	0.50	**2.28**	**1.69**	**1.93**	**14.96**	1.26	0.70	**0.16**
'Goldfinger'	**0.60**	**1.77**	1.27	**2.41**	**36.02**	1.11	0.85	**0.23**
'Kelat'	**0.39**	**1.21**	0.90	**0.59**	**5.97**	0.70	**0.41**	**0.20**
'Laknau'	**0.06**	**3.01**	**1.29**	1.64	**11.34**	1.23	1.46	**0.18**
'Mysore'	0.15	0.81	0.99	**1.51**	**12.66**	1.06	0.86	**1.84**
'Horn Plantain'	**0.05**	1.96	**1.53**	2.30	**10.06**	0.75	1.72	0.65
'Huamoa'	**0.06**	0.81	**1.28**	**3.15**	**16.33**	0.32	**0.52**	1.21
'Manzano'	**2.65**	**2.60**	**1.57**	**4.43**	**14.22**	**2.68**	**4.19**	**2.76**
'Dwarf Chamaluco'	**0.45**	3.07	0.81	**2.43**	1.40	**0.60**	0.83	1.61
'Nam Wah'	**0.38**	**4.10**	**1.46**	**10.53**	**60.15**	**1.94**	**0.45**	**4.70**
'Pisang Awak'	1.17	**2.51**	1.05	**5.01**	**11.79**	**1.29**	**2.26**	**1.80**

Table 5.3 (cont'd)

cultivar	proline	serine	threonine	tryptophan	tyrosine	valine
'Senorita'	**0.50**	**1.53**	0.99	0.75	**0.46**	**3.17**
'Gran Nain'	1.18	**2.62**	**1.43**	1.54	**3.12**	**11.80**
'Valery'			**1.17**			**6.04**
'Williams'	**4.15**	**2.91**	**2.01**	**18.65**	**9.58**	**18.83**
'Gros Michel'	**1.83**	**3.71**	**1.84**	**1.95**	**2.21**	**26.89**
'Goldfinger'	0.93	**3.75**	1.11	1.43	**2.59**	**26.76**
'Kelat'	**0.86**	**1.52**	0.86	1.29	1.07	**7.12**
'Laknau'	**2.40**	**1.96**	**1.44**	1.17	**1.57**	**10.95**
'Mysore'	0.63	1.38	**0.56**	0.61	0.95	**15.49**
'Horn Plantain'	**1.59**	0.86	0.74	1.98	**7.42**	**3.60**
'Huamoa'	0.80	0.93	0.51	0.98	**4.61**	**4.36**
'Manzano'	**1.94**	**3.01**	**1.98**	**2.79**	**3.76**	**9.81**
'Dwarf Chamaluco'	**0.52**	**1.37**	**0.81**	**2.05**	1.31	**1.69**
'Nam Wah'	1.27	**4.57**	**1.83**	**2.20**	**5.23**	**17.83**
'Pisang Awak'	1.09	**1.81**	**1.26**	**2.98**	**3.91**	**4.87**

m/z	volatile
TIC[a]	1-methylbutyl acetate
TIC[a]	1-methylbutyl butanoate
71	2-heptanone
33	2-methylpropanol
56	2-methylpropyl 2-methylpropanoate
103	2-methylpropyl 3-methylbutanoate
56	2-methylpropyl acetate
TIC[a]	2-pentanol
86	2-pentanone
57	3-methylbutanol
71	3-methylbutyl 2-methylpropanaote
103	3-methylbutyl 3-methylbutanoate
73	3-methylbutyl acetate
55	3-methylbutyl butanoate
33	butanol
103	butyl 3-methylbutanoate
61	butyl acetate
89	butyl butanoate
31	ethanol
71	ethyl 2-methylpropanoate
102	ethyl 3-methylbutanoate
61	ethyl acetate
88	ethyl butanoate
56	hexyl acetate
41	mix of 2-methylpropyl butanoate and butyl 2-methylpropanoate

Table 5.4. Ions used for integration of volatile compounds. [a] No standard was available for several compounds, thus they were integrated under their total ion count and then quantified against an isoform within the standard.

compound	parent ion (*m/z*)	daughter ion (*m/z*)	cone voltage	collision voltage	approximate retention time (min)	phase
Gly	76	30	17	8	2.05	1
[13C2,15N]-Gly	79	32	17	8	2.05	1
Ala	90.1	44	35	17	3.54	1
[13C3,15N]-Ala	94.1	47.1	17	8	3.54	1
Ser	106.1	60	30	10	1.79	1
[13C3,15N]-Ser	110.1	63	19	10	1.79	1
Thr	120.1	74	19	8	2.46	1
[13C4,15N]-Thr	125.1	78.1	19	8	2.46	1
Cys	122	76	18	15	2.32	1
[13C3,15N]-Cys	126	79	18	15	2.32	1
Asn	133.1	74	35	14	1.79	1
Asp	134.1	74	35	10	1.42	1
[13C4,15N]-Asp	139.1	77	19	11	1.42	1
Gln	147.1	84	35	14	2.24	1
Glu	148.1	84	34	14	2.01	1
[13C5,15N]-Gln	154.1	89.1	17	14	2.24	1
Pro	116	70	35	10	5.13	2
[13C5,15N]-Pro	122.1	75.1	35	10	5.13	2
Val	118.1	72	35	9	6.05	2
[13C5,15N]-Val	124.1	77.1	35	9	6.05	2
Met	150.1	104	19	9	5.89	2
[13C5,15N]-Met	156.1	109.1	19	9	5.89	2
Tyr	182.1	136.1	20	12	5.44	2
[13C9,15N]-Tyr	192.1	145.1	20	12	5.44	2
Ile and Leu	132.1	86	35	9	6.76 and 6.9	3
[13C5,15N]-Ile and Leu	139.1	92	35	9	6.76 and 6.9	3
Lys	147.1	84	19	14	7.7	3
[13C6,15N2]-Lys	155.1	90.1	19	14	7.7	3
His	156.1	110	20	12	7.73	3
[13C6,15N3]-His	165.1	118.1	20	12	7.73	3
Phe	166.1	120	20	10	6.98	3
[13C9,15N]-Phe	176.1	129.1	20	10	6.98	3
Arg	175.1	70	24	18	7.85	3
[13C6,15N4]-Arg	185.1	75	24	18	7.85	3
Trp	205.1	146	19	14	7.04	3
[13C11,15N2]-Trp	218.1	156	19	14	7.04	3

Table 5.5. Ions and other parameters used for amino acid analysis.

CHAPTER VI – CONCLUDING REMARKS

Fruits may be sacrificial organs, but that does not mean they are necessarily suicidal. The modifications brought about during ripening to induce consumption and seed dispersal have been selected upon for greater fitness. Such metabolic alterations would not be present today if they were not the product of a tried and tested risk-reward balance. The preceding work focused on only on one of the many metabolic and physiological changes that plants undergo for the success of their offspring: aroma synthesis.

As demonstrated, apple and banana fruits actively engage the biosynthetic processes that directly subvert the products of primary metabolism for the production of specialized volatiles. In doing so, both fruits circumvent guard rails meant to protect tissues from the overaccumulation of the very metabolites necessary for volatile production. The author of this work helped to demonstrate several important aspects of citramalate synthase's role in apple volatile formation (Sugimoto, Engelgau, Jones, Song, & Beaudry, 2021). The above research in banana represents a likewise novel solution to an analogous problem. It would thus seem very likely that many fruits employ specialized means for the production of volatile precursors.

This work, as a whole, also illustrated two themes that may not be obvious from the microscopic scale of the previous chapters.

The first theme is that of biochemical "nodes" that act to support the synthesis of specialized molecules within branched-chain amino acid metabolism. The first node is the enzyme isopropylmalate synthase. The enzyme was found to be a central figure of how banana fruit synthesize their characteristic aroma (Chapter IV). Furthermore, citramalate synthase, the critical element of apple fruit aroma synthesis, is believed to have evolved from isopropylmalate synthase (Sugimoto, Engelgau, Jones, Song, & Beaudry, 2021). The enzyme has likewise been neofunctionalized several times, as previously stated, for the production of defense compounds in a diversity of taxa. Undoubtedly the enzyme, and its ability to internally extend α-ketoacids, will be found to act as a critical player to the synthesis of other specialized metabolites in future studies. The second node is much less recognized as having an interaction between primary and specialized metabolism: α-ketobutyrate. The citramalate synthase pathway is able to supply flux into anteiso-branched-chain metabolism through α-ketobutyrate, but it can also extend this compound further to prepare precursors for straight-chain esters with α-ketobutyrate acting as a potential precursor for propyl and propanoate esters as well. Furthermore, muskmelons (*Cucumis*

melo L.) have been found to provide for the synthesis of anteiso-branched-chain compounds through the processing of methionine to α-ketobutyrate (Gonda, et al., 2013). It seems likely that connections to α-ketobutyrate and specialized metabolism will continue to be uncovered in the future as well.

The second theme is that of the five-carbon ester element. Some of the most intriguing results of this dissertation have concerned each of the four possible isomers, listed here as acetate esters: pentyl acetate, 1-methylbutyl acetate, 2-methylbutyl acetate, and 3-methylbutyl acetate. In Chapter III, the synthesis of 2-methylbutyl and 3-methylbutyl esters was found to be dependent upon the activity of acetohydroxyacid synthase, whereas 1-methylbutyl ester synthesis was independent. Pentyl ester production, after inhibitor application, was found to have a nuanced relationship with 2-methylbutyl ester synthesis. Furthermore, the work of Chapter IV focused on the metabolic shifts needed for 3-methylbutyl ester synthesis in banana fruits. These compounds, their unique aromas, and their likewise unique biochemical origins highlight the exciting ways that plants attempt to attract consumers.

To conclude this work, I would like to provide a brief plea to the field of biochemistry. Our world is full of biochemicals critical to the health and wellbeing of humans, to the betterment of our society, and to future treatments and products for our species' continuation into man's ever evolving brave new world. However, it has appeared to me as I have pursued my studies that there exists a dearth of research upon some of the most commonplace biochemicals that all persons regularly encounter. These are the tangible compounds that provide fruits and vegetables with the colors, tastes, and aromas that have propelled them to be of such importance to every human culture.

Do these chemicals cure cancers? No. Will they provide a solution to combat climate change? No. Can they boost food production for a growing population? No.

These compounds do something else. They provide, in the simplest terms, happiness. This was their service to humankind in past millennia and it continues to be what they provide today. They represent one of the likely few remaining direct connections that humans have with their primordial forefathers. The vibrant red of an apple, the alluring scent of a banana, the sour pucker of citrus; these same sensations were once experienced by primaeval man and contributed to the further propagation and domestication of these crops. Today, these exact phenomena are experienced the world over.

However, the biosynthesis of these compounds seems to be largely taken for granted. Banana fruit do in fact produce their characteristic aroma and the conquests of chemistry have devised means for synthesizing these same compounds on a massive scale. Why bother understanding how a banana fruit does it?

While “logical” reasons may be conceived to answer such a question, I think the most earnest answer can be attributed simply to the intrinsic value that humankind places on these compounds.

Why should man explore the dark side of the moon? Perhaps there may be rich ore deposits there. Maybe a relic lies left behind for an intelligent species to one day find. However, I would argue that the best reason for exploring the dark side of the moon, and likewise the best reason for understanding the synthesis of these compounds, is as a service to humankind. For eons primaeval man has gazed upon our celestial partner and pondered upon that familiar face in the night. Undoubtedly many have wondered what may lie behind. Exploring these questions does not necessarily provide capital gains in a tangible sense, but it does provide an explanation to those facets of the natural world that, through their interaction with humankind, give meaning and interest to our lives.

To research the biosynthetic origins of these horticultural biochemicals sheds light on the natural mechanisms that provide humankind with the simple but joyous sensations experienced everyday around the world. For these reasons have I found my research to be so rewarding and for these same reasons do I implore others to research these otherwise unassuming compounds appreciated by persons today, in the past, and hopefully for a long time into the future.

LITERATURE CITED

Adebesin, F., Widhalm, J. R., Boachon, B., Lefèvre, F., Pierman, B., Lynch, J. H., . . . Dudareva, N. (2017). Emission of volatile organic compounds from petunia flowers is facilitated by an ABC transporter. *Science, 356*, 1386-1388.

Alsmairat, N., Engelgau, P., & Beaudry, R. (2018). Changes in free amino acid content in the flesh and peel of 'Cavendish' banana fruit as related to branched-chain ester production, ripening and senescence. *Journal of the American Society for Horticultural Science, 143*(5), 370-380.

Asif, M. H., Lakhwani, D., Pathak, S., Gupta, P., Bag, S. K., Nath, P., & Trivedi, P. K. (2014). Transcriptome analysis of ripe and unripe fruit tissue of banana identifies major metabolic networks involved in fruit ripening process. *BMC Plant Biology, 14*(316), 1471-2229.

Baraniuk, C. (2014, August 28). *The secrets of fake flavours*. Retrieved February 2023, from BBC: https://www.bbc.com/future/article/20140829-the-secrets-of-fake-flavours

Beaudry, R. M., Cameron, A. C., Shirazi, A., & Dostal-Lange, D. L. (1992). Modified-atmosphere packaging of blueberry fruit: effect of termperature on package O2 and CO2. *Journal of the American Society for Horticultural Science, 117*(3), 436-441.

Beaudry, R. M., Paz, N., Black, C. C., & Kays, S. J. (1987). Banana ripening: implications of changes in internal ethylene and CO2 concentrations, pulp fructose 2,6-bisphosphate concentration, and activity of some glycolytic enzymes. *Plant physiology, 85*, 277-282.

Beaudry, R. M., Severson, R. F., Black, C. C., & Kays, S. J. (1989). Banana ripening: implications of changes in glycolytic intermediate concentrations, glycolytic and gluconeogenic carbon flux, and fructose 2,6-bisphosphate concentration. *Plant physiology, 91*(4), 1436-1444.

Becot, F. A., Bradshaw, T. L., & Conner, D. S. (2016). Apple market expansion through value-added hard cide production: Current production and prospects in Vermont. *HortTechnology, 26*(2), 220-229.

Bedewitz, M., Jones, A., D'Auria, J. C., & Barry, C. S. (2018). Tropinone synthesis via an atypical polyketide synthase and P450-mediated cyclization. *Nature communications, 9*, 5281.

Beekwilder, J., Alvarez-Huerta, M., Neef, E., Verstappen, F., Bouwmeester, H., & Aharoni, A. (2004). Functional characterization of enzmyes forming volatile esters from strawberry and banana. *Plant physiology, 135*, 1865-1878.

Borges, R. M., Bessière, J.-M., & Hossaert-McKey, M. (2008). The chemical ecology of seed dispersal in monoecious and dioecious figs. *Functional ecology, 22*, 484-493.

Borges, R. M., Ranganathan, Y., Krishnan, A., Ghara, M., & Pramanik, G. (2011). When should fig fruit produce volatiles? Pattern in a ripening process. *Acta oecologica, 37*, 611-618.

Burg, S. P., & Burg, E. A. (1967). Molecular requirements for the biological activity of ethylene. *Plant physiology, 42*(1), 144-152.

Bushdid, C., Magnasco, M. O., Vosshall, L. B., & Keller, A. (2014). Humans can discriminate more than 1 trillion olfactory stimuli . *Science, 343*, 1370-1372.

Campbell, W. F., Evans, J. O., & Reed, S. C. (1976). Effects of glyphosate on chloroplast ultrastructure of quackgrass mesophyll cells. *Weed science, 24*(1), 22-25.

Carqueijeiro, I., Koudounas, K., Dugé de Bernonville, T., Sepúlveda, L., Mosquera, A., Bomzan, D., . . . Cruz, P. (2020). Alternative splicing creates a pseudo-strictosidine β-D-glucosidase modulating alkaloid synthesis in Catharanthus roseus. *Plant Physiology, 185*(3), 836-856.

Chen, L., Zhong, H.-y., Kuang, J.-f., Li, J.-g., Lu, W.-j., & Chen, J.-y. (2011). Validation of reference genes for RT-qPCR studies of gene expression in banana fruit under different experimental conditions. *Planta*(234), 377-390.

Contreras, C., & Beaudry, R. (2013). Lipoxygenase-associated apple volatiles and their relationship with aroma perception during ripening. *Postharvest biology and technology, 82*, 28-38.

Daccord, N., Celton, J.-M., Linsmith, G., Becker, C., Choisne, N., Schijlen, E., . . . Di Pierro, E. (2017). High-quality de novo assembly of the apple genome and methylome dynamics of early fruit development. *Nature Genetics, 49*, 1099-1106.

Dale, J., James, A., Paul, J.-Y., Khanna, H., Smith, M., Peraza-Echeverria, S., . . . Harding, R. (2017). Transgenic Cavendish with resistance to Fusarium wilt tropical race 4. *Nature Communications, 8*, 1496.

de Kraker, J.-W., & Gershenzon, J. (2011). From amino acid to glucosinolate biosynthesis: protein sequence changes in the evolution of methylthioalkylmalaate synthase in Arabidopsis. *The plant cell, 23*, 38-53.

de Kraker, J.-W., Luck, K., Textor, S., Tokuhisa, J. G., & Gershenzon, J. (2007). Two Arabidopsis genes (IPMS1 and IPMS2) encode isopropylmalate synthase, the branchpoint step in the biosynthesis of leucine. *Plant physiology, 143*, 970-986.

Dickinson, J., Harrison, S., & Hewlins, M. (1998). An investigation of the metabolism of valine to isobutyl alcohol in Saccharomyces cerevisiae. *The journal of biological chemistry, 273*(40), 25751-25756.

Dickinson, J., Harrison, S., Dickinson, J., & Hewlins, M. (2000). An investigation of the metabolism of isoleucine to active amyl alcohol in Saccharomyces cerevisiae. *The journal of biological chemistry, 275*(15), 10937-10942.

Dickinson, J., Lanterman, M., Danner, D., Pearson, B., Sanz, P., Harrison, S., & Hewlins, M. (1997). A 13C nuclear magnetic resonance investigation of the metabolism of leucine to isoamyl alcohol in Saccharomyces cerevisiae. *The journal of biological chemistry, 272*(43), 26871-26878.

Emanuelsson, O., Nielsen, H., & Von Heijne, G. (1999). ChloroP, a neural network-based method for predicting chloroplast transit peptides and their cleavage sites. *Protein Science, 8*(5), 978-984.

FAO. (2022). *Banana Market Review - Preliminary results 2022.* Rome.

Farrell, K. (2020, July 24). *Why bananas aren't as good as they used to be*. Retrieved February 2023, from USA Today: https://www.10best.com/interests/food-culture/bananas-arent-good-as-they-were-why-cavendish-gros-michel/

Feng, B.-h., Han, Y.-c., Xiao, Y.-y., Kuang, J.-f., Fan, Z.-q., Chen, J.-y., & Lu, W.-j. (2016). The banana fruit Dof transcription factor MaDof23 acts a repressor and interacts with MaERF9 in regulating ripening-related genes. *Journal of Experimental Botany, 67*(8), 2263-2275.

Ferenczi, A., Sugimoto, N., & Beaudry, R. (2021). Emission patterns of esters and their precursors throughout ripening and senescence in 'Redchief Delicious' apple fruit and implications regarding biosynthesis and aroma perception. *Journal of the American Society for Horticultural Science, 146*(5), 297-328.

Gawel, N. J., & Jarret, J. L. (1991). A modified CTAB DNA extraction procedure for Musa and Ipomoea. *Plant Moleuclar Biology Reporter, 3*(9), 262-266.

Goldberg, A., & St. John, A. C. (1976). Intracellular protein degradation in mammalian and bacterial cells: part 2. *Annual review of biochemistry, 45*(747-803).

Golding, J. B., Shearer, D., McGlasson, W. B., & Wyllie, S. G. (1999). Relationships between respiration, ethylene, and aroma production in ripening banana. *Journal of agricultural and food chemistry, 47*(4), 1646-1651.

Golding, J. B., Shearer, D., Wyllie, S. G., & McGlasson, W. B. (1998). Application of 1-MCP and propylene to identify ethylene-dependent ripening processes in mature banana fruit . *Postharvest biology and technology, 14*(1), 87-98.

Gonda, I., Bar, E., Portnoy, V., Lev, S., Burger, J., Schaffer, A. A., . . . Lewinsohn, E. (2010). Branched-chain and aromatic amino acid catabolism into aroma volatiles in Cucumis melo L. fruit. *Journal of experimental botany, 61*(4), 1111-1123.

Gonda, I., Lev, S., Bar, E., Sikron, N., Portnoy, V., Davidovich-Rikanati, R., . . . Lewinsohn, E. (2013). Catabolism of L-methionine in the formation of sultur and other volatiles in melon (Cucumis melo L.) fruit. *The Plant Journal, 74*, 458-472.

Gortner, W. A., Dull, G. G., & Krauss, B. H. (1967). Fruit development, maturation, ripening, and senescence: a biochemical basis for horticultural terminology. *HortScience, 2*(4), 141-144.

Guo, Y.-f., Zhang, Y.-l., Shan, W., Cai, Y.-j., Liang, S.-m., Chen, J.-y., . . . Kuang, J.-f. (2018). Identification of two transcriptoinal activators MabZIP4/5 in controlling aroma biosynthetic genes during banana ripening. *Journal of Agricultural and Food Chemistry, 66*, 6142-6150.

Halgand, F., Wessel, P., Laprévote, O., & Dumas, R. (2002). Biochemical and mass spectrometric evidence for quaternary structure modification of plant threonine deaminase induced by isoleucine. *Biochemistry, 41*, 13767-13773.

Harbach, C. J., Allen, T. W., Bowen, C. R., Davis, J. A., Hill, C. B., Leitman, M., . . . Hartman, G. L. (2016). Delayed senescence in soybean: terminology, research update, and survey results from growers. *Plant health progress, 17*(2), 64-154.

Harrison's flavoring extracts. (1853). Retrieved March 2023, from Library of Congress: https://www.loc.gov/item/2003680538/

Hawkes, T. R., Howard, J. L., & Pontin, S. E. (1989). Herbicides that inhibit the biosynthesis of branched chain amino acids. In A. D. Dodge, *Herbicides and plant metabolism.* Cambridge: Press Syndicate of the University of Cambridge.

Howard, N., Micheletti, D., Luby, J., Durel, C.-E., Denancé, C., Muranty, H., . . . Albach, D. (2023). Pedigree reconstruction for triploid apple cultivars using single nucleotide polymorphism array data. *Plants People Planet, 5*, 98-111.

Humphrey, J. E. (1894, February). Where bananas grow. *The Popular Science Monthly*, 486-502.

Jayanty, S., Song, J., Rubinstein, N., Chong, A., & Beaudry, R. (2002). Temporal relationships between ester biosynthesis and ripening events in bananas. *Journal of the American Society for Horticultural Science, 127*(6), 998-1005.

Jiang, G., Zhang, D., Li, Z., Liang, H., Deng, R., Zu, X., . . . Duan, X. (2021). Alternative splicing of MaMYB16L regulates starch degradation in banana fruit during ripening. *Journal of Integrative Plant Biology, 63*(7), 1341-1352.

Johnston, J. (1860). *A manual of chemistry, on the basis of Turner's elements of chemistry.*

Kaminaga, Y., Schnepp, J., Peel, G., Kish, C. M., Ben-Nissan, G., Weiss, D., . . . Vainstein, A. (2006). Plant phenylacetaldehyde synthase is a bifunctional homotetrameric enzyme that catalyzes phenylalanine decarboxylation and oxidation. *The journal of biological chemistry, 281*(33), 23357-23366.

Kent, E. N. (1854). *Descriptive Catalogue of Chemical Apparatus, Chemicals and Pure Reagents.*

Kitchen, L. M., Witt, W. W., & Rieck, C. E. (1981). Inhibition of chlorophyll accumulation by glyphosate. *Weed science, 29*(4), 513-516.

Kleber, C. (1912). The occurrence of amyl acetate in bananas. *The American Perfumer, 7*, 235-236.

Klee, H. J., & Tieman, D. M. (2018). The genetics of fruit flavour preferences. *Nature review genetics, 19*, 347-356.

Kletzinski, M. (1867). On fruit essences. *The American Journal of Pharmacy, 39*(5), 238-239.

Kochevenko, A., & Fernie, A. R. (2011). The genetic architecture of branched-chain amino acid accumulation in tomato fruits. *Journal of Experimental Botany, 62*(11), 3895-3906.

Kohlaw, G. (1988). α-Isopropylmalate synthase from yeast. *Methods enzymol, 166*, 414-423.

Koon, N., Squire, C. J., & Baker, E. N. (2004). Crystal structure of LeuA from Mycobacterium tuberculosis, a key enzyme in leucine biosynthesis. *PNAS, 101*(22), 8295-8300.

Kroumova, A. B., & Wagner, G. J. (2003). Different elongation pathways in the biosynthesis of acyl groups of trichome exudate sugar esters from various solanaceous plants. *Planta, 216*, 1013-1021.

Lam, P., Wang, L., Lo, C., & Zhu, F.-Y. (2022). Alternative splicing and its role in plant metabolism. *International Journal of Molecular Sciences, 23*(13), 7355.

Lambert, J. (2019, August 19). *Alarm as devastating banana fungus reaches the Americas*. Retrieved February 2023, from nature: https://doi.org/10.1038/d41586-019-02489-5

Lamprecht, W., & Heinz, F. (1984). Pyruvate. In H. U. Bergmeyer, *Methods of enzymatic analysis, third edition* (Vol. IV). Deerfield Beach, Florida, United State of America: Weinheim.

Lee, Y.-T., & Duggleby, R. G. (2001). Identification of the regulatory subunit of Arabidopsis thaliana acetohydroxyacid synthase and reconstitution with its catalytic subunit. *Biochemistry, 40*, 6836-6844.

Liao, P., Ray, S., Boachon, B., Lynch, J., Deshpande, A., McAdam, S., . . . Dudareva, N. (2021). Cuticle thickness affects dynamics of volatile emission from petunia flowers. *Natural chemical biology, 17*, 138-145.

Lomáscolo, S. B., Levey, D. J., Kimball, R. T., Bolker, B. M., & Alborn, H. T. (2010). Dispersers shape fruit diversity in Ficus (Moraceae). *Proceedings of the national academy of sciences, 107*(33), 14668-14672.

Lonhienne, T., Low, Y. S., Garcia, M. D., Croll, T., Gao, Y., Wang, Q., . . . Guddat, L. W. (2020). Structures of fungal and plant acetohydroxyacid synthases. *Nature, 586*, 317-321.

Lopez-Gomez, R., & Gomez-Lim, M. A. (1992). A method for extracting intact RNA from fruits rich in polysaccharides using ripe mango mesocarp. *HortScience, 27*(5), 440-442.

Macku, C., & Jennings, W. G. (1987). Production of volatiles by ripening bananas . *Journal of agricultural and food chemistry, 35*(5), 845-848.

Maisch, J. M. (1879). Artifical fruit essences. *The American Journal of Pharmacy, 51*(9), 144-146.

Maoz, I., Lewinsohn, E., & Gonda, I. (2022). Amino acids metabolism as a source for aroma volatiles biosynthesis . *Current opinion in plant biology, 67*, 102221.

Martin, G., Baurens, F.-C., Droc, G., Rouard, M., Cenci, A., Kilian, A., . . . D'Hont, A. (2016). Improvement of the banana "Musa acuminata" reference sequence using NGS data and semi-automated bioinformatics methods. *BMC Genomics*(17), 243.

McCarthy, A., Palmer, J. K., Shaw, C. P., & Anderson, E. E. (1963). Correlation of gas chromatographic data with flavor profiles of fresh banana fruit. *Journal of food science, 28*(4), 379-384.

McCourt, J. A., Pang, S. S., King-Scott, J., Guddat, L. W., & Duggleby, R. G. (2006). Herbicide-binding sites revealed in the structure of plant acetohydroxyacid synthase. *Proceedings of the National Academy of Sciences, 103*(3), 569-573.

McMurchie, E. J., McGlasson, W. B., & Eaks, I. L. (1972). Treatment of fruit with propylene gives information about the biogenesis of ethylene. *Nature, 237*(5352), 235-236.

Migicovsky, Z., Gardner, K., Richards, C., Chao, C., Schwaninger, H., Fazio, G., . . . Myles, S. (2021). Genomic consequences of apple improvement. *Horticulture Research, 8*(9).

Mirdita, M., Schutze, K., Moriwaki, Y., Heo, L., Ovchinnikov, S., & Steinegger, M. (2022). ColabFold: making protein folding accessible to all. *Nature methods, 19*, 679-682.

Morton, I., & MacLeod, A. (1990). *Food Flavours Part C. The Flavour of Fruits* (Vol. 3). London: Elsevier Science Publishers B.V.

Muranty, H., Denancé, C., Feugey, L., Crépin, J.-L., Barbier, Y., Tartarini, S., . . . Durel, C.-E. (2020). Using whole-genome SNP data to reconstruct a large multi-generation pedigree in apple germplasm. *BMC Plant Biology, 20*(2).

Murphy, C., Cain, W. S., & Bartoshuk, L. M. (1977). Mutual action of taste and olfaction. *Sensory Processes, 1*(3), 204-211.

Myers, M. J., Issenberg, P., & Wick, E. L. (1969). Vapor analysis of the production by banana fruit of certain volatile constituents. *Journal of food science, 34*(6), 504-509.

Myers, M. J., Issenberg, P., & Wick, E. L. (1970). L-Leucine as a precursor of isoamyl alcohol and isoamyl acetate, volatile aroma constituents of banana fruit discs. *Phytochemistry, 9*(8), 1693-1700.

Ning, J., Moghe, G. D., Leong, B., Kim, J., Ofner, I., Wang, Z., . . . Last, R. L. (2015). A feedback-insensitive isopropylmalate synthase affects acylsugar composition in cultivated and wild tomato. *Plant physiology, 169*, 1821-1835.

Noiton, D., & Alspach, P. (1996). Founding clones, inbreeding, coancestry, and status number of modern apple cultivars. *Journal of the American Society for Horticultural Science, 121*(5), 773-782.

Ortiz, R., & Swennen, R. (2014). From crossbreeding to biotechnology-facilitated improvement of banana and plantain. *Biotechnology Advances, 32*(1), 158-169.

Palmer, J., & McGlasson, W. (1969). Respiration and ripening of banana fruit slices. *Australian journal of biological sciences, 22*, 87-99.

Palmer, M., & Molloy, C. (2020, November 3). *It can cost over $10 million and 22 years to create a new apple variety. See what it took to markey the new 'Cosmic Crisp'*. Retrieved March 2023, from Business Insider: https://www.businessinsider.com/cosmic-crisp-apple-washington-state-scientists-2020-11

Peng, C., Uygun, S., Shiu, S.-H., & Last, R. L. (2015). The impact of the branched-chain ketoacid dehydrogenase complex on amino acid homeostasis in Arabidopsis . *Plant physiology, 169*, 1807-1820.

Perrier, X., De Langhe, E., Donohue, M., Lentfer, C., Vrydaghs, L., Bakry, F., . . . Denham, T. (2011). Multidisciplinary perspectives on banana (Musa spp.) domestication. *Proceedings of the national academy of sciences, 108*(28), 11311-11318.

Ploetz, R. C., Kepler, A. K., Daniells, J., & Nelson, S. C. (2007). Banana and plantain - an overview with emphasis on Pacific island cultivars. *Species profiles for Pacific island agroforestry*(1), 21-32.

Robert, X., & Gouet, P. (2014). Deciphering key features in protein structures with the end ENDscript server. *Nucleic Acids Research, 42*(W1), W320-W324.

Rodríguez, A., Alquézar, B., & Peña, L. (2013). Fruit aromas in mature fleshy fruits as signals of readiness for predation and seed dispersal. *New phytologist, 197*, 36-48.

Rodriquez, D. W. (1955). *Bananas.* South Africa: Government Printer.

Rogers, H. S., Donoso, I., Traveset, A., & Fricke, E. C. (2021). Cascading impacts of seed disperser loss on plant communities and ecosystems. *Annual review of ecology, evolution, and systematics, 52*, 641-666.

Rowan, D. D., Allen, J. M., Fielder, S., & Hunt, M. B. (1999). Biosynthesis of straight-chain ester volatiles in Red Delicious and Granny Smith apples using deuterium-labeled precursors. *Journal of agricultural and food chemistry, 47*, 2553-2562.

Rowan, D. D., Lane, H. P., Allen, J. M., Fielder, S., & Hunt, M. B. (1996). Biosynthesis of 2-methylbutyl, 2-methyl-2-butentyl, and 2-methylbutanoate esters in Red Delicious and Granny Smith apples using deuterium-labeled substrates. *Journal of agricultural and food chemistry*(44), 3276-3285.

Sainsbury, F., Thuenemann, E. C., & Lomonossoff, G. P. (2009). pEAQ: versatile expression vectors for easy and quick transient expression of heterologous proteins in plants. *Plant Biotechnol J., 7*, 682-693.

Schiller, D., Contreras, C., Vogt, J., Dunemann, F., Defilippi, B., Beaudry, R., & Schwab, W. (2015). A dual positional specific lipoxygenase functions in the generation of flavor compounds during climacteric ripening of apple. *Horticulture Research, 2*, 15003.

Schlegel, E. (2022, January 18). *The history of Gros Michel bananas* . Retrieved February 2023, from Miami Fruit: https://miamifruit.org/blogs/news/the-history-of-gros-michel-bananas#:~:text=From%201870%20until%20the%20late,even%20modeled%20after%20this%20flavor.

Schwieterman, M. L., Colquhoun, T. A., Jaworski, E. A., Bartoshuk, L. M., Gilbert, J. L., Tieman, D. M., . . . Clark, D. (2014). Strawberry flavor: diverse chemical compositions, a seasonal influence, and effects on sensory perception. *PLoS ONE, 9*(2), e88446.

Scientific American. (1853, September 3). Artificial Fruit Essences. *Scientific American, 8*(51), 402.

Shaner, D. L., & Reider, M. L. (1986). Physiological responses of corn (Zea mays) to AC 243,997 in combination with valine, leucine, and isoleucine. *Pesticide biochemistry and physiology, 25*(2), 248-257.

Shaner, D. L., & Singh, B. K. (1997). Acetohydroxyacid synthase inhibitors. In R. M. Roe, J. D. Burton, & R. J. Kuhr, *Herbicide activity: toxicology, biochemistry and molecular biology.* Amsterdam, Netherlands: IOS Press.

Shiota, H. (1993). New esteric components in the volatiles of banana fruit (Musa sapientum L.). *Journal of Agricultural and Food Chemistry, 41*(11), 2056-2062.

Sievers, F., Wilm, A., Dineen, D., Gibson, T., Karplus, K., Li, W., . . . Higgins, D. (2011). Fast, scalable generation of high-quality protein multiple sequence alignments using Clustal Omega. *Molecular Systems Biology, 7*(539).

Soluri, J. (2005). *Banana cultures.* Austin: University of Texas Press.

Sugimoto, N., Engelgau, P., Jones, A. D., Song, J., & Beaudry, R. (2021). Citramalate synthase yields a biosynthetic pathway for isoleucine and straight- and branched-chain ester formation in ripening apple fruit. *Proceedings of the national academy of sciences, 118*(3).

Sugimoto, N., Forsline, P., & Beaudry, R. (2015). Volatile profiles of members of the USDA Geneva Malus Core Collection: utility in evaluation of a hypothesized biosynthetic pathway for esters derived from 2-methylbutanoate and 2-methylbutan-1-ol . *Journal of agricultral and food chemistry*(63), 2106-2116.

Sugimoto, N., Jones, A. D., & Beaudry, R. (2011). Changes in free amino acid content in 'Jonagold' apple fruit as related to branched-chain ester production, ripening, and senescence. *Journal of the American Society for Horticultural Science, 136*(6), 429-440.

Sugimoto, N., Park, S., van Nocker, S., & Beaudry, R. (2008). Gene expression associated with apple aroma biosynthesis. *Acta Horticulturae, 768*, 57-64.

Suttle, J. C., & Schreiner, D. R. (1982). Effects of DPX-4189 (2-chloro-N-((4-methoxy-6-methyl-1,3,5-triazin-2-yl)amino-carbonyl)benzenesulfonamide) on anthocyanin synthesis, phenylalanine ammonia lyase activity, and ethylene production in soybean hypocotyls . *Candaian journal of botany, 60*(6), 741-745.

Thorpe, T. (1894). *A dictionary of applied chemistry* (Vol. 1). London: Longmans, Geen, and Co.

Tieman, D., Taylor, M., Schauer, N., Fernie, A., Hanson, A., & Klee, H. (2006). Tomato aromatic amino acid decarboxylases participate in synthesis of the flavor volatiles 2-phenylethanol and 2-phenylacetaldehyde. *Proceedings of the national academy of sciences, 103*(21), 8287-8292.

Tieman, D., Zhu, G., Resende Jr., M. F., Lin, T., Nguyen, C., Bies, D., . . . Zam. (2017). A chemical genetic roadmap to improved tomato flavor. *Science, 355*(6323), 391-394.

Tressl, R., & Drawert, F. (1973). Biogenesis of banana volatiles. *Journal of agricultural and food chemistry, 21*(4), 560-565.

Tressl, R., & Jennings, W. G. (1972). Production of volatile compounds in the ripening banana . *Journal of agricultural and food chemmistry, 20*(2), 189-192.

Trimmer, C., Keller, A., Murphy, N., Snyder, L., Willer, J., Nagai, M., . . . Mainland, J. (2019). Genetic variation across the human olfactory receptor repertoire alters odor perception. *Proceedings of the National Academy of Sciences, 116*(19), 9475-9480.

USDA. (2021, July 16). *Food Availability (Per Capita) Data System.* Retrieved March 2023, from USDA: https://www.ers.usda.gov/data-products/food-availability-per-capita-data-system/

Wang, C., Wang, Y., Chen, J., Liu, L., Yang, M., Li, Z., . . . Xu, H. (2022). Synthesis of 4-methylvaleric acid, a precursor of pogostone, involves a 2-isobutylmalate synthase related to 2-isopropylmalate synthase of leucine biosynthesis. *New phytologist, 235*, 1129-1145.

Weed Science Society of America. (2021, May 5). *Herbicide Site of Action Classification List.* Retrieved from WSSA: https://wssa.net/wssa/weed/herbicides/

Wyllie, S. G., & Fellman, J. K. (2000). Formation of volatile branched chain esters in bananas (Musa sapientum L.). *Journal of agricultural and food chemistry, 48*(8), 3493-3496.

Xing, A., & Last, R. L. (2017). A regulatory hierarchy of the Arabidopsis branched-chain amino acid metabolic network. *The plant cell, 29*, 1480-1499.

Xu, Q., Cheng, L., Mei, Y., Huang, L., Zhu, J., Mi, X., . . . Wei, C. (2019). Alternative splicing of key genes in LOX pathway involves biosynthesis of volatile fatty acid derivatives in tea plant (Camellia sinensis). *Journal of Agricultural and Food Science, 67*, 13021-13032.

Yabumoto, K., Jennings, W. G., & Pangborn, R. M. (1975). Evaluation of lactose as a transfer carrier for volatile flavor constituents . *Journal of food science, 40*(1), 105-108.

Yan, X., Bai, D., Song, H., & Pang, E. (2021). Alternative splicing during fruit development among fleshy fruits. *BMC Genomics, 22*, 762.

Yin, P., Zhen, Y., & Li, S. (2019). Identification and functional classification of differentially expressed proteins and insight into regulatory mechanism about flower color variegation in peach. *Acta Physiologiae Plantarum, 41*, 95.

Ziosi, V., Noferini, M., Fiori, G., Tadiello, A., Trainotti, L., Casadoro, G., & Costa, G. (2008). A new index based on vis spectroscopy to characterize the progression of ripening in peach fruit. *Postharvest biology and technology, 49*(3), 319-329.

APPENDIX A – THE HISTORY AND MYTH OF ARTIFICIAL BANANA FLAVOR

Within the United States, 'Gros Michel' was the dominant cultivar from the turn of the 20th century to 1965 when mounting disease pressure from *Fusarium oxysporum* f. sp. *cubense* forced production from the highly susceptible 'Gros Michel' to those with natural resistance. Cultivars of the 'Cavendish' group, although disliked by shippers and handlers due to the thinner peel, increased sensitivity to cold, and required ethylene application to induce even ripening, eventually won out among trialed cultivars (Soluri, 2005). Today, the vast monocultures of 'Cavendish' plantations are threatened by a new race of the same pathogen that caused the downfall of 'Gros Michel'. The fungus has recently spread to the Americas and seriously threatens the future of 'Cavendish' production (Lambert, 2019). There are currently no other cultivars that are resistant and are believed to be able to fulfil market requirements, meanwhile efforts to imbue 'Cavendish' with resistance are ongoing but have yet to be successful (Dale, et al., 2017) (Ortiz & Swennen, 2014).

During the years following the fall of 'Gros Michel' and rise of 'Cavendish', a mythos has formed concerning the lasting effects that the 'Gros Michel' has had on modern society. This myth, however, does not necessarily concern itself with an aspect of fruit production or the meteoric fall of 'Gros Michel', but rather with the role that 'Gros Michel' had on shaping the flavor of artificially banana-flavored candies and foodstuffs. Simply put, it is widely believed and disseminated that artificial banana flavor much more closely resembles the flavor of the now scarce 'Gros Michel' rather than of modern day's 'Cavendish' (Baraniuk, 2014) (Schlegel, 2022) (Farrell, 2020). However, to the best of our knowledge, no scientific study has been published that addresses this widespread myth.

'Gros Michel' are, however, not extinct. While production of the fruit within *Fusarium* impacted regions of Central America and the Caribbean are economically untenable, the fruit are still capable being produced, usually so in small quantities, by local growers in areas of low disease pressure. Thus, for the exploration of banana aroma diversity in Chapter V, 'Gros Michel' were acquired from small scale growers in southern Florida. Given our ability to sample *bona fide* 'Gros Michel' fruit, we felt that it was incumbent of us to investigate this myth.

To do so, we investigated what constitutes artificial banana flavor by collecting and sampling twenty-six banana-flavored products, including candies, schnapps, puddings, and baking mixes, purchased from American grocery stores throughout the United States, and

compared their aroma profiles to that of ripe ‘Valery’ (the common ‘Cavendish’ cultivar within the United States) and ‘Gros Michel’ fruit (Table A.1).

The aroma profiles of ‘Valery’ and ‘Gros Michel’ fruit were found to be remarkably similar (Table A.1). Over twenty compounds populate the headspaces with no single volatile composing more than 15% of the aroma profiles. The distribution of these compounds was also highly similar. The greatest divergence observed was a 5.6% difference of 3-methylbutanol content. 3-Methylbutyl acetate, which is often described in pop flavor science articles as being of much greater concentration in ‘Gros Michel’ fruit, only composed 2.3% more of the headspace of ‘Gros Michel’ fruit compared to ‘Valery’.

Among the food products tested, none had aroma profiles that were comparable to that of either cultivar (Table A.1). 3-Methylbutyl acetate, which is regularly attested to in pop articles as being of much greater abundance in ‘Gros Michel’ fruit, was found to dominate the profiles of every product, representing, on average, 64% of the aroma profile. The headspaces of ‘Valery’ and ‘Gros Michel’ are composed of only 11.8% and 14.1% of 3-methylbutyl acetate, respectively. The lowest proportion found in a product, 24.8% was from a banana-based baby food. The next lowest, 34.1%, was of a banana-flavored candy chew. Furthermore, more than 40% of products, whether listed as naturally or artificially flavored, contained 2-methylbutyl acetate, a compound not normally produced by bananas. However, in these instances 3-methylbutyl acetate was still the dominant isomer. The most extreme example of reliance upon 3-methylbutyl acetate was in a banana-flavored schnapps whose only aroma compounds detected were 3-methylbutyl acetate with trace amounts of 2-methylbutyl acetate.

Many of the volatiles naturally produced by banana fruit were not detected in the products tested, including in those with banana listed as an ingredient (Table A.1). For example, 2-methylpropanol and 2-pentanol, which together represent 8.6% and 6.9% of the aroma profiles of ‘Valery’ and ‘Gros Michel’, respectively, were not detected in any product. Overall, no foodstuffs matched the complexity of either cultivar.

There were also many volatiles that are not produced by ‘Valery’ or ‘Gros Michel’ fruit that were found in the products tested (Table A.1). The most common additive, limonene, a staple of citrus aroma, composed more than 15% of the aroma profile of a popular banana-flavored hard candy. Many products also had substantial quantities of ethyl butanoate. While this

compound is naturally present in the headspace of banana fruit, it constitutes less than 1% of ‘Gros Michel’ and ‘Valery’ aroma profiles.

Overall, beyond the omnipresent dominance of 3-methylbutyl acetate, no pattern could be discerned for banana or banana-related flavored products. Ultimately the banana-flavored candy Hi-Chew (Morinaga & Company), which contains banana and is listed as being artificially and naturally flavored, was most emblematic of banana fruits, however it was still deficient of several naturally occurring compounds and the distribution of its volatiles diverged from that of real fruit.

Together, our results clearly dispute the notion that artificial banana flavor is a stand-in for ‘Gros Michel’ fruit.

The similarity of aroma profiles between ‘Gros Michel’ and ‘Valery’ fruit is, perhaps, not of great surprise: the discerned pedigrees of these cultivars indicate them to be closely related. Both cultivars are believed to be derived from the same 2N donor and closely related N donors (Perrier, et al., 2011). Perhaps it is no wonder that a society, who had for decades strongly resisted moving on from ‘Gros Michel’ (Soluri, 2005), would accept ‘Cavendish’ when disease pressure made production of the former economically unfeasible; their aroma profiles are nearly identical.

It may be that the ultimate source of the now defunct myth concerning the ‘Gros Michel’ origin of artificial banana flavor was from interpretations of a 1963 study that included a flavor panel sampling these same cultivars (McCarthy, Palmer, Shaw, & Anderson, 1963). The five-person panel, which openly discussed the perceived flavor of, at times, only two fruit per ripeness stage, attributed ‘Valery’ fruits as having *“a much fuller and more interesting flavor than… ‘Gros Michel’ fruit”*. The study also concluded that the *“chromatograms of the ‘Gros Michel’ fruit revealed the presence of those compounds responsible for the ‘banana-like’ flavor, but showed little or none of the volatiles associated with ‘fruitiness’. The ‘Valery’ fruit, however, contained substantial amounts of the compounds contributing to both ‘banana’ and ‘fruity’ impressions”*. Such chromatogram findings clearly clash with those described herein and published previously (Tressl & Drawert, 1973). It may be that faulty sampling methods, biased panelists, minimal sample sizes, as well as ‘Gros Michel’ fruit sourced from Honduras at the height of the first Fusarium wilt epidemic (Soluri, 2005) led to these misleading results.

A question, however, still remains: if artificial banana flavor is not emblematic of 'Gros Michel' fruit, then what is it based on?

While the first documented bunch of bananas to reach New York City was in 1804 (Rodriquez, 1955), it took nearly a century for the fruit to reach their current popularity. By the 1840's, red Cuban bananas still sold for $0.25 a fruit (~$10, 2023) (Soluri, 2005) and in 1876 banana plants were exhibited at the 1876 Centennial Exposition in Philadelphia as a novelty. Perhaps the best indication of the dramatic rise of banana consumption in the United States was by American botanist James Ellis Humphrey (1861-1897), who commented in 1894 that bananas had transcended from a rare childhood luxury to a commonplace item of adulthood, rivaling apples as a staple article of the American diet (Humphrey, 1894).

Imitation banana essence, however, was displayed at the New York City Exhibition of the Industry of All Nations World's Fair in 1853 (Scientific American, 1853). That same year an advertisement in Philadelphia was published to market, among many other flavors, banana flavoring extract (Harrison's flavoring extracts, 1853). A year later, 3-methylbutyl acetate, the chemical found to be dominant in every banana-flavored product tested, was listed in a chemical catalog as banana essence (Kent, 1854).

These seemingly anachronistic records illustrate a history unlike what is regularly shared today (Figure A.1). The combinations of chemicals used to artificially flavor sweets were not selected upon due to their known presence in the fruit being mimicked, but because they were sufficient to remind chemists of their flavor target. The natural presence of 3-methylbutyl acetate in banana fruit aroma was not determined until 1912 (Kleber, 1912). Furthermore, 3-methylbutyl acetate, despite not being present in high amounts in any other commercially produced fruits (Morton & MacLeod, 1990), was likewise used regularly in a variety of fruit flavorings, including that of strawberry, raspberry, orange and pear (Kletzinski, 1867). The compound's precursor, 3-methylbutanol, was regularly available as the major component of fusel oil, a byproduct from the fermentation and distillation of spirits (Thorpe, 1894).

It is then very likely that many Americans would have experienced eating a banana-flavored treat before, or at least more regularly than, eating an actual banana fruit in the mid-1800s. Thus, the use of 3-methylbutyl acetate as artificial banana flavoring in the United States, for many, predated real banana fruits.

This work demonstrates the risk from the continuous amplification of unreproduced and unproved results, culminating in a disregard for history and the transformation of misinterpretations into accepted fact.

Figures & Tables

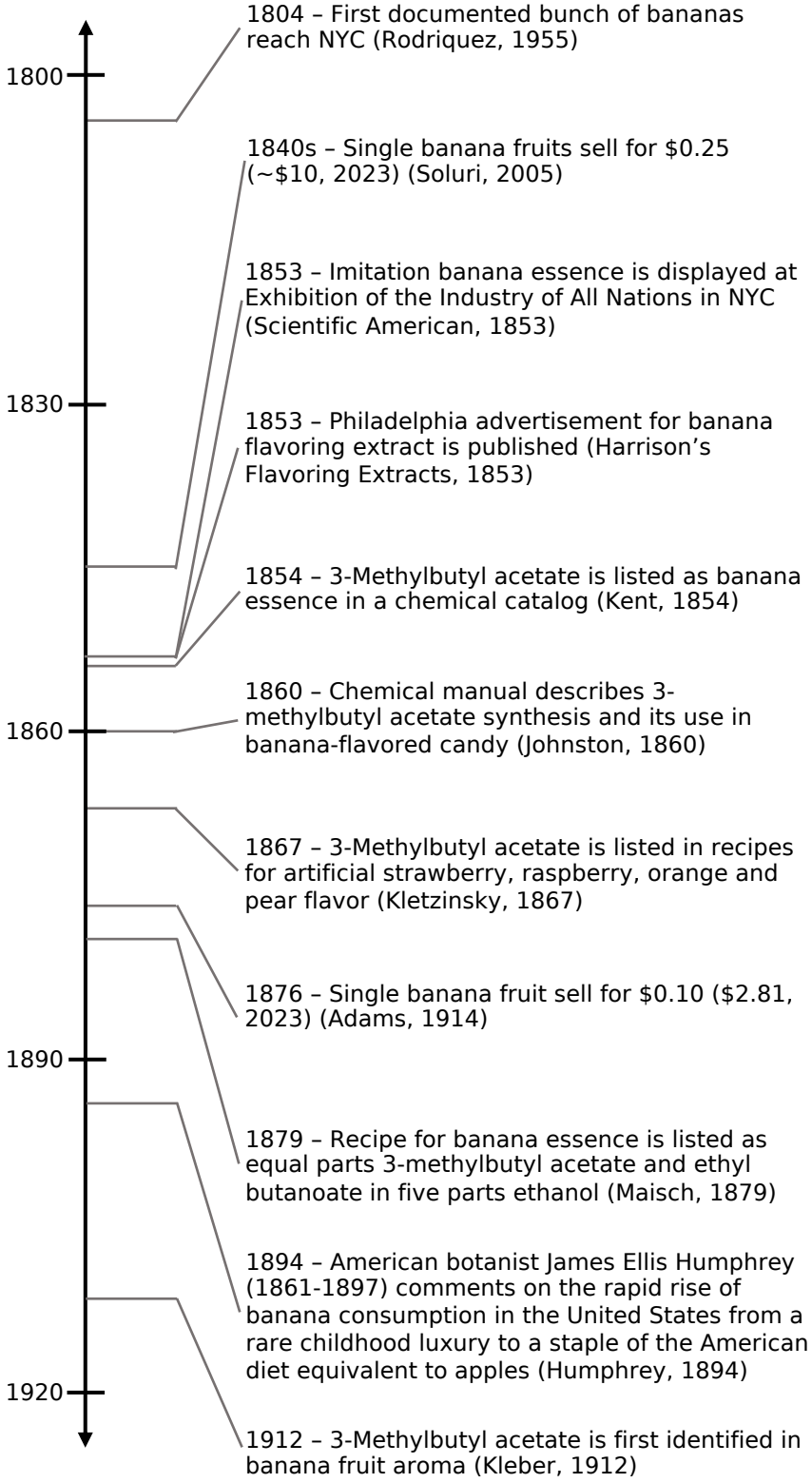

Figure A.1. Timeline of artificial banana flavoring in the United States.

no.	product	product type	listed flavor	flavoring source	contains banana
1	whole 'Valery' banana fruit	ripe fruit	-	-	-
2	whole 'Gros Michel' banana fruit	ripe fruit	-	-	-
3	Kroger Imitation Banana Flavor	flavorant	banana	artificial	no
4	99 Bananas Schnapps	schnapps	banana	NA[b]	NA[b]
5	Now & Later Candy	candy	banana	artificial	no
6	Dubble Bubble Bananarama Candy	candy	banana	artificial	no
7	Dubble Bubble Crazy Bananas Candy (yellow pieces)	candy	banana	artificial	no
8	Hi-Chew	candy	banana	natural and artificial	yes
9	Lolli & Pops Giant Gummy Banana	candy	banana	natural and artificial	no
10	Taffy Town Banana Taffy	candy	banana	natural and artificial	no
11	Taffy Town Banana Cream Pie Taffy	candy	BCP	natural and artificial	no
12	Nestle Runts Candy (banana pieces)	candy	banana	natural	no
13	Nestle Laffy Taffy Candy Laff Bites	candy	gone bananas	natural	no
14	Jelly Belly Top Banana Jelly Beans	candy	top banana	natural and artificial	yes

Table A.1. Headspaces of banana-flavored foodstuffs and ripe fruit. BCP = banana cream pie, B&C = bananas and cream. Volatile concentrations presented as precent of total ion count normalized by molecular weight. [a] some 3-methylbutyl acetate peaks were found to also contain some 2-methylbutyl acetate. [b] alcoholic beverages are not required to have their ingredients disclosed. [c] those naturally found in banana are listed in italics.

Table A.1 (cont'd)

no.	ethyl butanoate	butyl acetate	butyl butanoate	2-methyl-propanol	2-methylpropyl acetate	2-methylpropyl butanoate	3-methyl-butanol	3-methylbutyl acetate[a]
1	0.5%	4.1%	2.9%	4.2%	8.5%	7.4%	14.9%	11.8%
2	0.6%	4.7%	2.6%	2.6%	9.1%	7.0%	9.3%	14.1%
3	0.0%	0.0%	0.0%	0.0%	0.0%	0.0%	2.5%	67.3%
4	0.0%	0.0%	0.0%	0.0%	0.0%	0.0%	0.0%	100%[a]
5	17.0%	0.0%	0.0%	0.0%	0.0%	0.0%	0.0%	51.1%
6	7.4%	0.0%	0.0%	0.0%	0.0%	0.0%	0.5%	86.3%[a]
7	6.3%	1.4%	0.6%	0.0%	0.0%	0.0%	1.0%	64.3%[a]
8	3.9%	16.8%	2.1%	0.0%	22.2%	1.3%	1.6%	34.1%[a]
9	0.3%	0.0%	0.0%	0.0%	0.0%	0.0%	0.0%	48.6%[a]
10	24.5%	0.0%	0.0%	0.0%	15.5%	0.0%	0.0%	41.6%
11	28.4%	0.0%	0.0%	0.0%	15.3%	0.0%	0.0%	44.2%
12	4.1%	0.5%	0.0%	0.0%	3.7%	0.0%	3.2%	71.9%
13	5.9%	1.3%	0.0%	0.0%	6.5%	0.0%	1.0%	73.4%
14	9.4%	0.0%	0.0%	0.0%	0.0%	0.0%	0.0%	90.6%

Table A.1 (cont'd)

no.	3-methylbutyl butanoate	3-methylbutyl 3-methylbutanoate	2-pentanol	2-pentanone	1-methylbutyl acetate	1-methylbutyl butanoate	limonene
1	8.6%	3.2%	4.5%	4.6%	7.7%	2.7%	0.0%
2	10.2%	5.7%	4.4%	6.2%	8.0%	3.7%	0.0%
3	0.0%	29.8%	0.0%	0.0%	0.0%	0.0%	0.4%
4	0.0%	0.0%	0.0%	0.0%	0.0%	0.0%	0.0%
5	0.0%	0.0%	0.0%	0.0%	0.0%	0.0%	0.0%
6	5.7%	0.0%	0.0%	0.0%	0.0%	0.0%	0.0%
7	19.1%	0.0%	0.0%	0.0%	0.0%	0.0%	5.3%
8	3.0%	2.6%	0.0%	4.8%	3.1%	0.0%	0.0%
9	14.0%	22.6%	0.0%	0.0%	0.0%	0.0%	0.0%
10	0.0%	3.6%	0.0%	0.0%	0.0%	0.0%	0.0%
11	0.0%	1.4%	0.0%	0.0%	0.0%	0.0%	0.0%
12	0.0%	0.0%	0.0%	0.0%	0.0%	0.0%	15.5%
13	0.0%	0.0%	0.0%	0.0%	0.0%	0.0%	10.9%
14	0.0%	0.0%	0.0%	0.0%	0.0%	0.0%	0.0%

Table A.1 (cont'd)

no.	other compounds[c]
1	*ethyl acetate (4.7%), propyl acetate (3.8%), butanol (1.6%), 2-heptanone (0.8%), 2-methylpropyl 2-methylpropanoate (0.7%), 2-methylpropyl 3-methylbutanoate (1.1%), mix of hexyl acetate and 3-methylbutyl 2-methylpropanoate (1.8%)*
2	*ethyl acetate (5.1%), propyl acetate (0.3%), butanol (0.9%), 2-heptanone (0.8%), 2-methylpropyl 2-methylpropanoate (0.8%), 2-methylpropyl 3-methylbutanoate (1.8%), mix of hexyl acetate and 3-methylbutyl 2-methylpropanoate (2.1%)*
3	
4	
5	pentyl acetate (31.9%)
6	
7	ethyl hexanoate (2.0%)
8	*2-heptanone (1.2%)* , 2-hexenal (2.4%)
9	ethyl hexanoate (1.6%), cyclohexyl acetate (12.9%)
10	3-methylbutanal (3.4%), ethyl 2-methylbutanoate (5.3%), cis-3-hexenyl acetate (4.9%), 2-butyl-4-methyl-1,3-dioxolane (1.2%)
11	3-methylbutanal (2.4%), ethyl 2-methylbutanoate (3.9%), cis-3-hexenyl acetate (2.2%), 2-butyl-4-methyl-1,3-dioxolane (2.2%)
12	
13	*ethyl acetate (1.0%)*
14	

Table A.1 (cont'd)

no.	product	product type	listed flavor	flavoring source	contains banana
15	Budget $aver Twin Pops	popsicle	banana	natural and artificial	no
16	Simply Delish Sugar Free Keto Pudding	pudding	banana	natural	no
17	Jello Instant Pudding & Pie Filling	pudding	banana cream	natural and artificial	no
18	Kroger Pudding and Pie Filling	pudding	banana cream	artificial	no
19	Snack Pack Banana Cream Pie Pudding (mixed)	pudding	BCP	natural and artificial	yes
20	Kroger Bananas & Cream Instant Oatmeal	oatmeal	B&C	natural	yes
21	Quaker Bananas & Cream Instant Oatmeal	oatmeal	B&C	natural	yes
22	Gerber Grain & Grow Puffs	baby food	banana	natural	no
23	Gerber Natural for Baby	baby food	banana	natural	yes
24	King Arthur Baking Company Gluten Free Banana Bread Mix	baking mix	banana	natural	yes
25	Krusteaz Banana Quick Bread Mix	baking mix	banana	natural	yes
26	Krusteaz Banana Nut Muffin Mix	baking mix	banana nut	natural	yes
27	Martha White Banana Nut Muffin Mix	baking mix	banana nut	natural and artificial	yes
28	Duncan Hines Dolly Parton's Southern Style Cake Mix	baking mix	banana	natural	yes

Table A.1 (cont'd)

no.	ethyl butanoate	butyl acetate	butyl butanoate	2-methyl-propanol	2-methylpropyl acetate	2-methylpropyl butanoate	3-methyl-butanol	3-methylbutyl acetate[a]
15	0.0%	0.0%	0.0%	0.0%	9.7%	0.0%	0.0%	65.6%
16	0.0%	0.0%	0.0%	0.0%	5.4%	0.0%	0.0%	90.0%[a]
17	0.0%	0.0%	0.0%	0.0%	0.0%	0.0%	0.0%	78.5%[a]
18	0.0%	0.0%	0.0%	0.0%	0.0%	0.0%	0.0%	81.5%[a]
19	0.0%	0.0%	0.0%	0.0%	0.0%	0.0%	0.0%	95.6%[a]
20	6.5%	0.0%	0.0%	0.0%	19.3%	1.6%	0.1%	67.6%
21	0.0%	0.0%	0.0%	0.0%	13.4%	0.0%	0.0%	86.3%
22	5.5%	0.0%	0.0%	0.0%	5.6%	0.0%	2.1%	86.8%
23	1.1%	3.7%	0.4%	0.0%	13.7%	1.9%	0.0%	24.8%
24	0.0%	0.0%	0.0%	0.0%	0.0%	0.0%	0.0%	51.1%[a]
25	0.0%	0.0%	0.0%	0.0%	13.8%	0.0%	0.0%	68.1%
26	10.7%	0.0%	0.0%	0.0%	13.4%	0.0%	0.0%	72.3%
27	0.0%	0.0%	0.0%	0.0%	0.0%	0.0%	0.0%	49.6%[a]
28	0.0%	0.0%	0.0%	0.0%	0.0%	0.0%	0.0%	53.8%

Table A.1 (cont'd)

no.	3-methylbutyl butanoate	3-methylbutyl 3-methylbutanoate	2-pentanol	2-pentanone	1-methylbutyl acetate	1-methylbutyl butanoate	limonene
15	4.3%	0.0%	0.0%	0.0%	0.0%	0.0%	4.2%
16	0.0%	0.8%	0.0%	0.0%	0.0%	0.0%	3.8%
17	19.1%	1.9%	0.0%	0.0%	0.0%	0.0%	0.5%
18	0.0%	6.0%	0.0%	0.0%	0.0%	0.0%	2.1%
19	0.0%	4.4%	0.0%	0.0%	0.0%	0.0%	0.0%
20	0.7%	0.0%	0.0%	1.9%	0.0%	0.0%	0.0%
21	0.0%	0.0%	0.0%	0.0%	0.0%	0.0%	0.0%
22	0.0%	0.0%	0.0%	0.0%	0.0%	0.0%	0.0%
23	5.5%	2.2%	0.0%	28.1%	8.2%	0.8%	0.0%
24	0.0%	22.5%	0.0%	0.0%	0.0%	0.0%	0.0%
25	0.0%	0.0%	0.0%	0.0%	0.0%	0.0%	0.0%
26	0.0%	0.0%	0.0%	0.0%	0.0%	0.0%	0.0%
27	18.3%	20.8%	0.0%	0.0%	0.0%	0.0%	0.0%
28	14.3%	28.0%	0.0%	0.0%	0.0%	0.0%	3.9%

Table A.1 (cont'd)

no.	other compounds[c]
15	butyl 2-methylpropanoate (16.3%)
16	
17	
18	pentyl formate (2.1%), pentyl butanoate (5.1%), 2-methylbutyl butanoate (3.2%)
19	
20	*ethyl acetate (2.4%)*
21	*ethyl acetate (0.3%)*
22	
23	*ethyl acetate (3.6%)* , dimethyl sulfide (6.2%)
24	*2-heptanone (3.8%)* , pentyl acetate (22.7%)
25	*ethyl acetate (0.9%)* , assorted monoterpenes (17.2%)
26	*ethyl acetate (1.1%)* , benzaldehyde (2.5%)
27	pentyl 3-methylbutanoate (4.6%), cis-3-hexenyl acetate (6.7%)
28	

APPENDIX B – NANOPORE SEQUENCING OF THE CITRAMALATE SYNTHASE LOCUS

Summary

Upon my arrival to the lab, much of the research concerning citramalate synthase and its role as a facilitator to the biosynthesis of 2-methylbutyl and 2-methylbutanoate esters in ripening apple fruits was complete. It was also already known that there exists a great diversity among apple cultivars with regards to the content of 2-methylbutyl and 2-methylbutanoate esters that they may produce (Sugimoto, Forsline, & Beaudry, 2015). However, there was no understanding of what mechanisms may be leading to such a breadth of volatile content between different cultivars. To discern these underlying mechanisms was my initial charge when joining the lab.

When reviewing an early draft manuscript concerning citramalate synthase's role in apple aroma biosynthesis, I was drawn to the description of an inactive allele of citramalate synthase (MdCMS_2). That this allele may be responsible for the virtual absence of 2-methylbutyl and 2-methylbutanoate esters in some cultivars seemed to be a reasonable hypothesis. I promptly tested this idea, performing Sanger sequencing of the consequential SNP of citramalate synthase in the dozen cultivars identified by Sugimoto et al., (2015) to have exceptionally high or low levels of 2-methylbutyl and 2-methylbutanoate esters as compared to other common apple esters. My initial hypothesis was right: cultivars homozygous for MdCMS_2 produce only slight quantities of 2-methylbutyl and 2-methylbutanoate esters, whereas those with at least one copy of the active MdCMS_1 allele have moderate to high amounts. I subsequently sequenced a total of 99 apple cultivars previously investigated by Sugimoto et al., (2015) to be certain. These results, as well as metabolic data from the transient expression of MdCMS in tobacco leaves, were published with the major publication describing citramalate synthase (Sugimoto, Engelgau, Jones, Song, & Beaudry, 2021).

The relative ease with which I verified the importance of this SNP was misleading. Surely such a key finding to my assigned task should take more effort. Under this misconception, I pursued what I now retroactively consider to be a bloated and callow experiment that mirrored the previously described succinct and focused one.

I hypothesized that other genetic variants, either within the MdCMS gene or of the surrounding locus, may be likewise imparting an outsized and thus easily detectable role on the activity of citramalate synthase. I was specifically hopeful of the potential results to illuminate

the variation of 2-methylbutyl and 2-methylbutanoate ester content among cultivars with at least one copy of MdCMS_1.

To pursue this idea, I considered various sequencing strategies. Variants, such as SNPs or indels, may have synergistic activity with one another. Thus I was interested in methods that allow for haplotyping. Sanger sequencing of amplified DNA may indicate SNPs, but they cannot be associated with one another and data following an indel is unusable. Cloning of the desired regions followed by Sanger sequencing can suffice to produce phased haplotypes due to the presence of a single sequence in a sample, but the initial cost greatly increases as the number of samples and length of sequence increase. Short-read sequencing, such as that by Illumina, would avoid the problem caused by indels in mixed-amplicon Sanger sequencing, but any variants greater than double the typical read-length, or 100-600 bp apart on average, cannot be associated. Longer reads, such as those produced by PacBio and Oxford Nanopore instruments, although of much lesser quality than short-read technologies, do allow for haplotype phasing. Thus, given the availability of the latter at the Michigan State University Genomics Research Technology Support Facility, Oxford Nanopore sequencing was performed.

About two dozen cultivars, composed of popular past and present cultivars, as well as those with exceptionally high or low levels of 2-methylbutyl and 2-methylbutanoate esters as compared to other common apple esters, had the citramalate synthase locus amplified and sequenced. This region was composed of citramalate synthase as well as the upstream sequence prior to the next predicted gene (Daccord, et al., 2017).

Many variants were detected in this region, including two large structural variants within 1 kb of the start codon of citramalate synthase (Table B.1). However, many of the SNPs identified through the analysis had to be discarded as they were within or in close proximity to stretches of repeating nucleotides, motifs that are known to be error prone when using long-read sequencing technologies. Ultimately, despite the extensive amount of time taken to analyze the data, including forming a novel analysis pipeline for the still nascent and poorly supported technology, no correlation could be discerned between the variants detected and their cultivar's aroma profiles.

I learned many lessons from this experience.

While cloning and Sanger would in fact have been expensive, the time saved by performing a mundane but known method, and the increased quality of sequencing data, would

have far outweighed the extensive amount of time taken to process the only moderately accurate Nanopore data. Thus, the prosaic but understood method may very well be more efficient than the clever but unknown one.

Furthermore, the overall experimental premise was questionable. While enzymatic data of MdCMS_2 provided a viable platform to hypothesize upon, the notion that such a potent association may be made by blindly sequencing a locus is naïve. If I were to perform this experiment again, with the goal of finding genetic variants that associate with a trait, I would cast a much greater net and sequence the entire genome of my experimental cultivars. However, it should be said that such an experiment still lacks a definitive hypothesis and, by nature of the enormous number of variants considered, lends itself to substantial noise and false positives.

Thus, while this experiment lacked the desired scientific results, I ultimately gained valuable perspective with regard to the value of time versus money spent, as well as the importance of pursing experiments with feasible and promising outcomes, as opposed to those where a great quantity of work may ultimately result in nothing to show for.

Materials and Methods

DNA from the following cultivars was extracted from leaf or petal tissues with a Qiagen Dneasy Plant Mini Kit: ‘Empire’, ‘Red Chief Delicious’, ‘Spur McIntosh’, ‘Nova Easygro’, ‘Burgundy’, ‘Cox’s Orange Pippin’, ‘Jonafree’, ‘PRI 1850-4’, ‘Virginiagold’, ‘Honeycrisp’, ‘Fulford Gala’, ‘Idared’, ‘Jonathan’, ‘Fuji’, ‘Granny Smith’, ‘Braeburn’, ‘Pink Lady’, ‘Kanzi’, ‘Trent’, ‘PRI 1312-6’, ‘Cortland’, ‘Golden Delicious’, ‘SweeTango’, ‘Jonagold’, and ‘PRI 1176-1’. The cultivars were selected based on their past or present popularity, contribution to apple breeding, or if they were found to have exceptionally high or low ratios of 2-methylbutyl and 2-methylbutanoate esters to straight chains esters (Sugimoto, Forsline, & Beaudry, 2015).

MdCMS (Md05g1155100) as well as the upstream genetic region spanning from MdCMS to the next gene (Daccord, et al., 2017) were amplified using Thermofisher Phusion High Fidelity Polymerase. Per 25 µL reaction: 5 µL 5X High Fidelity Buffer, 0.5 µL 10 mM dNTPs, 1.25 µL 10 µM of each primer, 2.5 µL DNA, 0.25 µL High Fidelity Polymerase, 0.2 µL 50 mM $MgCl_2$. Thermocycler conditions: 30 s 98 ℃, followed by 30 cycles of 5 s 98 ℃, 10 s 63 ℃, 60 s 72 ℃, followed by 10 min 72 ℃. The forward primer of each cultivar had a 5’ 16 bp unique section of sequence to serve as a barcode for multiplexing. Forward primer: NNNNNNNNNNNNNNNCATCTCCACCTTTGAAGCCCTCT. Reverse primer:

CCCAGAATCGACAATGGAGGA. Amplicons were then purified with a New England Biolabs Monarch PCR & DNA Cleanup Kit and quantified with a Qubit and dsDNA High Sensitivity Assay Kit before being mixed in an equimolar concentration for sequencing library preparation.

Nanopore sequencing was performed using Oxford Nanopore Technologies kits and instruments. Amplicons were prepared with an SQK-LSK108 1D kit and sequenced on a GridION (flowcell: FLO-MIN106 R9.4.1, GridION Release: 18.04.1-0).

Reads were basecalled with Guppy (v3.1.5) prior to demultiplexing with Porechop (v0.2.3) and filtering to quality scores > 15 with NanoFilt (v2.2.0). Reads were indexed against the amplified region of the Golden Delicious Double Haploid genome (Daccord, et al., 2017) using minimap2 (v2.16-r922) and samtools (v1.9). Reads were then phased by haplotype via WhatsHap (v0.18) based on known SNPs. Haplotyped reads were then assembled into a draft sequence by canu (v1.8). For this process a seed contig was hand-selected to match with known variants. The draft sequence was then polished against raw electrical nanopore reads by Nanopolish (v0.11.0). Variants were then curated to disregard those within tandem repeats greater than 7 bp as these were predicted to likely be an artefact of sequencing/basecalling. Other tools and programs used: htslib (v1.9), seqtk (v1.3-r106), Python 3.7.1.

Code Used

```
#STEP ONE
#HPCC basecalling script using Guppy

#!/bin/bash
#SBATCH --job-name=<JOB_NAME>
#SBATCH --nodes=1
#SBATCH --gres=gpu:4
#SBATCH --ntasks-per-node=1
#SBATCH --cpus-per-task=4
#SBATCH --time=0-12:00:00
#SBATCH --mem=3102
#SBATCH --mail-type=ALL
#SBATCH --mail-user=<YOUR_EMAIL>
#SBATCH --constraint="intel18&v100"
module purge && module use /mnt/home/johnj/software/modulefiles
module load Guppy/3.1.5
nvidia-smi
guppy_basecaller -i <PATH_TO_INPUT_FAST5_DIRECTORIES> \
```

```
--recursive \
-s  <PATH_TO_OUTPUT_BASECALLED_FASTQS> \
--flowcell FLO-MIN106 \
--kit SQK-LSK108 \
-x auto \
--num_callers 8 \
--qscore_filtering true \
--min_qscore 7 \
--disable_pings \
-q 0

#STEP TWO
#Demultiplex reads by cultivar using barcodes via Porechop (split up data into three sets to not overload computer)

python3 porechop-runner.py -i /Volumes/TeraPhil/nanopore/Data/20180817_ONT_Amplicon/basecalls/set_one/pass/ -b /Volumes/TeraPhil/nanopore/new_data/set_1_demulti/ --adapter_threshold 50

#STEP THREE
#Filter reads to greater than Qscore of 15 via NanoFilt (Below is an example from a loop)

#cat ${cult}/${cult}1all.fastq | NanoFilt -q 15 > ${cult}/${cult}1above15.fastq
#cat ${cult}/${cult}2all.fastq | NanoFilt -q 15 > ${cult}/${cult}2above15.fastq

#STEP FOUR
#Index reads against the Golden Delicious Double Haploid (GDDH) corresponding to what I sequenced via minimap2 and samtools (below is example for TRE)

minimap2 -ax map-ont GDDH_cms2_updown_LplusQ.fasta TREabove11.fastq > TREabove11.unsorted.bam
samtools sort -o TREabove11.sorted.bam -T TREabove11.tmp TREabove11.unsorted.bam
samtools index TREabove11.sorted.bam

#STEP FIVE
#Phase reads by haplotype via WhatsHap based on known SNPs (performed using several scripts)

#!/bin/bash
#PHILIP ENGELGAU
```

```
cult={}
for cult in COP CTL EMP FUJ GAL GDE GSM HYC IDA JFR JGO JON KAN MAC NOV
PNK PR1 PR2 PR3 RCH SWE TRE VIG BRB #BUR
do
#MODIFY THE ALT
#modified HYCabove12.vcf to HYCabove12alt.vcf to only have known SNPs at 3283 and 5540
#whatshap phase uses the provided variant files (vcf) to phase the reads and tags them with HP1
or HP2 for what variant they have
#whatshap haplotag then makes a bam of the tag reads
#bamtools then separates the reads by this tag
#bgzip ${cult}above12alt.vcf
#tabix vcfs/${cult}above11alt.vcf.gz
whatshap phase -o ${cult}/${cult}above12altphased.vcf --reference
GDDH_cms2_updown_LplusQ.fasta --ignore-read-groups --tag HP
vcfs/${cult}above11alt.vcf.gz ${cult}/${cult}above12.sorted.bam
echo ${cult} "First whatshap done"
bgzip ${cult}/${cult}above12altphased.vcf
tabix ${cult}/${cult}above12altphased.vcf.gz
whatshap haplotag -o ${cult}/${cult}above12altphased.bam --ignore-read-groups
${cult}/${cult}above12altphased.vcf.gz ${cult}/${cult}above12.sorted.bam
echo ${cult} "Second whatshap done"
bamtools split -in ${cult}/${cult}above12altphased.bam -tag HP
echo ${cult} "DONE"
done
#!/bin/bash
#PHILIP ENGELGAU
cult={}
for cult in COP CTL EMP FUJ GAL GDE GSM HYC IDA JFR JGO JON KAN MAC NOV
PNK PR1 PR2 PR3 RCH SWE TRE VIG BRB BUR
do
#modify the altphasedbam files to be numbered
#in these steps samtools is converting the bam files (which is a compressed file format) into a txt
file format called sam
#I then have all the reads names pulled out and put into a list
#seqtk then goes through the fastq file and pulls out just the ones from the list
#there's then an additional filtering step if needed
PATH=$PATH:/Users/vannockerlab/Documents/Phil_pls_dont_delete/seqtk/seqtk
samtools view -h ${cult}/${cult}above12altphased1.bam >
${cult}/${cult}above12altphased1.sam
tail -n+5 ${cult}/${cult}above12altphased1.sam | awk '{print $1}' > ${cult}/${cult}1names.txt
```

```
seqtk subseq ${cult}/${cult}above12.fastq ${cult}/${cult}1names.txt > ${cult}/${cult}1all.fastq
echo ${cult} "1 done"
samtools view -h ${cult}/${cult}above12altphased2.bam >
${cult}/${cult}above12altphased2.sam
tail -n+5 ${cult}/${cult}above12altphased2.sam | awk '{print $1}' >${cult}/${cult}2names.txt
seqtk subseq ${cult}/${cult}above12.fastq ${cult}/${cult}2names.txt > ${cult}/${cult}2all.fastq
echo ${cult} "2 done"
#cat ${cult}1all.fastq | NanoFilt -q 12 >> ${cult}1above12.fastq
#cat ${cult}2all.fastq | NanoFilt -q 12 >> ${cult}2above12.fastq #again, reduced to ~16%
#echo ${cult}" filtering done"
done
```

#STEP SIX
#Assemble haplotyped reads into a 'draft genome' via canu. Canu requires a seed read to start with. This was hand-selected among the phased reads to correctly match previously known variants. Below is an example from a script that refiltered, did canu and then did Nanopolish

```
/Users/vannockerlab/Documents/Phil_pls_dont_delete/canu/canu-1.8/*/bin/canu -p
${cult}1alldraft5 -d ${cult}1alldraft5 genomeSize=5600 -nanopore-raw
${cult}/${cult}1above15.fastq contigFilter="2 0 1.0 0.5 0" correctedErrorRate=0.12
readSamplingCoverage=100 minReadLength=4000
```

#STEP SEVEN
#Polish the haplotypes against the original electrical data to improve quality. Below is my step_three.sh script, which ran several steps at once

```
#!/bin/bash
#PHILIP ENGELGAU
cult={}
for cult in COP CTL EMP FUJ GAL GDE GSM HYC IDA JFR JGO JON KAN MAC NOV
PNK PR1 PR2 PR3 RCH SWE TRE VIG BRB BUR
do
#check the draft number
#this is making a draft haplotype via canu and the polishing this draft on nanopolish by making a
vcf file
#vcf2fasta will then use this vcf file to generate a complete, polished sequence
PATH=$PATH:/Users/vannockerlab/Documents/Phil_pls_dont_delete/minimap2/minimap2
PATH=$PATH:/Users/vannockerlab/Documents/Phil_pls_dont_delete/nanopolish
#cat ${cult}/${cult}1all.fastq | NanoFilt -q 15 > ${cult}/${cult}1above15.fastq
#cat ${cult}/${cult}2all.fastq | NanoFilt -q 15 > ${cult}/${cult}2above15.fastq
```

```
#/Users/vannockerlab/Documents/Phil_pls_dont_delete/canu/canu-1.8/*/bin/canu -p
${cult}1alldraft5 -d ${cult}1alldraft5 genomeSize=5600 -nanopore-raw
${cult}/${cult}1above15.fastq contigFilter="2 0 1.0 0.5 0" correctedErrorRate=0.12
readSamplingCoverage=100 minReadLength=4000
#/Users/vannockerlab/Documents/Phil_pls_dont_delete/canu/canu-1.8/*/bin/canu -p
${cult}2alldraft5 -d ${cult}2alldraft5 genomeSize=5600 -nanopore-raw
${cult}/${cult}2above15.fastq contigFilter="2 0 1.0 0.5 0" correctedErrorRate=0.12
readSamplingCoverage=100 minReadLength=4000
#echo ${cult} "canu done"
#make sure contigs were produced
minimap2 -ax map-ont ${cult}1alldraft5/${cult}1alldraft5.contigs.fasta
${cult}/${cult}1above15.fastq > ${cult}1alldraft5/${cult}1alldraft6.contigs.unsorted.bam
samtools sort -o ${cult}1alldraft5/${cult}1alldraft6.contigs.sorted.bam -T
${cult}1alldraft5/${cult}1alldraft6.contigs.tmp
${cult}1alldraft5/${cult}1alldraft6.contigs.unsorted.bam
samtools index ${cult}1alldraft5/${cult}1alldraft6.contigs.sorted.bam
nanopolish index -d ../20180817_ONT_Amplicon/fast5s/allfast5s/
${cult}/${cult}1above15.fastq -s
../20180817_ONT_Amplicon/newoldbasecalls/newsuper_sequencing_summary.txt
echo ${cult} "index done for 1"
nanopolish variants --consensus -o ${cult}1alldraft5/${cult}1alldraft6_polished.vcf -r
${cult}/${cult}1above15.fastq -b ${cult}1alldraft5/${cult}1alldraft6.contigs.sorted.bam  -g
${cult}1alldraft5/${cult}1alldraft5.contigs.fasta
echo ${cult} "variants done for 1"
nanopolish vcf2fasta --skip-checks -g ${cult}1alldraft5/${cult}1alldraft5.contigs.fasta
${cult}1alldraft5/${cult}1alldraft6_polished.vcf >
../new_finished_seqs/${cult}1alldraft5_final.fasta
echo ${cult} "DONE for 1"
minimap2 -ax map-ont ${cult}2alldraft5/${cult}2alldraft5.contigs.fasta
${cult}/${cult}2above15.fastq > ${cult}2alldraft5/${cult}2alldraft6.contigs.unsorted.bam
samtools sort -o ${cult}2alldraft5/${cult}2alldraft6.contigs.sorted.bam -T
${cult}2alldraft5/${cult}2alldraft6.contigs.tmp
${cult}2alldraft5/${cult}2alldraft6.contigs.unsorted.bam
samtools index ${cult}2alldraft5/${cult}2alldraft6.contigs.sorted.bam
nanopolish index -d ../20180817_ONT_Amplicon/fast5s/allfast5s/
${cult}/${cult}2above15.fastq -s
../20180817_ONT_Amplicon/newoldbasecalls/newsuper_sequencing_summary.txt
echo ${cult} "index done for 2"
```

```
nanopolish variants --consensus -o ${cult}2alldraft5/${cult}2alldraft6_polished.vcf -r
${cult}/${cult}2above15.fastq -b ${cult}2alldraft5/${cult}2alldraft6.contigs.sorted.bam  -g
${cult}2alldraft5/${cult}2alldraft5.contigs.fasta
echo ${cult} "variants done for 2"
nanopolish vcf2fasta --skip-checks -g ${cult}2alldraft5/${cult}2alldraft5.contigs.fasta
${cult}2alldraft5/${cult}2alldraft6_polished.vcf >
../new_finished_seqs/${cult}2alldraft5_final.fasta
echo ${cult} "DONE for 2"
#rm ../finished_seqs/${cult}alldraft5_final.fasta
done
```

cultivar	haplotype	contig # for canu	-1967 SNP	-1965 SNP	-1723 SNP	-1544 SNP	-1029 SNP	-994 indel	-809 SNP	-316 SNP	-289 SNP	-287 SNP	-239 SNP
Braeburn	1	29	C	T	C	C	T	PLUS	G	A	C	C	C
Braeburn	2	1	A	G	C	T	T	MINUS	T	G	C	C	A
Burgundy	1	14	C	G	C	C	T	MINUS	G	G	C	T	A
Burgundy	2	1	C	G	T	C	T	MINUS	G	G	C	T	A
Cortland	1	35	C	T	C	C	C	PLUS	G	G	C	C	C
Cortland	2	32	C	G	C	C	T	HALF	G	G	C	C	C
Cox's Orange Pippin	1	6	C	G	C	C	T	MINUS	G	G	C	T	A
Cox's Orange Pippin	2	10	C	G	T	C	T	MINUS	G	G	C	T	A
Empire	1	7	C	T	C	C	C	PLUS	G	G	C	C	C
Empire	2	17	C	T	C	C	C	PLUS	G	G	T	C	C
Fuji	1	20	C	G	C	C	T	MINUS	G	G	C	T	A
Fuji	2	5	C	T	C	C	T	PLUS	G	A	T	C	C
Fulford Gala	1	4	C	G	C	C	T	MINUS	G	G	C	T	A
Fulford Gala	2	1	A	G	C	T	T	MINUS	T	G	C	C	A
Golden Delicious	1	23	C	G	C	C	T	MINUS	G	G	C	T	A
Golden Delicious	2	39	A	G	C	T	T	MINUS	T	G	C	C	A
Granny Smith	1	6	C	T	C	C	C	PLUS	G	G	T	C	C
Granny Smith	2	19	A	G	C	T	T	MINUS	T	G	C	C	A
Honeycrisp	1	32	C	G	C	C	T	MINUS	G	G	C	T	A
Honeycrisp	2	9	A	G	C	T	T	MINUS	T	G	C	C	A
Idared	1	5	A	G	C	T	T	MINUS	T	G	C	C	A
Idared	2	7	A	G	C	T	T	MINUS	T	G	C	C	A
Jonafree	1	2	C	G	T	C	T	MINUS	G	G	C	T	A
Jonafree	2	2	C	G	C	C	T	MINUS	G	G	C	T	A

Table B.1. Variants detected via Nanopore sequencing. Location of SNP or indel in reference to basepairs ± start codon. Variants within coding regions identified by codon affected and have resulting amino acid residues likewise listed. Due to pipeline limitations only two haplotypes could be determined per cultivar, regardless of ploidy.

Table B.1 (cont'd)

cultivar	-187 indel	-145 SNP	-121 SNP	codon 36	AA 36	codon 68	AA 68	codon 92	AA 92	+1073 SNP	+1100 SNP	+1208 SNP	+1784 SNP	+2025 SNP
Braeburn	PLUS	T	C	CCC	P	GAA	E	CAG	Q	A	C	C	G	A
Braeburn	PLUS	C	C	CTC	L	GAA	E	CAA	Q	C	A	C	C	C
Burgundy	MINUS	T	T	CCC	P	GAA	E	CAA	Q	A	C	T	G	C
Burgundy	MINUS	T	C	CCC	P	GAA	E	CAA	Q	A	C	T	G	C
Cortland	PLUS	T	T	CCC	P	AAA	K	CAG	Q	A	C	C	G	A
Cortland	PLUS	T	T	CCC	P	GAA	E	CAA	Q	A	C	C	G	C
Cox's Orange Pippin	MINUS	T	C	CCC	P	GAA	E	CAA	Q	A	C	T	G	C
Cox's Orange Pippin	MINUS	T	C	CCC	P	GAA	E	CAA	Q	A	C	T	G	C
Empire	PLUS	T	T	CCC	P	AAA	K	CAG	Q	A	C	C	G	A
Empire	PLUS	T	T	CCC	P	AAA	K	CAG	Q	A	C	C	G	A
Fuji	MINUS	T	C	CCC	P	GAA	E	CAA	Q	A	C	T	G	C
Fuji	PLUS	T	T	CCC	P	GAA	E	CAG	Q	A	C	C	G	A
Fulford Gala	MINUS	T	C	CCC	P	GAA	E	CAA	Q	A	C	T	G	C
Fulford Gala	PLUS	C	C	CTC	L	GAA	E	CAA	Q	C	A	C	C	C
Golden Delicious	MINUS	T	C	CCC	P	GAA	E	CAA	Q	A	C	T	G	C
Golden Delicious	PLUS	C	C	CTC	L	GAA	E	CAA	Q	C	A	C	C	C
Granny Smith	PLUS	T	T	CCC	P	AAA	K	CAG	Q	A	C	C	G	A
Granny Smith	PLUS	C	C	CTC	L	GAA	E	CAA	Q	C	A	C	C	C
Honeycrisp	MINUS	T	C	CCC	P	GAA	E	CAA	Q	A	C	T	G	C
Honeycrisp	PLUS	C	C	CTC	L	GAA	E	CAA	Q	C	A	C	C	C
Idared	PLUS	T	C	CTC	L	GAA	E	CAA	Q	C	A	C	C	C
Idared	PLUS	T	C	CTC	L	GAA	E	CAA	Q	C	A	C	C	C
Jonafree	MINUS	T	C	CCC	P	GAA	E	CAA	Q	A	C	T	G	C
Jonafree	MINUS	T	C	CCC	P	GAA	E	CAA	Q	A	C	T	G	C

Table B.1 (cont'd)

cultivar	+2070 SNP	intron4 indel	codon 387	AA 387
Braeburn	G	MINUS	CAG	Q
Braeburn	G	PLUS	CAG	Q
Burgundy	T	MINUS	CAG	Q
Burgundy	T	MINUS	CAG	Q
Cortland	G	MINUS	CAG	Q
Cortland	G	MINUS	CAG	Q
Cox's Orange Pippin	T	MINUS	GAG	E
Cox's Orange Pippin	T	MINUS	GAG	E
Empire	G	MINUS	CAG	Q
Empire	G	MINUS	CAG	Q
Fuji	T	MINUS	GAG	E
Fuji	G	MINUS	CAG	Q
Fulford Gala	T	MINUS	GAG	E
Fulford Gala	G	PLUS	CAG	Q
Golden Delicious	T	MINUS	GAG	E
Golden Delicious	G	PLUS	CAG	Q
Granny Smith	G	MINUS	GAG	E
Granny Smith	G	PLUS	CAG	Q
Honeycrisp	T	MINUS	GAG	E
Honeycrisp	G	PLUS	CAG	Q
Idared	G	PLUS	CAG	Q
Idared	G	PLUS	CAG	Q
Jonafree	T	MINUS	GAG	E
Jonafree	T	MINUS	GAG	E

Table B.1 (cont'd)

cultivar	haplotype	contig # for canu	-1967 SNP	-1965 SNP	-1723 SNP	-1544 SNP	-1029 SNP	-994 indel	-809 SNP	-316 SNP	-289 SNP	-287 SNP	-239 SNP
Jonagold	1	32	C	G	C	C	T	MINUS	G	G	C	T	A
Jonagold	2	3	A	G	C	T	T	MINUS	T	G	C	C	A
Jonathan	1	33	A	G	C	T	T	MINUS	T	G	C	C	A
Jonathan	2	31	C	G	C	C	T	MINUS	G	G	C	T	A
Kanzi	1	20	C	G	C	C	T	MINUS	G	G	C	T	A
Kanzi	2	1	A	G	C	T	T	MINUS	T	G	C	C	A
Nova Easygro	1	23	C	G	C	C	T	MINUS	G	G	C	T	A
Nova Easygro	2	39	C	T	C	C	C	PLUS	G	G	C	C	C
Pink Lady	1	4	C	T	C	C	T	MINUS	G	A	C	C	C
Pink Lady	2	3	C	G	C	T	T	HALF	G	G	C	C	A
PRI 1176-1	1	4	C	T	C	C	C	PLUS	G	G	C	C	C
PRI 1176-1	2	10	A	G	C	T	T	MINUS	T	G	C	C	A
PRI 1312-6	1	19	C	T	C	C	T	PLUS	G	A	C	C	C
PRI 1312-6	2	2	A	G	C	T	T	MINUS	T	G	C	C	A
PRI 1850-4	1	1	C	G	T	C	T	MINUS	G	G	C	T	A
PRI 1850-4	2	7	C	G	C	C	T	MINUS	G	G	C	T	A
Red Chief Delicious	1	23	C	T	C	C	C	PLUS	G	G	C	C	C
Red Chief Delicious	2	2	C	T	C	C	T	PLUS	G	A	C	C	C
Spur McIntosh	1	25	C	T	C	C	C	PLUS	G	G	C	C	C
Spur McIntosh	2	28	C	T	C	C	C	PLUS	G	G	C	C	C
SweeTango	1	17	A	G	C	T	T	MINUS	T	G	-	-	A
SweeTango	2	19	A	G	C	T	T	MINUS	T	G	A	T	A
Trent	1	1	C	G	C	C	T	MINUS	G	G	A	T	A
Trent	2	18	C	T	C	C	C	PLUS	G	G	A	C	C
Virginiagold	1	3	C	G	C	C	T	MINUS	G	G	A	T	A
Virginiagold	2	27	C	G	T	C	T	MINUS	G	G	A	T	A

Table B.1 (cont'd)

cultivar	-187 indel	-145 SNP	-121 SNP	codon 36	AA 36	codon 68	AA 68	codon 92	AA 92	+1073 SNP	+1100 SNP	+1208 SNP	+1784 SNP	+2025 SNP
Jonagold	MINUS	T	C	CCC	P	GAA	E	CAA	Q	A	C	T	G	C
Jonagold	PLUS	C	C	CTC	L	GAA	E	CAA	Q	C	A	C	C	C
Jonathan	MINUS	T	C	CTC	P	GAA	E	CAA	Q	C	A	C	C	C
Jonathan	MINUS	T	C	CCC	L	GAA	E	CAA	Q	A	C	T	G	C
Kanzi	MINUS	T	C	CCC	L	GAA	E	CAA	Q	A	C	T	G	C
Kanzi	PLUS	C	C	CTC	P	GAA	E	CAA	Q	C	A	C	C	C
Nova Easygro	MINUS	T	C	CCC	L	GAA	E	CAA	Q	A	C	T	G	C
Nova Easygro	PLUS	T	T	CCC	L	AAA	K	CAG	Q	A	C	C	G	A
Pink Lady	PLUS	T	T	CCC	L	GAA	E	CAG	Q	A	C	C	G	A
Pink Lady	PLUS	C	C	CTC	P	GAA	E	CAA	Q	C	A	C	C	C
PRI 1176-1	PLUS	T	T	CCC	L	AAA	K	CAG	Q	A	C	C	G	A
PRI 1176-1	PLUS	C	C	CTC	P	GAA	E	CAA	Q	C	A	C	C	C
PRI 1312-6	PLUS	T	T	CCC	L	GAA	E	CAG	Q	A	C	C	G	A
PRI 1312-6	PLUS	T	C	CTC	P	GAA	E	CAA	Q	C	A	C	C	C
PRI 1850-4	MINUS	T	C	CCC	L	GAA	E	CAA	Q	A	C	T	G	C
PRI 1850-4	MINUS	T	C	CCC	L	GAA	E	CAA	Q	A	C	T	G	C
Red Chief Delicious	PLUS	T	T	CCC	L	AAA	K	CAG	Q	A	C	C	G	A
Red Chief Delicious	PLUS	T	T	CCC	L	GAA	E	CAG	Q	A	C	C	G	A
Spur McIntosh	PLUS	T	T	CCC	L	AAA	K	CAG	Q	A	C	C	G	A
Spur McIntosh	PLUS	T	T	CCC	L	AAA	K	CAG	Q	A	C	C	G	A
SweeTango	PLUS	T	C	CTC	P	GAA	E	CAA	Q	C	A	C	C	C
SweeTango	PLUS	T	C	CTC	P	GAA	E	CAA	Q	C	A	C	C	C
Trent	MINUS	T	C	CCC	L	GAA	E	CAG	Q	A	C	T	G	C
Trent	PLUS	T	T	CCC	L	AAA	K	CAG	Q	A	C	C	G	A
Virginiagold	MINUS	T	C	CCC	L	GAA	E	CAA	Q	A	C	T	G	C
Virginiagold	MINUS	T	C	CCC	L	GAA	E	CAA	Q	A	C	T	G	C

Table B.1 (cont'd)

cultivar	+2070 SNP	intron4 indel	codon 387	AA 387
Jonagold	T	MINUS	GAG	E
Jonagold	G	PLUS	CAG	Q
Jonathan	G	PLUS	CAG	Q
Jonathan	T	MINUS	GAG	E
Kanzi	T	MINUS	GAG	E
Kanzi	G	PLUS	CAG	Q
Nova Easygro	T	MINUS	GAG	E
Nova Easygro	G	MINUS	CAG	Q
Pink Lady	G	MINUS	CAG	Q
Pink Lady	G	PLUS	CAG	Q
PRI 1176-1	G	MINUS	CAG	Q
PRI 1176-1	G	PLUS	CAG	Q
PRI 1312-6	G	MINUS	CAG	Q
PRI 1312-6	G	PLUS	CAG	Q
PRI 1850-4	T	MINUS	GAG	E
PRI 1850-4	T	MINUS	GAG	E
Red Chief Delicious	G	MINUS	CAG	Q
Red Chief Delicious	G	MINUS	CAG	Q
Spur McIntosh	G	MINUS	CAG	Q
Spur McIntosh	G	MINUS	CAG	Q
SweeTango	G	PLUS	CAG	Q
SweeTango	G	PLUS	CAG	Q
Trent	T	MINUS	GAG	E
Trent	G	MINUS	CAG	Q
Virginiagold	T	MINUS	GAG	E
Virginiagold	T	MINUS	GAG	E

APPENDIX C – NORTH AMERICAN BIRDS IDENTIFIED WHILE IN GRADUATE SCHOOL

common name	date	location
Ring-Billed Gull	5/23/20	Saugatuck, MI
Scarlet Tanager	5/23/20	Saugatuck, MI
Spotted Sandpiper	5/23/20	Saugatuck, MI
Chipping Sparrow	6/1/20	MSU Gardens, MI
Sandhill Crane	6/7/20	East Lansing, MI
American Goldfinch	6/7/20	Lansing, MI
Mallard	6/9/20	Red Cedar River, MI
Eastern Bluebird	6/11/20	Fenner Nature Center, MI
Blue Jay	6/16/20	Pidgeon Creek, MI
Cardinal	6/18/20	MSU Gardens, MI
Robin	6/18/20	MSU Gardens, MI
Canada Goose	6/19/20	Lansing, MI
Great Blue Heron	6/19/20	Red Cedar River, MI
Mourning Dove	6/20/20	Lansing, MI
Red-Winged Blackbird	6/22/20	Hawk Island, MI
Rock Dove	6/25/20	Lansing, MI
Starling	6/26/20	Lansing, MI
House Sparrow	7/2/20	East Lansing, MI
Downy Woodpecker	7/3/20	Lansing, MI
Cedar Waxwing	7/8/20	Hawk Island, MI
Common Crow	7/10/20	Lansing, MI
Black-Capped Chickadee	7/12/20	East Lansing, MI
Green Heron	8/29/20	Hawk Island, MI
Belted Kingfisher	9/7/20	Hawk Island, MI
American Redstart	9/13/20	Fenner Nature Center, MI
Turkey	9/13/20	Fenner Nature Center, MI
White-Breasted Nuthatch	9/13/20	Fenner Nature Center, MI
Yellow-Shafted Flicker	9/13/20	Fenner Nature Center, MI
Wood Duck	9/19/20	Fenner Nature Center, MI
Red-Bellied Woodpecker	11/26/20	Fenner Nature Center, MI
Slate-Colored Junco	11/26/20	Fenner Nature Center, MI
Tufted Titmouse	11/26/20	Fenner Nature Center, MI

Table C.1. North American birds identified while in graduate school.

Table C.1 (cont'd)

common name	date	location
Pileated Woodpecker	12/6/20	Fenner Nature Center, MI
Purple Finch	12/13/20	Hawk Island, MI
Brown Creeper	12/22/20	Central Park, NY
White-Throated Sparrow	12/22/20	Central Park, NY
Brant	12/23/20	Liberty Island, NY
Greater Scaup	12/23/20	Liberty Island, NY
Shoveler	12/26/20	Central Park, NY
Red-Breasted Nuthatch	12/29/20	Lansing, MI
Tree Sparrow	1/2/21	Fenner Nature Center, MI
Cooper's Hawk	1/9/21	Woldumar, MI
Bald Eagle	3/10/21	MSU Campus, MI
Killdeer	3/20/21	Sycamore Creek, MI
American Coot	3/27/21	Hawk Island, MI
Bufflehead	4/17/21	Pinckney, MI
Mute Swan	4/17/21	Pinckney, MI
Whistling Swan	4/17/21	Pinckney, MI
Wood Thrush	4/17/21	Pinckney, MI
Red-Breasted Merganser	4/18/21	Saugatuck, MI
Barn Swallow	4/24/21	Lansing, MI
Common Grackle	4/24/21	Lansing, MI
Tree Swallow	4/24/21	Lansing, MI
Blue-Winged Teal	4/25/21	Sleepy Hollow, MI
Brown-Headed Cowbird	4/25/21	Sleepy Hollow, MI
Eastern Towhee	4/25/21	Sleepy Hollow, MI
Hermit Thrush	4/25/21	Sleepy Hollow, MI
Eastern Phoebe	5/9/21	Fenner Nature Center, MI
House Finch	5/9/21	Lansing, MI
Baltimore Oriole	5/15/21	Fenner Nature Center, MI
Eastern Kingbird	5/15/21	Fenner Nature Center, MI
Indigo Bunting	5/15/21	Fenner Nature Center, MI
Yellow Warbler	5/16/21	Grand River, MI
Double-Crested Cormorant	5/16/21	Maple River, MI
Osprey	5/16/21	Maple River, MI
Solitary Sandpiper	5/16/21	Maple River, MI
White-Crowned Sparrow	5/16/21	Maple River, MI
Yellowthroat	5/16/21	Maple River, MI
Sharp-Shinned Hawk	5/18/21	Lansing, MI

Table C.1 (cont'd)

common name	date	location
Hairy Woodpecker	5/22/21	Grand River, MI
Prothonotary Warbler	5/22/21	Grand River, MI
Catbird	6/30/21	Fenner Nature Center, MI
Black-Billed Magpie	8/3/21	Eldorado Canyon, CO
Lesser Goldfinch	8/4/21	Mt. Gailbraith, CO
Ruby-Crowned Kinglet	8/4/21	Mt. Gailbraith, CO
Spotted Towhee	8/4/21	Mt. Gailbraith, CO
Western Bluebird	8/4/21	Mt. Gailbraith, CO
Western Tanager	8/4/21	Mt. Gailbraith, CO
Great Horned Owl	8/5/21	Rocky Mountain Arsenal National Wildlife Refuge, CO
Western Kingbird	8/5/21	Rocky Mountain Arsenal National Wildlife Refuge, CO
Western Meadowlark	8/5/21	Rocky Mountain Arsenal National Wildlife Refuge, CO
White Pelican	8/5/21	Rocky Mountain Arsenal National Wildlife Refuge, CO
Chestnut-Backed Chickadee	8/10/21	Monte Sereno, CA
Oak Titmouse	8/10/21	Monte Sereno, CA
California Scrub Jay	8/12/21	Monte Sereno, CA
Oregon Junco	8/12/21	Monte Sereno, CA
Brewer's Blackbird	8/14/21	Capitola, CA
Brown Pelican	8/14/21	Capitola, CA
Black Phoebe	8/16/21	Monte Sereno, CA
Acorn Woodpecker	8/19/21	Monte Sereno, CA
Stellar's Jay	8/19/21	Monte Sereno, CA
Common Egret	9/6/21	Priggoris Park, MI
Canada Warbler	9/12/21	Grand River, MI
American Pipit	9/25/21	Cheboygan, MI
Barred Owl	10/3/21	Sycamore Creek, MI
Pacific Wren	10/30/21	Mt. Tabor, OR
Varied Thrush	10/30/21	Mt. Tabor, OR
Red-Tailed Hawk	11/27/21	Bronx Zoo, NY
Ruddy Duck	11/28/21	Central Park, NY
Black Duck	11/28/21	Little Island, NY
Gadwall	11/28/21	Little Island, NY
Great Cormorant	11/28/21	Little Island, NY

Table C.1 (cont'd)

common name	date	location
Mockingbird	11/28/21	Little Island, NY
Golden-Crowned Sparrow	12/17/21	Monte Sereno, CA
California Quail	12/18/21	Monte Sereno, CA
Red-Breasted Sapsucker	12/18/21	Monte Sereno, CA
Red-Shafted Flicker	12/18/21	Monte Sereno, CA
California Towhee	12/19/21	Monte Sereno, CA
Audubon's Warbler	12/21/21	Monte Sereno, CA
Bewick's Wren	12/21/21	Monte Sereno, CA
Common Bushtit	12/21/21	Monte Sereno, CA
Nuttall's Woodpecker	12/21/21	Monte Sereno, CA
Turkey Vulture	12/22/21	Monte Sereno, CA
Pied-Billed Grebe	12/23/21	Vasona Park, CA
Anna's Hummingbird	12/24/21	Monte Sereno, CA
American Avocet	12/26/21	Elkhorn Slough, CA
Black Brant	12/26/21	Elkhorn Slough, CA
Black-Necked Stilt	12/26/21	Elkhorn Slough, CA
Brandt's Cormorant	12/26/21	Elkhorn Slough, CA
Eared Grebe	12/26/21	Elkhorn Slough, CA
Forster's Tern	12/26/21	Elkhorn Slough, CA
Long-Billed Curlew	12/26/21	Elkhorn Slough, CA
Marbled Godwit	12/26/21	Elkhorn Slough, CA
Snowy Egret	12/26/21	Elkhorn Slough, CA
Snowy Plover	12/26/21	Elkhorn Slough, CA
Surf Scoter	12/26/21	Elkhorn Slough, CA
Willet	12/26/21	Elkhorn Slough, CA
Townsend's Warbler	12/27/21	Monte Sereno, CA
Carolina Wren	1/8/22	Fenner Nature Center, MI
Common Goldeneye	1/16/22	Discovery Park, WA
American Widgeon	1/18/22	Duck Bay, WA
Green-Winged Teal	1/18/22	Duck Bay, WA
Pintail	1/18/22	Duck Bay, WA
Song Sparrow	1/18/22	Marsh Island, WA
Common Merganser	1/19/22	Marsh Island, WA
Ring-Necked Duck	1/19/22	Marsh Island, WA

Table C.1 (cont'd)

common name	date	location
Field Sparrow	4/16/22	Fenner Nature Center, MI
Winter Wren	4/16/22	Fenner Nature Center, MI
Pine Warbler	4/19/22	Fenner Nature Center, MI
Brown Thrasher	4/24/22	Fenner Nature Center, MI
Myrtle Warbler	4/24/22	Fenner Nature Center, MI
Palm Warbler	4/24/22	Fenner Nature Center, MI
Yellow-Bellied Sapsucker	4/24/22	Fenner Nature Center, MI
Rough-Winged Swallow	4/30/22	Woldumar, MI
Black-And-White Warbler	5/7/22	Fenner Nature Center, MI
House Wren	5/7/22	Fenner Nature Center, MI
Magnolia Warbler	5/10/22	Fenner Nature Center, MI
Swainson's Thrush	5/10/22	Fenner Nature Center, MI
Eastern Wood Pewee	5/24/22	Fenner Nature Center, MI
Rose-Breasted Grosbeak	5/24/22	Fenner Nature Center, MI
Hooded Merganser	6/2/22	Fenner Nature Center, MI
Hooded Warbler	6/25/22	Saugatuck, MI
Chimney Swift	7/24/22	Fenner Nature Center, MI
Least Sandpiper	9/5/22	Billy Frank Jr. Nisqually National Wildlife Refuge, WA
Pectoral Sandpiper	9/5/22	Billy Frank Jr. Nisqually National Wildlife Refuge, WA
Semipalmated Plover	9/5/22	Billy Frank Jr. Nisqually National Wildlife Refuge, WA
Black-Throated Green Warbler	9/25/22	Fenner Nature Center, MI
Golden-Crowned Kinglet	10/16/22	Woldumar, MI
Nashville Warbler	10/16/22	Woldumar, MI
Black Oystercatcher	12/22/22	Point Lobos, CA
Heermann's Gull	12/22/22	Point Lobos, CA
Fox Sparrow	4/9/23	Fenner Nature Center, MI
Purple Martin	7/14/23	Escanaba, MI
Cliff Swallow	7/17/23	Yellowstone, WY
Common Raven	7/17/23	Yellowstone, WY
Louisiana Heron	8/2/23	Orlando, FL
White Ibis	8/2/23	Orlando, FL
Greater Yellowlegs	8/20/23	Billy Frank Jr. Nisqually National Wildlife Refuge, WA